A decentralized approach for enabling advanced ancillary services through distributed energy sources

Department of Electrical and Information Engineering

ELECTRICAL AND INFORMATION ENGINEERING
Ph.D. Program
SSD: ING-IND/33– Electrical Energy Systems

**Final Dissertation**

---

# A Decentralized Approach for Enabling Advanced Ancillary Services through Distributed Energy Sources

---

by

Carmine Rodio

Supervisors:

Prof. Massimo La Scala

Eng. Antonio Araldo

Eng. Andrea Caregari

Eng. Giovanni Valtorta

*Coordinator of Ph.D. Program:*
*Prof. Mario Carpentieri*

---

*XXXV Cycle - November 1st, 2019 - January 31st, 2023*

Politecnico di Bari

# LIBERATORIA PER L'ARCHIVIAZIONE DELLA TESI DI DOTTORATO

Al Magnifico Rettore
del Politecnico di Bari

Il sottoscritto ___Carmine_Rodio_____ nato a ___Cisternino_(BR)__ il__22/12/1986___

residente a __Fasano_(BR)__ in via_____Sisto,10_____ e-mail__carmine.rodio@poliba.it_____

iscritto al 3° anno di Corso di Dottorato di Ricerca in__Ingegneria Elettrica e dell'Informazione_____ciclo_XXXV____

ed essendo stato ammesso a sostenere l'esame finale con la prevista discussione della tesi dal titolo:

__**A Decentralized Approach for Enabling Advanced Ancillary Services through Distributed Energy Sources**___

**DICHIARA**

1) di essere consapevole che, ai sensi del D.P.R. n. 445 del 28.12.2000, le dichiarazioni mendaci, la falsità negli atti e l'uso di atti falsi sono puniti ai sensi del codice penale e delle Leggi speciali in materia, e che nel caso ricorressero dette ipotesi, decade fin dall'inizio e senza necessità di nessuna formalità dai benefici conseguenti al provvedimento emanato sulla base di tali dichiarazioni;
2) di essere iscritto al Corso di Dottorato di ricerca in Ingegneria Elettrica e Dell'Informazione ciclo XXXV, corso attivato ai sensi del "*Regolamento dei Corsi di Dottorato di ricerca del Politecnico di Bari*", emanato con D.R. n.286 del 01.07.2013;
3) di essere pienamente a conoscenza delle disposizioni contenute nel predetto Regolamento in merito alla procedura di deposito, pubblicazione e autoarchiviazione della tesi di dottorato nell'Archivio Istituzionale ad accesso aperto alla letteratura scientifica;
4) di essere consapevole che attraverso l'autoarchiviazione delle tesi nell'Archivio Istituzionale ad accesso aperto alla letteratura scientifica del Politecnico di Bari (IRIS-POLIBA), l'Ateneo archivierà e renderà consultabile in rete (nel rispetto della Policy di Ateneo di cui al D.R. 642 del 13.11.2015) il testo completo della tesi di dottorato, fatta salva la possibilità di sottoscrizione di apposite licenze per le relative condizioni di utilizzo (di cui al sito http://www.creativecommons.it/Licenze), e fatte salve, altresì, le eventuali esigenze di "embargo", legate a strette considerazioni sulla tutelabilità e sfruttamento industriale/commerciale dei contenuti della tesi, da rappresentarsi mediante compilazione e sottoscrizione del modulo in calce (Richiesta di embargo);
5) che la tesi da depositare in IRIS-POLIBA, in formato digitale (PDF/A) sarà del tutto identica a quelle **consegnate**/inviate/da inviarsi ai componenti della commissione per l'esame finale e a qualsiasi altra copia depositata presso gli Uffici del Politecnico di Bari in forma cartacea o digitale, ovvero a quella da discutere in sede di esame finale, a quella da depositare, a cura dell'Ateneo, presso le Biblioteche Nazionali Centrali di Roma e Firenze e presso tutti gli Uffici competenti per legge al momento del deposito stesso, e che di conseguenza va esclusa qualsiasi responsabilità del Politecnico di Bari per quanto riguarda eventuali errori, imprecisioni o omissioni nei contenuti della tesi;
6) che il contenuto e l'organizzazione della tesi è opera originale realizzata dal sottoscritto e non compromette in alcun modo i diritti di terzi, ivi compresi quelli relativi alla sicurezza dei dati personali; che pertanto il Politecnico di Bari ed i suoi funzionari sono in ogni caso esenti da responsabilità di qualsivoglia natura: civile, amministrativa e penale e saranno dal sottoscritto tenuti indenni da qualsiasi richiesta o rivendicazione da parte di terzi;
7) che il contenuto della tesi non infrange in alcun modo il diritto d'Autore né gli obblighi connessi alla salvaguardia di diritti morali od economici di altri autori o di altri aventi diritto, sia per testi, immagini, foto, tabelle, o altre parti di cui la tesi è composta.

Luogo e data _Bari, 25/03/2023__ Firma _____

Il sottoscritto Rodio Carmine, con l'autoarchiviazione della propria tesi di dottorato nell'Archivio Istituzionale ad accesso aperto del Politecnico di Bari (POLIBA-IRIS), pur mantenendo su di essa tutti i diritti d'autore, morali ed economici, ai sensi della normativa vigente (Legge 633/1941 e ss.mm.ii.),

**CONCEDE**

- al Politecnico di Bari il permesso di trasferire l'opera su qualsiasi supporto e di convertirla in qualsiasi formato al fine di una corretta conservazione nel tempo. Il Politecnico di Bari garantisce che non verrà effettuata alcuna modifica al contenuto e alla struttura dell'opera.
- al Politecnico di Bari la possibilità di riprodurre l'opera in più di una copia per fini di sicurezza, back-up e conservazione.

Luogo e data __Bari, 25/03/2023_____ Firma _____

Politecnico di Bari

Department of Electrical and Information Engineering

ELECTRICAL AND INFORMATION ENGINEERING
Ph.D. Program
SSD: ING-IND/33 – Electrical Energy Systems

**Final Dissertation**

---

# A Decentralized Approach for Enabling Advanced Ancillary Services through Distributed Energy Sources

---

by

Rodio Carmine:

_____

Referees:

Prof. Stefania Conti

Prof. Andrea Bonfiglio

Supervisors:

Prof. Massimo La Scala

_____

Eng. Antonio Araldo

_____

Eng. Andrea Caregari

_____

Eng. Giovanni Valtorta

_____

*Coordinator of Ph.D. Program:*

*Prof. Mario Carpentieri*

---

*XXXV Cycle - November 1st, 2019 - January 31st, 2023*

This work has been founded by e-distribuzione S.p.A.

# Contents

# List of Figures

# List of Tables

# Abstract

This thesis reports the results carried out by the author during the three-year activities of the XXXV cycle of the Ph.D. course in Electrical and Information Engineering at Politecnico di Bari. The main goal of this work was to implement a decentralized approach to enable the provision of Ancillary Services (AS) by means of Distributed Energy Resources (DERs).

As a first step, an analysis of Regulations, Directives, and Network Codes at the national and European level was carried out to define the future framework of the electricity market. In addition, papers and technical reports concerning eight European projects, such as SmarNet, CoordiNet, FLEXCoop, OSMOSE, inteGRIDy, eDREAM, ADDRESS, and evolvDSO have been analyzed with the aim to define the state of the art about the provision of AS by means of DERs. In particular, a set of coordination schemes was identified from those proposed in the literature to coordinate the use of DERs among Transmission System Operators (TSOs) and Distribution System Operators (DSOs). These coordination schemes are classified into centralized and decentralized architectures, depending on the possibility of System Operators of managing their respective networks. In addition, the main methodologies proposed in the literature to perform optimal dispatch of flexibility resources in a TSO-DSO coordination framework, taking technical and grid constraints into account, have been identified and presented.

In order to enable DERs in AS provision and coordinate system operators in their usage, a few methodologies suitable for decentralized architectures were developed and presented in this work. In particular, a new algorithm based on a three-phase optimal power flow routine for mapping the flexibility area at the point of interconnection

(POI) between transmission and distribution grids was provided. Furthermore, two alternative methodologies to aggregate flexibility resources located in distribution networks interfaced with the TN in multiple POIs were described. In addition, a Benders decomposition algorithm able to optimize TN and DN flexibility resources for congestion management in a few decentralized coordination schemes was also implemented. The proposed methodologies were validated by means of simulation tests conducted on a power system including transmission and distribution grids.

The last part of this thesis investigated how innovative grid services, such as Synthetic Inertia (SI) and Fast Frequency Response (FFR), may be also provided through fast control dispatchable resources located at the distribution grid level. With this aim, a low-cost controller for end-user applications able to generate a SI law for dispatchable DERs was developed and tested through Power Hardware-in-the-Loop (PHIL) tests. Similarly, PHIL tests were also carried out to investigate the capability of LED lamps of public lighting systems to be controlled with the aim to provide SI and FFR actions. Experimental results validated the proposed decentralized approaches.

# Publications

Publications resulting from this research work are listed below in chronological order.

**Conferences**

1. S. Bruno, G. Giannoccaro, C. Iurlaro, M. La Scala, and C. Rodio, "A Low-cost Controller to Enable Synthetic Inertia Response of Distributed Energy Resources," in *2020 IEEE EEEIC/ICPS Europe*, 2020, pp. 1–6

2. C. Rodio, G. Giannoccaro, S. Bruno, M. Bronzini, and M. La Scala, "Optimal Dispatch of Distributed Resources in a TSO-DSO Coordination Framework," in *2020 AEIT International Annual Conference*, 2020, pp. 1–6

3. E. Bompard, S. Bruno, S. Frittoli, G. Giannoccaro, M. La Scala, A. Mazza, E. Pons, and C. Rodio, "Remote PHIL Distributed Co-Simulation Lab for TSO-DSO-Customer Coordination Studies," in *2020 AEIT International Annual Conference*, 2020, pp. 1–6

4. S. Bruno, G. Giannoccaro, C. Iurlaro, M. La Scala, L. Notaristefano, and C. Rodio, "Mapping Flexibility Region through Three-phase Distribution Optimal Power Flow at TSO-DSO Point of Interconnection," in *2021 AEIT International Annual Conference*, 2021, pp. 1–6

5. S. Bruno, G. De Carne, C. Iurlaro, C. Rodio, and M. Specchio, "A SOC-feedback Control Scheme for Fast Frequency Support with Hybrid Battery/Supercapacitor

Storage System," in *2021 6th IEEE Workshop on the Electronic Grid (eGRID)*, 2021, pp. 1–8

6. S. Bruno, G. Giannoccaro, C. Iurlaro, M. La Scala, C. Rodio, and R. Sbrizzai, "Fast Frequency Regulation Support by LED Street Lighting Control," in *2021 EEEIC/ICPS Europe Conference*, 2021, pp. 1–6

7. S. Bruno, G. Giannoccaro, M. M. Islam, C. Iurlaro, M. La Scala, M. Menga, and C. Rodio, "Control and Power Hardware-in-the-Loop tests for low-inertia power systems," in *2022 AEIT International Annual Conference*, 2022, pp. 1–6

8. C. Rodio, G. Giannoccaro, S. Bruno, and M. La Scala, "Benders Decomposition for TSO-DSO Coordination in Local Ancillary Services Market," in *Accepted with mandatory changes to 2023 IEEE PES General Meeting*

**Journal**

1. P. A. Lombardi, K. R. Moreddy, A. Naumann, P. Komarnicki, C. Rodio, and S. Bruno, "Data centers as active multi-energy systems for power grid decarbonization: A technical and economic analysis," *Energies*, vol. 12, no. 21, 2019

2. E. Bompard, S. Bruno, G. Chicco, G. Giannoccaro, M. La Scala, A. Mazza, E. Pons, and C. Rodio, "Co-simulazione real-time multi-sito e cooperazione tra laboratori," *AEIT*, vol. 106 num. 7, pp. 38–55, 2020

3. S. Bruno, G. Giannoccaro, C. Iurlaro, M. La Scala, and C. Rodio, "Power Hardware-in-the-Loop Test of a Low-Cost Synthetic Inertia Controller for Battery Energy Storage System," *Energies*, vol. 15, no. 9, 2022

4. S. Bruno, G. Giannoccaro, C. Iurlaro, M. La Scala, M. Menga, C. Rodio, and R. Sbrizzai, "Fast Frequency Support Through LED Street Lighting in Small Non-Synchronous Power Systems," *IEEE Transactions on Industry Applications*, pp. 1–11, 2022

5. C. Rodio, G. Giannoccaro, S. Bruno, and M. La Scala, “Benders Decomposition Methodology for TSO-DSO Cooperation in Ancillary Services Markets,” *submitted to IEEE Transactions on Power Systems*

# Introduction

## Background and Motivation

In recent years, EU power systems and electricity markets are undergoing drastic changes to implement the energy transition. In this direction, numerous initiatives and regulations have been adopted to reach by 2030 a share of Renewable Energy Sources of 40 % and reduce greenhouse gas emissions of at least 55 % with respect to 1990 levels [14], [15]. In order to achieve this goal, fossil-fueled generation is gradually being replaced with renewable sources. Although the progressive replacement of conventional power plants with non-programmable units is introducing additional uncertainties in power system management [16], the presence of Distributed Energy Resources (DERs) at distribution network (DN) level represents also an opportunity for power system operators and the Ancillary Services (AS) market design [17]. Small dispatchable generators, controllable loads, and storage systems may be exploited as flexibility resources [4] for improving power system operation and facing power fluctuations introduced by renewable sources [18], load changes, line outages, and forecasting errors [19]. In this perspective, distributed generation, Demand Response (DR), and microgrids will be considered as the major flexibility providers [20].

In the coming years, it is expected that the growing presence of DERs connected to the distribution grid will negatively affect the DN operation [21]. In this sense, as highlighted by the Italian Regulatory Authority, ARERA, the increasing number of renewable sources, electrical vehicle (EV) charging stations and Heating, Ventilation and Air Conditioning (HVAC) units located at the DN level might cause voltage profile and congestion issues [22]. These issues pointed out the necessity to involve the

DSO in the provisioning of Ancillary Services from DERs to the TSO as well as allow it in using grid services to ensure optimal use of DERs and improve the trading efficiency of TN and DN [20]. This idea is also shared by Regulation EU 2019/943 [23] and Directive EU 2019/944 [24]. In accordance with European regulations, several studies investigated how DERs can be exploited as grid services for both TN and DN in a TSO-DSO cooperation framework, distinguishing *centralized* and *decentralized* coordination architectures. In general, the former assigns the control of resources to a single operator, which may be the TSO or and Independent Market Operator (IMO). This condition does not well fits with contexts in which transmission and distribution grids are operated by separated grid operators, as in the Italian context, in which there are one Transmission System Operator (TSO) and 55 DSOs [25]. As an alternative to the centralized architectures, this thesis investigated different decentralized approaches aimed to enable the provision of advanced Ancillary Services by means of Distributed Energy Resources. Below are the main contributions of this thesis work and its outline.

# Contributions

The two main topics of this thesis are the provision of grid services by means of Distributed Energy Resources and the coordination between the Transmission System Operator and Distribution System Operator in using such resources as Ancillary Services. The main contributions are resumed below.

1. Definition of the European and Italian regulatory framework about the provision of Ancillary Services through DERs and assessment of the main TSO-DSO coordination schemes proposed in the literature.

2. Development of a three-phase optimal power flow (TOPF) to estimate the amount of active and reactive power available at the TN/DN point of interconnection (POI). This TOPF is suitable to deal with both medium voltage and low voltage resources, unbalanced DNs, and coordinated active and reactive resources.

3. Development of two methodologies to aggregate DERs located in a distribution

grid interfaced with the distribution network through multiple points of interconnection.

4. Implementation of a Benders decomposition algorithm (BDA) able to optimize flexibility resources located at TN and DN levels with different TSO-DSO coordination scheme. The proposed BDA can also be applied to power system models in which transmission networks are interfaced with the distribution grids in multiple POIs.

5. Analysis of data exchanged between TSOs and DSOs in coordination schemes investigated at point 4.

6. Development of three different algorithms based on the autocorrelation of voltage signals to be implemented in a low-cost controller for fast frequency measurement.

7. Development a low-cost controller able to autonomously measure frequency as well as Rate of Change of Frequency (RoCoF), and implement a Synthetic Inertia (SI) control law on the management system of remotely controllable DERs.

8. Design of a centralized control to provide SI and Fast Frequency Response (FFR) through real LED lamps of public street lighting systems.

## Outline of the Thesis

This thesis is organized into five Chapters plus the Introduction and Conclusion parts below described.

**Chapter 1 - The provision of Ancillary Services:** defines the regulatory framework at European and national levels and provides an overview of studies conducted on the provision of Ancillary Services through DERs.

**Chapter 2 - TSO-DSO Coordination Schemes and Market Models:** describes the need for coordination between transmission and distribution system operators in using flexibility of DERs as Ancillary Services and provides an overview of the main TSO-DSO coordination schemes proposed in the literature.

**Chapter 3 - Methods for coordinated provision of flexibility in CM and Balancing:** illustrates the main methodology proposed in the literature for an optimal dispatch of flexibility resources in a TSO- DSO coordination framework, with a focus on balancing and congestion management (CM).

**Chapter 4 - New methodologies for CM and Balancing:** describe the methodologies developed with the aim to provide AS in decentralized coordination schemes, and the simulation tests carried out to validate them.

**Chapter 5 - Innovative Ancillary Services through DERs:** describes simulation tests concerning the provision Synthetic Inertia (SI) by means of actual controllable DERs located at the distribution grid level.

# Chapter 1

# The provision of Ancillary Services

An electricity grid is designed with the aim to interconnect generating units with power loads. By means of transmission (TN) and distribution network (DN) power lines, the energy produced by conventional power plants and renewable sources, or stored in energy storage systems, is delivered to the final customers, such as homes and industries. System Operators (SOs) responsible for the planning, development, and operation of TN and DN are, respectively, the Transmission System Operator (TSO) and the Distribution System Operator (DSO). By acting on generating and load units, they ensure that TN and DN power flows fulfill technical constraints. Moreover, since, to date, large amounts of electricity cannot be stored economically, TSOs and DSOs are also responsible for ensuring a real-time balancing between power generation and load demand [14]. This issue is exacerbated by the increasing share of renewable sources, such as wind and photovoltaic power plants, which are intermittent and add uncertainties in power system management [15], [16].

In order to accomplish their tasks and ensure the stable operation of the whole power system, SOs procure grid services, better known as Ancillary Services (AS), from flexibility resources. *Flexibility* is usually defined as the capability of controllable units to change power production and/or consumption in reaction to external prices or activation signals with the aim to contribute to the grid operation in a cost-effective manner [6]. Traditionally, AS were provided by means of power plants based on fossil fuels, such as gas and coal plants, located at the TN level [17], [18] and electricity mar-

kets were tailored for these so-called "conventional" energy sources [19]. Due to the decarbonization of the energy sector [20] and the replacement of conventional power plants with Renewable Energy Sources, in the coming years, flexibility for Ancillary Services will be also obtained by dispatching the active and reactive power of Distributed Energy Resources (DERs) located in the transmission and distribution grds [19], [21]. With this aim, in the last years, several projects and research groups are studying how DERs could replace conventional power plants in providing effective grid services [22]. Applications of controllable DERs as flexibility resources, like battery energy storage systems (BESS), thermostatic loads [23] or even coiling systems for data centers [24], have also been proposed in the literature [25]. Nevertheless, the possibility of exploiting controllable DERs for Ancillary Services is requiring a change of roles of the TSO and DSO in power system operation as well as improved coordination between them in exploiting such resources [22], [26].

## 1.1 Need for Ancillary Service in a TSO-DSO cooperation framework

Traditionally, at the European level, the Transmission System Operators has been the only operator allowed in procuring Ancillary Services for power system management, whereas DSOs role was limited to a passive DN management, with both energy consumption and generation of DERs at distribution level not yet optimized, nor coordinated with the overall system [4], [27], [28]. In a future scenario, as also recognized by the Regulation Authority ARERA for the Italian case [10], the increasing presence of electrical vehicle (EV) charging points, Heating, Ventilation and Air Conditioning (HVAC) units, and PV systems connected to the low voltage grid, will negatively affect the distribution grids with voltage profile or line congestion issues [10], [28], [29]. Based on this, in the coming years, there will be a need of Ancillary Services for both system operators. For instance, AS may be offered to the TSO for frequency/voltage regulation and congestions management, and to the DSO to manage local congestions and voltage control [30]. Based on descriptions provided in [31] and [31] on rele-

vant grid services (conventional and future), an overview of main AS is provided in Table 1.1

Table 1.1: Description of the main Ancillary Services

| AS | Description |
|---|---|
| **Congestion management** | Actions aimed at solving power line congestion problems [32]. |
| **Voltage control** | Voltage Control is aimed at facilitating the transfer of active power through power system nodes in an economic, efficient and safe manner [32]. Products for Voltage Control can be diversified depending on whether the operation is normal or under disturbances. |
| **Frequency control** | **Frequency Containment Reserve (FCR)**<br>Active power reserves available to contain frequency deviations after imbalances [32], [33]. |
| | **Frequency Restoration Reserve (FRR)**<br>Active power reserves available to restore the grid frequency to the nominal value [32], [33].<br>It can be differentiated in **automatic-FRR** or **manual-FRR**. |
| | **Replacement Reserve (RR)**<br>Active power reserves available to restore the required level of FRR in order to be prepared for next system imbalances [32], [33]. |
| **Inertial response** | Rapid injections/withdraws of active power following a contingency with the aim to mitigate the Rate of Change of Frequency and frequency deviations [32].<br>It can be differentiated in **Synthetic Inertia (SI)** or **Fast Frequency Response (FFR)**. |
| **Black start** | Service aimed at ensuring the capability of the electric system to be able to be restored effectively and economically. [32]. |
| **Controlled islanding** | The last stage of power system defense plans to operate electrical systems in a safe way [32]. |

## 1.2 Projects focusing on provision of AS through DERs

With the aim of enabling DERs to participate in the Ancillary Services market and provide grid services for the transmission and distribution networks, several initiatives and

research projects have been deployed at the European level in the last years. In order to provide an overview of the regulatory framework and the state of the art, as a basis for this thesis, a study of scientific papers, National and European regulations as well as deliverables of a few projects of the FP7 and H2020 [34] programs, promoted by the European Commission, has been performed. An overview of the projects concerning the addressed topic is provided below:

**SmarNet** [35] (*H2020*, 2016-2019)
The SmartNet project was aimed at developing TSO-DSO interaction schemes and market architectures to obtain AS from demand side management and distributed generation. This project was one of the first to move steps in the field of coordination between transmission and distribution operators. The performed research activities permitted stakeholders to understand how real-time markets should be revised to enable the participation of such flexibility resources and to analyze the exchange of information between System Operators to ensure the observability and the control of DERs. Moreover, the project developed five TSO-DSO coordination models [36], which have been discussed in Section 2.1. As shown in Figures 1.1 and 1.2, the project also investigated the capability of the most common DERs of complying with current technical requirements of specific Ancillary Services [25]. In this sense, the project differentiated into three different categories the Ancillary Services that should be provided by DERs. In particular, as shown in Figure 1.3, it is possible to distinguish AS widely implemented, but only provided by conventional generation up to date, emerging AS, which are not widely deployed, and new functions that will be implemented in DERs to allow them to provide specific Ancillary Services [31]. Three different pilots, respectively, located in Denmark, Spain, and Italy, were carried out with the aim to test a few AS in specific use cases, such as balancing, FCR, FRR, and voltage regulation.

**CoordiNet** [37] (*H2020*, 2019-2022)
The CoordiNet project was proposed as a large-scale campaign to demonstrate how TSO and DSO shall operate in a coordinated manner to procure grid services in the most reliable and efficient way. The main objectives of this project were of identifying

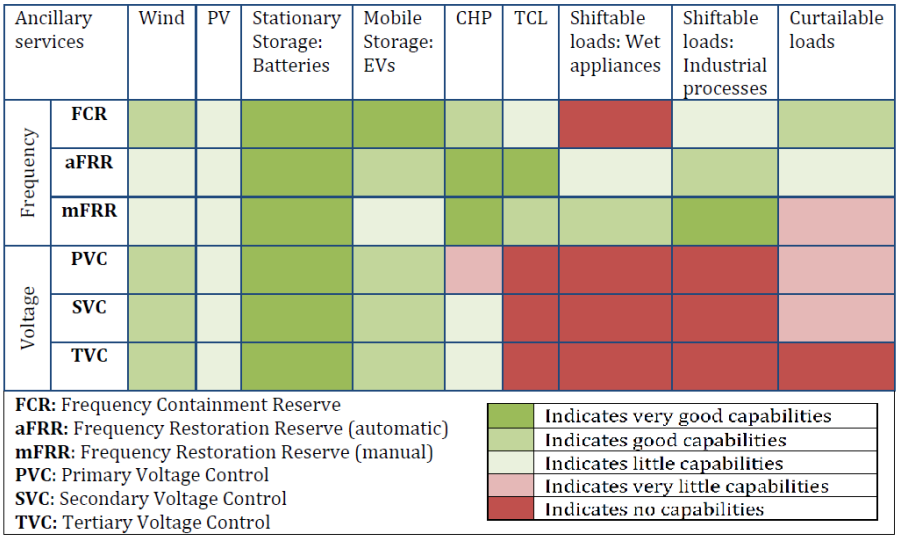


Figure 1.1: Capability of DERs to provide current AS (source: SmartNet).

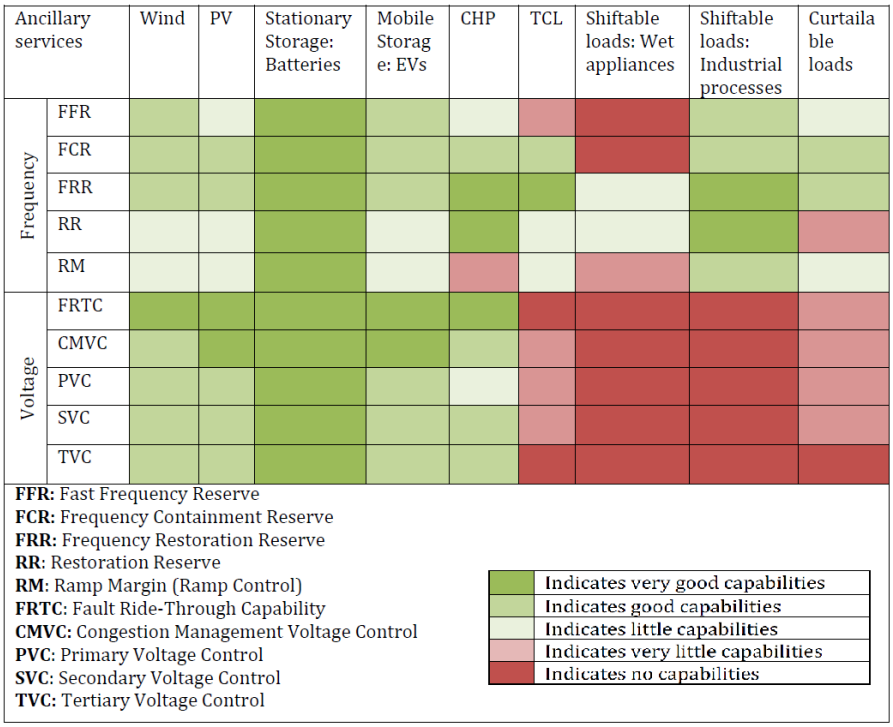


Figure 1.2: Capability of DERs to provide future AS (source: SmartNet).

| | A<br>AS Widespread Today | B<br>Emerging AS | C<br>Future DER AS |
|---|---|---|---|
| Ancillary services for frequency control | FCR<br>FRR<br>RR | | Fast frequency reserve: Inertia emulation<br>Ramp margin: Ramp control |
| Ancillary services for voltage control | Congestion management through voltage control | Primary Voltage Control<br>Secondary Voltage Control<br>Tertiary Voltage Control | Fault ride-through capability |
| Ancillary services for power quality improvement | | | Injection of negative sequence voltages<br>Damping of low-order harmonics<br>Mitigation of flicker<br>Damping of power system oscillations |
| Other ancillary services | | Black start capability<br>Compensation of power losses | Power factor control |

Figure 1.3: Classification of AS (source: SmartNet).

the main gaps, barriers, and drivers for the TSO-DSO coordination, providing insights and recommendations for the development of the European internal energy market, and defining and testing a series of AS standardized products. Based on the outcomes of SmartNet, this project developed seven groups of coordination possibilities [32] (see Section 2.1 for further details) and a set of AS standard products, illustrated in Figure 1.4. In order to test the products for congestion management (CM), balancing, voltage control and controlled islanding, three large-scale demonstrators (located in Greece, Spain, and Sweden), described in Figure 1.5, were developed.
In order to implement the described pilots, the project developed suitable platforms aimed at managing the interactions among TSOs, DSOs and flexibility service providers, tools for resources aggregation and for the control and the monitoring of DERs.

**FLEXCoop** [38] (*H2020*, 2017-2020)
The FlexCoop project was aimed at developing innovative tools and business models to exploit the flexibility of consumers and obtain, through demand aggregators, AS for grid stability and congestion management. In order to reach this target, the project defined a series of business models and use cases to be applied in the performed pilots. Considering two types of users, i.e. prosumers, which were the demand flexibility providers, and cooperatives, which played the role of demand flexibility aggregators, two different demonstrators were carried out. In the Dutch pilot, it was investigated

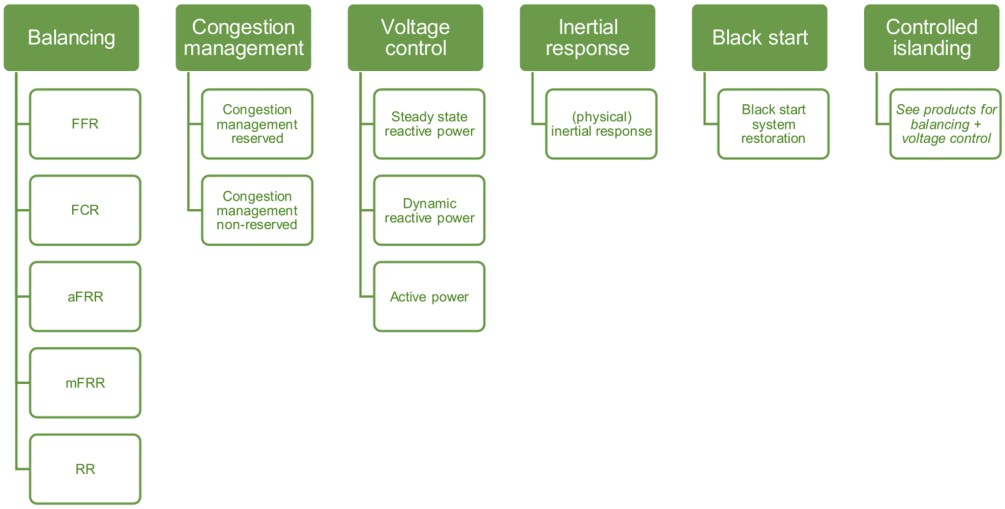


Figure 1.4: Mapping of the investigated Ancillary Services (source: CoordiNet).

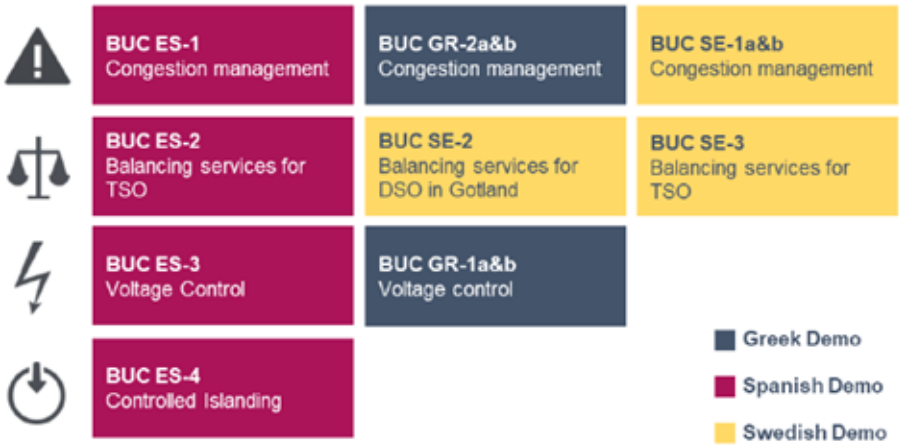


Figure 1.5: Demonstrators and tested AS products (source: CoordiNet).

how cooperatives could provide grid services like aFRR. While, in the Spanish pilot, it was addressed the maximization of self-consumption of rooftop PV units and the improvement of the bidding process in the Day-ahead market (DAM). To carry out these pilot projects, suitable tools were developed, such as those aimed to enable consumers to be informed about their home's environmental conditions, for generation monitoring and forecasting, or for DERs aggregation.

**OSMOSE** [39] (*H2020*, 2018-2021)
The OSMOSE project analyzed how the need for flexibility will be satisfied in a future energy scenario characterized by high shares of renewable energy and low carbon emissions. With this aim, it focused on studying the optimal mix of flexibilities for the European electricity system. Four different demonstrators were developed to test the capability of specific resources to provide effective grid services. Innovative solutions like a Hybrid Energy Storage System (HESS), consisting of a few batteries and capacitors, were tested. In the Italian pilot, solutions aimed at improving total system inertia or voltage profiles and solving congestion issues affecting the transmission lines in southern Italy were also tested. In this context, among various pilots, the possibility of using a Dynamic Thermal Rating strategy for power lines and the Demand Side Response for industrial loads was also investigated [40]. In addition, the capability of wind power plants equipped with battery energy storage systems (BESS) of providing Synthetic Inertia (SI) or automatic voltage control was also analyzed.

As part of this project, the author collaborated on a study aimed at assessing the feasibility of proposed flexibility solutions to be implemented in the Italian context [41].

**inteGRIDy** [42] (*H2020*, 2017-2020)
The inteGRIDy project investigated how cutting-edge technologies and mechanisms can be integrated into a scalable cross-functional platform that connects energy networks with stakeholders. This was with the aim of achieving optimal and dynamic operation of distribution networks and coordinating the share of DERs and BESS. Among the main objectives of this project, there were:

- integration of innovative smart grid technologies with optimal and dynamic operation of distribution grids;
- validation of innovative DR technologies and relevant business models;
- employment of storage systems to avoid renewable sources curtailment;
- providing predictive and forecasting tools;
- development of business models and services for the emerging electricity market.

With the aim to achieve this target, as shown in Figure1.6, ten demonstrators were developed using DR, smartening of distribution grids (SG), energy storage systems (ES), and EVs.

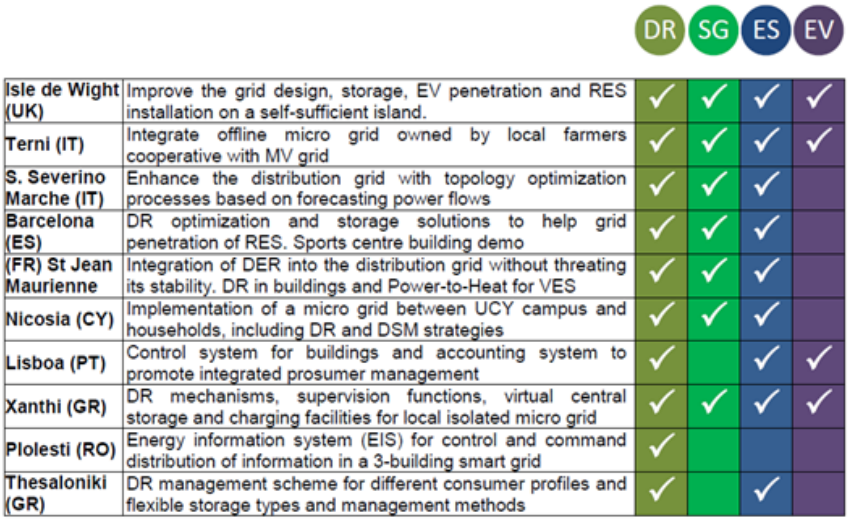


Figure 1.6: Use cases of demonstrators (source: inteGRIDy).

**eDREAM** [43] (*H2020*, 2018-2020)

This project, named eDREAM, was aimed to develop new solutions for Distribution System Operators and improve decision-making of aggregators and energy retailers. In particular, a new decentralized and community-driven energy ecosystem, integrating microgrids and Virtual Power Plants (VPPs) with the distribution networks was

implemented. Three pilots were carried out in the project with the aim to validate flexibility aggregation via smart contracts, peer-to-peer (P2P) local energy trading market, and VPP in energy communities. In addition, tools for power consumption/production forecasting, Renewable Sources degradation assessment, customer load profiling, and for blockchain-based energy marketplace were developed and tested.

**ADDRESS** [44] (*FP7-ENERGY*, 2008-2013)
The ADDRESS project was developed to implement a comprehensive commercial and technical framework for the development of Active Demand in future smart grids. The project focused on studying the active participation of domestic and small commercial customers in power system markets and the provision of gird services to the different power system participants [45].

Following test results of developed demonstrators, it provided recommendations and solutions to remove barriers against the Active Demand deployment and regulatory barriers. In particular, three different field test sites having different demographic and electricity supply characteristics (Spain, Italy and French) were carried out, and components like an energy box, interfacing the consumer with the aggregator, and aggregator tools were also developed and tested.

**evolvDSO** (*FP7-ENERGY*, 2013-2016)
The goal of the project evolvDSO was to define the roles of Distribution System Operators in future distribution network scenarios characterized by high penetration levels of renewable energy sources and the proactive demand for electricity. As specified in [46], ten priority processes were designed to implement the key services associated with the future of the DSOs, concerning the business domains of network planning, operational planning, operation and maintenance, market, and TSO-DSO cooperation. In more detail, management tools to support the TSO-DSO coordination, such as an interval-constrained Power Flow, to estimate the flexibility area at primary substations, and a sequential optimal power flow (OPF), to define the control actions to be undertaken to keep the active and reactive power flows at primary substations level within specific limits, were developed [47].

## 1.3 Regulatory framework

In order to assess the feasibility of various flexibility resources proposed in the literature to be exploited for the provisioning of Ancillary Services in a TSO-DSO coordination framework, several issues need to be considered. Aspects like the AS market structure, roles of system operators, regulatory framework, and the European trends toward the harmonization and integration of electricity markets need to be taken into account. With this aim, a study of the European and National regulations concerning this topic was performed and provided below.

### 1.3.1 The European Regulatory Framework

The European Union was an early mover away from fossil fuels in favor of cleaner energies [48]. The first steps were made with *Directive 2009/28/EC* through which the EU set to achieve a share of Renewable Energy Sources of 20%, or more, by 2020 [49]. Following it, in order to carry on this energy transition plan, with the 2015 Paris Climate Agreement, the EU set to reduce greenhouse gas emissions by at least 40% by 2030 and reach the total carbon neutrality (net-zero emissions) by 2050 [48]. With this aim, a new set of rules called the *"Clean Energy Package for all Europeans"* has been proposed in 2016 and approved in 2019 by the European Commission [48]. This package consists of 8 new European laws to be converted into national laws by each EU country and concerning the frameworks of energy security, Internal Energy Market [50], [51], energy efficiency, decarbonization, and research, innovation and competitiveness [50]. The implementation of the transition process has also been supported by the introduction of *Network Codes* (NCs), a set of rules drafted by the association of the European TSOs *"ENTSO-E"* [52] with the aim of facilitating the harmonization, integration, and efficiency of the European electricity market [53].

The *Clean Energy Package for all Europeans*, simply known as *"Clean Energy Package" (CEP)*, together with the Network Codes and national regulations establish a comprehensive regulatory framework to implement the energy transition of the electrical power systems and the electricity markets at the European level.

#### 1.3.1.1 The Clean Energy Package: towards 2030 targets

Since 2020, the Third energy package on electricity has been replaced by the Clean Energy Package [51], [54] with the aim of fitting the EU electricity market to the energy transition. In such context, Regulation EU 2019/943 and Directive EU 2019/944 were established to assign to the consumers a relevant role in the energy transition and create appropriate coordination between system operators [55].

#### 1.3.1.2 Regulation EU 2019/943

The *European Directive 2019/943 on Common rules for the internal market for electricity* [11] set the key principles for the design of a new electricity market. Replacing Regulation *EC/714/2009* [51], it introduced several changes for system operators. First, it allowed European DSOs to be associated in a new European DSO entity [56]. As specified in Article 52:

> *"Distribution system Operators shall cooperate at Union level through the EU DSO entity, in order to promote the completion and the functioning of the internal market for electricity, and to promote optimal management and a coordinated operation of distribution and transmission systems. Distribution System Operators who wish to participate in the EU DSO entity shall have the right to become registered members of the entity."*

Thanks to the efforts done by four electricity DSO associations (CEDEC, E.DSO, Eurelectric and GEODE), the European DSO entity has been created in 2021 with the aim to improve the efficiency of electricity distribution networks and ensure close cooperation with the Transmission System Operators and ENTSO-E [11], [56]. In this sense, as specified in [57] and [58], the EU DSO entity will be an important interlocutor with ENTSO-E on monitoring the implementation of the network codes and guidelines relevant for the operation and planning of DNs and their coordinated operation with the TNs. In addition, in accordance with what has been specified in Article 55, this entity will improve the cooperation between all European DSOs, facilitate the integration of renewable and dispatchable resources in distribution networks, and promote the

digitization of distribution grids through smart grids, smart meters, cybersecurity, and appropriate data protection [58].

As a novelty, the same Regulation introduced also the possibility for Distribution System Operators to play an active role in DN management in a TSO-DSO coordination framework. In this sense, Article 57 states:

> *"(1) Distribution System Operators and Transmission System Operators shall cooperate with each other in planning and operating their networks. In particular, Distribution System Operators and Transmission System Operators shall exchange all necessary information and data regarding the performance of generation assets and demand side response, the daily operation of their networks and the long-term planning of network investments, with the view to ensure the cost-efficient, secure and reliable development and operation of their networks.*
>
> *(2) Distribution System Operators and Transmission System Operators shall cooperate with each other in order to achieve coordinated access to resources such as distributed generation, energy storage or demand response that may support particular needs of both the Distribution System Operators and Transmission System Operators."*

#### 1.3.1.3 Directive EU 2019/944

Similarly to the previous Regulation, the *European Directive 2019/944 on Common rules for the internal market for electricity* [12], which replaced Regulation *EC/714/2009* [51], addressed the persisting obstacles to the completion of the Internal market for electricity. Furthermore, it establishes the need for cooperation between TSOs and DSOs, the integration of DERs in the energy and service markets, and the possibility for the DSO to provide grid services for the DN [59]. In this perspective, Article 31 defines the new tasks of neutral market facilitator and Ancillary Services buyer that Distribution System Operators should perform in line with the national regulations. About the former role, paragraph (5) of the same Article specifies that:

> *"Each Distribution System Operator shall act as a neutral market facilitator in procuring the energy it uses to cover energy losses in its system in accordance with transparent, non-discriminatory and market-based procedures, where it has such a function."*

While, about what concerns the role of Ancillary Services buyer, paragraph (6) clarify that:

> *"Where a Distribution System Operator is responsible for the procurement of products and services necessary for the efficient, reliable and secure operation of the distribution system, rules adopted by the distribution system operator for that purpose shall be objective, transparent and non-discriminatory, and shall be developed in coordination with Transmission System Operators and other relevant market participants. [...]"*

However, the possibility for Distribution System Operators to procure grid services for their own needs must be assessed and approved by the national regulatory authorities. In this sense, paragraph (7) of the same Article establishes that each DSO:

> *"[...] shall procure the non-frequency ancillary services needed for its system in accordance with transparent, non-discriminatory and market-based procedures, unless the regulatory authority has assessed that the market-based provision of non-frequency ancillary services is economically not efficient and has granted a derogation. [...]"*

As specified in paragraph (49) of Article 2, by *"non-frequency ancillary service"* is intended a service employed by the TSO or the DSO for steady state voltage regulation, fast injections of reactive currents, provision of inertia for local grids stability, short-circuit current, black start and island operation capability.

The same directive highlights also the necessity for coordination between DSO and TSO in using DERs as Ancillary Services. With this goal, paragraph (9) of Article 31, specifies:

> *"Distribution System Operators shall cooperate with Transmission System Operators for the effective participation of market participants connected to their grid in retail, wholesale and balancing markets. Delivery*

> *of balancing services stemming from resources located in the distribution system shall be agreed with the relevant Transmission System Operator in accordance with Article 57 of Regulation (EU) 2019/943 and Article 182 of Commission Regulation (EU) 2017/1485."*

A need for cooperation between TSOs and DSOs is also presented in paragraph (2) of Article 32, which states:

> *"[...] Distribution System Operators shall exchange all necessary information and shall coordinate with transmission system operators in order to ensure the optimal utilisation of resources, to ensure the secure and efficient operation of the system and to facilitate market development. Distribution System Operators shall be adequately remunerated for the procurement of such services to allow them to recover at least their reasonable corresponding costs, including the necessary information and communication technology expenses and infrastructure costs."*

In order to implement effective coordination between the Transmission and Distribution System Operators, the first paragraph of Article 32 sets that Member States must develop a regulatory framework that incentives DSOs to procure the necessary flexibility resources from providers of distributed generation, DR or energy storage, in order to operate their DNs efficiently and solve specific operative problems, e.g. local congestions. In addition, as outlined in Article 34, Member States shall ensure that all participants have non-discriminatory access to data, with clear and equal conditions and in accordance with the relevant data protection rules.
The same Directive also allows Energy Communities to exploit energy storage systems (e.g. of electric vehicles), Demand Response strategies, or energy efficiency schemes, to provide flexibility for the power system and participate in the electricity markets. In order to reach the target, recital (39) considers the possibility of DERs to be aggregated:

> *"All customer groups (industrial, commercial and households) should have access to the electricity markets to trade their flexibility and self-generated*

> *electricity. Customers should be allowed to make full use of the advantages of aggregation of production and supply over larger regions and benefit from cross-border competition. Market participants engaged in aggregation are likely to play an important role as intermediaries between customer groups and the market. [...].”*

As specified in Articles 33 and 36, it should be noted that Distribution System Operators are not allowed, to own, develop, manage, or operate recharging points for EVs or storage systems. Nevertheless, derogations may be set by Regulatory Authorities in case of particular needs.

#### 1.3.1.4 The Network Codes

In order to contribute to the processes of harmonization, integration, and efficiency of the European electricity market, a set of rules has been developed and published in the last years by ENTSO-E under the guidance of Agency for the Cooperation of Energy Regulators (ACER), briefly named “the Agency” [53]. In detail, a few network codes were set out from the Third Energy Package with the aim of providing effective and transparent access to the transmission networks across borders as well as guaranteeing a coordinated technical evolution of transmission systems. In accordance with requirements set by Regulation EU 2009/714 [60], nine different network codes have been defined and regrouped in three different categories, namely *“connection”*, *“operation”* and *“market” codes* [53] (see Table 1.2). As specified in [61], although such codes are often referred to as *“network codes”*, only the first four of those described in Table 1.2 are network codes, whereas the remaining ones are guidelines (GLs). Network codes and guidelines have the same legal value, but, in general, NCs are more detailed than GLs and are ready for implementation. Conversely, guidelines are more flexible than Network Codes because they need the development of methodologies to be implemented [61]. In this case, as happened for the definition of the European Balancing Platform (described below), it is necessary that a group of TSOs define a methodology, followed by a public consultation, and submit their proposal to the National Regulatory Authorities for approval [62].

Table 1.2: Network codes

| Group | Code | Regulation | Acronym |
|---|---|---|---|
| **Connection** | High Voltage Direct Current Connections | EU2016/1447 | HVDC NC |
| | Requirements for Generators | EU2016/631 | RfG NC |
| | Demand Connection Code | EU2016/1388 | DCC NC |
| **Operations** | Emergency and Restoration | EU2017/2196 | ER NC |
| | Cybersecurity | – | – |
| | Transmission System Operation | EU2017/1485 | SO GL |
| **Market** | Electricity Balancing | EU2017/2195 | EB GL |
| | Forward Capacity Allocation | EU2016/1719 | FCA GL |
| | Capacity Allocation and Congestion Management | EU1222/2015 | CACM GL |

NC: Network Code, GD: guideline

Among the NC ans GL codes listed in Table 1.2, some of them concern also the provision of Ancillary Services in a TSO-DSO coordination framework. Title III of the DCC NC set requirements and rules for the connection of demand units to provide Demand Response services to System Operators. In this sense, the regulation states that a demand facility owner or a Closed Distribution System Operator (CDSO) may offer DR services to the market and also to the system operators for grid security [63].

Regulation SO GL [33] lays down guidelines about *"rules and responsibilities for the coordination and data exchange between TSOs, between TSOs and DSOs, and between TSOs or DSOs and significant grid users (SGUs), in operational planning and in close to real-time operation"*. In detail, Article 29 specifies that each TSO shall operate the reactive power resources located within its control area, where possible, in coordination with the transmission-connected DSOs, in order to fulfill the operational security constraints of the transmission network. In Article 43, the same guideline set also the requirements about the data exchange among the two System Operators. In particular, by means of suitable methodologies, the TSO should be able to determine the observability areas of the transmission-connected distribution networks, in order to determine the state of the system accurately and efficiently. Structural information concerning the obseved area, described in paragraphs (1) and (2), must be updated at least every six months by each transmission-connected DSO. Furthermore, the same Regulation also establishes the rules about the cooperation among TSOs and DSOs in case of reserves providing units connected to the distribution grid. In this context, SO

GL indicates as *"reserve provider"* a legal entity enabled to supply, from at least one reserve providing unit or reserve providing group, the following services:

- Frequency Containment Reserve (FCR).
- Frequency Restoration Reserve (FRR).
- Replacement Reserve (RR).

With this aim, Article 182 highlights that TSOs and DSOs shall cooperate and exchange information in order to allow the delivery of active power by reserve units or groups connected at the distribution grid.

Regulation EB GL [64] also concerns the provision of Ancillary Services in a TSO-DSO coordination framework. According to Article 15, TSOs, DSOs, Balancing Service Provider (BSP), and Balance Responsible Party (BRP) shall cooperate in order to ensure efficient and effective balancing of the entire power system. This regulation provides a guideline on electricity balancing including common principles and methodologies for procurement, settlement and activation of frequency products and services like FCR, FRR, RR [64]. Among various objectives, this regulation aims to enhance the efficiency of balancing markets as well as the participation of Demand Response resources, including aggregation facilities and energy storage systems. To achieve this target, EB GL established the rules necessary to the TSOs to create the following European platforms for balancing services provisioning [62].

**Replacement Reserves platform - TERRE**

This platform aimed at the exchange of balancing energy for the replacement reserves has been derived from Article 19 of Regulation EU 2017/1485 [33]. Under the name of *"Trans European Replacement Reserves Exchange" (TERRE)*, this project developed a RR platform and set up a European RR balancing energy market [65]. Operational since January 2020, TERRE is currently under improvement [65], [66].

**manual Frequency Restoration Reserves platform - MARI**

The *"Manually Activated Reserves Initiative" (MARI)* platform is aimed at creating a

European manual Frequency Restoration Reserves (mFRR) platform complying with the Electricity Balancing Guideline. MARI was successfully launched on 5 October 2022 with the participation of 5 TSOs [67].

**automatic Frequency Restoration Reserves platform - PICASSO**

The *"Platform for the International Coordination of Automated Frequency Restoration and Stable System Operation"* (PICASSO) is the project implemented to develop a European platform for the balancing energy exchange of frequency restoration reserves with automatic activation (aFRR). The platform, complying with EB GL, SO GL and CACM GL codes, has the following main objectives [68]:

- improve economic and technical efficiency without affecting system security;
- develop an aFRR integrated market.

PICASSO has been brought successfully into operation on 1 June 2022 [68].

**Inbalance Netting (IN) platform – IGCC**

Imbalance netting is the process agreed between TSOs of two or more Load-Frequency Control Areas wit the aim to avoid the simultaneous activation of FRR in opposite directions, taking into account the amount of activated FRR and the related control errors [69]. The *"International Grid Control Cooperation"* (IGCC) is the project chosen by ENTSO-E in February 2016 to develop this common platform for the Imbalance Netting process [69] successfully launched on 25 June 2021 [69]. Figure 1.7 illustrates the European memberships for developed balancing platforms, distinguishing between members, project members, observers, and non-operational members.

**Frequency Containment Reserve Platform**

In accordance with the objectives of Regulation EU 2017/2195 (EB GL), the development of a common market for cooperation in FCR procurement was undertaken with the aim of promoting effective competition, non-discrimination, transparency, new entrants, and increased liquidity [70]. Currently, the project involves eleven TSOs from

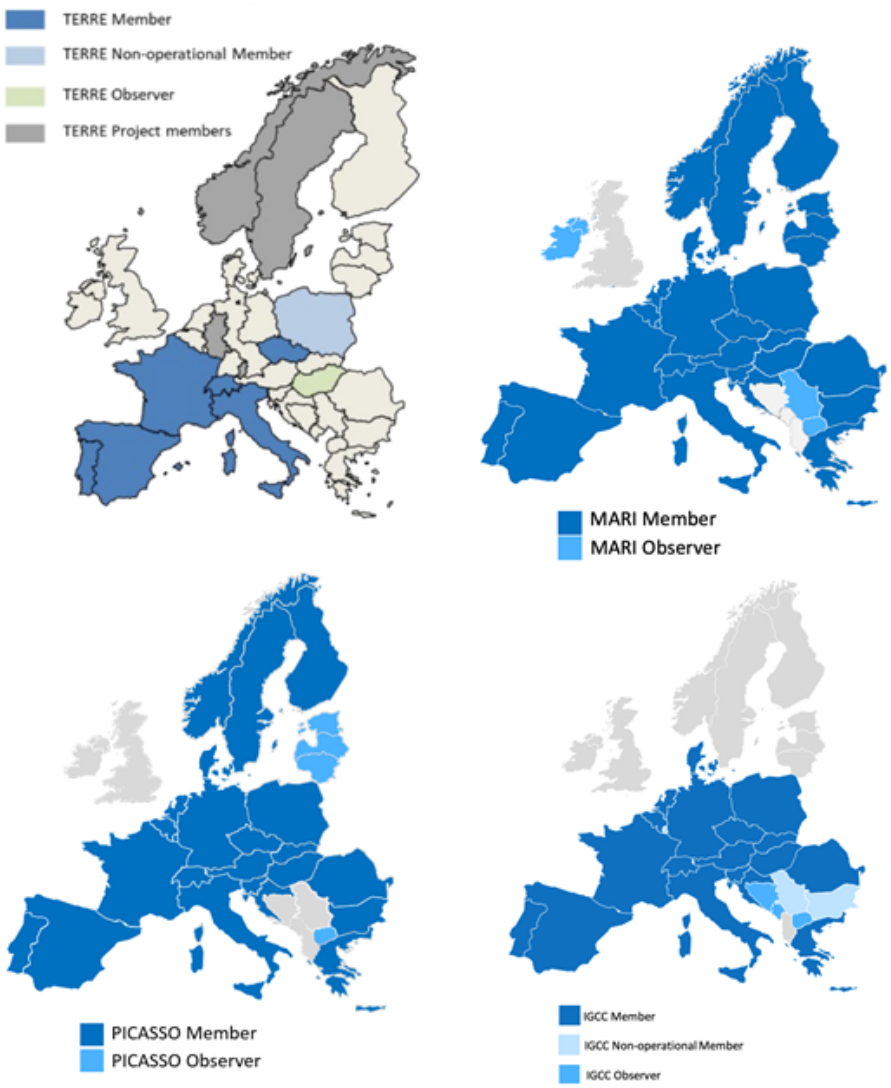


Figure 1.7: Balancing Platforms membership (source: ENTSO-E).

eight different countries (see Figure 1.8) and periodically promotes public consultations, gathering input and feedback from stakeholders [70].

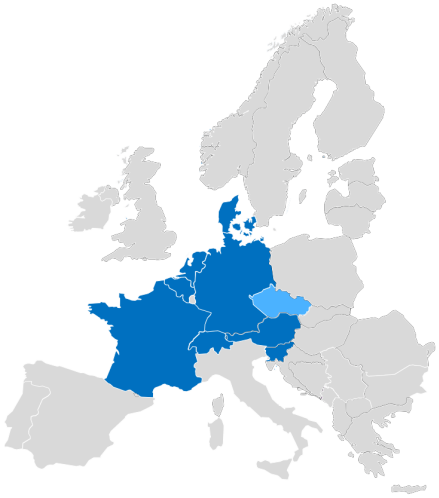

Figure 1.8: FCR common market membership (source: ENTSO-E).

### 1.3.2 The Italian Regulation Framework

In Italy, there is an Ancillary Services Market ("MSD") in which the National Transmission System Operator, Terna, acting as a sole counterparty, procures the flexibility resources needed to operate the entire power system. Currently, only programmable generating units having a minimum installed capacity of 10 MVA and satisfying the necessary technical requirements are allowed to participate in the MSD. Flexibility resources are offered as upward and downward regulation and can be provided with or without remuneration. In the former case, AS are remunerated at the price at which flexibility was offered (*pay-as-bid* pricing mechanism) [71]. To date, only the following Ancillary Services are remunerated in Italy[72]:

- infra-zonal congestions relief;
- secondary frequency control, corresponding to the aFRR [31];
- tertiary frequency control, which is divided into ready tertiary reserve, spinning tertiary reserve, and tertiary replacement reserve, comparable to the RR [31];

- real-time balancing.

The other Ancillary Services are provided without remuneration, as their provision is mandatory [72]:

- primary frequency control, corresponding to the FCR [31];
- primary voltage regulation, in which reactive power generation is adjusted locally by means of automatic controls [31];
- secondary voltage regulation, in which reactive power generation is controlled automatically according to a specified voltage set-point.

The Italian AS market is divided into two sub-markets, such as the *ex-ante MSD* and the *Balancing market*. In the former, corresponding to a planning phase, Terna accepts energy bids and submits offers with the aim to relieve residual congestions and procure both secondary and tertiary regulation reserves [72]. Conversely, the balancing market is a real-time phase in which Terna uses secondary and tertiary regulation reserve intervals and maintains real-time balancing between injections and withdrawals.

As specified above, only programmable resources having an installed capacity equal or higher than 10 MVA (properly called "relevant units") are allowed to participate in the MSD. Therefore, except hydroelectric power plants, renewable sources, such as wind and PV power plants, or DERs are, currently, not all allowed in the AS provisioning. With the goal of gradually opening up the MSD to those flexibility resources currently not yet allowed in it, by means of Resolution 300/2017 [73], the Italian Regulatory Authority allowed the development of pilot projects to gain useful insights to redesign the AS market.

Furthermore, in order to transpose Regulation EU 2019/943 [11] and Directive EU 2019/944 [12], new rules are about to be introduced in the Italian regulation framework regarding the Ancillary Services provision. With the Consultation Document (DCO) 322/2019/R/eel [74], known also as "TIDE", ARERA promoted a consultation procedure useful to support Terna, the Italian TSO, in the redefinition of the Ancillary Services necessary to the power system operation in the 2030 energy scenario. In defining this new AS framework, the national TSO should consider the new presence

of DERs aggregators as well as the possibility for Distribution System Operators to procure grid services for its own needs or act as a *neutral facilitator* in providing grid services to the TSO [74]. As specified in the same DCO, these orientations should be defined considering the outcomes of pilot projects started with Resolution 300/2017 [73] and concerning the provision of grid services through virtual units (called UVA) not yet enabled in participating in the Ancillary Services markets. In order to comply with the European regulatory framework, the same DCO 322/2019/R/eel is also aimed to identify the main guidelines for the integration of the Italian electricity market with those of other EU Members States. In this sense, the document describes the actions that should be undertaken to coordinate the Italian AS market with the balancing platforms developed at the European level, described in Section 1.3.1.4.

The DCO 322/2019 provides also the criteria for allowing the participation of DERs to the Ancillary Services market. In this perspective, it considered the negative impact that the increasing presence of renewable sources, HVAC systems, and electrical vehicle charging points connected to the DN will have on distribution networks. As specified by the Authority in [10], in future scenarios, distribution networks might be affected by congestions of power lines and voltage profile issues. In order to allow the DSO to solve such troubles and use efficiently DERs located at the DN level, the Authority highlighted the need to redefine the role of Distribution System Operators, specifying that:

- the DSO should play the role of *neutral facilitator* in providing *global* Ancillary Services trough DN resources to the TSO;
- in case of necessity, the DSO may procure *local* Ancillary Services for the distribution network operation.

In this sense, the DCO specifies that by Ancillary Services are intended such grid services necessary to the System Operators to ensure the safe operation of the electrical system. In turn, Ancillary Services are differentiated in *global* Ancillary Services, if necessary to operate the national power system, and *local* Ancillary Services, if employed to manage distribution grids o part of them.

On what concerns the DSO's role as a neutral facilitator, it should be able of monitoring its distribution grid in real-time and evaluate the effect of the activation of DERs considering the effective network state [74]. In addition, in accordance with Resolution 628/2018 [75], an appropriate level of data exchange between TSO, DSOs and Significant gird users should be implemented to improve the observability of resources located in the distribution networks.

As described in DCO 322/2019, the DSO has also the possibility to procure only non-frequency Ancillary Services, but it should operate in a transparent way and in collaboration with the TSO and stakeholders. In this perspective, ARERA evaluates the provision of AS from DERs in a TSO-DSO coordination framework (see Sect. 2.4 for further details) and, by means of Resolution 352/2021 [76], approved the development of pilot projects. In accordance with the DCO 685/2022 [77], outcomes of the implemented demonstrators as well as the feedback provided by various stakeholders will be analyzed and taken into account to produce the final document on the reform of the Italian AS market (TIDE) in 2023 [74].

## 1.4 Lines of investigation

Flexibility resources represent an effective way to meet decarbonization targets established with the transition processes. As above described, a redesign of the electricity markets is taking place in several States to allow the participation of DERs in the AS markets [78], [79]. Nevertheless, other challenges will also be addressed by System Operators to manage power systems in future scenarios. With the replacement of traditional power plants with Distributed Energy Resources, the composition of power systems is progressively changing and the role of traditional power plants will become less relevant in power system operation [31]. Furthermore, the growing presence of generating units interfaced with the electrical grid by means of power inverters will lead to a decrease in total system inertia. As a consequence, in addition to the conventional Ancillary Services, such as balancing, congestion management and frequency regulation, innovative grid services like Synthetic Inertia (SI) or Fast Frequency Response (FFR) will be also necessary to face SO needs. A paradigm shift in power sys-

tem operation is also required to assign an active role to the DSOs [27]. With the future provision of energy and Ancillary Services from resources connected to the distribution networks, the responsibility of the power system operation will be shared by the TSO with the DSO. This aspect highlights the relevance of implementing TSO-DSO coordination schemes based on decentralized architectures, in which the transmission and distribution grids are managed by separate and independent System Operators.

In order to address these two challenges, this thesis work was aimed at investigating methodologies for an optimal dispatch of flexibility resources in decentralized coordination schemes and to enable DERs located at DN level to provide SI/SI/ services in low-inertia power systems.

# Chapter 2

# TSO-DSO Coordination Schemes and Market Models

With the energy transition process, the provisioning of Ancillary Services in power systems is changing. Thanks to the technological progress made in monitoring and control fields, Distributed Energy Resources will be exploited as flexibility resources to provide grid services to the TSO and DSO [14]. However, as remarked in [12], strong cooperation and information exchange between SOs is fundamental to guarantee optimal use of flexibility and ensure that the activation of DERs does not conflict with the actions undertaken by other system operators [14],[80]. As a result, this cooperation can also lead to greater observability of the entire electrical system, with more transparency and quality for the acquired data [30].

## 2.1 Market schemes for TSO-DSO coopeartion

In the last years, several research projects investigated how Distributed Energy Resources can be effectively managed to provide Ancillary Services to the transmission and distribution grids. Among them, the H2020 European projects SmartNet [35] and CoordiNet [37] focused on the development of coordination schemes aimed at regulating the interaction between TSO and DSO in using flexibility resources. Although a multitude of coordination models and variants have been proposed in the literature

[36], the main ones may be recognized in those developed and tested by SmartNet and CoordiNet. In particular, based on a preliminary work of literature review, country surveys, theoretical analyses, and public consultations, five different coordination schemes were developed by SmartNet taking into account the level of engagement of the DSOs and the number of markets in which flexibility may be procured [36]. Following this work, additional schemes have been developed by CoordiNet [32]. Considering the schemes and findings carried out by these two projects, a set of coordination models, shown in Figure 2.1, was carried out according to a five-layers classification.

### 2.1.1 Main roles in coordination schemes

A *coordination scheme* is defined as the set of roles and responsibilities for TSO and DSO when procuring grid services from flexibility resources located in the distribution networks [30]. As defined in [81], by *role* is intended the behavior of a specific market party with specific responsibilities, which are unique and cannot be shared. Thus, each coordination scheme is characterized by specific market architecture, tasks, and responsibilities taken up by system operators and market players [36]. In general, coordination architectures can vary from Total TSO to Total DSO, passing through Hybrid DSO with regard to the coordination responsibility of DERs [78]. Therefore, processes and information exchanges between system operators can vary according to the adopted coordination architecture [36]. Nevertheless, the main differences between the coordination schemes can be observed in the *procurement* phase of these resources, as the *prequalification*, *operation*, *activation*, and *settlement* processes are quite similar across the investigated schemes [36]. A description of the main activities concerning the prequalification, grid operation, procurement, activation, and settlement of flexibility resources based on [14], [36] was provided in Table 2.1. These activities are defined considering the main roles of the TSOs in power system operation, described by ENTSO-E in [82], and tasks that should be performed by the DSOs in the next years [83].

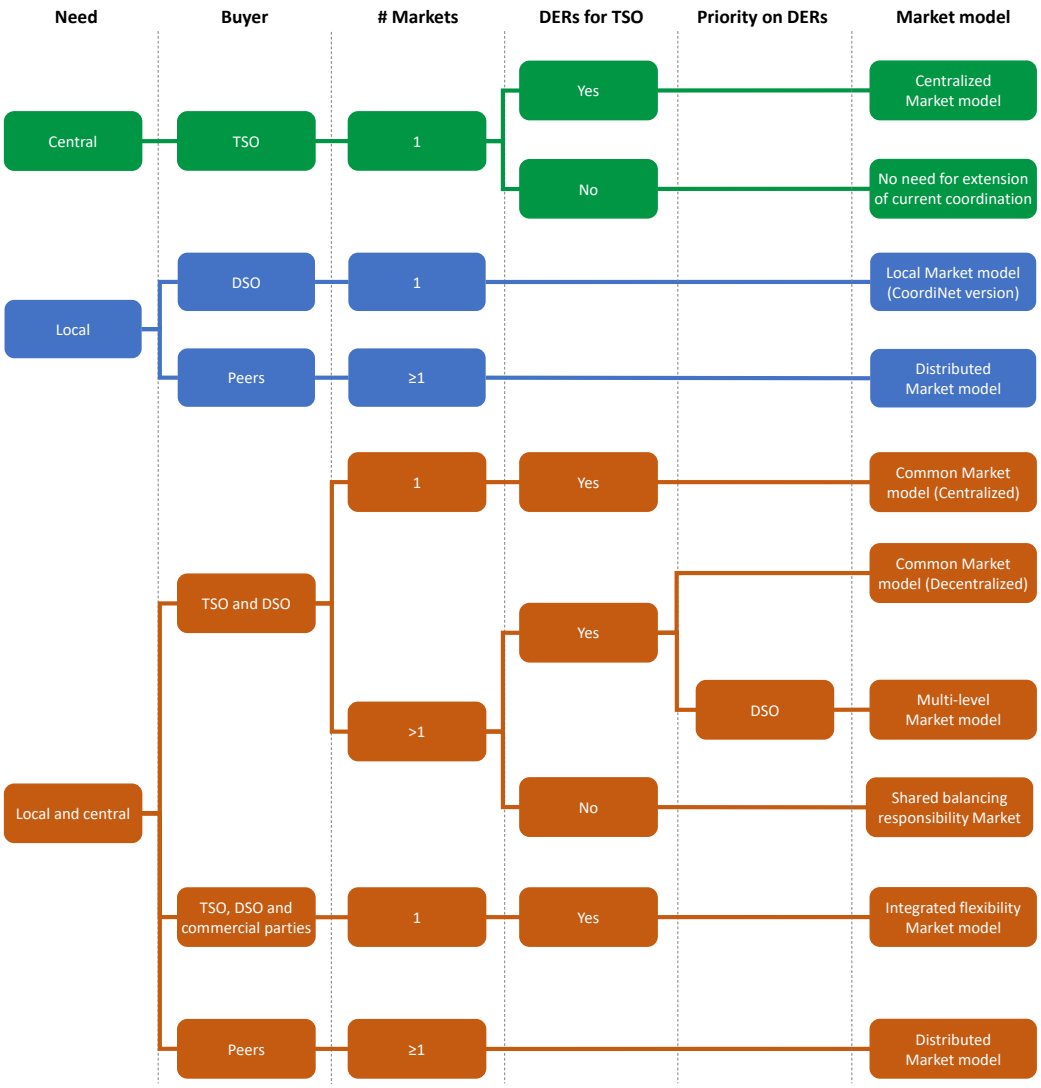


Figure 2.1: Mapping of main TSO-DSO coordination schemes

Table 2.1: Description of main roles

| | **Task** | **Description** |
|---|---|---|
| **Prequalification** | Flexibility feasibility checker (FFC) | Is responsible to check if the activation of flexibility resources at DN level does not negatively affect the DN |
| **Grid operation** | System Operator (SO) | Is responsible to operate a power system |
| | Balance Responsible Party (BRP) | Is responsible to guarantee the balancing for an electrical system |
| | Data Manager (DM) | Handles data relate a grid model or flexibility resources located in it |
| **Procurement** | Buyer | Acquires flexibility-based services in a market setup |
| | Seller | Sells flexibility-based services in a market setup |
| | Market Operator (MO) | Is responsible to manage a market and the related platform |
| | Reserve Allocator (RA) | Is responsible to determine the amount of services to be procured by means of flexibility resources |
| | Flexibility aggregator (FA) | The aggregation of TN and DN flexibility resources may be performed by the DSO (for non-commercial purposes) or by commercial market parties (CMP) |
| **Activation** | Flexibility resources dispatcher (FRD) | Generates and sends activation signals to the flexibility resources to be activated |
| **Settlement** | Measured Data Responsible (MDR) | Is responsible for measuring and communicating to MOs and SOs the value of activated energy |

### 2.1.2 Classification layers

Several TSO-DSO coordination schemes may be identified in the literature. Each model substantially changes depending on the number of markets, possibility of DERs to be offered to TSO and DSO, and priority of the DSO on their usage. Typically, each coordination scheme is identified by a specific name that reflects the adopted market architecture or the policy on DERs allocation. However, as described in [32], it is commonly recognized that there is no one-size-fits-all coordination scheme. This is because aspects like market and regulatory framework, grid characteristics, and roles of TSOs and DSOs change from country to country. In addition, there are also TSO-DSO market models that, although differently named, correspond to the same coordination scheme or present slight variations [36], [32]. In order to classify the investigated co-


Figure 2.2: Five-layers classification

ordination schemes, a five-layers classification model, shown in Fig. 2.2, was defined taking the following aspects into account:

- **need** to be satisfied by the acquired flexibility. It can be central (for the TSO), local (for the DSO), or both of them;
- **buyer** that may acquire flexibility, such as TSOs, DSOs, and commercial parties;
- **Number of markets** in the assumed coordination scheme;
- **Possibility of the TSO to use DERs**: has the Transmission System Operator access to flexibility resources located at the DN level?
- **Priority** of the TSO or the DSO in using DN flexibility than other system operators.

In general, as described also in [32], these coordination schemes are service independent and, therefore, can be applied to a set of Ancillary Services or to a combination of

them. However, in accordance with the classification above provided, the TSO-DSO coordination schemes can be regrouped in *centralized* or *decentralized* architectures [84], [85], as shown in Table 2.2.

Table 2.2: Classification in centralized and decentralized architectures

| **Centralized architectures** | **Decentralized architectures** |
|---|---|
| Centralized M. scheme | Local M. scheme (CoordiNet version) |
| Common M. scheme - Centralized v. | Multi-level M. scheme |
| Integrated flexibility M. scheme | Shared balancing responsibility M. scheme |
| | Common M. scheme - Decentralized v. |
| | Distributed M. scheme |

## 2.2 Centralized Architectures

In centralized TSO-DSO coordination architectures, the TSO is responsible for the whole dispatch of AS resources located at both TN and DN level [85], [36]. Therefore, in this case, there is one big central market in which flexibility resources located in the transmission and distribution grids are offered and contracted [36].

### 2.2.1 Centralized Market model

*Market organization and roles of system operators*

As a basic coordination scheme proposed by SmartNet, the Centralized AS Market model shown in Figure 2.3 is presented. According to the description given in [36], in this scheme, the TSO can procure Ancillary Services from flexibility located at TN and DN levels, while the DSO is not allowed to procure flexibility in real-time o near to real-time. Nevertheless, in the case of local issues such as grid congestions, the DSO may procure flexibility in other timeframes than the AS Centralized Market [36]. In case DERs cannot be offered even to the TSO, which can only use TN resources to solve central needs, no extension of the current coordination activities between TSO and DSO is necessary [32]. As shown in Figure 2.4, in the Centralized scheme, there is one only central AS market operated by the TSO, in which both TN and DN flexibility

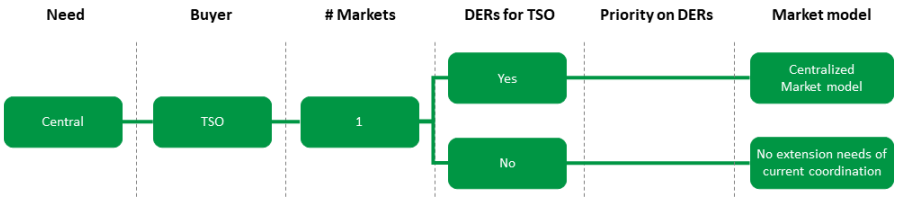


Figure 2.3: Mapping of the Centralized Market model

resources are offered. Therefore, in this case, the TSO is responsible for managing the transmission network and operating the central market [84], [36]. Differently, the

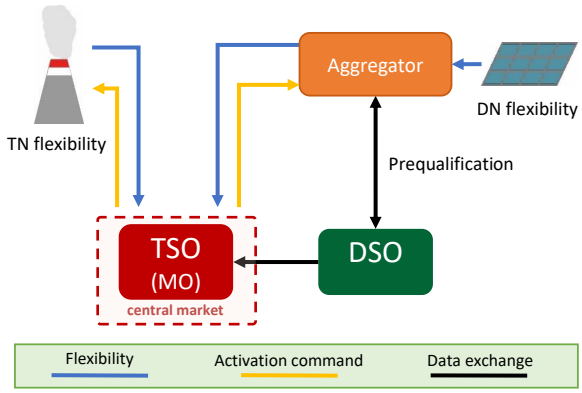


Figure 2.4: Centralized Market scheme

role of the DSO is limited to that of FFC for DN resources. In particular, since DN constraints are not taken into account in the flexibility optimization (see clearing process in Sect 3.1 for further details) performed by the TSO in the Central Market, the prequalification allows DSO to verify if the activation of DN flexibility by the TSO does not create any congestion in its own distribution network [36].

This market model was also presented by the CoordiNet project under the name of Central Market scheme. This project investigated a few variants of this market model, such as the Total TSO model, the Minimized DSO model, and the Fully Integration model, which proposed alternative approaches to consider DN constraints in the clearing process of the central market [32].

*Coordination scheme assessment*

This coordination scheme is the one most in line with the current practice since the TSO is the only system operator having access to the flexibility resources and the DSO role is limited to the prequalification process [4], [36]. Therefore, to obtain flexibility from distribution networks, a reduced exchange of information between TSO and DSO is required [36]. As an alternative, DN constraints may also be included in the market clearing performed by the TSO. However, in these conditions, the clearing process may be heavy to be managed as a whole and, furthermore, the TSO should also be able to interpret distribution network data. On the other side, having a single market operated by the TSO, which is the only MO and buyer, simplifies the market structure [36]. The main characteristics of this market model are resumed in Table 2.3, which describes its advantages and disadvantages in terms of market organization, roles of system and market operators and sharing of data.

### 2.2.2 Common Market model - Centralized version

*Market organization and roles of system operators*

In the Common Market model, flexibility resources at the TN and DN levels are shared between TSO and the DSO with the aim to address both central and local needs, minimizing the total AS activation costs [30], [36]. Depending on the number of markets in which resources are contracted, a centrlized variant (CV) and a decentrlized variant (DV) of this market model may be possible [36]. In the former, illustrated in Figure 2.5,

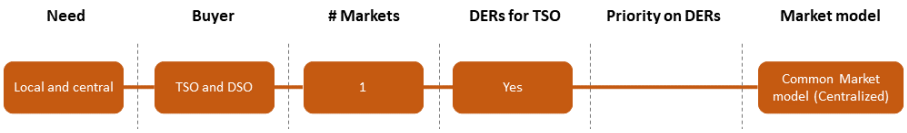


Figure 2.5: Mapping of the Common Market model - Centralized version

the TSO and DSO are jointly responsible for the organization and the operation of a common market platform. In this version, physical and operating limits concerning TN and DN grid models and flexibility resources are shared by the TSO and DSO with the aim to be included in the common optimization process [36]. Since, in this variant,

Table 2.3: Benefits and drawbacks of the Centralized Market model

| | **Benefits** | **Drawbacks** |
|---|---|---|
| **TSO** | • The TSO is SO for the TN and the only responsible for the central market, in which TN and DN flexibility resources are offered.<br>• Flexibility is not shared with the DSO. | • Need for experience to interpret DN data.<br>• DN constraints may be violated if not included in the optimization process performed by the TSO. |
| **DSO** | • DN constraints may be not communicated to the MO (TSO). | • The DSO is responsible for the distribution grid, but has no access to the AS resources to solve local issues.<br>• Passive role, limited to the DERs prequalification. |
| **Market organization** | • Single market platform, easier to be managed, with low operational costs and standardized processes/products. | • In case DN constraints are shared with the TSO:<br>- high computational burden;<br>- possible scalability issues and communication bottlenecks. |
| **Shared data** | • Reduced communication between TSO and DSO. | • DN contraints are communicated to the MO if included in the market clearing process. |
| **Implementation** | • In line with the current regulatory framework. | • Risks for security and privacy of data in the case DN constraints are shared with the TSO. |
| **References** | [36], [86], [87], [88] | |

the TSO and DSO are jointly responsible for the market operation, a neutral third party may be appointed by both system operators as an Independent Market Operator (IMO) to manage the common market under their supervision [36]. As shown in Figure 2.6, in this case, the MO is responsible for the common market operation and the optimal dispatch of flexibility resources for TN and DN needs. Once the common market has been cleared, it communicates the market outcomes to TSO, DSOs and flexibility providers (CMP) to activate the contracted AS resources [84]. This neutral third party is also responsible to guarantee the privacy of data acquired from System Operators [89].

A few variants to the Common Market model are resumed in [32]. However, as observed in [36], the Common Centralized Market model can be considered as an extension of the Centralized Market Model, with the difference that, in this case, central and local needs as well as TN and DN constraints are taken into account.

*Coordination scheme assessment*

This market model can represent a basic scheme to be extended for further collaboration among system operators [36]. Flexibility resources are shared between TSO and DSO with the aim to satisfy needs of both system operators and minimize the total AS activation costs. Nevertheless, due to the huge amount of flexibility resources and constraints (both TN and DN levels) to be processed, this market model requires high computational efforts. Furthermore, although in this scheme the overall activation costs of AS resources are minimized, the individual costs for TSO and DSOs might be

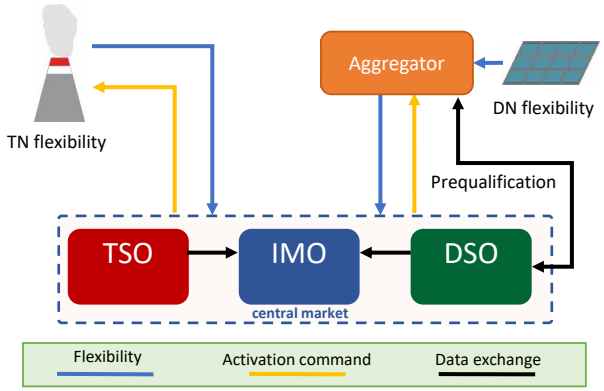


Figure 2.6: Common Market scheme - Centralized version

higher compared to those of other schemes [88]. About this issue, there is also a need to establish a criterion for allocating costs of flexibility resources between TSO and DSO [36]. Benefits and drawbacks of this scheme are resumed in Table 2.4.

### 2.2.3 Integrated flexibility Market model

*Market organization and roles of system operators*

Differently from the previous coordination schemes, the Integrated flexibility Market model promotes the possibility for flexibility resources to be procured by regulated operators (i.e. TSO and DSO) and commercial market parties (CMP) [36], [32]. This is performed without distinction between regulated and liberalized players [36]. As shown in Figures 2.7 and 2.8, there is a common market platform in which system operators and CMP may acquire flexibility from TN and DN resources. In this market,

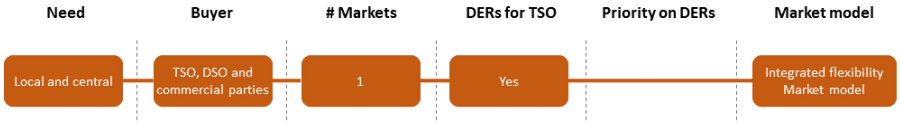


Figure 2.7: Mapping of the Integrated Market model

which is organized according to a discrete number of auctions, TN and DN resources are contracted in a single market managed by an IMO, with the aim to ensure neutrality, transparency, and efficiency in the market operation as well as a level playing field for all players [36], [32]. However, unlike the Common Market model, in which flexibility is allocated to the operator with the greatest need, in the Integrated Market model, AS resources are allocated to the operator with the greatest willingness to pay. In addition, flexibility resources previously contracted by the TSO or the DSO can be newly resold to other market operators.

*Coordination scheme assessment*

As specified above, in this market scheme, flexibility resources are allocated to market participants with the highest willingness to pay. As a result, if multiple market participants are interested in a specific resource, their competition may lead to an excessive increase in the price of that resource. This may be also caused by flexibility resources

Table 2.4: Benefits and drawbacks of the Common Market model - Centralized version

| | **Benefits** | **Drawbacks** |
|---|---|---|
| **TSO** | • The TSO is responsible for the operation of its own grid. | • The TSO share with the DSO the common market operation. |
| **DSO** | • The DSO is responsible for the operation of its own grid. | • The DSO share with the TSO the common market operation.<br>• Not priority in procuring DERs. |
| **Market organization** | • A third operator (IMO) is appointed by TSO and DSO to ensure the neutral market operation.<br>• Needs of system operators are satisfied minimizing the total AS activation costs.<br>• Market operational costs are shared between TSO and DSO. | • Reduced market operational costs than DV.<br>• Cost allocation between system operators may be difficult.<br>• Individual AS costs of TSOs and DSOs might be higher compared to other schemes. |
| **Shared data** | • Observability of the entire electrical system. | • Data about TN and DN models and resources are shared with a neutral MO, adding risks to the security and privacy of data. |
| **Implementation** | • The standardization process of products and communication requirements may be lower in the case of a CV. | • High computational efforts for the market clearing process. |
| **References** | [30], [36], [32], [88] | |

that, if activated, can negatively affect the operation of other grid operators [36]. On the other side, the presence of non-regulated parties may increase market liquidity. In this sense, flexibility resources procured in the Day-ahead market o intraday markets that are no longer needed may be resold (or procured) in the real-time market. This has the advantage to reduce imbalance penalties since grid operators can procure in real-time the necessary resources. However, since also non-regulated parties are allowed in procuring AS resources, the TSO has difficulties in estimating the effective amount of flexibility to be procured. As a result, there is a risk for system operators of not obtaining what they need, and they are forced to buy additional capacity upfront [32].

Due to the complexity of its mathematical model, which requires an application of the game theory, this market scheme has not been investigated by SmartNet [88]. However, the presence of a single common market platform enhances the participation of DERs and facilitates the standardization process of flexibility resources [36]. In addition, market operating costs can be shared over a higher number of participants [32]. Nevertheless, if the IMO is not involved in the prequalification process of AS resources located at the DN level, the activation of DERs may be in contrast with the DSO operation. Therefore, TSOs and DSOs should communicate to the IMO the reserved data about TN/DN models and constraints. In this case, clear rules need to be defined in order to ensure security and privacy for shared data [36].

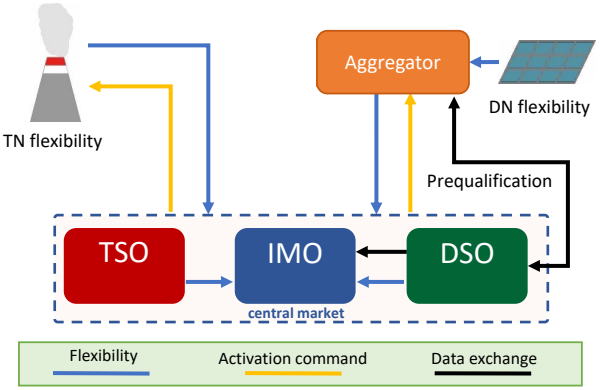


Figure 2.8: Integrated Market scheme

Table 2.5: Benefits and drawbacks of the Integrated flexibility Market model

| | **Benefits** | **Drawbacks** |
|---|---|---|
| **TSO** | • Access to resources previously acquired by other players and no longer needed (DSO, CMP ...).<br>• Flexibility previously procured and no longer needed can be resold to the DSO. | • Due to the presence of non-regulated parties, which can buy flexibility, the TSO has difficulties in estimating the effective amount of necessary flexibility. |
| **DSO** | • Access to resources previously acquired by other players and no longer needed (TSO, CMP ...).<br>• Flexibility previously procured and no longer needed can be resold to the TSO. | • No priority of the DSO in procuring DERs.<br>• If the IMO is not involved in the prequalification process, the activation of DERs may affect the DSO operation. |
| **Market organization** | • Grid operators can procure resources in real-time.<br>• DN flexibility resources may also be aggregated by different DSO-areas.<br>• Reduced AS costs due to the higher liquidity level.<br>• Operational costs of the common market are shared between market operators. | • The activation of AS resources may be in contrast with other grid operators.<br>• In case of competition between market stakeholders for the same product, unnecessary price increases may be generated.<br>• Liquidity for the intraday market might be reduced. |
| **Shared data** | • All flexibility resources are communicated to the IMO in order to guarantee the market neutrality. | • Need for sharing TN and DN data with the IMO, introducing risks for security and privacy of data. |
| **Implementation** | • The presence of a single market platform increases the participation of DERs and simplifies the standardization process of products. | • Since this market model has high mathematical complexity, it has not been investigated as other coordination schemes. |
| **References** | [30], [36], [32], [88] | |

## 2.3 Decentralized architectures

In decentralized TSO-DSO coordination architectures, each system operator is responsible for the operation and the procurement of AS resources for its own network. In this case, due to the coexistence of central and local markets, different pricing methods, such as pay-as-bid or pay-as-clear approaches (See Section 3.1 for further details), may be adopted. This aspect can be considered an advantage because it allows the use of pricing schemes tailored to the characteristics of a specific market, but it could be complicated to be managed in the case of multiple market platforms with different features [84].

### 2.3.1 Local Market model (CoordiNet version)

*Market organization and roles of system operators*

In the Local Market model proposed by Coordinet [32], as shown in Figure 2.9, there is one only local market in which the DSO procures DN flexibility to solve its own needs. Differently from the Local Market model proposed by SmartNet (see Section 2.3.2), resources located in the distribution grid cannot also be offered to the TSO.

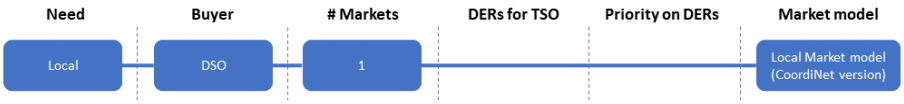


Figure 2.9: Mapping of the Local Market model (CoordiNet version)

In this case, as illustrated in Figure 2.10, the DSO is responsible for managing the distribution network and its local market. However, no coordination is supposed with the central market managed by the TSO (if existing).

*Coordination scheme assessment*

As observed in [32], due to the absence of coordination between the central and the local markets, this coordination model is suitable for controlled island distribution networks or for cases in which there are no transmission networks (e.g., islands). However, in case the distribution network is interfaced with the transmission grid, a minimum level of coordination between TSO and DSO must be ensured at the TN-DN

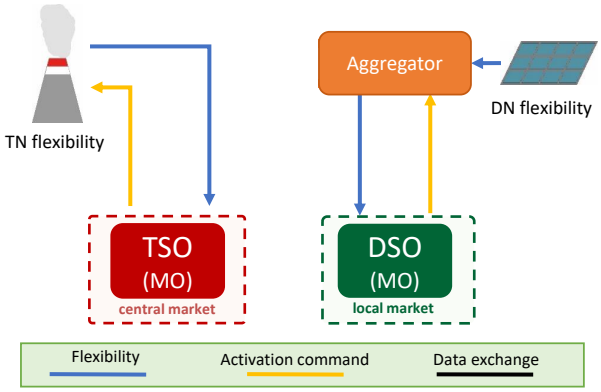


Figure 2.10: Local Market scheme (CoordiNet version)

interconnection point [32]. Table 2.6 resumes the main benefits and disadvantages of this coordination scheme.

### 2.3.2 Multi-level Market model

*Market organization and roles of system operators*

As introduced in the previous subsection, the Multi-level Market model described in [32] extends the use of DN flexibility resources to the TSO. In this case, there are a local market and a central market in which DERs located at the DN level may be offered to the DSO and TSO for, respectively, local and central needs. However, as shown in Figure 2.11, in this scheme, the DSO has priority in using flexibility located at the DN level to solve its own issues with respect to the TSO.

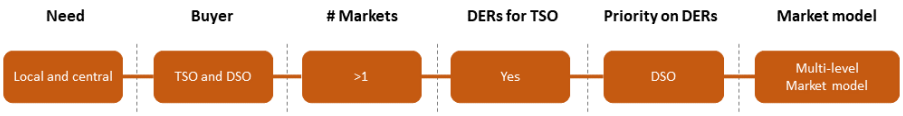


Figure 2.11: Mapping of the Multi-level Market model

This scheme has also been proposed by the SmartNet project under the name of Local AS Market model [36]. As shown in Figure 2.12, the DSO is responsible for the operation of both distribution network and the local AS market, while the TSO is responsible for the operation of the transmission network and the management of the

Table 2.6: Benefits and drawbacks of the Local Market model (CoordiNet version)

| | **Benefits** | **Drawbacks** |
|---|---|---|
| **TSO** | • Reduced amount of AS resources to be shared with the DN. | • The TSO cannot procure AS from DN flexibility. |
| **DSO** | • The DSO may manage and procure AS resources from the DN to solve its own need. | • Possibility to exploit only DN resources to procure AS: risk of illiquidity in case of small-sized local markets. |
| **Market organization** | • The local market is operated directly by the DSO, which is also responsible for the DN operation. | • No coordination of the local market with the central one (if existing). |
| **Shared data** | • Reduced communication between TSO and DSO, since only a coordination at the TN-DN interfacing point is required.<br>• No need to share data about distribution networks. | • Reduced observability of the entire electrical system. |
| **Implementation** | • The DSO must have a full control over its distribution network and, therefore, adequate investments in ICT are required.<br>• Suitable for distribution networks that are islanded or operated in controlled islanding mode. | • Non-optimal use of DERs since they cannot be shared with the TSO. |
| **References** | [32] | |

central market, in which TN and aggregated DN flexibility resources are contracted.

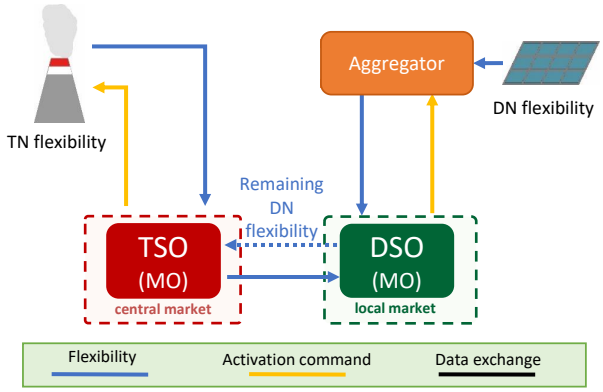


Figure 2.12: Multi-level Market scheme

In particular, the local market managed by the DSO is run first with the aim to solve local needs. Then, once the local market has been cleared, only the remaining DN resources are aggregated and offered by the DSO to the TSO in the central market [36]. In such a way, the TSO may procure flexibility from resources at the TN level and from the aggregated DERs provided by each DSO at the POI. After the TSO determined the AS necessary to solve central needs, clears the central market, and communicates to the DSO the amount of flexibility required at the POI from DN resources.

The aggregation process performed by the DSO (FA) allows DN flexibility resources to be offered to the central market without having to communicate to the TSO data about DN constraints and resources (prices, volumes, capability, ...). However, like for the Centralized AS market model, it must be ensured that the activation of DN resources for the TSO needs does not negatively affect the distribution grid. A *smart* aggregation solution was proposed by SmartNet in [36] with the aim to ensure that only distribution grid resources that do not cause any DN congestion are offered to the TSO. In any case, since the activation of flexibility at DN level may generate power imbalances, the DSO must notify this activation to the TSO in such a way that the TSO may re-establish the power balance [36].

Based on these assumptions, in the Multi-level market model, the DSO is responsible for the distribution grid and the local market operation, playing also the role of

the middleman (FA) between DERs located at the DN level and the TSO [36]. Due to the fragmentation in multiple local markets (one per DSO), the aggregation of DN flexibility resources cannot be performed for resources located in different DNs. Furthermore, although, in this case, AS products are tailored to the needs of each local market, resources offered to the TSO must be aggregated in a format complying with that of the central market [36].

*Coordination scheme assessment*

As previously specified, in this case, there is a local market managed by the DSO for local needs and a central market operated by the TSO for central needs. As a whole, the market operation of this coordination scheme can be very efficient in the case of large DNs, since characterized by higher numbers of Distributed Energy Resources [36]. Conversely, operative costs may increase in smaller local markets. This is because each marker platform should be equipped with an appropriate level of ICT resources and communication infrastructures. In addition, local markets may suffer from illiquidity risks and lower economies of scale, causing higher market operating costs [36]. Whenever local markets are affected by scarce amounts of DN flexibility resources, unwanted measures, such as load shedding or load curtailment, may be necessary to guarantee the correct operation of the distribution network [36].

In performing this kind of scheme, it is important that local and central markets are coordinated and closed at different timing. This is with the aim to avoid that flexibility resources presented at both markets are double accepted [88]. Table 2.7 resumes the main benefits and drawbacks of this coordination scheme.

### 2.3.3 Shared balancing responsibility Market model

*Market organization and roles of system operators*

In the Shared balancing responsibility Market model, the responsibility of balancing the distribution network is transferred to the DSO, which must use its own resources to fulfill this responsibility [30], [36]. Moreover, as shown in Figures 2.13, flexibility resources located at the DN level cannot be offered to the TSO [30], [36], [32]. The main difference with the other investigated schemes is that, in this case, AS resources cannot

Table 2.7: Benefits and drawbacks of the Multi-level Market model

| | **Benefits** | **Drawbacks** |
|---|---|---|
| **TSO** | • TSO responsible for the TN and the central market operation, in which TN and DN resources are contracted. | • The TSO may have higher operational costs since it can only use DERs non activated by the DSO. |
| **DSO** | • DSO responsible for the DN and local market operation, from which it can procure DN AS to solve local needs.<br>• Priority of the DSO on procuring DERs.<br>• The DSO aggregates remaining DERs at the POI. | • Small local markets may be affected by high operational costs (illiquidity of the markets and no economy of scale).<br>• Costs for ICT equipment can impact on the economy of small local markets. |
| **Market organization** | • DN constraints may be included in the central market optimization by means of the aggregated DERs cost curve provided by the DSO to the TSO.<br>• Small markets with reduced number of participants are easier to be managed. | • Additional operational costs due to the presence of multiple markets.<br>• Aggregation of DERs performed at the level of DSO area, reducing the possibility to combine DERs of different markets. |
| **Shared data** | • No data about DN model or DERs are shared with the TSO, reducing risks for security and privacy of data.<br>• The activation of DERs must be communicated to the TSO so it can restore the resulting imbalances. | • Resources at the DN level must be aggregated in a format complying with the central market. |
| **Implementation** | • Smaller markets offer lower entry barriers to small scaled DERs. | • Need to improve ICT for communication between central and local markets |
| **References** | [36], [32], [88] | |

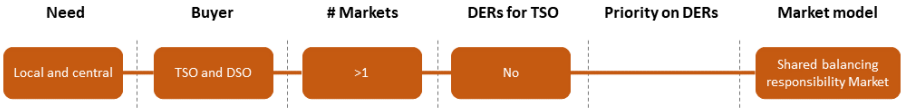


Figure 2.13: Mapping of the Shared balancing responsibility Market model

be shared between grid operators and that the DSO is also responsible for balancing its own DN according to predefined power exchanges [30], [36].

As shown in Figure 2.14, in this market model, there are a central market managed by the TSO for TN resources and a separate local market operated by the DSO for DN resources. Thus, TN and DN grid constraints are included in the clearing process of the respective central and local markets [36]. However, since each grid operator is responsible for the balancing of its own network and AS resources cannot be shared, pre-defined power exchanges need to be established for each TSO-DSO point of interconnection or for the whole DSO-area [30], [36]. These power exchange profiles can be based on Day-ahead market outcomes, forecasts, or historical data [4], [30].

Similarly to the Local Market model, in this case, there is a risk of illiquidity and higher operating costs for small local markets. However, since each market is managed by a specific grid operator and, thus, managed independently, it follows that rules, products, and market design may be tailored to the system operator's need [32].

This market model was presented by CoordiNet as Fragmented Market model, due

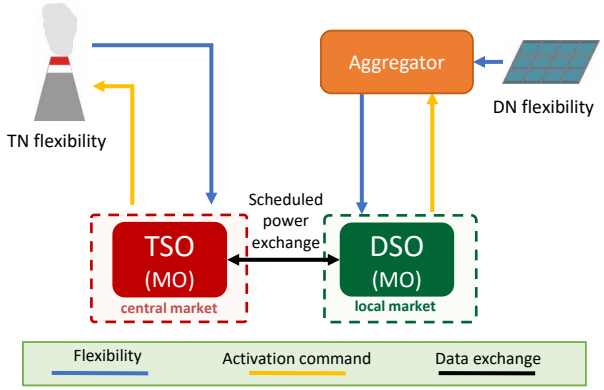


Figure 2.14: Shared balancing responsibility Market scheme

to the full separation between the central and local markets. Variants like the System Balancing Cost Allocation model [32] or based on the possibility to apply additional penalties, whenever programmed power exchanges at the POIs cannot be satisfied by the DSOs [90], [91], were also proposed in the literature.

*Coordination scheme assessment*

In this scheme, flexibility resources cannot be shared among grid operators who must also meet the scheduled power exchanges at the POIs. As a result, AS cost for the DSO may be higher than other schemes [36].

As the balancing responsibility of the distribution network is transferred to the DSO, in this scheme, the TSO has to provide less quantity of flexibility. On the contrary, a greater amount of resources has to be procured from the DN to solve both DN balancing and congestion issues. In the case of low penetration levels of controllable DERs, the lack of flexibility resources can jeopardize the stability of the entire power system. As a consequence, the DSO may be forced to implement unwanted measures, like load shedding or load curtailment. As an alternative, appropriate penalty mechanisms might be adopted to guarantee the power system stability also for those cases in which scheduled power exchanges cannot be satisfied [36]. Table 2.8 resumes the main benefits and drawbacks of this coordination scheme.

Table 2.8: Benefits and drawbacks of the Shared balancing responsibility Market model

| | **Benefits** | **Drawbacks** |
|---|---|---|
| **TSO** | • The TSO is responsible for managing its own network and the central market.<br>• Lower quantity of AS have to be procured by the TSO. | • DN flexibility resources cannot be offered to the central market. |
| **DSO** | • The DSO is responsible for managing its own network and the local market.<br>• As an additional role, the DSO is also responsible for the balancing of the distribution network. | • Unwanted measures must be undertaken in case of scarcity of AS resources necessary to solve local needs and fulfill power exchanges set at the POIs.<br>• Increased need for AS for the DSO. |
| **Market organization** | • Possibility to customize markets and products. | • Risk of illiquidity for small markets since flexibility cannot be pooled.<br>• Higher operational costs for local markets with low penetration level of DERs. |
| **Shared data** | • No need to share reserved data about grid models. | • Reduced observability of the entire power system. |
| **Implementation** | • No high standards are required for the TSO-DSO communication since only power exchanges at the POIs need to be communicated. | • The separation between global and local markets determines sub-optimal solutions.<br>• Risks for power system stability. |
| **References** | [30], [36], [32] | |

### 2.3.4 Common Market model - Decentralized version

*Market organization and roles of system operators*

Similarly to the Centralized version, in the Common Decentralized Market model, flexibility resources at the TN and DN levels are shared between TSO and the DSO with the aim to address both central and local needs and minimize the total AS activation costs [30], [36]. As indicated in Figure 2.15, in this case, there are multiple markets. One central market, managed by the TSO, and local markets managed by the

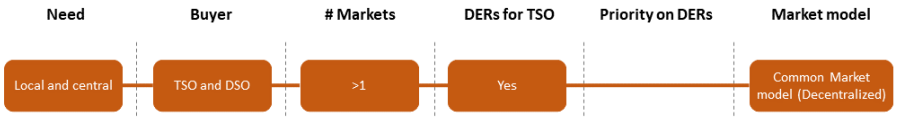


Figure 2.15: Mapping of the Common Market model - Decentralized version

DSOs [36]. All MOs are jointly responsible for the final outcome of the performed separate market runs [36] and, in contrast with the centralized version, data concerning grid models and resources are not shared between System Operators. Moreover, as in the Multi-level Market model, DN resources are offered to the TSO in aggregated form, although without any priority of the DSO. Therefore, in this case, the local market is run first, considering DN constraints and local needs, but without any commitment to the market participants [36]. Next, preliminary results are communicated (e.g. through aggregated DERs [84]) to the TSO and integrated into the central market optimization. Once the central market has been cleared, the volume of flexibility required by the central market at the POI is communicated back to the DSO, which will dispatch DN flexibility resources taking TN and DN needs into account [30], [36].

As observed in [36], the decentralized version of the Common Market model can be intended an extension of the Local Market Model, but without priority of the DSO on DERs procurement. The assignment of flexibility is performed considering the combined needs of both operators [36]. A few variants to the Common Market model are resumed in [32].

*Coordination scheme assessment*

Like in the Centralized version of the Common Market model, in this scheme, flexibil-

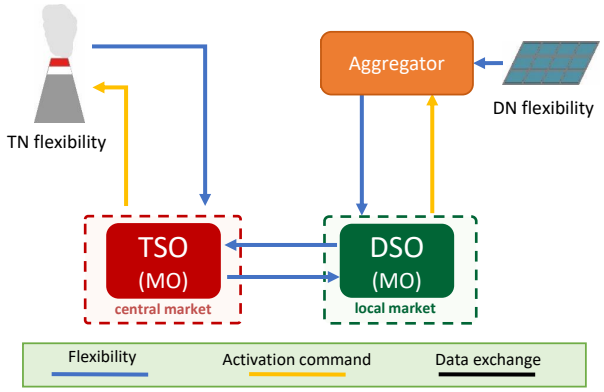


Figure 2.16: Common Market scheme - Decentralized version

ity resources are shared between TSO and DSO with the aim to satisfy needs of both system operators and minimize the total AS activation costs. Nevertheless, differently from the Centralized version, each market is cleared independently and this allows the entire computational burden to be distributed among the market operators. Instead, further efforts are needed to align the flexibility products of different market platforms [32].

As specified for the Centralized version, although, in this market model, the overall AS activation costs are minimized, the individual costs for TSO and DSOs might be higher compared with those of other coordination schemes [88]. In this sense, there is also a need to establish a criterion for allocating the activation costs of DERs between TSO and DSO [36]. These and other benefits/drawbacks of this market model are resumed in Table 2.9.

### 2.3.5 Distributed Market model

*Market organization and roles of system operators*

In the Distributed Market model, peers are the only ones authorized to buy and provide AS flexibility resources [32]. As shown in Figure 2.17, in this scheme, local or combinations of central and local needs can be satisfied [32]. An example of Distributed Market model is represented by a peer-to-peer (P2P) market in which each peer established a direct connection with the neighboring peers [32]. In this sense, as specified

Table 2.9: Benefits and drawbacks of the Common Market model - Decentralized version

| | **Benefits** | **Drawbacks** |
|---|---|---|
| **TSO** | • The TSO is responsible for managing its own network and the central market. | • The TSO has not direct access to the DN flexibility resources. |
| **DSO** | • The DSO is responsible for managing its own network and the local market. | • Not priority in procuring DERs. |
| **Market organization** | • Needs of system operators are satisfied minimizing the total AS activation costs.<br>• Markets are managed individually with AS products tailored on market characteristics. | • Additional operational costs due to the presence of multiple markets.<br>• Risk of illiquidity, with reduced amounts of DERs, may exist in case of small local markets.<br>• Individual costs for TSOs and DSOs might be higher than those of other schemes.<br>• Allocation of AS costs between system operators may be difficult. |
| **Shared data** | • No need to share reserved data about grid models with external operators. | • Need for strategies to offer DERs to the central market without communicating reserved data about the DN. |
| **Implementation** | • Computational efforts to optimize AS are distributed among market operators. | • Need for extensive communication and ICT resources for the communication among the central and the local markets. |
| **References** | [30], [36], [32], [88] | |

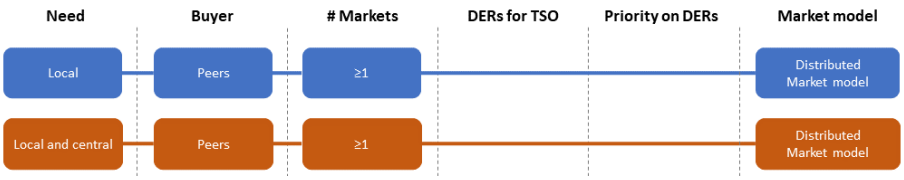


Figure 2.17: Mapping of the Distributed Market model

in [32], P2P is defined as a decentralized market architecture in which all peers can cooperate, with the available resources, to produce, exchange or distribute goods or services [92]. Therefore, to implement a Distributed Market model an ad-hoc market setup is needed [32]. Different P2P-based market structures, like the blockchain technology [32], have been proposed in the literature, but, currently, there is no agreement about how such markets should be structured. For instance, these maket models may differ according to the level of decentralization and topology. This consideration also applies to P2P-based power trading, in which it is necessary to have structures tailored to the specific context.

Blockchain could be efficiently applied in a Distributed Market model since it would allow flexibility resources to be offered in a digital platform in which system operators send their flexibility requests without the need for centralized control. Transactions would be confirmed by smart contracts which the involved users can access without being able to change them [17]. Based on these aspects, a Blockchain-based market platform can ensure security in energy transactions and equal rights for market participants, as they can submit and accepts flexibility freely [17].

*Coordination scheme assessment*

As specified in [32], drastic changes in the current market structure and regulatory framework are needed to implement this market model. Depending on the performed implementation, market participants can assume less or more autonomy. Consequently, this autonomy can reduce the system overview and lead to grid-constrained situations or power imbalances [32]. Moreover, one peer's goal may be at odds with that of other peers, penalizing the optimal social welfare [32]. In fact, as highlighted by [32], there is also a lot of uncertainty in defining how TSO and DSO needs will be taken into

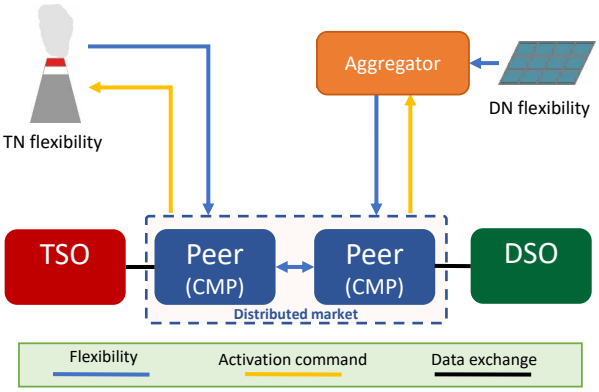


Figure 2.18: Distributed Market scheme

account in this market structure. Based on these aspects, a careful design is necessary to implement this market model. Table 2.10 resumes the main benefits and drawbacks of this coordination scheme.

## 2.4 TSO-DSO coordination in the Italian framework

As specified in Section 1.3, new rules have been introduced by the Italian Regulatory Authority ARERA with the transposing of Regulation EU 2019/943 [11] and Directive EU 2019/944 [12] into national codes. In the last years, through the DCO 322/2019/R/eel [74], ARERA promoted a consultation procedure aimed at identifying the main lines of action to establish the next dispatch framework at the national level. More in detail, this reform process, concerning the Ancillary Services provisioning through DERs and Renewable Energy Sources, has been promoted by the Authority since 2013, with the DCO 354/2013/R/eel [93]. As highlighted by [74], three TSO-DSO coordination schemes, similar to those later proposed by SmartNet in [36], were developed and described in Annex A [94] of the same DCO.

Among various proposals of the DCO 322/2019, it has been considered the possibility to enable the DSO to play the role of neutral facilitator for DN resources offered to TSO and of AS buyer for local issues. Furthermore, in accordance with the resolution 628/2018/R/eel [75], the same DCO remarks the need to enhance the data ex-

Table 2.10: Benefits and drawbacks of the Distributed Market model

| | **Benefits** | **Drawbacks** |
|---|---|---|
| **Peers** | • Possibility to buy or procure flexibility. | • Need for suitable trading mechanism to avoid power imbalances. |
| **Market organization** | • Each peer operates in order to reach its objective, which may be in contrast with those of other peers. | • Uncertainty in taking TSO and DSO needs into account.<br>• Multiple market platforms may exist. |
| **Shared data** | • Data about transactions may be communicated through encrypted data (Blockchain) | • High computational burden for transactions between peers. |
| **Implementation** | • Blockchain technology would enable transactions and smart contracts to be executed automatically. | • Not in line with the current regulatory framework and market setup. |
| **References** | [32] | |

change between the TSO, DSO and significant grid users to improve the provisioning of AS from DERs located at the DN level. In this perspective, a call for investigating the most effective ways of providing Ancillary Services by means of DERs, in a TSO-DSO coordination framework, was also issued. With this aim, the document refers to the five TSO-DSO coordination schemes proposed by the SmartNet project [36] and above described, such as:

**1-** Centralized AS Market model;

**2-** Local AS Market model (identified as Multi-level in Chapter 2);

**3-** Shared balancing responsibility Market model;

**4-** Common AS Market model;

**5-** Integrated flexibility Market model;

Based on an cost-benefit analysis (CBA) provided in the literature for these schemes [95], the DCO observed that:

- The Centralized Market scheme **1-** demonstrated to be less efficient than scheme **4-** in the case of congestions at the DN level;
- Coordination models **2-** and **3-** based on local markets are usually more expensive than models **1-** and **4-**. This may be due to the complexity of the algorithms employed in these schemes as well as the limited number of resources available in small local markets. This last trouble is also more evident in case of different smaller DSOs, as for Italy.
- The coordination scheme **2-** appears difficult to be implemented due to the presence of central and local markets that need to interact with each other. Coordination between the central and local market is necessary to ensure that the activation of flexibility at the DN level, to solve local congestions, does not negatively affect the global balancing performed by the TSO as well as that resources offered to both central and local markets are not activated twice.
- The market model **3-** is more expensive than the other schemes due to the balancing responsibility assigned to the DSOs, which must use its DN resources

first to balance its distribution grid. This market model also appears to be not in line with the European trends regarding regulation.

- Model **5-** is complicated to be implemented and, therefore, has not been implemented.

On the basis of these features, ARERA concluded that the most effective models are the Centralized scheme **1-**, in absence of relevant congestions at the DN level, and the Common AS Market model **4-** for the other cases. In order to test the provision of Ancillary Services for the DSO, the DCO also highlighted the need for additional resolutions to set the requirements of pilot projects (defined in 352/2021/R/EEL [76]). In this sense, the DCO also specified that such pilot projects should be aimed at solving local issues that, as discussed in Report 428/2018/I/efr [10], may affect the distribution networks in future scenarios. In particular, to improve voltage profiles (e.g. in the proximity of generating units) and solve congestion issues caused by excessive Renewable Energy Sources production, or, conversely, by EV charging points and HVAC systems. Tests results of performed pilot projects will be employed to carry out the final document on the reform of the Italian AS market (TIDE [74]) in 2023 [77].

## 2.5 Final assessments

Based on the characteristics of the investigated market schemes, the advantages and disadvantages of the centralized and decentralized architectures are evaluated. Tables 2.12 and 2.13 resume the main roles performed, respectively, by system and market operators in each investigated centralized/decentralized coordination scheme. As it can be seen in Table 2.11, centralized architectures are able to provide more effective solutions in terms of optimal dispatch because including all data about TN/DN grid models and resources. However, this approach requires a huge computational effort to optimize the entire power system. In this sense, the huge amount of data to be shared and processed in centralized architectures may also lead to communication bottlenecks, slowing down the whole communication process.

Table 2.11: Centralized vs. decentralized architectures

| | |
|---|---|
| | **CENTRALIZED ARCHITECTURE** |
| **Advantages** | ✓ TSOs and DSOs share costs for market organization<br>✓ The overall optimal dispatch is reached |
| **Disadvantages** | ✗ Share of reserved data<br>✗ High computational burden<br>✗ Scalability issues<br>✗ Risk of communication bottlenecks |
| | **DECENTRALIZED ARCHITECTURE** |
| **Advantages** | ✓ The calculation burden is distributed among operators<br>✓ Reduced data exchange between system operators<br>✓ Security and privacy for data of TN/DN models and status<br>✓ More engagement of the DSO (is also market operator)<br>✓ Possibility of using customized OPF tools for subproblems |
| **Disadvantages** | ✗ High needs of ITC and communication infrastructures<br>✗ Reduced economy of scale<br>✗ Additional operative costs than centralized version<br>✗ Approximations for decentralization: less optimal solutions<br>✗ Need to align local products to the central market features |

As an alternative, decentralized market schemes may be employed, since they represent a suitable trade-off between data to be shared among system operators and optimality in dispatching TN and DN flexibility resources. As a benefit, the presence of multiple market platforms allows the computational burden to be shared among various players and the AS products to be tailored to the characteristics of the specific markets. However, small local markets can be affected by the scarcity of dispatchable resources and, therefore, illiquidity problems. This can also result in additional operational costs for decentralized architectures than single (larger) markets of centralized architectures.

Although a CBA has been carried out by SmartNet for specific coordination schemes [95], it is clear that the adoption of a specific coordination model should be performed taking into account further several aspects, such as socio-techno-economic challenges [18]. In general, any coordination scheme, to be implemented, requires improved observability of networks and controllability of physical devices, resulting in higher

capital and operating expenditures [18]. In addition, TSO-DSO coordination schemes rely on access to accurate information about transmission and distribution networks, making the whole power system more vulnerable and exposed to cyberattacks [18]. Therefore, cyber-security is also a relevant issue to be addressed. Further complexity is also given by the greater number of DERs to be dispatched, in particular at the DN level [18]. All these aspects suggest how any comparison between coordination schemes is relative to specific regulatory, organizational, and market contexts [18].

Although the Centralized Market model is the TSO-DSO coordination scheme that is most in line with the current regulatory framework [88] and EU power systems [14], decentralized schemes, such as the Common Decenralized Market model, may offer to the DSO the possibility of using AS to remove local congestions, minimizing the total AS activation costs for both operators. The same is for the Multi-level and the Shared balancing responsibility Market models, which are probably easier to be implemented from an operational perspective [14]. However, with a shift from the Centralized Market model to other coordination schemes, there is a gradual increase in roles and responsibilities of the DSO [88]. The choice of the more appropriate coordination model should be performed considering aspects like type of AS, state of grid, normal operation vs. emergency condition, amount of flexibility resources, and penetration of Renewable Sources. In addition, national regulatory framework, ICT requirements, national organization, amount and interaction between TSOs and DSOs have to be considered for evaluating the feasibility of a coordination scheme [30], [88]. In this perspective, a coordination model could also be adapted to a specific application context [88] or assumed for a particular Ancillary Services product [14].

In conclusion, several aspects need to be taken into account when assessing the feasibility of a coordination scheme, including the fact that its adoption will introduce inevitable and drastic changes in business models, information exchanges, and structure ICT [14].

Table 2.12: Comparison of roles in centralized architectures

| | Task | Centralized Market | Common Centralized Market | Integrated Market |
|---|---|---|---|---|
| **Prequal.** | FFC | DSO (DN) | DSO (DN) | DSO (DN) |
| **Grid operation** | SO | TSO (TN)<br>DSO (DN) | TSO (TN)<br>DSO (DN) | TSO (TN)<br>DSO (DN) |
| | BRP | TSO (TN,DN) | TSO (TN,DN) | TSO (TN,DN) |
| | DM | TSO (TN)<br>DSO (DN) | TSO,DSO (TN,DN)<br>IMO (TN,DN) | TSO (TN)<br>DSO (DN)<br>IMO (TN,DN) |
| **Procurement** | Buyer | TSO (TN,DN) | TSO,DSO (TN,DN) | TSO,DSO,CMP (TN,DN) |
| | Seller | CMP (TN,DN) | CMP (TN,DN) | TSO (TN,DN)<br>DSO (DN)<br>CMP (TN,DN) |
| | MO | TSO (TN,DN) | TSO,DSO (TN,DN)<br>IMO (TN,DN) | IMO (TN,DN) |
| | RA | TSO (TN,DN) | TSO (TN)<br>DSO (DN) | TSO (TN)<br>DSO (DN) |
| | FA | CMP (TN,DN) | CMP (TN,DN) | CMP(TN,DN) |
| **Activation** | FRD | TSO,CMP (TN,DN) | TSO (TN)<br>DSO (DN)<br>IMO,CMP (TN,DN) | TSO (TN)<br>DSO (DN)<br>IMO,CMP (TN,DN) |
| **Settlement** | MDR | TSO (TN)<br>DSO (DN)<br>CMP (TN,DN) | TSO (TN)<br>DSO (DN)<br>CMP (TN,DN) | TSO (TN)<br>DSO (DN)<br>CMP (TN,DN) |

Table 2.13: Comparison of roles in decentralized architectures

| | Task | Local (CoordiNet v.) Market | Multi-level Market | Shared Balancing responsibility Market | Common Decentralized Market | Distributed Market |
|---|---|---|---|---|---|---|
| **Prequal.** | FFC | DSO (DN) | DSO (DN) | DSO (DN) | DSO (DN) | DSO (DN) |
| **Grid operation** | SO | TSO (TN)<br>DSO (DN) | TSO (TN)<br>DSO (DN) | TSO (TN)<br>DSO (DN) | TSO (TN)<br>DSO (DN) | TSO (TN)<br>DSO (DN) |
| | BRP | TSO (TN,DN) | TSO (TN,DN) | TSO (TN)<br>DSO (DN) | TSO (TN,DN) | - |
| | DM | TSO (TN)<br>DSO (DN) | TSO (TN)<br>DSO (DN) | TSO (TN)<br>DSO (DN) | TSO (TN)<br>DSO (DN) | TSO (TN)<br>DSO (DN)<br>IMO (TN,DN) |
| **Procur.** | Buyer | DSO (TN,DN) | TSO,DSO (TN,DN) | TSO (TN)<br>DSO (DN) | TSO,DSO (TN,DN) | CMP (TN,DN) |
| | Seller | CMP (TN,DN) | CMP (TN,DN) | CMP (TN,DN) | CMP (TN,DN) | CMP (TN,DN) |
| | MO | TSO (TN)<br>DSO DN) | TSO (TN)<br>DSO DN) | TSO (TN)<br>DSO DN) | TSO (TN)<br>DSO DN) | IMO (TN,DN) |
| | RA | DSO (DN) | TSO (TN)<br>DSO (DN) | TSO (TN)<br>DSO (DN) | TSO (TN)<br>DSO (DN) | TSO (TN)<br>DSO (DN) |
| | FA | CMP (DN) | DSO (DN)<br>CMP (TN,DN) | CMP (TN,DN) | DSO (DN)<br>CMP (TN,DN) | CMP (TN,DN) |
| **Activation** | FRD | DSO,CMP (DN) | TSO (TN)<br>DSO (DN)<br>CMP (TN,DN) | TSO (TN)<br>DSO (DN)<br>CMP (TN,DN) | TSO (TN)<br>DSO (DN)<br>CMP (TN,DN) | CMP (TN,DN) |
| **Settlement** | MDR | DSO,CMP (DN) | TSO (TN)<br>DSO (DN)<br>CMP (TN,DN) | TSO (TN)<br>DSO (DN)<br>CMP (TN,DN) | TSO (TN)<br>DSO (DN)<br>CMP (TN,DN) | TSO (TN)<br>DSO (DN)<br>CMP (TN,DN) |

# Chapter 3

# Methods for coordinated provision of flexibility in CM and Balancing

In this Chapter, an overview of the main tools proposed in the literature to implement an effective dispatch of flexibility resources in a TSO-DSO coordination framework for congestion management and balancing Ancillary Services was provided. More in detail, the main algorithms employed to clear markets, estimating the flexibility available at the POI or aggregating DERs at the DN level are described.

## 3.1 Market clearing algorithms

A *Market Clearing* algorithm is typically employed by market operators to establish which resources participating in market sessions have been accepted and prices to be paid for their activation [84]. It consists of an optimal constrained problem including an objective cost function to be optimized as well as capability curves of resources and grid constraints to be satisfied [84]. Algorithms like OPF routines may be employed with this aim since they are able to perform an optimal dispatch of resources by acting on a set of controllable variables, taking into account grid model and unit constraints. An application of an OPF algorithm to dispatch flexibility DN resources in a Shared balancing responsibility Market model has been developed by the author in [90].

In general, to implement a market platform based on a market clearing process,

several aspects need to be defined [84]:

- **AC or DC OPF:** traditionally, DC optimal power flows are employed to optimize the transmission network operation. In distribution networks, DC OPF cannot be employed since resistance to reactance (R/X) ratios of distribution lines are higher than those of transmission ones [96].
- **Objective function:** may be aimed at minimizing the activation costs (or, equivalently, reducing operating costs) of dispatchable resources or maximizing the overall social welfare for sellers and buyers.
- **Type of bids:** linear, quadratic or piece-wise linear, divisible (curtailable) or non-divisible (non-curtailable), etc.
- **Ancillary Services products:** congestion management, balancing, frequency regulation, voltage regulastion, etc. [36].
- **Pricing of accepted resources:** *pay-as-bid* or *pay-as-clear* approaches. In the first case, each resource is remunerated at the price at which it was offered to the market. Differently, in the pay-as-clear strategy, named also *marginal price approach*, the activated resources receive the price corresponding to the most expensive flexibility selected in the market session.

Based on these aspects, it follows that the implemented optimal power flow formulation should comply with the characteristics of the addressed problem, regulation framework and, in particular, with the adopted TSO-DSO coordination architecture. In the literature, several methodologies and market-clearing methods, such as Lagrangian methods, data-driven approach, game-theoretic and heuristic methods have been proposed with the aim to perform an optimal dispatch [97], [98], [99]. However, as shown in Figure 3.1, three different categories of market clearing algorithms are typically employed in local markets, such as centralized optimization, bilevel optimization, and decomposition algorithms [100].
A description of these algorithms was provided below, with a focus on centralized optimization, as it was used as a benchmark method for simulation tests carried out in Section 4.3.3.

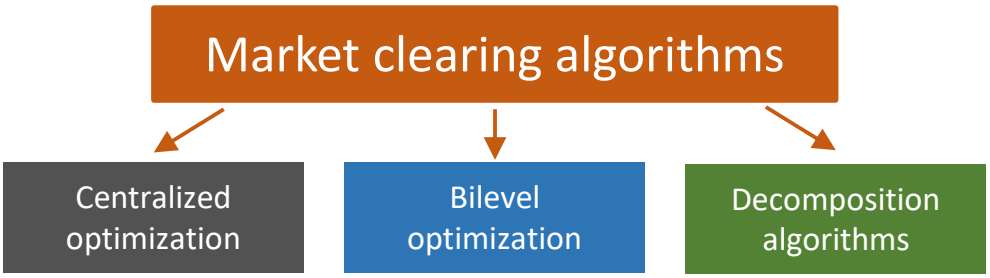


Figure 3.1: Markets clearing algorithms.

### 3.1.1 Centralized Optimization

As specified in Chapter 2, in centralized TSO-DSO coordination schemes, there is a single Market Operator which is responsible for the optimal dispatch of resources at TN and DN level. Then, in order to implement a *centralized* dispatch of resources, TN and DN grid constraints as well as the operational limits concerning the physical devices are shared by TSOs and DSOs with the MO, in order to to be included in the overall dispatch problem performed by the MO itself [30], [36].

In line with the Italian Ancillary Services market [71], in the present thesis, a pay-as-bid approach was adopted in the market clearing processes. Then, a centralized AC-optimal power flow algorithm, aimed at minimizing the activation cost of flexibility resources at TN and DN level, to provide AS for balancing and CM issues, can be formulated as follow:

$$\min_{\mathbf{u}^{TN},\mathbf{u}_l^{DN}} \left[ C^{TN}(\mathbf{u}^{TN}) + \sum_{l=1}^{n_{DSO}} C_l^{DN}(\mathbf{u}_l^{DN}) \right] \tag{3.1}$$

subjects to

$$\begin{aligned} \mathbf{g}^{TN}(\mathbf{x}^{TN},\mathbf{u}^{TN}) &= \mathbf{0} \\ \mathbf{h}^{TN}(\mathbf{x}^{TN},\mathbf{u}^{TN}) &\geq \mathbf{0} \end{aligned} \tag{3.2}$$

and

$$\begin{aligned} \mathbf{g}_l^{DN}(\mathbf{x}_l^{DN}, \mathbf{u}_l^{DN}) &= \mathbf{0} \\ \mathbf{h}_l^{DN}(\mathbf{x}_l^{DN}, \mathbf{u}_l^{DN}) &\geq \mathbf{0} \end{aligned} \tag{3.3}$$

with

$$\begin{aligned} \mathbf{x}_{POI,l,v}^{TN} + \mathbf{x}_{POI,l,v}^{DN} &= \mathbf{0} \\ v &= 1, 2, ..., n_{POI,l} \\ l &= 1, 2, ..., n_{DSO} \end{aligned} \tag{3.4}$$

in which $C^{TN}$ and $C_l^{DN}$ represent, respectively, the activation costs of AS resources for the transmission network and each $l$-th of the $n_{DSO}$ distribution grids. These costs depend on the control variables $\mathbf{u}^{TN}$ and $\mathbf{u}_l^{DN}$, which denote the arrays of the active and reactive power of dispatchable resources located, respectively, in the transmission and in the $l-$th distribution network. While, the arrays $\mathbf{x}^{TN}$ and $\mathbf{x}_l^{DN}$ represent the state variables for the transmission and the $l-$th distribution grids, respectively. Sets $\mathbf{g}^{TN}$ and $\mathbf{h}^{TN}$ denote, respectively, the equality and inequality constraints concerning the capability curves of dispatchable resources and power balance equations at nodes, as well as voltage and thermal limits of physical devices (power lines, transformers, etc.) located at the transmission level. Similarly, $\mathbf{g}_l^{DN}$ and $\mathbf{h}_l^{DN}$ for the the $l-$th distribution network. Assuming each $l$-th DSO interfaced with the transmission grid in $n_{POI,l}$ interconnection points, $\mathbf{x}_{POI,l}^{TN}$ and $\mathbf{x}_{POI,l}^{DN}$ are two generic sub-arrays of dimension $(2 \times 1)$ representing the active and reactive power flows at each $v$-th POI from the transmission and the distribution point of view, respectively.

Due to its characteristics, a centralized OPF appears suitable for cases in which the entire power system is managed by a single system operator. In contrast, this approach may not be feasible in electrical systems where transmission and distribution networks are managed by independent operators. In addition, other aspects such as those described below should also be taken into account in performing a centralized dispatch:

- **Grids topology**: common OPF tools, usually employed for meshed transmis-

sion networks, may not properly work with radial distribution grid models, leading to optimizing ill-conditioned problems. Moreover, differently from the TN, unbalanced load conditions may affect the distribution network. Therefore, unbalanced three-phase optimal power flow algorithms like the TOPF developed and proposed in Section 4.1 [5] should be employed at the DN level.

- **AC/DC OPF**: as above specified, transmission networks are characterized by low resistance to reactance $R/X$ ratios. This condition does not apply to distribution networks, in which resistance is dominant. Classical DC OPF algorithms used for transmission networks are not suitable for distribution grids and, therefore, comprehensive OPF tools able to optimize simultaneously TN and DN are necessary [101], [102], [103].

- **Data exchange**: traditionally, in dispatching generating units, only the transmission network models were considered, while the distribution grids were represented as a node [86]. In this case, DERs at the DN level are dispatched without considering their effective grid location and, thus, any possible following congestion affecting the DN lines has to be solved through a re-dispatch. Theoretically, this trouble can be solved with the sharing of DN grid models with the TSO, in order to implement a nodal approach also at DN level [86]. In the reality, TSO and DSO may be reluctant in sharing details about their grid models and status with external operators or commercial parties, with the risk of compromising the possibility of implementing an effective TSO-DSO coordination [21]. In addition, collecting all data about resources located at TN and DN level may be challenging for the dispatch centers, with the risk of generating communication bottlenecks [87].

- **Computational burden**: with the provisioning of AS from widespread DERs located at DN level, a greater amount of bids needs to be controlled and optimized. Therefore, performing optimal dispatch of large-size systems, including several interconnected transmission and distribution networks, could be troublesome and potentially not solvable in adequate timeframes [36].

### 3.1.2 Decomposition algorithms

As previously specified, grid operators are reluctant in sharing reserved data about their networks with external operators. Decomposition methodologies operate by breaking down a complex optimization problem into several sub-problems, which can be solved independently and, thus, easier to be solved than a single large problem [104]. As a result, this kind of approach may be very suitable to address optimal dispatch problems in a TSO-DSO coordination framework since TN and DN can be optimized separately, without the need of sharing confidential data between system operators. In addition, decomposition techniques are also advantageous when applied to large problems, as they allow the computational burden to be distributed among sub-problems [86], [104].

Several decomposition techniques have been proposed in the literature and also applied to linear and non-linear programming [105], for power system scheduling and resources dispatch [106], [107], [108]. Some of them are based on Lagrangian relaxation [109], augmented Lagrangian decomposition, optimality condition decomposition [110], cutting plane consensus [87] generalized Benders decomposition [111], [107] and Dantzig–Wolfe [112]. The application of a Benders decomposition algorithm implemented in this thesis for CM and Balancing Ancillary Services in a TSO-DSO coordination framework is described in Section 4.3.

### 3.1.3 Bilevel optimization

A bilevel algorithm is a kind of optimization in which a subset of variables is constrained to be optimal for another optimization problem, parameterized by the remaining variables [104]. Commonly, the outer problem is identified as the upper-level problem, while the inner one as the lower-level problem. As a result, the optimization performed at the upper level is also influenced by the response of the lower level problem [113].

Several applications of bilevel optimization techniques can be found in the literature about the optimal dispatch of DERs [114], [115]. However, in the market clearing context, this methodology is applied to optimization problems having a hierarchical structure, with "leader" players (at the upper level) and "follower" players (at the lower

level). As described in [100], a market optimization based on a bilevel approach can be performed with single-level reduction or nested methods. The former can be only used when the lower-level problems are linear, since they may be replaced by the corresponding KKT conditions only when the constraints are linear and convex. Differently, in the case of non-linearity of lower-level problems, nested methods may be employed to solve this kind of optimization [100]. Whenever, instead, the upper-level problem is non-linear, its non-linear terms can be linearized through the strong duality theorem [104]. In the case both the upper-level and lower-level problems are linear and KKT conditions are enough to reduce the whole problem into a single-level problem solvable with a commercial solver.

From a comparison between the BDA and the bilevel approach, the study described in [100] remarked as the decomposition methods are suitable to solve large-scale optimizations in which the complex problem may be decomposed into smaller ones. While, the bilevel optimization algorithms are suitable for hierarchical market structure, having leader and follower participants. Nevertheless, cases of bilevel algorithms integrating a decomposition technique are also described in the literature [116].

## 3.2 Mapping Flexibility Area

As specified by ENTSO-E in "Network Code on Operational Planning and Scheduling" [117], in order to increase the efficiency in power system operation, each TSO should be able to monitor the ratio of active and reactive power at the TSO-DSO interconnection point [117]. This need is also more evident in decentralized coordination architectures, in which the TSO has not the possibility to estimate the total amount of flexibility resources available at the DN level and that can be offered to it. In order to solve this issue, the concept of *flexibility area* (or region) has been introduced and widely described in the literature. It allows the DSO to estimate and communicate to the TSO the effective amount of active/reactive power available at the POI. An example of flexibility area was provided in Fig. 4.2. It consists of a graphical representation that, like a capability chart, describes the flexibility available at the TN/DN interfacing point in terms of active and reactive power.

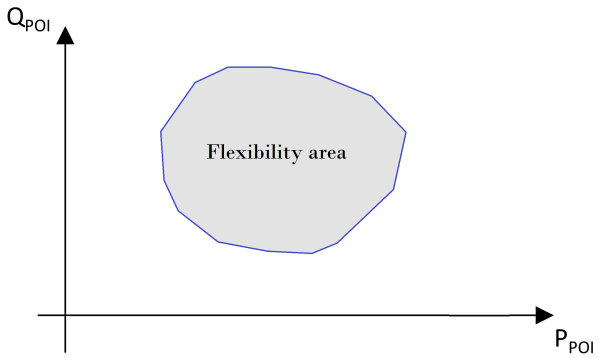


Figure 3.2: Example of flexibility area

Several solutions have been proposed in the literature with the aim to estimate the amounts of active and reactive power that can be exchanged at the TSO-DSO interface point [21], [118], [119]. Nevertheless, the proposed methods can be mainly regrouped into two types: Random Sampling (RS)- and OPF-based approaches [120], [121]. In the first case, resources are dispatched randomly and the feasibility of detected solutions is just verified after running power flow routines [119]. Differently, OPF-based methodologies are more effective since they aim to find both maximum and minimum power values at the POIs taking technical network constraints into account. More in detail, in RS-based methodologies, the overall flexibility is calculated by performing an established number of power flows in which each flexibility resource is randomly selected from its respective band. The disadvantage of this method is that the feasibility of calculated solutions is just verified after running the power flows [119]. The second approach is based on performing OPF routines considering technical constraints and non-linearities of distribution grids [18].

Typically, these flexibility area estimation strategies are referred to those cases in which there is a single interconnection point between the TSO and DSO, a condition common in power system operation. However, with the spread of DNs operated in meshed mode, which have multiple interconnections with the transmission network, the flexibility region estimation for multiple POIs has also been investigated in the literature [122], [123], [124].

This flexibility estimation process well complies with the possibility to be exploited

for an effective TSO-DSO coordination and included in a market-based application to provide grid services to the TSO [121]. For instance, this process could be used to estimate the effective amount of flexibility that can be offered from DN resources to the TSO in the congestion or balancing AS markets. In this context, a method to monetize the flexibility associated with the calculated flexibility area was also provided in [125].

With the aim of estimating the flexibility area at the POI, considering DERs located at both medium and low voltage level, an OPF-based algorithm was developed in this thesis and presented in Section 4.1.

## 3.3 Aggregation of DERs

As described in Chapter 2, in decentralized market schemes, local market operators (DSOs) have the task to transfer flexibility from the local to the central markets, managed by the TSO. In order to reach this aim without communicating confidential data about grid models and status, the DSOs can offer the flexibility available at the DN level to the TSO in an aggregated form. This strategy, for instance, is adopted in the Common (Decentralized version) and Local AS Market models proposed by SmartNet [36]. In more detail, as described in [84], the DSO collects the DN flexibility resources (aggregated or not) and submits them as one equivalent bid to the TSO in the central market. However, if this aggregation is performed by means of commercial aggregators, it is not ensured that distribution grid constraints are satisfied. In this case, follow-up controls should be performed by the DSO to verify that the activation of DERs does not create congestions or excessive voltage drops at the DN level.

As an alternative, a smart aggregation approach (SAA) to aggregate and offer flexibility resources located at the DN level to the TSO was proposed by SmartNet [84]. Differently from commercial aggregators, the SAA ensures that flexibility resources offered to the central market respect DN voltage and power line constraints. Conversely, in the case of a traditional aggregator, in which no smart aggregation is performed, all DN flexibility resources would be transferred to the TSO.

Denoting by $P_{POI}$ the active power flowing from the TN to the DN in a specific POI, the SAA of DERs can be performed through the following steps:

- **Step 1)** the minimum (maximum) value of the flexibility range $[P_{POI}^{min}; P_{POI}^{max}]$ is defined by assuming the lowest value between the sum of all upward (downward) flexibility bids and the remaining margin between the rating power at the POI (e.g. of the installed transformer) and a reference value $P_{POI}^{ref}$;

- **Step 2)** assuming a number of steps $N_s$ for which optimize the local market in the SAA, the incremental step of active power $\Delta P_{POI}$ is calculated as:

$$\Delta P_{POI} = \frac{P_{POI}^{max} - P_{POI}^{min}}{N_s} \tag{3.5}$$

- **Step 3)** by means of optimal power flow routines, aimed at minimizing the total AS activation costs, the local market is cleared for each calculated value of active power $P_{POI}^{i}$:

$$\begin{aligned} P_{POI}^{i} &= P_{POI}^{min} + i \cdot \Delta P_{POI} \\ &\forall i = 0, ..., N_s \end{aligned} \tag{3.6}$$

- **Step 4)** the total AS activation cost $C_i^{DN}$ of the distribution grid is calculated for each value of flexibility $P_{POI}^{i}$ in which the DN technical constraints are not violated;

- **Step 5)** all pairs of values ($C_i^{DN}$, $P_{POI}^{i}$) obtained for $i = 0, ..., N_s$ are interpolated through a polynomial interpolation in such a way to obtain a quadratic cost curve for the aggregated DERs [126];

- **Step 6)** the parameters $\alpha$, $\beta$ and $\gamma$ of the obtained cost curve are sent to the TSO;

- **Step 7)** the TSO clears the central market and communicates to the DSO the amount of flexibility desired at the POI;

- **Step 8)** the DSO performs a new dispatch of DERs located in the distribution grid taking into account its own needs and the flexibility required by the TSO.

Applications of the smart aggregation approach in a TSO-DSO coordination framework can be found in [84], in which the SAA was employed to the Common (Decentralized version) and Local AS Market models proposed by SmartNet. In the former market scheme, the SAA is directly applied to aggregate all flexibility resources available in the distribution network. While, in the Local market model of SmartNet (see Multi-level Market model in Section 2.3.2), the smart aggregation is performed only for resources not contracted by the DSO, which has priority on DERs procurement.

However, the aggregation of DERs performed according to this process may be affected by unwanted approximations. First, because the cost curve obtained through the interpolation process at **Step 6)** might not pass through all points calculated with the OPF routines, introducing estimation errors (See Figure 4.13). In addition, it should be considered that amount and cost of the active power available at the POI may depend on the reactive power at the TN/DN interconnection point. Therefore, the amount of flexibility available in a specific POI is influenced by the effective status of the interfaced transmission-distribution grids. Since DN flexibility is estimated by the DSO before the central market is cleared and a new generation asset at the TN level is implemented, a criterion to establish the reactive power to be assumed at the POI in aggregating DERs need to be defined. In thise sense, the SAA described in [84] does not provide details about the value of reactive power to be considered at the POI in performing the smart aggregation of DERs. However, in order to aggregate DERs with more realistic operating conditions, the value of reactive power at POI can be assumed taking Day-ahead market operating conditions into account.

Simulation tests of the above described SAA applied to the Common and Local Market models, with the aim to solve CM issues at TN and DN level, were performed in [127] and described in this work of thesis in Section 4.3.3.

# Chapter 4

# New methodologies for CM and Balancing

In this chapter, the methodologies developed with the aim to implement optimal dispatch of DERs in decentralized TSO-DSO coordination schemes were described. First, a new algorithm for mapping the flexibility area at TN-DN interfacing point, based on a three-phase optimal power flow routine, was provided. Then, the algorithms of two alternative methodologies to aggregate flexibility resources located in distribution networks interfaced with the TN through multiple POIs were described. Finally, a Benders decomposition algorithm able to optimize TN and DN flexibility resources in a few decentralized TSO-DSO coordination schemes was also presented. Proposed methodologies were validated by means of simulation tests below described.

## 4.1 Mapping flexibility area through Three-phase Distribution Optimal Power Flow

As specified in Section 3.2, establishing the flexibility area at TN-DN interfacing point allows the DSO to calculate and communicate to the TSO the amount of flexibility available at the same POI without having to share with it reserved data about DN model or status. Several methodologies have been proposed in the literature with the aim of

mapping this area. However, OPF-based approaches proposed in the literature mainly focused on medium voltage scenarios [21], [119], [120], [125]. Very few examples investigated cases of MV and LV distribution networks, as in [128], where a single-phase constrained OPF algorithm was applied. This aspect could be crucial, since, as highlighted from [18], tools suitable to handle the unbalanced nature of distribution networks, and therefore to implement an effective TSO-DSO coordination, are lacking. In this sense, the authors of [18] highlighted the necessity of comprehensive three-phase approaches able to investigate multiple voltages levels (e.g., MV and LV), as well as capture the effects of DERs and controllable assets.

In order to face this challenge, a new methodology derived from the TOPF approach described in [129], [130], suitable for MV/LV unbalanced distribution grids, was developed and described as follow. In order to validate the proposed approach, simulation tests were performed on a portion of an Italian distribution grid, comprising about six hundred MV/LV buses. Here, the availability of both active and reactive flexibility resources as controllable loads and PV resources was assumed.

### 4.1.1 TOPF Mathematical formualtion

In general, an optimal power flow problem can be formulated as follow:

$$\min_{\mathbf{u}} C(\mathbf{x}, \mathbf{u}) \tag{4.1}$$

subject to:

$$f(\mathbf{x}, \mathbf{u}) = 0 \tag{4.2}$$

$$g(\mathbf{x}, \mathbf{u}) \leq 0 \tag{4.3}$$

where $C$ is the overall function to minimize, $\mathbf{x} \in \Re^n$ is the $n-$dimension state variable vector, $\mathbf{u} \in \Re^m$ is the $m-$dimension control variable vector. The function $f$ is the set of load flow equations, taking into account the multi-phase representation instead of the typical single-line equivalent model. Function $g$ is associated to the set of inequality constraints that keep into account maximum active/reactive power of devices and transformers, nominal current of feeders, and further technical constraints. Cur-

rent and voltage constraints are aimed to avoid security violations at each phase of the controlled circuit elements.

By means of a penalty method, inequality constraints of $g$ can be treated as soft inequality constraints. Therefore, the overall formulation becomes:

$$\min_{\mathbf{u}} [C_O(\mathbf{x},\mathbf{u}) + C_P(\mathbf{x},\mathbf{u})] \tag{4.4}$$

subject to

$$f(\mathbf{x},\mathbf{u}) = 0 \tag{4.5}$$

and to the following domain of the control variables:

$$\mathbf{u_{min}} \leq \mathbf{u} \leq \mathbf{u_{max}}$$

The function $C_O$ is the *objective function* to be optimized together with $C_P$, which represents the overall *penalty cost function*. In particular, the objective function $C_O$ has been derived from [131]:

$$C_O(\mathbf{x},\mathbf{u}) = \sum_{i=1}^{n_{TR}} \alpha \cdot \left( \frac{P_{tr,i}}{S_{tr,i}^{max}} \right) + \sum_{i=1}^{n_{TR}} \beta \cdot \left( \frac{Q_{tr,i}}{S_{tr,i}^{max}} \right) \tag{4.6}$$

with:

$$\alpha = -cos(\theta) \;\; and \;\; \beta = -sin(\theta) \tag{4.7}$$

where $n_{TR}$ is the number of HV/MV transformers at the TSO/DSO point of interconnection, $\alpha$ and $\beta$ are the weight factors, $P_{tr,i}$ and $Q_{tr,i}$ are respectively the actual active and reactive power of the $i-$th HV/MV transformer at the TSO/DSO point of interconnection, and $S_{tr,i}^{max}$ is its rated apparent power. As shown in Fig. 4.1, the angle $\theta$ represents the direction of maximization of the power exchanged at the POI in the plane $(P,Q)$.

The overall penalty cost function $C_P$ was defined as:

$$C_P(\mathbf{x},\mathbf{u}) = C_{P,1}(\mathbf{x},\mathbf{u}) + C_{P,2}(\mathbf{x},\mathbf{u}) + C_{P,3}(\mathbf{x},\mathbf{u}) \tag{4.8}$$

where $C_{P,1}$, $C_{P,2}$ and $C_{P,3}$ are three different penalty functions taking into account grid

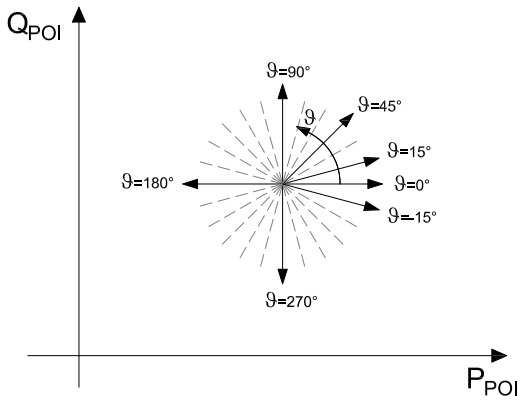


Figure 4.1: Directions of maximization in $(P,Q)$ plane

constraints. $C_{P,1}$ is the penalty cost that takes into account current limits of each $p-$th wire of the $j-$th medium/low voltage feeder.

$$C_{P,1}(\mathbf{x},\mathbf{u}) = \sum_{j=1}^{n_{feed}} \sum_{p=1}^{n_{wires}} \alpha_1 \cdot \left( \frac{I_{j,p} - I_{j,p}^{max}}{I_{j,p}^{max}} \right)^2 \tag{4.9}$$

with:

$$\alpha_1 = 0 \text{ if } I_{j,p} < I_{j,p}^{max}$$

where $\alpha_1$ is a weight factor, $n_{wires}$ the number of conductors of each one of the $n_{feed}$ feeders at medium and low voltage level. $I_{j,p}$ and $I_{j,p}^{max}$ are the actual and maximum current values of feeders.

The second penalty function, $C_{P,2}$, is associated to the maximum apparent power of the $n_{TR}$ HV/MV and $n_{tr}$ MV/LV transformers.

$$C_{P,2}(\mathbf{x},\mathbf{u}) = \sum_{i=1}^{n_{TR}+n_{tr}} \alpha_2 \cdot \left( \frac{S_{tr,i} - S_{tr,i}^{max}}{S_{tr,i}^{max}} \right)^2 \tag{4.10}$$

with:

$$\alpha_2 = 0 \text{ if } S_{tr,i} < S_{tr,i}^{max}$$

where $\alpha_2$ is a weight factor, $S_{tr,i}$ the actual apparent power flowing in the $i-$th HV/MV or MV/LV transformer, and $S_{tr,i}^{max}$ its rated power.

The third term of eq. (4.8), $C_{P,3}$, is related to the lower or upper voltage constraints, calculated for each phase of the $n_{bus}$ buses at both MV and LV level.

$$C_{P,3}(\mathbf{x},\mathbf{u}) = \sum_{k=1}^{n_{bus}} \sum_{p=1}^{n_{phases}} \alpha_3 \cdot \left( \frac{V_{k,p} - V_{k,p}^{lim}}{V_{k,p}^{lim}} \right)^2 \tag{4.11}$$

with:

$$\alpha_3{=}0 \quad \text{if} \quad V_{k,p}^{min} < V_{k,p} < V_{k,p}^{max}$$

$$V_{k,p}^{lim} = V_{k,p}^{min} \quad \text{if} \quad V_{k,p} < V_{k,p}^{min}$$

$$V_{k,p}^{lim} = V_{k,p}^{max} \quad \text{if} \quad V_{k,p} > V_{k,p}^{max}$$

where $\alpha_3$ is a weight factor, $V_{k,p}$ and $V_{k,p}^{lim}$ are respectively the actual and the min/max voltage of the $p-$th phase of the $k-$th MV/LV bus. Minimum and maximum voltages $V_{k,p}^{min}$ and $V_{k,p}^{max}$ can be specified for each bus and each phase.

### 4.1.2 Proposed methodology

The constrained problem described in (4.4)-(4.11) can be difficulty tackled, especially if the TOPF formulation requires the solution of multi-phase circuits and radial or weakly meshed networks. For this reason, in [130] it was proposed to simplify its formulation by applying the Implicit Function Theorem and reformulate the TOPF as an unconstrained problem:

$$\min_{\mathbf{u}} C(\gamma(\mathbf{u}),\mathbf{u}) \tag{4.12}$$

whose minimum can be obtained by solving

$$F(\mathbf{u}) = \frac{dC(\gamma(\mathbf{u}),\mathbf{u})}{d\mathbf{u}} = 0 \tag{4.13}$$

To solve equation (4.13), several non-linear programming techniques can be used. In this study, a quasi-Newton method was employed to avoid the calculation of the

second-order derivative of $C(\mathbf{u})$. Quasi-newton methods are characterized by an iterative approximation of the Hessian matrix, based on the calculation of the first-order derivatives. As in [130], first-order derivatives are calculated numerically exploiting the fast convergence properties of the OpenDSS software [132], whereas the Hessian can be approximated using full-matrix or even more simplified formulation. In this study, given the limited number of assumed variables, a diagonal matrix formulation, as in Barzilai and Borwein methods [133] , [134], was adopted.

### 4.1.3 TOPF application for flexibility region estimation

The procedure employed to estimate the flexibility region is described in the following. As a first step of the proposed approach, the blue coloured boundary represented in Fig. 4.2, is determined.

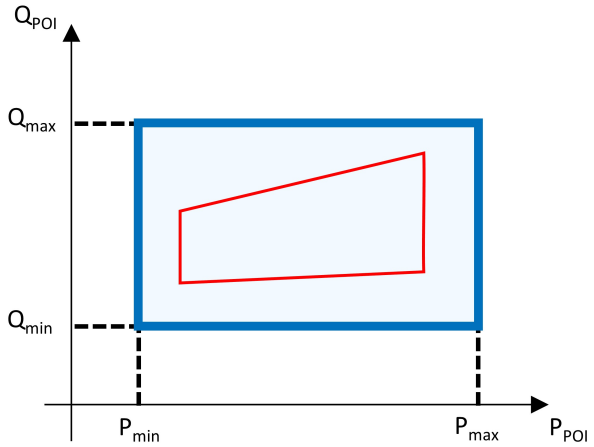


Figure 4.2: Example of flexibility region and ideal boundaries

It allows to draw approximated ideal boundaries in which the flexibility region will be situated. This theoretical area is drawn considering the results of four OPF routines aimed respectively at maximizing and minimizing, active and reactive power, neglecting all technical and security constraints. The solutions of these OPFs allow to dispatch all flexibility resources at their maximum or minimum value.

Afterwards, the actual flexibility region, which keeps into account technical grid constraints, and represented with a red line in Fig. 4.2, is calculated by means of the

proposed TOPF approach. The procedure consists of the following steps:

1. Maximum and minimum injections of active power $P_{POI}$ at the TSO-DSO interface point are searched for directions $\theta = 0°$ and $\theta = 180°$, respectively. Therefore TOPF routine is performed assuming in (4.6): $\alpha = -1$, $\beta = 0$ and, then, $\alpha = 1$, $\beta = 0$.

2. Maximum and minimum injections of reactive power $Q_{POI}$ at the TSO-DSO interface point are searched for directions $\theta = 90°$ and $\theta = 270°$, respectively. Therefore TOPF routine is performed assuming in (4.6): $\alpha = 0$, $\beta = -1$ and, then, $\alpha = 0$, $\beta = 1$.

3. The whole region perimeter can be mapped with more accuracy solving TOPF for a predefined number of directions $n_{dir}$, such that $\theta_k = k \cdot 360°/n_{dir}$, for $k = 1, ..., n_{dir}$ (as in Fig. 4.1 ). Each obtained solution is used to build the flexibility region, as vertex of a polygonal figure.

In order to speed up the whole process and increase the convergence behavior of the algorithm, each TOPF solution can use, as an initial guess, the solution already found using the closest direction (i.e. the solving algorithm for direction $\theta_k$ is initialized with the solution found for $\theta_{k-1}$). Each iterative TOPF routine is stopped when the mismatch on variable updates is less than an assumed tolerance.

### 4.1.4 TOPF Simulation Tests

The proposed approach was tested on the model of a real MV/LV distribution network, representing a portion of the distribution grid in the City of Bari (Italy). This network is radial and interfaced with the transmission by means of two 150/20 kV transformers located in the same primary substation (POI). This grid model comprises three whole MV feeders supplying 22 secondary substations and LV circuits represented by means of a 4-wire model. More specifically, it consists of 590 buses, 2289 nodes, 576 lines and 24 transformers. The concurrent presence of both single-phase or three-phase circuits and flexibility resources was assumed. In particular, 48 controllable loads and 21 photovoltaic units, connected at the low voltage level, were considered as flexible

resources. It was assumed that the controllable loads can be dispatched considering their own minimum and maximum active power limit values and a fixed power factor $cos(\varphi) = 0.9$. Therefore, active and reactive power of the controllable loads are interdependent, whereas it was assumed that PV generators can vary only their reactive power output. In particular, it was assumed that PV reactive power cannot exceed half of the active production. This condition corresponds to a minimum power factor of about 0.9 for both capacitive or inductive reactive generation.

Simulation tests were performed with an ordinary laptop PC having the following characteristics: Windows 10 Home, Intel® Core™ i7-7700HQ CPU @ 3.40 GHz (64 bits), and 16.0 GB RAM.

#### 4.1.4.1 Flexibility region mapping and comparison with Random Sampling

Firstly, the proposed methodology was applied to map the flexibility region of the distribution system described above in order to test the TOPF effectiveness. As presented in Tab. 4.1, the TOPF-based approach was run for three different tests.

Table 4.1: Estimation of the flexibility region

| **Applied method** | **Number of points** | **Flexibility area** $[A_{max}]$ | **Simulation time [s]** |
|---|---|---|---|
| *TOPF* | 4 | 37.1% | 404 |
| *TOPF* | 12 | 38.9% | 1391 |
| *TOPF* | 24 | 38.9% | 2880 |
| *RS* | 1000 | 10.6% | 128 |
| *RS* | 5000 | 17.8% | 1280 |
| *RS* | 50000 | 23.6% | 6390 |

Each test was characterized by a different number of points employed to construct the flexibility region boundary, namely 4, 12 and 24. This means that the optimal solutions were found for each direction at every 90°, 30°, and 15°, respectively. As shown in Fig. 4.3, the detail in the representation of the flexibility region improved when the number of calculated points increased. In this same figure, the region enclosed by the solid blue line represents the ideal boundary obtained by maximizing and minimizing

all active and reactive resources without considering security constraints. This area is

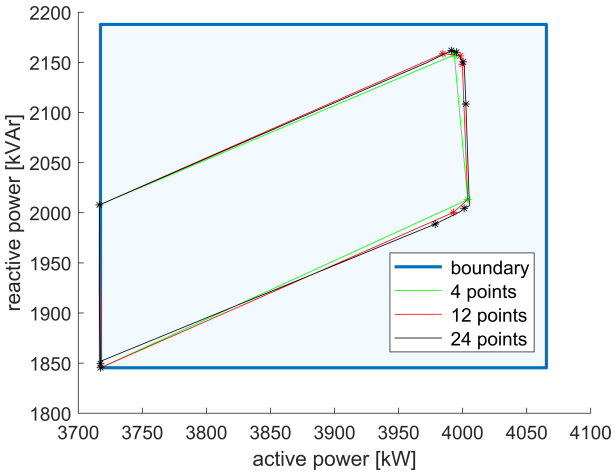


Figure 4.3: Flexibility regions comparison over different number of points

used as base value to compare the extension of the mapped areas. As shown in Tab. 4.1, the mapped region increased from 37.1 % to 38.9 % by employing 12 boundary points instead of 4, whereas simulation almost tripled. The third test showed that, by increasing the number of points from 12 to 24, no further significant improvements can be obtained. The mapped area was about the same of the previous test (38.9 %), whereas the required simulation time has almost doubled. The assumed interdependence of active and reactive power of flexible resources can be observed in Fig.4.3. The flexibility region is shaped as a parallelogram, laying in the $(P,Q)$ plane with lower and upper size sloping with respect to the $P_{axis}$. This slope is due to the assumption of the constant power factor of controllable loads. This is due to the fact that active power can be maximized (or minimized) only through an increase (decrease) of the overall consumption of reactive power. The proposed approach, based on a numerical evaluation of sensitivities, permits to deal very well with this kind of dependency.

Tab. 4.2 shows the convergence behaviour of the TOPF algorithm, applied to calculate the optimal solution for a specific slope θ (-30°). It can be noticed how the maximum value of flexibility was determined by balancing the objective function with respect to the penalty costs. It can be observed how, at iteration 9, TOPF converged towards an optimal point characterized by values of active and reactive power slightly

lower than previous iterations (e.g. iter. 3), but with reduced penalty costs.

Table 4.2: Iterative behaviour of the TOPF solution for slope $\theta = -30°$

| # *Iter.* | $P_{POI}$ [kW] | $Q_{POI}$ [kVAr] | $C_O$ [p.u.] | $C_{P,1}$ [p.u.] | $C_{P,2}$ [p.u.] | $C_{P,3}$ [p.u.] | *Tot. Cost* [p.u.] |
|---|---|---|---|---|---|---|---|
| 0 | 3978.61 | 1988.74 | -0.08461 | 0.00000 | 0.00000 | 0.00000 | -0.08461 |
| 1 | 3977.03 | 1988.91 | -0.08455 | 0.00000 | 0.00000 | 0.00000 | -0.08455 |
| 2 | 3992.50 | 2003.03 | -0.08477 | 0.00001 | 0.00001 | 0.00000 | -0.08476 |
| 3 | 4002.14 | 2000.73 | -0.08517 | 0.00004 | 0.00020 | 0.00006 | -0.08487 |
| 4 | 4000.45 | 2001.05 | -0.08510 | 0.00001 | 0.00016 | 0.00006 | -0.08488 |
| 5 | 3998.50 | 2001.09 | -0.08503 | 0.00000 | 0.00010 | 0.00005 | -0.08488 |
| 6 | 3995.29 | 2000.76 | -0.08493 | 0.00000 | 0.00001 | 0.00003 | -0.08489 |
| 7 | 3999.10 | 2001.47 | -0.08503 | 0.00003 | 0.00002 | 0.00000 | -0.08498 |
| 8 | 3998.32 | 2001.18 | -0.08501 | 0.00000 | 0.00002 | 0.00000 | -0.08499 |
| 9 | 3998.32 | 2001.18 | -0.08501 | 0.00000 | 0.00002 | 0.00000 | -0.08499 |

Further tests were carried out in order to compare the previous results with the ones obtainable through a Random Sampling (RS) approach. This second approach is based on performing a power flow for each sample, obtained by dispatching randomly flexibility resources, according to a uniform probability density function. Each solution was characterized by an overall penalty cost $C_p(\mathbf{x},\mathbf{u})$ calculated according to formulations (4.8) - (4.12). Among all obtained solutions, only the ones characterized by a penalty cost lower than a specific tolerance were considered feasible and, therefore, accepted. As described in Tab. 4.1, RS simulations were performed using 1000, 5000 and 50000 samples, respectively. Results are graphically shown in Figures 4.4, 4.5, 4.6 where all acceptable random samples are printed as blue dots.

Table 4.1 permits to compare numerically the RS approach with the proposed one. It can be noticed how increasing the number of samples from 1000 to 5000, and then to 50000, the estimated flexibility region can be considerably enlarged. However, in spite of a much higher computational burden, and even using 50000 samples, the mapped area is considerably smaller than the one obtained using just four points with the proposed TOPF approach. This result confirms the scarce efficacy of RS approaches in finding the most extreme power injection points [119].

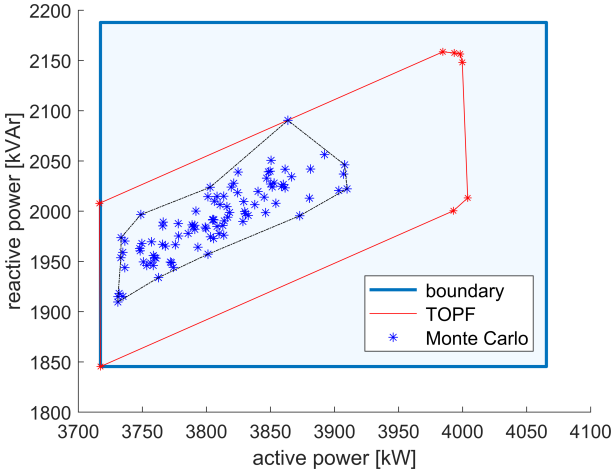


Figure 4.4: Flexibility region through Random Sampling approach using 1000 samples

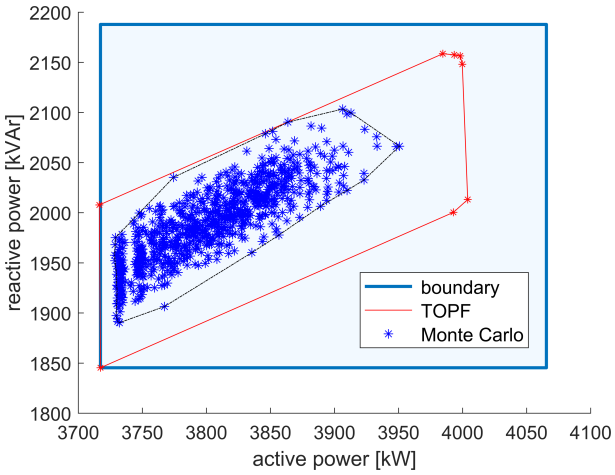


Figure 4.5: Flexibility region through Random Sampling approach using 5000 samples

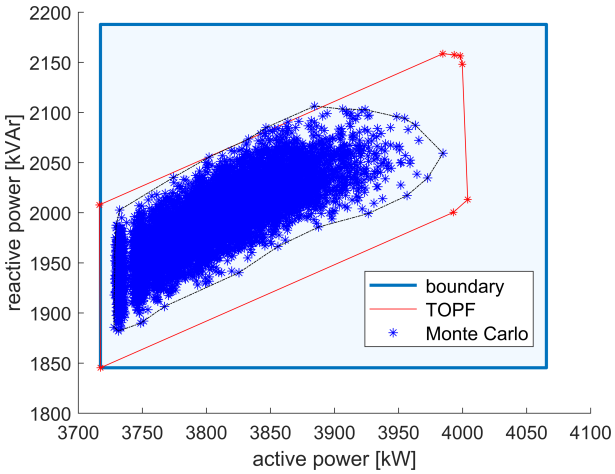


Figure 4.6: Flexibility region through Random Sampling approach using 50000 samples

#### 4.1.4.2 Influence of Voltage Constraints

Further tests were run in order to investigate the influence of security constraints on shape and boundary of the estimated flexibility region. In this context, the European Regulation EN 50160, with regard to the voltage characteristics of public electricity networks, establishes that, in ordinary conditions, grid voltages must be ranged between 0.90 p.u. and 1.10 p.u. [135]. Therefore, in our previous tests, the lower voltage limits were set accordingly.

A new test was run considering more severe voltage constraints with a lower and upper bound of 0.95-1.05 p.u., respectively. Fig. 4.7 shows the flexibility region obtained by using twelve points and two different lower voltage limits. As expected, stricter voltage constraints shrank the flexibility region from 38.9 % to 30.7 % (see Tab. 4.3). Nevertheless, as shown in Fig. 4.7, voltage limits had mainly influence on the right side of the estimated boundary. This is due to the fact that, with less strictly voltage requirements, a greater amount of power can be transferred at the POI. In this specific test case, upper voltage limits had no influence on the flexibility region. However, it can be easily imagined that upper voltage limits could be relevant in the case of reversed power flows and overgeneration conditions.

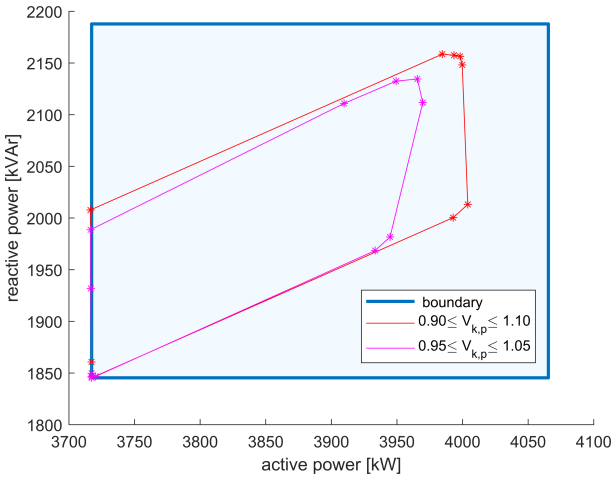


Figure 4.7: Flexibility region over different voltage limits

Table 4.3: Flexibility regions and voltage limits

| **Applied method** | **Number of points** | **Voltage limits [p.u.]** | **Flexibility area** $[A_{max}]$ |
|---|---|---|---|
| *TOPF* | 12 | $0.90 \leq V_{k,p} \leq 1.10$ | 38.9% |
| *TOPF* | 12 | $0.95 \leq V_{k,p} \leq 1.05$ | 30.7% |

### 4.1.5 TOPF Assessment

Test results of the three-phase unbalanced power flow algorithm proposed to estimate the flexibility region at the POI demonstrated the effectiveness of this approach. The performed simulations considered the availability of both active and reactive flexible resources, demonstrating the validity of the proposed methodology, which resulted more accurate and efficient with respect to the RS approaches. This advantage could also be more evident for larger network models, characterized by a wider number of flexible resources to be dispatched. Security constraints and operative technical limits can heavily influence shape and area of flexibility regions, and should be carefully chosen according to technical regulations and DSOs' operational practices.

This algorithm may find application in the AS market, allowing the DSO to estimate the amount of flexibility that can be provided from the DN to the TN without negatively affecting the DN constraints. In this sense, the proposed TOPF approach can be intended as a tool to implement any TSO-DSO coordination scheme in which flexibility resources are offered from the DSO to the TSO without communicating reserved data about the DN model or state. However, it should be considered that the estimation of the available flexibility should be done in advance or near real-time with respect to the time slots to which the AS market sessions relate. Consequently, according to the adopted strategy, such flexibility levels are estimated on the basis of forecasts or historical data and, thus, taking not into account the effective operating status of distribution networks (load conditions). The compliance of the activated flexibility should be verified in real-time, ensuring that DN constraints are respected during the AS provisioning. Distribution network constraints assumed in the proposed TOPF algorithm are enough conservative. Therefore, eventual significant power fluctuations should not jeopardize the distribution network operation. Additional TOPF routines might also be performed and repeated every 15/30 minutes, in what could be intended as an extended real-time framework of SCADA/DMS control function.

## 4.2 Aggregation of DERs for Multiple TSO-DSO interconnection points

As described in Chapter 2, in decentralized coordination schemes, like the Common (Decentralized version) and the Multi-level Market models, the DSO needs to aggregate DN DERs to be offered to the TSO in the central market. With this target, an aggregation methodology based on the SAA proposed by SmartNet was described in Section 3.3. This methodology refers to cases in which TSO and DSO are interfaced in a single point of interconnection (POI) and, therefore, with DN operated in a radial manner. However, although operating DN in this way is common among DSOs, in recent power systems, DN are also managed in a meshed manner. As a result, estimating the amount of flexibility that can be offered from the distribution to the transmission network in such conditions may be arduous. As described in [122], the main difficulty in these cases is in estimating with enough accuracy the impact of any active/reactive power variation for a specific POI on the other TN-DN interconnection points. Addressing this challenge, a few authors proposed suitable procedures for evaluating the flexibility area (See Section 3.2) at the TSO-DSO borders in case of multiple TN-DN interconnection points [122, 123, 124]. Nevertheless, as far as the author knows, a procedure for aggregating DERs and obtaining a cost curve of flexibility in case of multiple POIs has not been provided in the literature. In order to tackle this issue, two different procedures to aggregate flexibility resources in case of multiple POIs were derived from the SAA proposed by SmartNet in [84].

### 4.2.1 Smart Aggregation for Multiple POIs - Variant A (SAA-A)

This first proposed procedure, indicated as SAA-A, consists of the following steps:

- **Step 1)** in accordance with the first step described in Section 3.3, a flexibility range $[P_{POI}^{min}; P_{POI}^{max}]$ is individually calculated for all $n_{POI}$ POIs of the same DSO-area;
- **Step 2)** the minimum, $P_{DN}^{min}$, (maximum, $P_{DN}^{max}$,) value of flexibility that can be

provided from each DN to the TN is calculated as the sum of all $P_{POI}^{min}$ ($P_{POI}^{max}$) of POIs concerning the same DSO;

- **Step 3)** assuming a number of steps $N_s$ for which optimize the local market in the SAA, an incremental step of active power $\Delta P_{DN}$ is defined for the whole DN as:

$$\Delta P_{DN} = \frac{P_{DN}^{max} - P_{DN}^{min}}{N_s} \tag{4.14}$$

- **Step 4)** by means of optimal power flow routines, aimed at minimizing the total AS activation costs, the local market is cleared for each calculated value of active power $P_{DN}^{i}$:

$$\begin{aligned} P_{DN}^{i} &= P_{DN}^{min} + i \cdot \Delta P_{DN} \\ &\forall i = 0, ..., N_s \end{aligned} \tag{4.15}$$

Considering that, for each value $P_{DN}^{i}$, the active power exchanges at the POIs are treated as dependent variables, the following equation needs to be added to the OPF associated with the local market clearing process:

$$P_{POI,1} + ... + P_{POI,n_{POI}} = P_{DN}^{i} \tag{4.16}$$

- **Step 5)** the total AS activation cost $C_i^{DN}$ is calculated for each value $P_{DN}^{i}$ of flexibility globally provided by the DN, in which the DN technical constraints are not violated;

- **Step 6)** all pairs of values ($C_i^{DN}$, $P_{DN}^{i}$) obtained for $i = 0, ..., N_s$ are interpolated through a polynomial interpolation in such a way to obtain a quadratic cost curve for the aggregated DERs;

- **Step 7)** the parameters $\alpha$, $\beta$ and $\gamma$ of the obtained cost curve are sent to the TSO;

- **Step 8)** the TSO clears the central market considering the overall cost of the flexibility that can be provided from the DN through the $n_{POI}$ POIs;

- **Step 9)** the TSO communicates to the DSO the amount of flexibility desired at each POI;
- **Step 10)** the DSO performs a new optimal dispatch of DERs considering its own needs and the values of flexibility demanded at each POI by the TSO.

### 4.2.2 Smart Aggregation for Multiple POIs - Variant B (SAA-B)

This second aggregation method, named SAA-B, was also derived from the smart aggregation approach proposed by SmartNet. It can be described as follow:

- **Step 1)** in accordance with the first step described in Section 3.3, a flexibility range $[P^{min}_{POI}; P^{max}_{POI}]$ is individually calculated for both two $n_{POI}$ interfacing points belonging to the same DSO-area;
- **Step 2)** assuming a number of steps $N_s$, the incremental active power change for each $v$-th POI is defined as:

$$\Delta P_{POI,v} = \frac{P^{max}_{POI,v} - P^{min}_{POI,v}}{N_s} \qquad \forall v = 1, ..., n_{POI} \tag{4.17}$$

- **Step 3)** $(N_s \cdot N_s)$ OPF routines are performed at DN level considering all possible combinations of active power values at the POIs, assuming at the $v$-th generic interfacing point:

$$P^{i}_{POI,v} = P^{min}_{POI,v} + i \cdot \Delta P_{POI,v} \qquad \forall v = 1, ..., n_{POI} \qquad i = 0, ..., N_s \tag{4.18}$$

- **Step 5)** the AS activation cost $C^{DN}$ is calculated for those combinations of active power at the POIs in in which the DN technical constraints are not violated;

- **Step 6)** in order to obtain the quadratic cost curves associated with each POI, an interpolation procedure like that described in **Step 5)** of Sect. 3.3 may be applied. However, since in this case, the operational costs are calculated for $n_{POI}$ interconnection points, a multi-dimensional interpolation procedure has to be employed. Then, assuming $n_{POI} = 2$ for sake of clarity, the interpolated surface may be represented through the following expression:

$$p_{00} + p_{10} \cdot P_{POI,1} + p_{20} \cdot P_{POI,1}^2 + p_{11} \cdot P_{POI,1} P_{POI,2} + p_{01} \cdot P_{POI,2} + p_{02} \cdot P_{POI,2}^2 \tag{4.19}$$

- **Step 7)** the parameters $(p_{00}, p_{10}, p_{20}, p_{11}, p_{01}, p_{02})$ obtained through the performed interpolation are communicated to the TSO in order to take AS activation costs of flexibility provided through both POIs of DNs into account.

- **Step 8)** the procedures follows as in Variant A.

An application of these methodologies was carried out and described in Section 4.3.3.6. In performed simulation tests, two different interpolations were performed for Variant B, indicated as SAA-B1 and SAA-B2, depending on whether the parameter $p_{11}$ was assumed to be null or not.

As an attention point, it should be considered that the proposed SAA methodologies are based on a discrete number of OPF routines and, thus, eventual discontinuities related to unfeasible solutions might be not taken into account in the interpolated curves. Consequently, in cases where the power exchange values resulting from the central market correspond to unfeasible solutions, the procedure must be repeated assuming constrained values.

## 4.3 Benders Decomposition algorithm

Decomposition algorithms represent a suitable approach to implement a coordinated dispatch of DERs in decentralized architectures, as an alternative to the flexibility area estimation and the aggregation of DERs above presented. As described in Section 3.1.2, decomposition methodologies operate by dividing a complex optimization

problem into several sub-problems, which can be solved independently and, thus, easier to be solved than a single complex problem [104]. Therefore, this approach is very suitable for decentralized TSO-DSO coordination frameworks in which each grid operator is responsible for its own system.

Among various decomposition approaches proposed in the literature [110], there is the Benders decomposition algorithm (BDA). This methodology was initially developed for linear problems [116], [136], [137] and later extended also to non-linear formulations (Generalized Benders algorithm) [110], [111], as well as to integer, stochastic, multi-stage, bilevel and other optimization problems [112]. This methodology operates by breaking down the structure of a complex problem into one *Master problem (MP)* and one (or more) *Slave problem (SP)*, each one including part of the overall variables [106], [110]. In such a way, each system operator can also implement the OPF tool that best fits the features of the optimized system (radial or meshed grid, DC or AC, ...).

Thanks to its characteristics, the Benders decomposition algorithm is able to ensure decentralization and hierarchical priority in procuring resources from DSOs as well as to avoid approximations generated by the resource aggregation performed by other techniques. In addition, a BDA can also address the TSO-DSO coordination problems in which the transmission and distribution grids are interfaced with each other in multiple POIs. A focus on this issue was provided in Section 4.2.

In the literature, several applications of the BDA are proposed [112]. A Benders algorithm application for scheduling power plant preventive maintenance can be found in [137], while a BDA for corrective risk-based security-constrained OPF is described in [138]. In addition, BDA applications have been also proposed for transmission-constrained unit commitment [108], TN design [139], and planning of TN and DN with the integration of smart grid technologies [140].

Cases of the BDA application in a TSO-DSO coordination framework can be found in [106] and [141]. Both of them focused on a DERs optimal dispatch problem in the presence of a Common AS market scheme. In particular, [141] proposed a hierarchical coordination mechanism based on the communication of a set of parameters (Generalized Bid Function) of an affine approximator associated with the Benders cuts (see

Section 4.3.1 for further details).

The present work investigated the possibility to implement a full-iterative Benders decomposition algorithm to be applied on three different TSO-DSO coordination schemes [127], [142]. In particular, it was applied on the Common (decentralized version), Local, and Shared balancing responsibility AS market schemes proposed by the SmartNet project [36]. These coordination schemes play an important role in Italy since they have been examined by the Italian regulator ARERA in the consultation document 322/2019/R/EEL [74] for the exploitation of DERs in Congestion Management issues. In order to test the proposed methodology based on a Benders decomposition algorithm, four different test cases of CM issues have been solved for a power system including one transmission network interfaced with two distribution grids. In order to assess the proposed approach, test results were also compared with those obtained from the application of the aggregation strategy proposed by SmartNet (see Section 3.3). Furthermore, since the proposed algorithm is able to also address cases of multiple interconnections between the TSO and a DSO, an additional test was performed assuming two POIs for each TN-DN interconnection. Obtained test results were also compared with those obtained from the aggregation approach proposed for multiple POIs, described in Section 4.2. Please, note that, although the applications of the proposed Benders decomposition strategy have been reported in [127] and [142], only test results of [127] are described in this thesis for sake of brevity. In fact, this first reference concerns the application of the BDA on all of the three investigated market models. Whereas, [142] focused only on the Local AS market model and assumed a single TN-DN interconnection point.

### 4.3.1 Algorithm description

In accordance with the structure of the Benders decomposition algorithm, the optimal dispatch problem described in Section 3.1.1, concerning the centralized dispatch of the AS resources, is decomposed. In particular, the formulation (3.1)-(3.4) can be split in such a way to obtain a Master problem, associated with the cost function $C^{TN}(\mathbf{u}^{TN})$ of (3.1) and the respective TN constraints in (3.2), and $n_{DSO}$ Slave problems (one for

DSO), associated with the $C_l^{DN}(\mathbf{u}_l^{DN})$ of (3.1), the DN constraints of (3.3) and the boundary constraints of (3.4). Based on this assumption, the proposed BDA can be described as follows.

### Master problem

At the generic iteration, the following MP is solved:

$$\begin{aligned} \min_{\mathbf{u}^{TN},\alpha} \; & C^{TN}(\mathbf{u}^{TN}) + \alpha \\ & < \textit{Benders cuts} > \\ & \mathbf{g}^{TN}(\mathbf{x}^{TN},\mathbf{u}^{TN}) = \mathbf{0} \\ & \mathbf{h}^{TN}(\mathbf{x}^{TN},\mathbf{u}^{TN}) \geq \mathbf{0} \\ & \alpha \geq 0 \end{aligned} \tag{4.20}$$

in which $C^{TN}$ represent the activation costs of AS resources at TN level. These costs depend on control variable $\mathbf{u}^{TN}$, which denotes the arrays of the active and reactive power of dispatchable resources located in the transmission network. The array $\mathbf{x}^{TN}$ represents the state variable for the transmission grid. While, $\mathbf{g}^{TN}$ and $\mathbf{h}^{TN}$ denote, respectively, the TN equality and inequality constraints. The control variable $\alpha$ is additional with respect to the formulation (3.1) and represents the cost contribution of each distribution network on the MP objective function. For each iteration, the optimal value of $\alpha$ is evaluated considering the Benders cuts obtained from previous iterations. Therefore, at the initial iteration, $< \textit{Benders cuts} >$ is empty [143]. The Master problem represented in (4.20) is assumed to be feasible, otherwise, the decomposed problem is proven to be unfeasible and the BDA is stopped.

### Slave problem

After that the Master problem has been solved, the solutions $\hat{\mathbf{x}}_{POI,l,v}^{TN}$ obtained for all

$n_{POI,l}$ TN-DN interfacing points of the $l$-th DSO are passed to the corresponding $l$-th Slave problem:

$$\begin{aligned} &\min_{\mathbf{u}_l^{DN}} C_l^{DN}(\mathbf{u}_l^{DN}) \\ &\mathbf{g}_l^{DN}(\mathbf{x}_l^{DN}, \mathbf{u}_l^{DN}) = \mathbf{0} \\ &\mathbf{h}_l^{DN}(\mathbf{x}_l^{DN}, \mathbf{u}_l^{DN}) \geq \mathbf{0} \\ &\mathbf{x}_{POI,l,v}^{TN} + \mathbf{x}_{POI,l,v}^{DN} = \mathbf{0} \\ &\mathbf{x}_{POI,l,v}^{TN} = \hat{\mathbf{x}}_{POI,l,v}^{TN} \quad \xrightarrow[\text{variable}]{dual} \lambda_{l,v} \\ &l = 1,2,...,n_{DSO} \\ &\forall v = 1,2,...,n_{POI,l} \end{aligned} \tag{4.21}$$

in which $C_l^{DN}$ represents the activation costs of AS resources at DN level. These costs depend on the control variable $\mathbf{u}_l^{DN}$, which denotes the arrays of the active and reactive power of dispatchable resources located in the $l-$th distribution network. The array $\mathbf{x}_l^{DN}$ represents the state variable for the $l-$th distribution grid. While, $\mathbf{g}_l^{DN}$ and $\mathbf{h}_l^{DN}$ denote, respectively, the equality and inequality constraints for the $l-$th distribution grid. The vector $\lambda_{l,v}$ of dimension $(2 \times 1)$ is obtained by solving the dual of (4.21) and is associated with the boundary variable $\mathbf{x}_{POI,l,v}^{TN}$.

### Unfeasible Slave problem

According to the values of $\hat{\mathbf{x}}_{POI,l,v}^{TN}$ set by the Master problem at each iteration, if a $l$-th SP is proven to be unfeasible, formulation (4.21) needs to be modified for the

corresponding $l$-th SP by adding two sets of slack variables and a penalty cost:

$$\begin{aligned}
\min_{\mathbf{u}_l^{DN},\mathbf{t}_{l,v},\mathbf{w}_{l,v}} \quad & C_l^{DN}(\mathbf{u}_l^{DN}) + \mathbf{m}_l[\mathbf{t}_{l,v} + \mathbf{w}_{l,v}] \\
& \mathbf{g}_l^{DN}(\mathbf{x}_l^{DN}, \mathbf{u}_l^{DN}) = \mathbf{0} \\
& \mathbf{h}_l^{DN}(\mathbf{x}_l^{DN}, \mathbf{u}_l^{DN}) \geq \mathbf{0} \\
& \mathbf{x}_{POI,l,v}^{TN} + \mathbf{x}_{POI,l,v}^{DN} + (\mathbf{t}_{l,v} - \mathbf{w}_{l,v}) = \mathbf{0} \\
& \mathbf{x}_{POI,l,v}^{TN} = \hat{\mathbf{x}}_{POI,l,v}^{TN} \quad \xrightarrow[\text{variable}]{dual} \lambda_{l,v} \\
& 0 \leq \mathbf{t}_{l,v} \leq \mathbf{t}_{l,v}^{max} \\
& 0 \leq \mathbf{w}_{l,v} \leq \mathbf{w}_{l,v}^{max} \\
& l = 1,2,...,n_{DSO} \\
& \forall\, v = 1,2,...,n_{POI,l}
\end{aligned} \tag{4.22}$$

The arrays $\mathbf{t}_{l,v}$ and $\mathbf{w}_{l,v}$ are two non-negative slack variables of dimension $(2 \times 1)$, which are limited to $\mathbf{t}_{l,v}^{max}$ and $\mathbf{w}_{l,v}^{max}$, respectively. While, $\mathbf{m}_l$ is a large enough positive constant associated with the $l$-th Slave problem and set arbitrarily [110]. The reason for using this high penalty is aimed at avoiding that non-feasible values of $\mathbf{x}_{POI,l,v}^{TN}$ are recalculated by the MP and proposed newly to the $l$-th SP at following iterations [110].

### Benders cuts

In order to reflect the solutions obtained from all Slave problems on the Master problem at the following BDA iteration, an *Optimal cut* is generated. Indicating by $(s)$ the index of the generic iteration, each Benders cut generated in $s = 1,2,...,n_{BD}$ is added to the original MP at each $(s+1)$-th iteration.

$$\begin{aligned}
\sum_{l=1}^{n_{DSO}} [C_l^{DN(s)}(\mathbf{u}_l^{DN(s)}) \; + \sum_{l=1}^{n_{DSO}} \left[ \sum_{v=1}^{n_{POI,l}} \lambda_{l,v}^{(s)} (\mathbf{x}_{POI,l,v}^{TN(s+1)} - \hat{\mathbf{x}}_{POI,l,v}^{TN(s)}) \right] \leq \alpha^{(s+1)} \\
s = 1,2,...,n_{BD}
\end{aligned} \tag{4.23}$$

in which $n_{BD}$ indicates the performed iterations.

In case the Slave problem has been solved through (4.22), the Benders cut generated by (4.23) is named *Feasibility cut* [144]. It avoids new unfeasible solutions being assigned again to the SP, but without affecting the final optimal solution [110].

The set of parameters $(\lambda_{l,v}^{(s)}, C_l^{DN(s)}, \hat{\mathbf{x}}_{POI,l,v}^{TN(s)})$ in (4.23) reflect the overall costs of the power injected at the POIs of distribution networks towards the transmission grid at the $s$-th iteration. Therefore, these parameters allow each DSO to communicate to the TSO the marginal costs of the resources activated at the $s$-th iteration taking into account grid constraints and losses of its own distribution grid. Figure 4.8 shows the data exchange between the TSO and all the DSOs at each iteration.

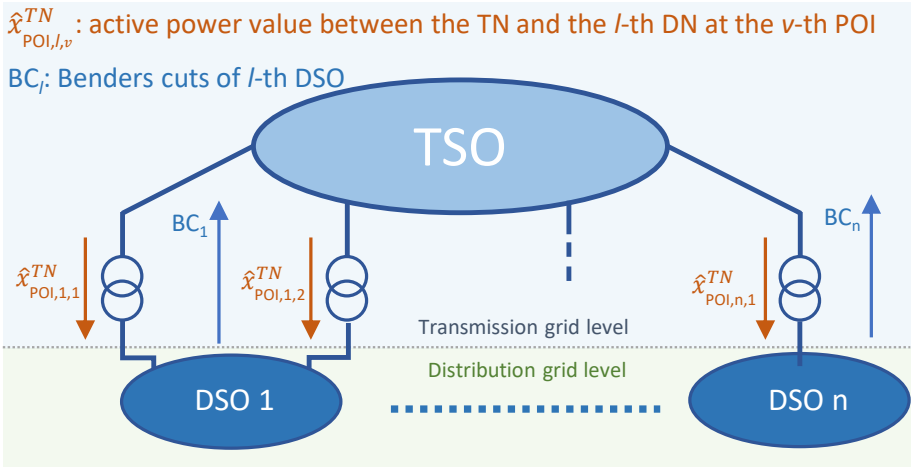


Figure 4.8: Data exchange between TSO and DSOs

### Convergence checking

As the last step, an *upper bound*, $z_{up}^{(s)}$, and a *lower bound*, $z_{low}^{(s)}$, defined as follow, are calculated to verify if an optimal solution has been reached [21]:

$$\begin{aligned} z_{up}^{(s)} &= C^{TN(s)}(\mathbf{u}^{TN(s)}) + \sum_{l=1}^{n_{DSO}} C_l^{DN(s)}(\mathbf{u}_l^{DN(s)}) \\ z_{low}^{(s)} &= C^{TN(s)}(\mathbf{u}^{TN(s)}) + \alpha^{(s)} \end{aligned} \tag{4.24}$$

Formulation (4.20)-(4.24) concerning the Benders decomposition algorithm is reiter-

ated until an established relative cost tolerance ε has been reached:

$$(z_{up}^{(s)} - z_{low}^{(s)})/z_{up}^{(s)} > \varepsilon \tag{4.25}$$

The implemented BDA is illustrated in Figure 4.9.

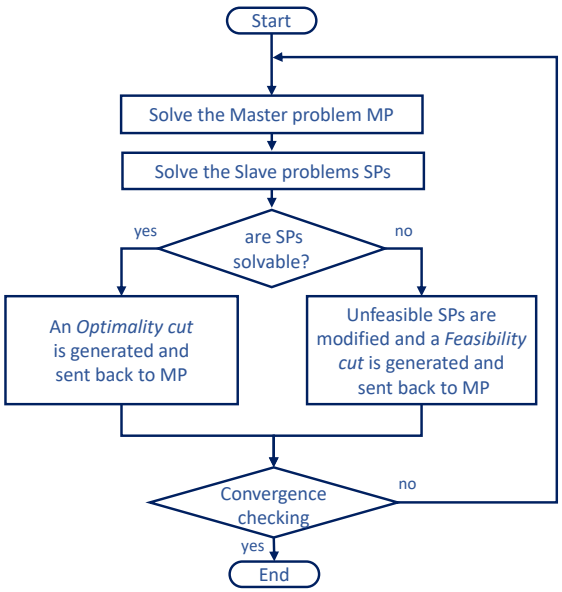


Figure 4.9: The Benders decomposition algorithm

### 4.3.2 Application of Benders Decomposition Algorithm

With the aim to apply the proposed Benders decomposition Algorithm to the Common (Decentralized version), Local and Shared balancing responsibility AS market models proposed by SmartNet [36], described in Chapter 2, details about the application of the BDA on these market schemes are provided below.

**Common AS Market model (Decentralized version)**

The application of the proposed BDA to the Common Decentralized AS Market model is straightforward. In this case, the Master problem can be associated with the mathematical problem of the TSO and the Slave problems with those of the respective DSOs.

**Local AS Market model**

As specified in Chapter 2, in this market model, the DSO has priority on procuring flexibility resources located at the DN level. Therefore, as a preliminary step (PS), the local market is run first with the aim to solve the DSO needs. Next, once the local market has been cleared, the remaining DERs are offered to the TSO to solve the central needs also.

In this coordination scheme, the proposed BDA is employed subsequently to the PS to clear the central market considering both TN and DN remaining AS resources. Therefore, a new feasible domain is introduced by means of $\mathbf{x}_l^{*DN}$ and $\mathbf{u}_l^{*DN}$ to indicate the residual DN DERs that can be offered from the local to the central market. Formulation (4.26) replaces the DN constraints in the Slave problem (4.21), (4.22).

$$\begin{aligned} \mathbf{g}_l^{DN}(\mathbf{x}_l^{*DN}, \mathbf{u}_l^{*DN}) &= \mathbf{0} \\ \mathbf{h}_l^{DN}(\mathbf{x}_l^{*DN}, \mathbf{u}_l^{*DN}) &\geq \mathbf{0} \end{aligned} \tag{4.26}$$

**Shared balancing responsibility Market model**

The formulated BDA may also be applied to the Shared balancing responsibility Market model without the need to introduce relevant changes to the BDA mathematical formulation. In this case, each DSO is responsible for balancing its own area and ensuring that the power exchange scheduled at each POI $\tilde{\mathbf{x}}_{POI,l,v}$ is satisfied.

With this aim, in accordance with the strategy proposed in [91], an additional penalty cost is introduced into the objective function of the MP (4.20) to find alternative optimal solutions for those cases in which the DSOs are not able to fulfill the scheduled power exchanges for their own areas:

$$\min_{\mathbf{u}^{TN},\alpha} C^{TN}(\mathbf{u}^{TN}) + M_{l,v}(\mathbf{x}_{POI,l,v} - \tilde{\mathbf{x}}_{POI,l,v}) + \alpha \tag{4.27}$$

in which $M_{l,v}$ is the penalty factor applied when the power exchange set at the $v$-th POI of the $l$-th DSO is not satisfied.

### 4.3.3 Test Cases

In order to test the proposed BDA, a congestion management issue at both DN and DN levels was simulated and solved in the Common, Local, and Shared TSO-DSO AS market models [127]. Solutions obtained by using the formulas of the centralized approach (3.1)-(3.4) were assumed as an ideal benchmark since obtained by assuming that the MO had complete knowledge of both DN and DNs and, thus, without introducing any approximation. This algorithm was identified as Ideal Centralized Approach (ICA). The same simulations were also been carried out through the above-described smart aggregation approach (SAA). This second method was employed to aggregate and offer DN resources to the TSO at the TN-DN point of interconnection, without communicating data about distribution grid constraints.

#### 4.3.3.1 Solver and grid models

Test results reported in this thesis are based on simulations described in [127]. These simulation tests were carried out on a simulated electrical system consisting of one transmission network, indicated as TN, connected to two separate distribution networks, DN #1 and DN #2. The TN is based on the IEEE 118-bus test case (Figure 4.10) [145], which includes nodes at 138 kV, 161 kV, and 345 kV. Thermal ratings of the transmission network were reasonably assumed to be 1000 MVA for the 345 kV branches, and 100 MVA for lower voltage lines. About what concerns distribution networks, DN #1 and DN #2 were built replicating (respectively 7 and 10 times) a modified version of the IEEE 33-node test feeder [146] shown in Figure 4.11, in which each feeder operates at 12.6 kV with a thermal rating of 7 MVA. The first and the second distribution networks include 226 and 322 medium voltage nodes, respectively. Table 4.4 lists the feeders of DN #1 (DN1_01-DN1_07) and DN #2 (DN2_01-DN2_10 ) and the respective nodes. It can be observed that the IDs assigned to the DN #1 and DN #2 nodes follows the IDs (#1-118) assigned to the TN nodes. In more detail, DN #1 is interfaced with the bus #19 of the TN by means of two 138 kV/12.6 kV, 25 MVA, parallel transformers, assumed located in the same primary substation. DN #2 is connected to the TN bus #49 by means of two 138 kV/12.6 kV parallel transformers having

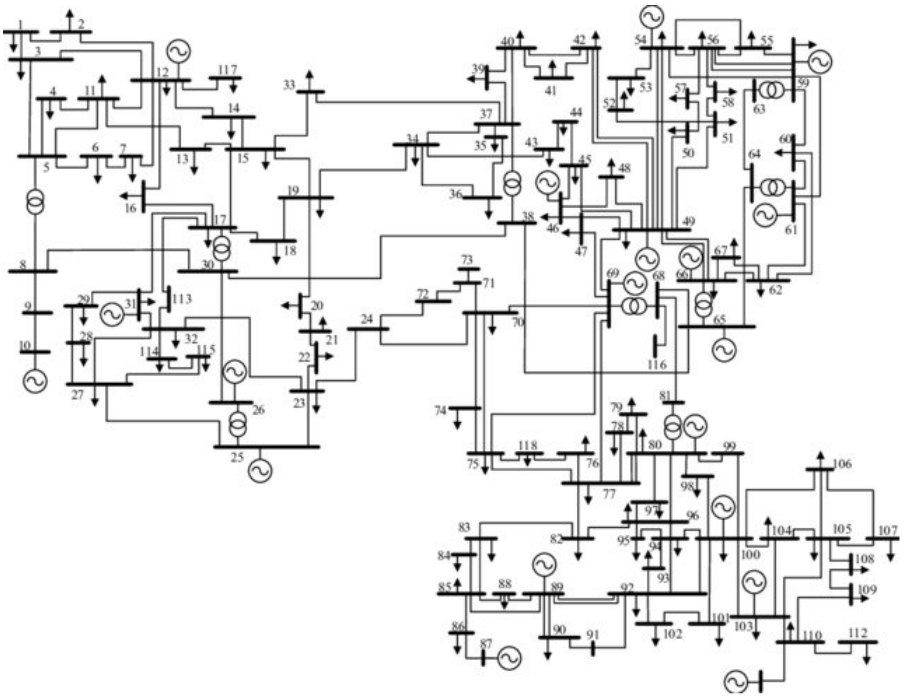

Figure 4.10: Diagram of IEEE 118-bus test case
(Source: [147])

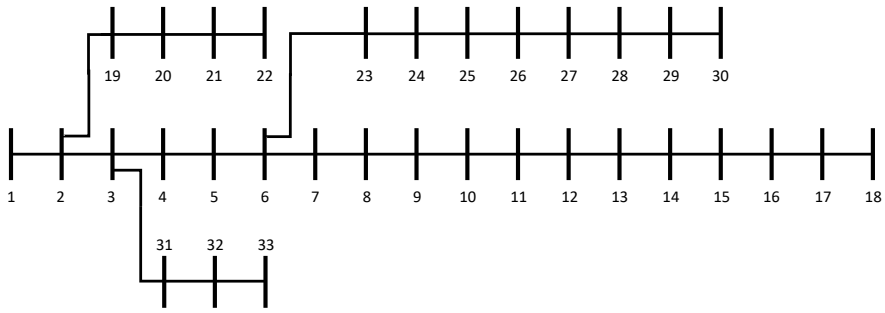


Figure 4.11: Diagram of the 33-bus test feeder

| Distribution grid | Feeder ID | From bus-To bus |
|---|---|---|
| DN #1 | DN1_01 | 187-223 |
| | DN1_02 | 224-260 |
| | DN1_03 | 261-297 |
| | DN1_04 | 298-334 |
| | DN1_05 | 335-371 |
| | DN1_06 | 372-408 |
| | DN1_07 | 409-446 |
| DN #2 | DN2_01 | 447-483 |
| | DN2_02 | 484-520 |
| | DN2_03 | 521-557 |
| | DN2_04 | 558-594 |
| | DN2_05 | 595-631 |
| | DN2_06 | 632-668 |
| | DN2_07 | 669-705 |
| | DN2_08 | 706-742 |
| | DN2_09 | 743-779 |
| | DN2_10 | 780-817 |

Table 4.4: Feeders description

sizes of 50 MVA and 25 MVA, respectively. Flexibility was assumed to be provided by dispatchable resources located at the TN and DN levels, having linear or quadratic activation costs. Tables 4.5-4.9 resume the BUS ID to which the dispatchable resources are connected, the active power ranges of load units (0-$P_{Load}$), the capability curves of generators ($P_{Gen}^{min}, P_{Gen}^{max}, Q_{Gen}^{min}, Q_{Gen}^{max}$) and the parameters defining the total cost function ($\alpha, \beta, \gamma$). Please, note that only generating units were assumed as flexibility resources at the TN level.

To test the proposed BDA methodology, simulations of the three investigated AS Market schemes were performed with the aim to remove congestion at TN and DN level. These simulations were carried through OPF routines based on Matpower Interior Point Solver (MIPS) [148], [149]. With the aim to perform a fair comparison with the proposed BDA, a convergence relative cost tolerance $\varepsilon$ of $10^{-4}$ p.u. was set for all tested methodologies (ICA, BDA, SAA). Simulations were run on an ordinary laptop PC with these characteristics: Windows 10 Home, Intel Core i7-7700HQ, CPU 3.40Ghz (64bits) and 16.0 GB RAM.

Dispatchable generators in the transmission grid

| Bus | $P_{Gen}^{min}$ | $P_{Gen}^{max}$ | $Q_{Gen}^{min}$ | $Q_{Gen}^{max}$ | α | β | γ |
|---|---|---|---|---|---|---|---|
| 1 | 0.00 | 100.00 | -5.00 | 15.00 | 0.01 | 400 | 0 |
| 4 | 0.00 | 100.00 | -300.00 | 300.00 | 0.01 | 400 | 0 |
| 6 | 0.00 | 100.00 | -13.00 | 50.00 | 0.01 | 400 | 0 |
| 8 | 0.00 | 100.00 | -300.00 | 300.00 | 0.01 | 400 | 0 |
| 10 | 0.00 | 550.00 | -147.00 | 200.00 | 0.02 | 200 | 0 |
| 12 | 0.00 | 185.00 | -35.00 | 120.00 | 0.12 | 200 | 0 |
| 15 | 0.00 | 100.00 | -10.00 | 30.00 | 0.01 | 400 | 0 |
| 18 | 0.00 | 100.00 | -16.00 | 50.00 | 0.01 | 400 | 0 |
| 19 | 0.00 | 100.00 | -8.00 | 24.00 | 0.01 | 400 | 0 |
| 24 | 0.00 | 100.00 | -300.00 | 300.00 | 0.01 | 400 | 0 |
| 25 | 0.00 | 320.00 | -47.00 | 140.00 | 0.05 | 200 | 0 |
| 26 | 0.00 | 414.00 | -1000.00 | 1000.00 | 0.03 | 200 | 0 |
| 27 | 0.00 | 100.00 | -300.00 | 300.00 | 0.01 | 400 | 0 |
| 31 | 0.00 | 107.00 | -300.00 | 300.00 | 1.43 | 200 | 0 |
| 32 | 0.00 | 100.00 | -14.00 | 42.00 | 0.01 | 400 | 0 |
| 34 | 0.00 | 100.00 | -8.00 | 24.00 | 0.01 | 400 | 0 |
| 36 | 0.00 | 100.00 | -8.00 | 24.00 | 0.01 | 400 | 0 |
| 40 | 0.00 | 100.00 | -300.00 | 300.00 | 0.01 | 400 | 0 |
| 42 | 0.00 | 100.00 | -300.00 | 300.00 | 0.01 | 400 | 0 |
| 46 | 0.00 | 119.00 | -100.00 | 100.00 | 0.53 | 200 | 0 |
| 49 | 0.00 | 304.00 | -85.00 | 210.00 | 0.05 | 200 | 0 |
| 54 | 0.00 | 148.00 | -300.00 | 300.00 | 0.21 | 200 | 0 |
| 55 | 0.00 | 100.00 | -8.00 | 23.00 | 0.01 | 400 | 0 |
| 56 | 0.00 | 100.00 | -8.00 | 15.00 | 0.01 | 400 | 0 |
| 59 | 0.00 | 255.00 | -60.00 | 180.00 | 0.06 | 200 | 0 |
| 61 | 0.00 | 260.00 | -100.00 | 300.00 | 0.06 | 200 | 0 |

Continued on next page

Table 4.5 – continued from previous page

| Bus | $P_{Gen}^{min}$ | $P_{Gen}^{max}$ | $Q_{Gen}^{min}$ | $Q_{Gen}^{max}$ | α | β | γ |
|---|---|---|---|---|---|---|---|
| 62 | 0.00 | 100.00 | -20.00 | 20.00 | 0.01 | 400 | 0 |
| 65 | 0.00 | 491.00 | -67.00 | 200.00 | 0.03 | 200 | 0 |
| 66 | 0.00 | 492.00 | -67.00 | 200.00 | 0.03 | 200 | 0 |
| 69 | 0.00 | 805.20 | -300.00 | 300.00 | 0.02 | 200 | 0 |
| 70 | 0.00 | 100.00 | -10.00 | 32.00 | 0.01 | 400 | 0 |
| 72 | 0.00 | 100.00 | -100.00 | 100.00 | 0.01 | 400 | 0 |
| 73 | 0.00 | 100.00 | -100.00 | 100.00 | 0.01 | 400 | 0 |
| 74 | 0.00 | 100.00 | -6.00 | 9.00 | 0.01 | 400 | 0 |
| 76 | 0.00 | 100.00 | -8.00 | 23.00 | 0.01 | 400 | 0 |
| 77 | 0.00 | 100.00 | -20.00 | 70.00 | 0.01 | 400 | 0 |
| 80 | 0.00 | 577.00 | -165.00 | 280.00 | 0.02 | 200 | 0 |
| 85 | 0.00 | 100.00 | -8.00 | 23.00 | 0.01 | 400 | 0 |
| 87 | 0.00 | 104.00 | -100.00 | 1000.00 | 2.50 | 20 | 0 |
| 89 | 0.00 | 707.00 | -210.00 | 300.00 | 0.02 | 200 | 0 |
| 90 | 0.00 | 100.00 | -300.00 | 300.00 | 0.01 | 400 | 0 |
| 91 | 0.00 | 100.00 | -100.00 | 100.00 | 0.01 | 400 | 0 |
| 92 | 0.00 | 100.00 | -3.00 | 9.00 | 0.01 | 400 | 0 |
| 99 | 0.00 | 100.00 | -100.00 | 100.00 | 0.01 | 400 | 0 |
| 100 | 0.00 | 352.00 | -50.00 | 155.00 | 0.04 | 20 | 0 |
| 103 | 0.00 | 140.00 | -15.00 | 40.00 | 0.25 | 200 | 0 |
| 104 | 0.00 | 100.00 | -8.00 | 23.00 | 0.01 | 400 | 0 |
| 105 | 0.00 | 100.00 | -8.00 | 23.00 | 0.01 | 400 | 0 |
| 107 | 0.00 | 100.00 | -200.00 | 200.00 | 0.01 | 400 | 0 |
| 110 | 0.00 | 100.00 | -8.00 | 23.00 | 0.01 | 400 | 0 |
| 111 | 0.00 | 136.00 | -100.00 | 1000.00 | 0.28 | 20 | 0 |
| 112 | 0.00 | 100.00 | -100.00 | 1000.00 | 0.01 | 400 | 0 |
| 113 | 0.00 | 100.00 | -100.00 | 200.00 | 0.01 | 400 | 0 |
| 116 | 0.00 | 100.00 | -1000.00 | 1000.00 | 0.01 | 400 | 0 |

| Bus ID | $P_{Gen}^{min}$ [MW] | $P_{Gen}^{max}$ [MW] | $Q_{Gen}^{min}$ [MVAr] | $Q_{Gen}^{max}$ [MVAr] | α [€/MW$^2$] | β [€/MW] | γ [€] |
|---|---|---|---|---|---|---|---|
| 120 | 0 | 5.00 | -5.00 | 5.00 | 0.05 | 350 | 0.00 |
| 165 | 0.00 | 1.20 | -1.20 | 1.20 | 0.05 | 150 | 0.00 |
| 180 | 0.00 | 0.80 | -0.80 | 0.80 | 0.8 | 240 | 0.00 |
| 220 | 0.00 | 2.00 | -1.00 | 1.00 | 0.62 | 180 | 0.00 |
| 225 | 0.00 | 1.00 | -0.50 | 0.50 | 0.41 | 240 | 0.00 |
| 235 | 0.00 | 1.00 | -0.80 | 0.80 | 0.04 | 150 | 0.00 |
| 242 | 0.00 | 0.20 | -0.20 | 0.20 | 1.00 | 180 | 0.00 |
| 285 | 0.00 | 1.60 | -1.50 | 1.50 | 8.40 | 250 | 0.00 |
| 290 | 0.00 | 0.40 | -0.40 | 0.40 | 0.12 | 150 | 0.00 |
| 305 | 0.00 | 0.80 | -0.60 | 0.60 | 0.6 | 200 | 0.00 |

Table 4.6: Dispatchable generators in distribution network #1

| Bus ID | $P_{Load}$ [MW] | α [€/MW$^2$] | β [€/MW] | γ [€] |
|---|---|---|---|---|
| 140 | 0.50 | 0.00 | 1100 | 0.00 |
| 145 | 0.80 | 0.00 | 1000 | 0.00 |
| 205 | 1.20 | 0.00 | 1200 | 0.00 |
| 270 | 0.70 | 0.00 | 2000 | 0.00 |
| 330 | 1.00 | 0.00 | 1500 | 0.00 |

Table 4.7: Dispatchable loads in distribution network #1

| Bus ID | $P_{Gen}^{min}$ [MW] | $P_{Gen}^{max}$ [MW] | $Q_{Gen}^{min}$ [MVAr] | $Q_{Gen}^{max}$ [MVAr] | α [€/MW$^2$] | β [€/MW] | γ [€] |
|---|---|---|---|---|---|---|---|
| 345 | 0.00 | 8.00 | -8.00 | 8.00 | 0.05 | 350 | 0.00 |
| 357 | 0.00 | 1.50 | -1.20 | 1.20 | 0.50 | 250 | 0.00 |
| 385 | 0.00 | 0.70 | -0.70 | 0.70 | 0.04 | 400 | 0.00 |
| 423 | 0.00 | 0.80 | -0.50 | 0.50 | 0.20 | 180 | 0.00 |
| 432 | 0.00 | 1.20 | -1.00 | 1.00 | 0.06 | 400 | 0.00 |
| 456 | 0.00 | 1.00 | -1.00 | 1.00 | 0.15 | 260 | 0.00 |
| 493 | 0.00 | 1.40 | -1.20 | 1.20 | 0.33 | 322 | 0.00 |
| 529 | 0.00 | 0.40 | -0.40 | 0.40 | 0.42 | 420 | 0.00 |
| 565 | 0.00 | 1.20 | -1.00 | 1.00 | 0.18 | 220 | 0.00 |
| 546 | 0.00 | 0.60 | -0.50 | 0.50 | 0.22 | 312 | 0.00 |
| 585 | 0.00 | 2.00 | -2.00 | 2.00 | 0.26 | 415 | 0.00 |
| 591 | 0.00 | 1.40 | -1.40 | 1.40 | 0.15 | 240 | 0.00 |
| 603 | 0.00 | 1.50 | -1.30 | 1.30 | 0.80 | 310 | 0.00 |
| 615 | 0.00 | 0.30 | -0.20 | 0.20 | 0.70 | 200 | 0.00 |

Table 4.8: Dispatchable generators in distribution network #2

| Bus ID | $P_{Load}$ [MW] | α [€/MW$^2$] | β [€/MW] | γ [€] |
|---|---|---|---|---|
| 360 | 0.40 | 0.00 | 1500 | 0.00 |
| 450 | 0.70 | 0.00 | 1600 | 0.00 |
| 480 | 1.20 | 0.00 | 1000 | 0.00 |
| 498 | 1.00 | 0.00 | 1200 | 0.00 |
| 520 | 0.40 | 0.00 | 1800 | 0.00 |
| 540 | 0.80 | 0.00 | 1100 | 0.00 |
| 580 | 0.60 | 0.00 | 1200 | 0.00 |
| 605 | 0.40 | 0.00 | 1300 | 0.00 |
| 612 | 0.50 | 0.00 | 1400 | 0.00 |

Table 4.9: Dispatchable loads in distribution network #2

#### 4.3.3.2 Case #1: congestion of TN lines

In the first test case, the congestion of some TN power lines was generated by an increase of load of 160 MW in proximity to the TN-DN #1 primary substation with respect to the Day-ahead market (DAM) operating conditions. Thus, separate sessions of the Common, Local and Shared AS Markets were performed in order to solve the existing congestion. Table 4.10 describes the simulation time, the active power flows at the POIs and the dispatch costs of resources located at TN, DN #1 and DN #2 level. In particular, $P_{POI,1}$ and $P_{POI,2}$ indicate the active power flowing from TN to DN #1 and DN #2, respectively.

Table 4.10: Case #1 AS market outcomes

| | **Time** | **TN** | **DN #1** | | **DN #2** | | **Total** |
|---|---|---|---|---|---|---|---|
| | [s] | Cost [€] | Cost [€] | $P_{POI,1}$ [MW] | Cost [€] | $P_{POI,2}$ [MW] | Cost [€] |
| | | | **Common** | | | | |
| ICA | 1 | 56960 | 3819 | 14.80 | 347 | 41.89 | **61126** |
| BDA | 24 | 57192 | 3821 | 14.75 | 463 | 41.20 | **61476** |
| SAA | 25 | 58922 | 2195 | 19.40 | 630 | 40.45 | **61747** |
| | | | **Local** | | | | |
| PS | 1 | - | 0 | 30.88 | 0 | 44.21 | ***0*** |
| ICA | 1 | 56964 | 3817 | 14.86 | 362 | 41.92 | **61143** |
| BDA | 31 | 57231 | 3818 | 14.75 | 428 | 41.37 | **61477** |
| SAA | 25 | 58922 | 2195 | 19.40 | 630 | 40.45 | **61747** |
| | | | **Shared** | | | | |
| ICA | 1 | 63809 | 0 | 30.68 | 0 | 44.09 | |
| Pen. | | | 40 | | 13 | | **63862** |
| BDA | 4 | 63809 | 0 | 30.68 | 0 | 44.09 | |
| Pen. | | | 41 | | 13 | | **63863** |

As expected, the ICA method was more effective than other methodologies in terms of total dispatch costs. In particular, in the Common AS Market model simulation, the

solution closest to that provided by the ICA was obtained by the BDA in terms of total costs and final power exchanges at the POIs. However, a longer computational time was required by the BDA and SAA (about 25 s) with respect the ICA (1 s). Figure 4.12 shows the active power exchanges $P_{POI,1}$ and $P_{POI,2}$ in the 11 iterations performed by the Benders decomposition algorithm.

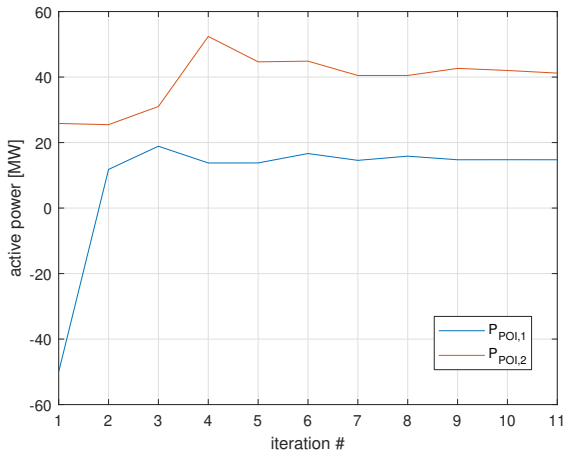


Figure 4.12: Case #1 - Common Market: active power flows at the POIs

Figures 4.13 and 4.14 represent the quadratic polynomial cost curves (in blue color) and the interpolated points (in red) of the flexibility values obtained by applying the SAA. In this case, $N_s = 40$ points were assumed to calculate the amount of flexibility at the POI, assuming the same voltage level present on its HV bus before the congestion was applied. The amounts of flexibility offered by the DSOs to the TSO were calculated with respect to the active power values $P_{POI,1} = 30.88$ MW and $P_{POI,2} = 44.21$ MW, which correspond to a flexibility demand of 0 MW at POI #1 and POI #2, respectively, and therefore characterized by cost null.

In the Local Market model simulation, the first performed optimization (PS), concerning the local markets of DN #1 and DN #2, was common to all three of the investigated methodologies. Next, the ICA, BDA and SAA were also performed. Please, note that the dispatch costs of DN #1 and DN #2 for the ICA, BDA and SAA include the dispatch costs of the PS. However, in this specific case, dispatch costs in PS were zero due to the absence of congestion at the DN level to be solved.

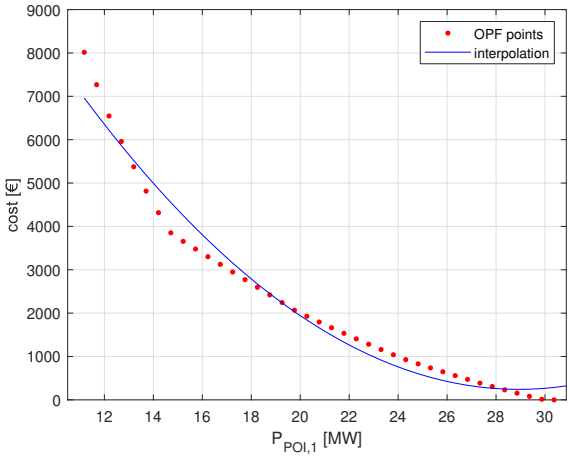


Figure 4.13: Case #1 - Common Market: costs of aggregated DERs of DN #1

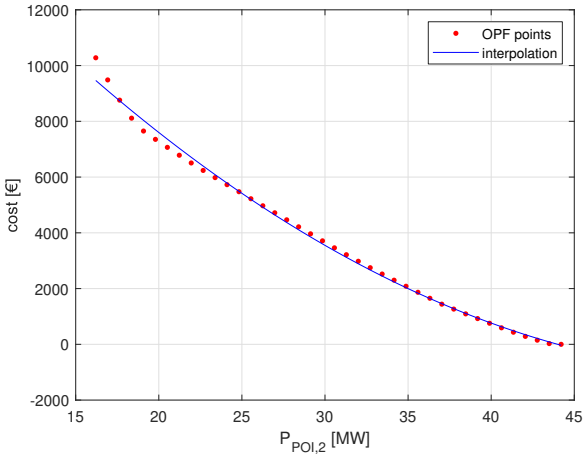


Figure 4.14: Case #1 - Common Market: costs of aggregated DERs of DN #2

It can be observed that the final solutions achieved in the Common and Local Market simulations were quite similar. This aspect is also more evident for the BDA results. This is because, in this case, there was no need for Ancillary Services in the distribution networks. Figures 4.15 and 4.16 show the final dispatch of DN #1 resources, in terms of active and reactive power, respectively, for the Local Market model implemented with the three different strategies. Like before, the BDA achieved the closest

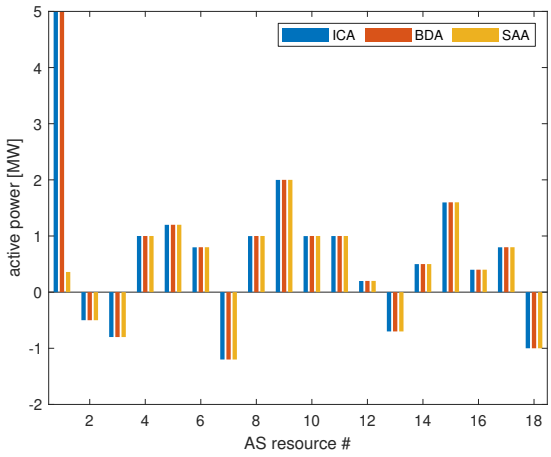


Figure 4.15: Case #1 - Local Market: active power of DERs in DN #1

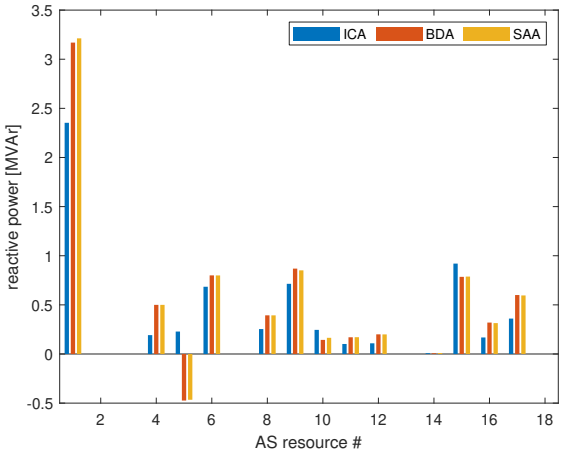


Figure 4.16: Case #1 - Local Market: reactive power of DERs in DN #1

solution to that provided by the ICA in terms of total costs and power exchanges at the

POIs. Nevertheless, the SAA converged in less time than the BDA due to the 24 iterations required by this last algorithm to achieve the final solution. Figure 4.17 shows the active power exchanges $P_{POI,1}$ and $P_{POI,2}$ in the Benders decomposition algorithm iterations.

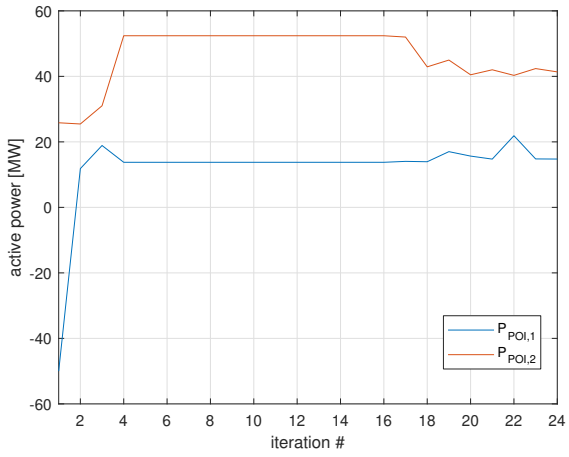


Figure 4.17: Case #1 - Local Market: active power flows at the POIs

In the Shared balancing responsibility Market model, the power exchanges at the TSO-DSO interconnection points were set to the DAM outcomes at the POI #1 and POI #2, respectively equal to 30.88 MW and 44.21 MW. A penalty of 1000 €/MW$^2$ was applied to the active power mismatches whenever the scheduled power exchanges cannot be fulfilled. Simulation results demonstrated that similar solutions were obtained by the ICA and BDA in terms of total costs and power exchanges at the POIs. Since power exchanges at the POIs were set to the DAM values, the BDA converged in only 2 iterations. The penalties (denoted as "Pen." in Table 4.10) of about 40 € and 13 € were due to the misalignment of the active power flows at the POI #1 and POI #2 with the respective DAM values.

From a comparison between the investigated methodologies, the ICA proved to be more effective than the two other methods in terms of total AS costs and running time. This is because the ICA was able to perform a better dispatch of flexibility resources at both TN and DN levels. In turn, the BDA provided better solutions than the SAA in terms of active power exchanges at the POIs and total dispatch costs.

About the simulated market models, in this case, the Common and the Local schemes were characterized by similar dispatch solutions, due to the absence of congestion to be solved for the DSOs, which have priority on DERs procurement. While, as expected, the Shared Market model proved to be less efficient than the other two Market models since, in this scheme, flexibility resources could not be shared between the different grid operators, leading to sub-optimal solutions [150].

#### 4.3.3.3 Case #2: congestion of DN #1 lines

In the second simulation test, a uniform load increase of about 40 % was applied to the DN #1. Test results, shown in Table 4.11, demonstrated that total AS activation costs were lower than in the previous case, due to the reduced amount of congestion to be solved. As before, results of the ICA were assumed as a benchmark for the BDA and SAA methodologies applied to all three investigated markets. Due to the presence of congestion only in DN #1, AS activation costs for TN and DN #2 were reduced. In this case, BDA achieved close results to the ICA than SAA for both Common and Local Market schemes. In addition, it was executed in fewer time than the SAA, since 9 iterations (less than in Case #1) were required by the BDA for both Common and Local market simulations (see Figure 4.18). As it can be observed, the active power

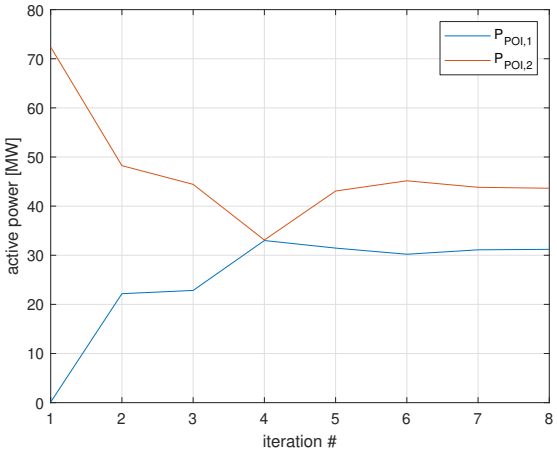


Figure 4.18: Case #2 - Local Market: active power flows at the POIs

exchanges at the POIs after the local markets have been cleared (PS) are, respectively,

Table 4.11: Case #2 AS market outcomes

| | **Time** | **TN** | **DN #1** | | **DN #2** | | **Total** |
|---|---|---|---|---|---|---|---|
| | [s] | Cost [€] | Cost [€] | $P_{POI,1}$ [MW] | Cost [€] | $P_{POI,2}$ [MW] | Cost [€] |
| | | | **Common** | | | | |
| ICA | 1 | 12 | 997 | 31.59 | 5 | 43.83 | **1014** |
| BDA | 15 | 0 | 1056 | 31.20 | 2 | 43.64 | **1058** |
| SAA | 25 | 0 | 1116 | 30.89 | 1 | 44.21 | **1117** |
| | | | **Local** | | | | |
| PS | 1 | - | 408 | 37.56 | 0 | 44.21 | ***408*** |
| ICA | 1 | 12 | 1152 | 31.54 | 5 | 43.88 | **1169** |
| BDA | 15 | 0 | 1192 | 31.20 | 2 | 43.64 | **1194** |
| SAA | 22 | 0 | 1251 | 30.89 | 1 | 44.21 | **1252** |
| | | | **Shared** | | | | |
| ICA | 1 | 182 | 1104 | 30.95 | 0 | 44.22 | |
| Pen. | | | 6 | | 0 | | **1292** |
| BDA | 4 | 184 | 1104 | 30.95 | 0 | 44.22 | |
| Pen. | | | 9 | | 0 | | **1297** |

of 30.56 MW and 44.21 MW. In this test case, the dispatch costs for the Local Market model were slightly higher than those of the Common Market scheme. In fact, although similar final power exchanges were achieved at the POIs for the Common and the Local Markets, the DN #1 dispatch costs were higher in the Local scheme. This was because resources already procured by the DSOs in the SP to solve local needs could not be re-despatched to achieve new overall optimal solutions.

As expected, like in Case #1, the Shared balancing responsibility Market was affected by higher costs than the other two market models. The solutions provided for this Market model by the ICA and the BDA, which converged in 2 iterations, were similar in terms of total dispatch costs and active power exchanges at the POIs.

#### 4.3.3.4 Case #3: congestion of DN #1 and DN #2 lines

In this third test case, the capability of the proposed BDA to address congestions on multiple distribution networks was assessed. With this aim, in addition to the overload applied to DN #1 of Case #2, a uniform load increase of 28 % was also assumed in DN #2. As in the previous cases, the Common, Local and Shared schemes were tested in the congestion management AS market. Test results are shown in Table 4.12. The BDA provided the closest solutions to those of the ICA in terms of total dispatch costs and power exchanges at both POIs. Furthermore, the BDA converged in less time than the SAA for both Common and Local Market models. Figure 4.19 and 4.20 show the active power exchanges $P_{POI,1}$ and $P_{POI,2}$ in the 11 and 12 iterations of the BDA for the respective Common and Local Market schemes.
In this case, it is possible to observe a higher cost of the Shared balancing responsibility Market than the Common and Local schemes. This can be explained by the fact that flexibility resources cannot be pooled among system operators and both the DSOs are responsible for the CM and balancing of their respective distribution grids. Differently from the previous tests, in this case, the BDA applied to the Shared Market scheme converged in three iterations.

Table 4.12: Case #3 AS market outcomes

| | **Time** | **TN** | **DN #1** | | **DN #2** | | **Total** |
|---|---|---|---|---|---|---|---|
| | [s] | Cost [€] | Cost [€] | $P_{POI,1}$ [MW] | Cost [€] | $P_{POI,2}$ [MW] | Cost [€] |
| | | | **Common** | | | | |
| ICA | 1 | 478 | 1839 | 27.93 | 807 | 51.11 | **3124** |
| BDA | 14 | 552 | 1908 | 27.57 | 825 | 50.96 | **3285** |
| SAA | 22 | 524 | 1695 | 28.40 | 1079 | 49.84 | **3298** |
| | | | **Local** | | | | |
| PS | 1 | - | 408 | 37.56 | 185 | 55.68 | ***593*** |
| ICA | 1 | 488 | 1959 | 28.02 | 886 | 50.95 | **3333** |
| BDA | 15 | 504 | 1976 | 27.80 | 941 | 50.47 | **3421** |
| SAA | 22 | 486 | 1813 | 28.44 | 1135 | 49.62 | **3434** |
| | | | **Shared** | | | | |
| ICA Pen. | 1 | 0 | 1100 9 | 30.97 | 2561 23 | 44.36 | **3693** |
| BDA Pen. | 4 | 0 | 1100 9 | 30.97 | 2562 23 | 44.36 | **3694** |

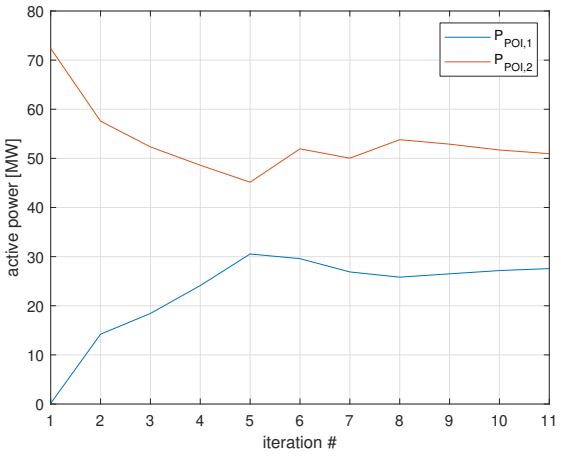


Figure 4.19: Case #3 - Common Market: active power flows at the POIs

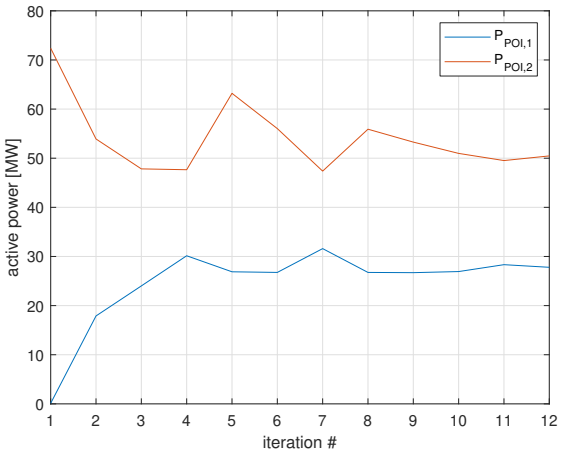


Figure 4.20: Case #3 - Local Market: active power flows at the POIs

#### 4.3.3.5 Case #4: congestion of TN, DN #1 and DN #2 lines

As a fourth test case, it was investigated the capability of the proposed BDA to handle congestions at both TN and DN levels. With this aim, the congestions assumed in Case #1 (at TN level) and Case #3 (DN #1 and DN #2) were applied simultaneously to the simulated power system. Test results of the three investigated methodologies applied to the different market models are described in Table 4.13. As for the previous cases, the ICA methodology provided the best solution in terms of total AS activation costs. Therefore, considering newly the ICA results as a benchmark, the BDA was more effective than the SAA strategy in terms of total dispatch costs, active power exchanges at the POIs and convergence time. Figure 4.21 and 4.22 show the active power exchanges $P_{POI,1}$ and $P_{POI,2}$ in the 14 and 11 iterations of the BDA for the respective Common and Local Market schemes.

From a comparison of the total dispatch costs in the Common and Local Markets, based on the same methodology, slight differences of a few hundred € can be observed. This proved that, in this case, the amount of flexibility located in DN #1 and DN #2 was enough to satisfy the needs of both the DSOs themselves and (partially) of the TSO. Greater differences of total dispatch costs may be observed with respect to the Shared balancing responsibility Market model, which resulted (about 1000 €)

Table 4.13: Case #4 AS market outcomes

| | **Time** | **TN** | **DN #1** | | **DN #2** | | **Total** |
|---|---|---|---|---|---|---|---|
| | [s] | Cost [€] | Cost [€] | $P_{POI,1}$ [MW] | Cost [€] | $P_{POI,2}$ [MW] | Cost [€] |
| | | | **Common** | | | | |
| ICA | 1 | 60923 | 4082 | 21.03 | 1477 | 48.18 | **66482** |
| BDA | 20 | 61255 | 4064 | 21.01 | 1576 | 47.71 | **66895** |
| SAA | 25 | 63372 | 2590 | 25.24 | 1184 | 49.38 | **67146** |
| | | | **Local** | | | | |
| PS | 1 | - | 408 | 37.56 | 184 | 55.68 | ***592*** |
| ICA | 1 | 60884 | 4224 | 20.93 | 1483 | 48.19 | **66591** |
| BDA | 12 | 61186 | 4227 | 20.88 | 1596 | 47.65 | **67009** |
| SAA | 22 | 63045 | 2928 | 24.60 | 1253 | 49.10 | **67226** |
| | | | **Shared** | | | | |
| ICA Pen. | 1 | 63882 | 1139 11 | 30.77 | 2597 1 | 44.24 | **67630** |
| BDA Pen. | 3 | 63883 | 1139 11 | 30.77 | 2596 2 | 44.24 | **67631** |

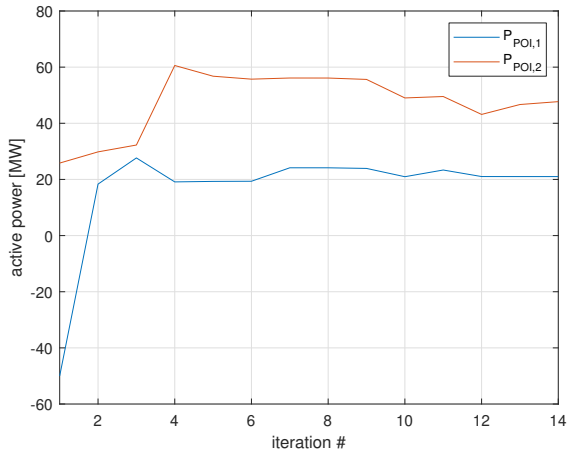


Figure 4.21: Case #4 - Common Market: active power flows at the POIs

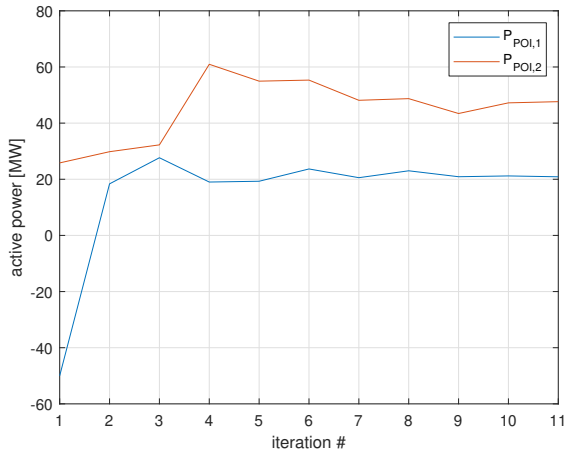


Figure 4.22: Case #4 - Local Market: active power flows at the POIs

more expansive than the other coordination schemes). It was due to the impossibility of sharing flexibility among system operators. This aspect can be also deduced by observing that dispatch costs of resources in TN and DN #2 increased in the Shared Market model with respect to the dispatch costs of the same grids in the Common and Local schemes. This was because, due to the impossibility in sharing flexibility, less flexibility was provided to TN and DN #2 by DN #1, whose activation costs decreased.

#### 4.3.3.6 Case #5: Multiple TSO-DSO interconnection

As an additional test, it was investigated the capability of the proposed BDA to be applied to cases in which the distribution networks are interfaced with the transmission grid in multiple TN-DN interfacing points. As described in [122], this aspect concerns a common issue of recent power systems, in which DN may be operated in a meshed manner. Therefore, with the aim to test the proposed BDA, two points of interconnection were added to the simulation model desribed in Sect. 4.3.3.1. In particular, two 138 kV/12.6 kV, 25 MVA, parallel transformers, located in the new primary substation, were connected with the bus #35 of the TN and the bus #120 of the DN #1. Similarly, two 138 kV/12.6 kV parallel transformers having sizes of 50 MVA and 25 MVA, respectively, and located in the second added primary substation were employed to interconnect the bus #60 of the TN with the bus #401 of the DN #2. The values of active

power flowing from the TN to DN #1 and DN #2 through the two added POIs was denoted as $P_{POI,3}$ and $P_{POI,4}$, respectively. Considering the same congestion of Case #4, a Common Market model was tested and implemented through the ICA, BDA, and SAA methodologies. However, since the SAA applied in the previous tests (and described in Section 3.3) is not suitable for multiple POIs, in this case, the smart aggregation of DERs was performed through the three methodologies SAA-A SAA-B1 and SAA-B2 developed for multiple TN-DN interfacing points (see Section 4.3.3.6). Test results of the investigated methods are described in Table 4.14. Figure 4.23 show the active power exchanges $P_{POI,1}$, $P_{POI,2}$, $P_{POI,3}$ and $P_{POI,4}$ in the 38 performed iterations of the BDA.

Table 4.14: Case #4 AS market outcomes with multiple POIs

| | **Time** | **TN** | **DN #1** | | | **DN #2** | | | **Total** |
|---|---|---|---|---|---|---|---|---|---|
| | [s] | Cost [€] | Cost [€] | $P_{POI,1}$ [MW] | $P_{POI,3}$ [MW] | Cost [€] | $P_{POI,2}$ [MW] | $P_{POI,4}$ [MW] | Cost [€] |
| ICA | 12 | 56865 | 4080 | 13.59 | 7.45 | 1463 | 43.20 | 4.91 | **62408** |
| BDA | 56 | 56876 | 4064 | 12.56 | 8.47 | 1551 | 42.86 | 4.88 | **62491** |
| SAA-A | 39 | 58510 | 2317 | 17.65 | 8.35 | 2049 | 42.84 | 3.08 | **62876** |
| SAA-B1 | 830 | 58451 | 2322 | 17.64 | 8.35 | 2122 | 42.84 | 2.83 | **62895** |
| SAA-B2 | 830 | 58580 | 3030 | 21.49 | 2.48 | 1115 | 46.44 | 3.08 | **62725** |

As it can be observed from the obtained results, the solution closest to those provide by the ICA in terms of total dispatch costs was given by the BDA, which converged in 38 iterations, followed by the SAA-B1. Table 4.14 describes the computational time required by each methodology. Figures 4.24 and 4.25 represent the overall costs of the flexibility aggregated for each DSO-area through the SAA-A method, thus considering the total active power $P_{POI,1}$+ $P_{POI,3}$ for DN #1 and $P_{POI,2}$+ $P_{POI,4}$ for DN #2. Differently, Figures 4.26 and 4.27 represent the calculated costs (blue points) and their interpolation (3-D grid surface) of DN #1 and DN #2, based on SAA-B1 and SAA-B2 methodologies, respectively. Simulation tests demonstrated that SAA-B1 and SAA-B2 were much slower (830 s) than the other methodologies. This was due to the huge number of OPF routines required to evaluate the flexibility costs for each candidate

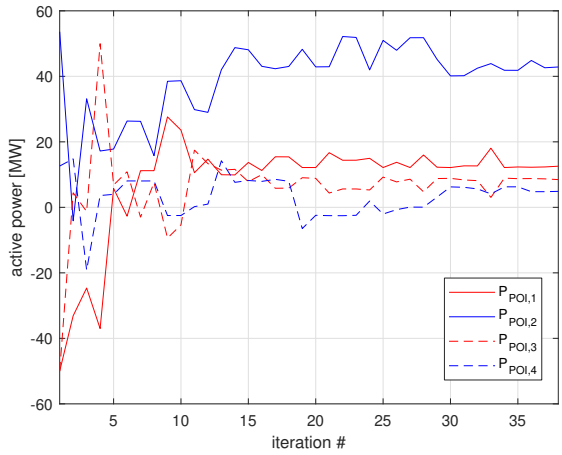


Figure 4.23: Case #5 - Common Market: active power flows at the POIs

pair of active power values ($P_{POI,1}$, $P_{POI,3}$) and ($P_{POI,2}$, $P_{POI,4}$) assumed for DN #1 and DN #2, respectively.

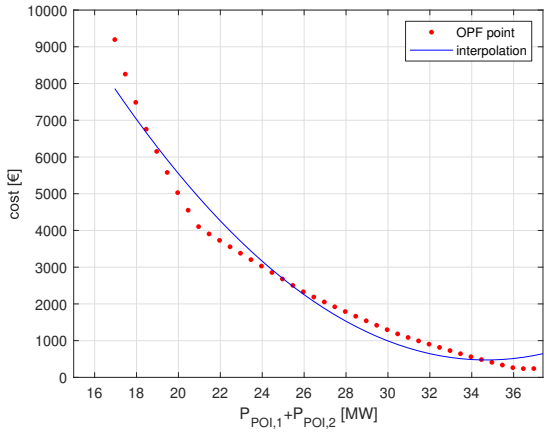


Figure 4.24: Aggregation of DERs through the SAA-A method for the whole DN #1-area

### 4.3.4 Data Exchange Analysis

As a final investigation, in order to assess the feasibility of the proposed BDA in practical implementation, a comparison of data exchanged between system operators in both Benders decomposition and smart aggregation methodologies was performed. Then,

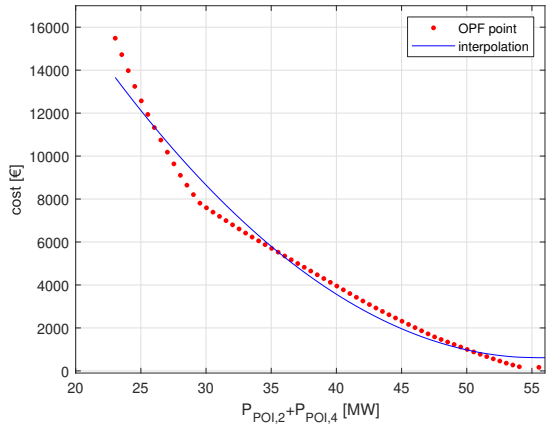


Figure 4.25: Aggregation of DERs through the SAA-A method for the whole DN #2-area

to extend this study to those cases in which there are multiple POIs, a generic number $n_{POI,l}$ of TN/DN interconnection points was assumed for each $l$-th distribution network. Furthermore, without loss of generality, it was assumed that one aggregated cost curve is defined in the Common and Local Market schemes for each individual interconnection point. This condition well fits with the previously investigated SAA, SAA-B1 and SAA-B2.

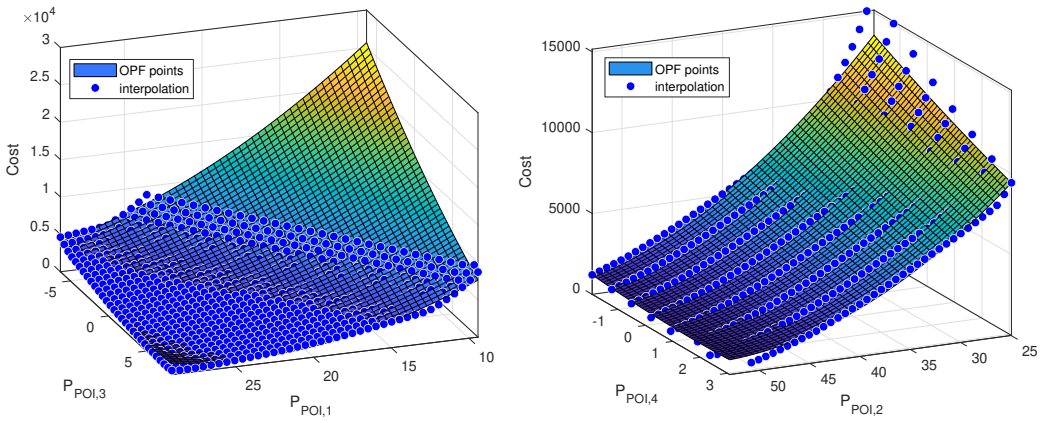


Figure 4.26: 3-D aggregation of DERs in DN #1 and DN #2 through SAA-B1

Table 4.15 describes, for each tested market scheme, direction and amount of data exchanged between the TSO (Master problem) and the DSO (Slave problem) in the

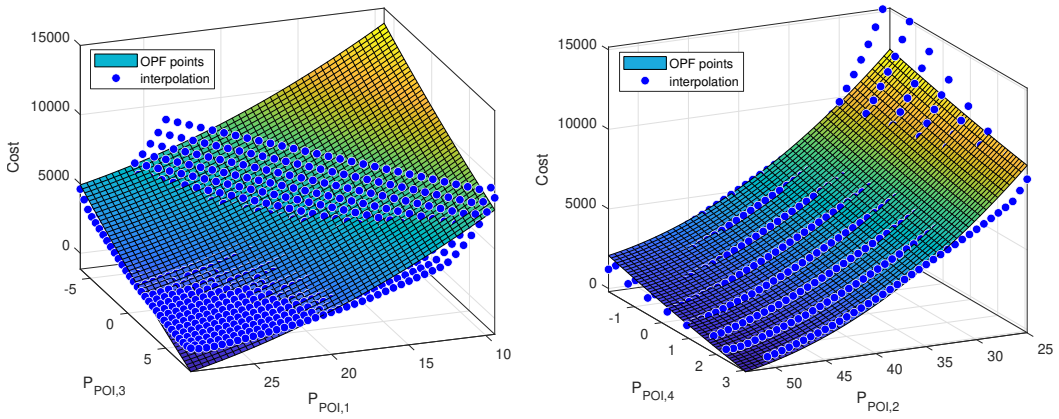


Figure 4.27: 3-D aggregation of DERs in DN #1 and DN #2 through SAA-B2

Common, Local and Shared balancing responsibility Market models. Looking at the detail, in the smart aggregation approach applied to the Common and Local Markets, it was assumed that each $l$-th DSO communicates to the TSO the three parameters ($\alpha$, $\beta$, $\gamma$) associated with the quadratic cost curve of the DERs aggregated at the $l$-th POI as well as the minimum and maximum active power values of the available flexibility. In the opposite direction, once the central market has been closed, the TSO communicates to the DSO the active and reactive power values of flexibility required at the POI. As a whole, an overall exchange of $7 \cdot \sum_{l=1}^{n_{DSO}} n_{POI,l}$ data is required for each Common or Local Market session performed through the SAA.

In the Shared Balancing responsibility Market model, the aggregation of DERs is not required since power exchanges at the POIs are scheduled. Therefore, there is no need to exchange data between the two system operators in such conditions. Differently, this need may exist for those POIs in which the scheduled power exchange cannot be satisfied. In this case, the DSO communicates to the TSO two new values (active and reactive power) to be set at the corresponding points of interconnection. Thus, indicating by $n'_{POI}$ the number of TN/DN interfacing points for which scheduled powers are not respected, a total number of $2 \cdot n'_{POI}$ parameters are communicated from the local to the central market.

A similar analysis can also be performed about the data exchange between the Mas-

Table 4.15: TSO-DSO data exchange in the investigated coordination schemes

| | **Smart aggregation** | | | **Benders decomposition** | | |
|---|---|---|---|---|---|---|
| **Coordination scheme** | **Exchanged data** | **Direction** | **Amount of exchanged data** | **Exchanged data** | **Direction** | **Amount of exchanged data** |
| **Common AS Market model (decentralized vers.)** | Aggregated DERs | From DSO to TSO | $(3+2) \cdot \sum_{l=1}^{n_{DSO}} n_{POI,l}$ | Power exchange at the POIs | From TSO to DSO | $2 \cdot n_{BD} \cdot \sum_{l=1}^{n_{DSO}} n_{POI,l}$ |
| **Local AS Market model** | Power exchange at the POIs | From TSO to DSO | $2 \cdot \sum_{l=1}^{n_{DSO}} n_{POI,l}$ | Marginal and total costs | From DSO to TSO | $2 \cdot n_{BD} \cdot \sum_{l=1}^{n_{DSO}} n_{POI,l}$ |
| | **Total** | | $7 \cdot \sum_{l=1}^{n_{DSO}} n_{POI,l}$ | **Total** | | $4 \cdot n_{BD} \cdot \sum_{l=1}^{n_{DSO}} n_{POI,l}$ |
| | **Power exchange-based approach** | | | **Benders decomposition** | | |
| **Shared balancing Market model (when scheduled power exchanges cannot be respected)** | Power exchanges at the POIs | From DSO to TSO | $2 \cdot n'_{POI}$ | Power exchange at the POIs | From TSO to DSO | $2 \cdot n_{BD} \cdot n'_{POI}$ |
| | | | | Marginal and total costs | From DSO to TSO | $2 \cdot n_{BD} \cdot n'_{POI}$ |
| | **Total** | | $2 \cdot n'_{POI}$ | **Total** | | $4 \cdot n_{BD} \cdot n'_{POI}$ |

ter problem (TSO) and the $n_{DSO}$ Slave problems (DSOs). As specified in Section 4.3.1, at each iteration, the Master problem communicates to each $l$-th Slave problem the values of candidate active and reactive power at each POI. While, each DSO sends to the TSO the parameters $\lambda_{l,v}$ and $C_l^{DN}$ concerning the performed local optimization. Therefore, assuming that the BDA converges in $n_{BD}$ iterations, $4 \cdot n_{BD}$ parameters need to be exchanged between TSO and the $l$-th DSO for each single TN-DN interfacing point. As a whole, an overall exchange of $4 \cdot n_{BD} \cdot \sum_{l=1}^{n_{DSO}} n_{POI,l}$ data is required for each Common or Local Market session performed through the BDA. In the Shared balancing responsibility Market scheme, this amount is reduced to $4 \cdot n_{BD} \cdot n'_{POI}$ since the BDA need to be applied only to those $n'_{POI}$ TN/DN interconnection points in which the scheduled power exchanges cannot be satisfied.

### 4.3.5 Final assessments

Simulation tests demonstrated the effectiveness of the proposed BDA methodology in finding optimal solutions in the Common, Local, and Shared Market models, without having to introduce any approximation in the mathematical formulation. Furthermore, the computational time of the BDA on performed tests was comparable with that of the other methods . On the other side, although the BDA demonstrated also to be faster than the SAA in some cases, the higher accuracy of this approach was penalized by higher data exchange between TSO and DSO. In fact, since the BDA requires at least 2 iterations to converge, the SAA appears to be more advantageous than the BDA in terms of exchanged data.

Test results also confirmed the effectiveness of the Common AS Market model in dispatching flexibility resources than the other two investigated market schemes. Although slight differences can be observed between the total dispatch costs of the Common and Local AS Markets, the former provided more efficient solutions. This advantage would increase by assuming more expensive resources at the distribution level. In fact, under such conditions, the DSOin the Local Market, is forced to solve its own congestion with higher dispatch costs.

Future tests will be aimed at testing in-depth the proposed BDA assuming further

realistic scenarios with DNs interfaced with the TN in multiple interconnection points. Moreover, acceleration strategies [144] to enhance the BDA convergence will be also investigated with the aim to reduce the exchange of information between Transmission and Distribution System Operators.

# Chapter 5

# Innovative Ancillary Services through DERs

In this chapter, the possibility of providing innovative Ancillary Services through DERs located at the DN level was investigated by means of Power Hardware-in-the-Loop simulation tests. In particular, the development of a low-cost controller for end-user applications able to generate a SI law for dispatchable DERs was described. In addition, the capability of LED lamps of public lighting systems to be controlled with the aim to provide SI and FFR was also analyzed. Tests result were described and discussed below.

## 5.1 Synthetic Inertia and Fast frequency regulation

The power stability and reliability depend on the system capability of keeping frequency excursions within a narrow interval around the nominal value, even following large perturbations which alter the balance between generation and power demand. Conventional generators adopt traditional control schemes, such as Frequency Containment Reserve, to control power system response. The ability of a power system to keep stable frequency after a grid disturbance, even before FCR exhibits its effect, is known as system *inertia*. As recalled in [151], this parameter is essential for power system stability, because its value influences the Rate of Change of Frequency

(RoCoF) following sudden variation of load and generation balance. In conventional power plants, the inertia is intrinsically linked to the kinetic energy that synchronous generator masses can inject or absorb from the network whent rotating.

Non-synchronous generators that produce energy from intermittent sources are usually interfaced with the electrical network by means of power converters that decouple them from the electrical grid and do not contribute to system inertia. As non-synchronous generators keep conventional units out of the economic dispatch, as they are characterized by low marginal costs, power systems are beginning to be characterized by low rotational inertia. [151].

The primary effect of low rotational inertia is to accelerate and amplify frequency transients leading to possible improper operation of protections, tripping of tie-lines, and load shedding [152]. These phenomena are very dangerous for small power systems and non-synchronous islands, but they also affect larger interconnected systems because global rotational inertia tends to assume local heterogeneous distributions [152] and this can cause instability in case of system separation and islanding [1].

As a consequence, the need for providing additional inertia has been recognized by a large number of system operators. As acknowledged in [153], some examples of ancillary services and incentive schemes aimed at improving the frequency response have been proposed by operators in UK and Ireland. In Italy, under Regulation 300/2017/R/EEL [154], the Energy Regulator, set the requirements for pilot projects to demonstrate the possibility of providing demand response fast load reduction and FCR services for generating units integrated by storage systems. Theoretically, as remarked in [155], additional synchronous condensers could theoretically be installed to improve system inertia and contain frequency excursions, with the drawback of increasing system costs and complexity. As an alternative, further solutions aimed at providing additional inertia through the electronic control of existing inverter-based resources have been also proposed in the literature [155]. These solutions are usually known as Virtual Synchronous Machines, which are grid-connected power converters that emulate the synchronous generator behavior [156]. Several recent studies focused also on the possibility to obtain additional inertia from controllable DERs, including generators, storage, and loads devices [157], [158].

However, to provide additional inertia to the electrical grid and limit the frequency and RoCoF excursions, control actions like the Synthetic Inertia (SI) and Fast Frequency Response (FFR) need to be implemented on DERs and controllable devices. Although many studies do not focus on the distinction between Synthetic Inertia and Fast Frequency Response [159], a separate description can be given for each of them. According to the SI description given by ENTSO-E in [160]:

> *"**Synthetic Inertia** is defined as the controlled contribution of electrical torque from a unit that is proportional to the rate of change of frequency measured at the terminals of the unit".*

Therefore, although in the literature there is no unified definition of SI [159], it can be intended as a control law proportional to the measured frequency derivative (RoCoF) [161], [162]. While, considering the description given in [159], the FFR is defined as:

> *"**Fast Frequency Response** is the controlled contribution of electrical torque from a unit which responds quickly to changes in frequency [...]".*

According to this definition, the Fast Frequency Response aims at providing inertial support by means of units able to quickly respond to frequency excursions. Several examples of FFR controls have been proposed in the literature with this aim [163], [164]. Most of studies showed that Synthetic Inertia and Fast Frequency Response are both able to improve the frequency excursions and the frequency nadir after a disturbance has been applied [159].

Following, the capability of controllable DERs, like BESS or loads, to be effectively employed as flexibility resources to provide SI and FFR support was investigated. Simulation tests carried out to validate the proposed solutions were described and discussed. Additional studies, not reported here for the sake of brevity, were also performed by the author to investigate the capability of hybrid systems, such as supercapacitor/battery storage systems, to be exploited with this aim [165].

## 5.2 Need for Accurate measurements of frequency and frequency derivative through low-cost devices

Improving the inertial response along with the diffusion of Renewable Energy Sources and distributed generation will be a relevant challenge in the incoming years. In this regard, recent developments have shown that also prosumers and active end-users at the distribution level are theoretically able to provide SI or FFR contribution [161]. However, to implement effective SI or FFR actions, the availability of real-time and accurate grid frequency measurements is necessary for end-users located at the DN level.

As remarked in [153], in practical implementation, assuming the availability of RoCoF signals at the distribution level is an unrealistic hypothesis, due to measurement noise. In the context of SI, RoCoF is a metric of paramount importance, since excessive RoCoF error (RFE) can compromise the efficacy of frequency control [166]. The central issue is that frequency measurement speed and accuracy tend to be mutually exclusive. In [166], it is recognized that a control scheme based on the adoption of M-Class Phasor Measurement Units (PMUs), characterized by slow reporting (11 cycles) but higher accuracy, can provide much better results than using P-Class PMUs with a faster reporting rate (3 cycles) and lower accuracy.

An effective SI control scheme based on RoCoF measurement should find a good compromise among these two parameters. Reference [166] suggests that ideal frequency measurements should have a reporting rate of maximum 100 ms with an accuracy of about 0.01 Hz in the presence of total harmonic distortion (THD) up to 3%. Similar, but less strict requirements, are set by the European Network Code on Demand Connection [167]. The Article 29 of this Code, establishes that demand facilities and closed distribution systems which participate to Demand Response system frequency control must be equipped with controllers able to measure the frequency at least every 200 ms and to detect 0.01 Hz changes. For SI applications at distribution or end-users levels, obtaining accurate and fast RoCoF estimation is even more problematic. The adoption of expensive instruments such as PMUs is clearly not sustainable for small-sized end-users. Moreover, frequency measurements at low voltage level

can be affected by high harmonic distortion, fast varying voltages, unbalanced load conditions and the presence of three-phase and single-phase circuits.

In the literature, applications for low-cost fast frequency measurement can be found. Simplest methodologies are usually based on zero crossing (ZC) detection, as proposed in [168], where a near-zero-cross-detector circuit generates pulses at each crossing which are totaled in a fixed time window. According to the author, by adopting a high-frequency oscillator (8MHz), an accuracy of about 1.25 mHz can be theoretically reached. However, typical problems of simple ZC techniques, such as scarce immunity to noise, distortion and DC components, are not addressed. In [169], the authors have compared different algorithms for frequency and RoCoF measurement, based on phasor estimation and ZC. Tests showed that ZC can obtain better RFE performances (30 mHz/s) than phasor algorithms, which can reach RFE up to 500 mHz/s. The algorithms have been tested off-line in a Matlab simulation environment, without addressing the problem of how high computational burdens, typically associated to ZC algorithms, can affect real-time implementations. The authors in [170] proposed the implementation of a PMU on a low-cost embedded platform, investigating also the estimation of frequency and RoCoF. A Discrete Fourier Transform (DFT) estimator and a Taylor-Fourier Transform have been implemented in C++ and transferred on a BeagleBone Black board. Tests, based on simulations, obtained a processing time of about 20 ms and accuracies potentially compatible with M-Class and P-Class PMUs. However, these timings do not take into account synchronization and acquisition which are only emulated. In [171], an accurate real-time voltage, frequency and phase angle monitoring hardware platform has been designed and tested. The system adopts a microprocessor-based analog-to-digital (AD) sampling module and a primary synchronization signal harvested from a 4G LTE smartphone. Reporting rate is 100 ms with an expected frequency accuracy of 1.7 mHz. The main drawback is that synchronization depends on the availability of the cellular signal.

Based on this preliminary survey, the present thesis investigated the possibility to develop an efficient frequency measurement algorithms that can be implemented on a low-cost equipment to be employed for providing frequency regulation services such as SI and FFR at distribution and end-users level.

## 5.3 A new algorithm for accurate frequency measurements and SI

In order to develop a low-cost controller suitable for end-user applications, three different algorithms for frequency measurements and SI evaluation were carried out. Such algorithms are based on the frequency definition given in [172], where the author have demonstrated, through simulations, the possibility to use of signal autocorrelation to provide frequency measurement, suitably immune to noise, harmonic distortion and continuous components, for applications in synchrophasors and time-tagged protections. Therefore, once the algorithms were defined, they were tested with specific signals to assess their immunity to noise and disturbance, conditions that typically affect distribution grids.

### 5.3.1 A framework for Frequency Assessment through Signal Autocorrelation

The frequency of a periodic signal expresses how many times a signal repeats itself over a time unit. However, this definition is valid only for steady-state conditions, since in a dynamic-state it is not possible to define frequency in the same way. In an electric power grid, continuous disturbances and switching events can make voltage signals non-sinusoidal and non-periodic. For such reason, it has been introduced the concept of instantaneous frequency (IF), with several possible definitions [173] and different methods for its evaluation [174]. In practice, with a lack of a common definition of IF, most methods assume that signals are near-stationary, and the industry relies on tests based on canonic signals such as ramps and oscillations [172]. Several methods usually adopted for IF assessment such as ZC, Clarke transformation, DFT, Gauss-Newton algorithm have been compared in [175], showing how each method has some drawbacks. Trying to overcome ZC and DFT-based phasor estimation method, typically adopted in PMUs [176], the author in [172] presented a novel approach to fast frequency measurement, proving it to be suitably immune to noise and distortion, in a simulated environment. The implementation of algorithms based on this formu-

lation has been considered suitable for applications at end-users level because of the wide range of signals which can be processed, without assumptions on periodicity and waveform. Calculations are mostly discretized autocorrelation integrals that can be easily obtained with sums and multiplications. The formulation is also intrinsically immune to the presence of DC components, which contributes also to eliminate the errors due to the off-set of the transduced signals. Given a generic waveform $x$ and a starting time $t_0$, a suitable definition of the period $\tilde{\tau}$ is the value that maximizes the autocorrelation integral

$$A(t,\tau) = \int_{t_0}^{t_0+\tau} x(t) \cdot x(t+\tau)\, dt \tag{5.1}$$

normalized by the wave magnitude $C(t,\tau)$ so defined:

$$\hat{A}(t,\tau) = \frac{A(t,\tau)}{C(t,\tau)} = \frac{\int_{t_0}^{t_0+\tau} x(t) \cdot x(t+\tau)\, dt}{0.5 \cdot \int_{t_0}^{t_0+2\tau} x^2(t)\, dt} \tag{5.2}$$

In [172], the computational effort needed to solve this maximization problem is avoided adopting a similar and less time consuming method based on the correlation of the $x$ waveform with its derivative

$$B(t,\tau) = \int_{t_0}^{t_0+\tau} x(t) \cdot x'(t+\tau)\, dt \tag{5.3}$$

This method is based on the search of the period $\tilde{\tau}$ such that function (5.3) is null as

$$B(t,\tilde{\tau}) = 0 \tag{5.4}$$

In the performed study, an analytical approach to maximize index $\hat{A}$ was proposed to understand its full potentialities. The mathematical developments that follow will permit to define three different algorithms for frequency estimation that are tested and compared. The analytical approach to maximize (5.2) is based on the consideration that a maximum can be evaluated finding the value of $\tilde{\tau}$ such that its partial derivative

is zero:

$$\frac{\partial \hat{A}(t,\tilde{\tau})}{\partial \tau} = \frac{\partial}{\partial \tau}\left(\frac{A(t,\tilde{\tau})}{C(t,\tilde{\tau})}\right) = 0 \tag{5.5}$$

By applying the Leibniz integral rule, it can be easily verified that

$$\frac{\partial A}{\partial \tau} = [x(t_0+\tau)\cdot x(t_0+2\tau)] + \int_{t_0}^{t_0+\tau} x(t)\cdot x'(t+\tau)\,dt \tag{5.6}$$

and

$$\frac{\partial C}{\partial \tau} = x^2(t_0+2\tau) \tag{5.7}$$

Thus, the derivative in (5.5) can be written as

$$D(t,\tau) = \frac{\partial \hat{A}}{\partial \tau} = \frac{\partial A/\partial \tau \cdot C - A \cdot \partial C/\partial \tau}{C^2} \tag{5.8}$$

Consequently the analytical approach to evaluate the period $\tilde{\tau}$ can be obtained solving the following equation:

$$D(t,\tilde{\tau}) = 0 \tag{5.9}$$

It is possible to demonstrate that the approach proposed in [172] can be obtained from (5.9) under certain approximations. If $x$ is a periodic signal with period $\tilde{\tau}$, for $\tau$ close to $\tilde{\tau}$ it is reasonable to assume that:

$$x(t) \approx x(t+\tau) \qquad \forall t \tag{5.10}$$

From (5.10), it follows that:

$$[x(t_0+\tau)\cdot x(t_0+2\tau)] \approx x^2(t_0+2\tau) \tag{5.11}$$

By posing:

$$G = x^2(t_0+2\tau) \tag{5.12}$$

under assumption (5.11), and taking into account eqn. (5.3), function (5.6) can be approximated as

$$\frac{\partial A}{\partial \tau} \approx G + B \tag{5.13}$$

Hence, from (5.8)

$$D \approx \frac{(G+B)\cdot C - A\cdot G}{C^2} \tag{5.14}$$

Equation (5.14) can also be written as

$$D \approx \left(1-\frac{A}{C}\right)\cdot\frac{G}{C}+\frac{B}{C} \tag{5.15}$$

Please note that, if assumption (5.10) holds, from (5.2) it can be derived that

$$\hat{A} = A/C \approx 1 \tag{5.16}$$

and, thus, substituting (5.16) in (5.15),

$$D = \frac{\partial \hat{A}}{\partial \tau} \approx \frac{B}{C} \tag{5.17}$$

Since the wave magnitude function $C$ is always positive, when $B$ equals zero, based on (5.17), also $\partial\hat{A}/\partial\tau$ is null. This demonstrates that, as long as condition (5.10) stands, finding the zero of the correlation of the waveform with its derivative (5.3) is equivalent to finding the maximum of the autocorrelation index (5.2). Clearly, since the period of the waveform is in general not known, the error introduced in approximating derivative (5.8) with (5.17) for a general $\tau$ can lead to incorrect evaluations. Furthermore, the implementation of equation (5.4) on a calculator will require the use of discretized values of $\tau$ that, in most cases, will deviate considerably from the exact waveform period $\tilde{\tau}$. Hence, the approximation (5.10) might be fallacious and cause deviations in the assessed frequency values. These deviations are probably considered not influent in [172], since the implementation on a synchrophasor framework allows to average errors with a large number of measurements. Differently, in the proposed architecture, which is based on the use of low-cost equipment for end-users applications, the number of measurements is limited and, therefore, the accuracy plays a more significant role.

Hereinafter, the use of the analytic approach (5.9) for the estimation of the maximum index $\hat{A}$ will be proposed and assumed as a benchmark. Moreover, based on the formulation above described, three different algorithms are developed and compared

with each other.

### 5.3.2 Algorithms for Frequency Estimation

The algorithms here proposed are based on the previous mathematical formulation and on the assumption that a sampled set of measurements was obtained using a voltage transducer, an ADC converter and an acquisition board. Furthermore, in the algorithms' formulation, it was assumed that samples were equally spaced. However, in practical implementation on a single-board computer, this requirement is hardly satisfiable without introducing idle times and reducing the sample rate. For this reason a resampling procedure was employed to interpolate samples yielding regularly-spaced input data. Since in the tested algorithms sampled data are used, all previous expressions are discretized. Therefore, in the following, the square brackets were used to represent discrete functions and values. Each candidate period $[\tau]$ is a discrete value that corresponds to a multiple of the sampling period. In order to evaluate a continuous value of period (and frequency) each algorithm adopts an interpolation rule between consecutive values of $[\tau]$. This is due to the fact that discretization leads to resolution errors not suitable with the accuracy requirements for frequency measurement. For example, adopting a sampling rate of 20 kHz, discrete frequency values are spaced about 0.125 Hz from each other around the nominal value of 50 Hz.

#### 5.3.2.1 Algorithm "B"

The first method replicates with sufficient fidelity the one proposed in [172]. It is based on the observation that the function $[B]$ assumes values with different sign if evaluated using a $[\tau_0]$ and a $[\tau_2]$ that are respectively smaller and greater of the actual period $\tilde{\tau}$. In other words, the method will search the value of $\tilde{\tau}$ that corresponds to a null value of $B$ as in (5.4). The method is also based on the observation that the function $B$ assumes, around the solution, a trajectory that can be approximated with a linear expression.

This first algorithm is organized as follows:

1. An initial guess $\tau_1$ of the signal period is made (a suitable guess is the frequency measured at the previous acquisition);

2. The neighborhood of $\tau_1$ is analyzed; then, two discrete values of $[\tau]$ are selected:

$$[\tau_0] \approx (\tau_1 - \Delta\tau) \qquad [\tau_2] \approx (\tau_1 + \Delta\tau);$$

3. Using the discretized formulation of (5.3) the values $[B_0]$ and $[B_2]$ are evaluated at $[\tau_0]$ and $[\tau_2]$, respectively;

4. $\tau_1$ is updated considering a linear interpolation

$$\tau_1 = [\tau_0] - [B_0] \cdot \frac{[\tau_2] - [\tau_0]}{[B_2] - [B_0]};$$

5. The neighborhood of $\tau_1$ is studied considering a $\Delta\tau$ equal to the sampling period. Steps 2), 3) and 4) are thus repeated;

6. $\tilde{\tau} \approx \tau_1$ *and* $\tilde{f} = \frac{1}{\tilde{\tau}}$;

Please note that at the point 4) of the algorithm an evaluation of $\tau_1$ is possible even if both $B_0$ and $B_2$ have the same sign. This happens when the guessed $\tau_1$ is far from the actual value. Nevertheless, this is not a problem since steps 2), 3) and 4) can be repeated until the zero crossing is found. However, based on the acquired experience two iterations are enough to find the zero in most cases.

#### 5.3.2.2 Algorithm "D"

This second algorithm, differently from Algorithm "*B*", which gives an approximate solution to the maximization problem of $\hat{A}$, utilizes the full expression of $D = \partial\hat{A}/\partial\tau$ in eqn.(5.8) to solve (5.9).

The algorithm is organized as follows:

1. An initial guess $\tau_1$ of the signal period is made (a suitable guess is the frequency measured at the previous acquisition);

2. The neighborhood of $\tau_1$ is analyzed; two discrete values of $[\tau]$ are selected:

$$[\tau_0] \approx (\tau_1 - \Delta\tau) \qquad [\tau_2] \approx (\tau_1 + \Delta\tau);$$

3. Using the discretized formulation of (5.8) the values $[D_0]$ and $[D_2]$ are evaluated at $[\tau_0]$ and $[\tau_2]$, respectively;

4. $\tau_1$ is updated considering a linear interpolation

$$\tau_1 = [\tau_0] - [D_0] \cdot \frac{[\tau_2] - [\tau_0]}{[D_2] - [D_0]};$$

5. The neighborhood of $\tau_1$ is studied considering a $\Delta\tau$ equal to the sampling period. Steps 2), 3) and 4) are thus repeated;

6. $\tilde{\tau} \approx \tau_1$ *and* $\tilde{f} = \frac{1}{\tilde{\tau}}$;

This second algorithm uses a more complex formulation and therefore is expected to require more computational resources and time. However, the solution is expected to be more precise since no approximation of the derivative $\partial\hat{A}/\partial\tau$ is made, as proved in Section 5.3.3. As for the previous case, repeating steps 2), 3) and 4) can improve the results if the initial guess is very far from the actual solution.

#### 5.3.2.3 Algorithm "A"

This third algorithm is based on the idea of using directly the full expression of $[\hat{A}]$, in eqn. 5.2, avoiding the calculation of its derivative. The trajectory of this function is studied around a discrete guess of the signal period using a polynomial approximation. In order to simplify calculations and accelerate the convergence of the method, a second order expression of $\hat{A}$ is calculated using three points.

The algorithm is organized with the following structure:

1. An initial guess $\tau_1$ of the signal period is made (a suitable guess is the frequency measured at the previous acquisition);

2. Having posed $[\tau_1] \approx \tau_1$, the neighbourhood of $[\tau_1]$ is analysed; then, two discrete values are selected:

$$[\tau_0] = [\tau_1] - \Delta\tau \qquad [\tau_2] = [\tau_1] + \Delta\tau;$$

3. Using the discretized formulation of eqn. 5.2 the values $[\hat{A_0}], [\hat{A_1}]$ and $[\hat{A_2}]$ are evaluated at $[\tau_0], [\tau_1]$ and $[\tau_2]$, respectively;

4. $\tau_1$ is recalculated as the abscissa of the vertex of the parabola passing by the three points $([\tau_0], [\hat{A_0}])$, $([\tau_1], [\hat{A_1}])$ and $([\tau_2], [\hat{A_2}])$;

5. The neighborhood of $[\tau_1] \approx \tau_1$ is studied considering a $\Delta\tau$ equal to the sampling period. Steps 2), 3) and 4) are repeated;

6. $\tilde{\tau} \approx \tau_1$ *and* $\tilde{f} = \frac{1}{\tilde{\tau}}$;

The use of index $[\hat{A}]$ to find the frequency was discarded in [172] because the evaluation of $[B]$ is simpler from a computational point of view. This is true because it requires the calculation of both integral functions $[A]$ and $[C]$. However, as it will be demonstrated through experimental results, an optimized coding of integral calculations and the skipping of the evaluation of the derivative $[x']$ ensure comparable computational timings.

### 5.3.3 Experimental Results

The three algorithms "*B*", "*D*" and "*A*", proposed in the previous section, were programmed in Python language and implemented on a single-board computer Raspberry Pi 3 Model B (cost of about 40$). It represents a versatile and powerful tool to be utilized with different devices and applications. Since the device can only work with digital signals only, an analog-to-digital converter is required. In the present tests, an ADC chip with a cost of about $ 10 was employed. The ADC is mounted on the prototype shield connected to the Raspberry PI through the GPIO interface. The proposed architecture is affordable, reliable and compact, since the same processing board is also used for data sampling. A transducer is needed to convert the voltage signal into a voltage range acceptable for the ADC shield (i.e. 0-3.3 V). A detailed description of this equipment will be provided in Section 5.4.1 In order to test the proposed algorithms, four different tests were made.

#### 5.3.3.1 Accuracy Test #1

In the first test, different signals generated by Agilent 33250A waveform generator were analyzed. This instrument is characterized by 2 ppm (parts per million) frequency accuracy and ±1mV ±1% voltage output accuracy. The error introduced by the signal generator is negligible when compared to the errors introduced by the low cost equipment. Therefore this test allows to assess the errors associated to calculations, sampling and ADC conversion. The proposed algorithms were tested at 50 Hz with three different waveforms (sinusoidal, triangular and square) in order to verify the device capability to measure frequency of signals with high harmonic content. Table 5.1 illustrates the results on 1000 frequency measurements, reporting the corresponding mean value, standard deviation, Maximum Absolute Error (Max AE) and Mean Absolute Percentage Error (MAPE). Please note that the three algorithms were run on the same sampled data in order to allow a fair comparison. From Table 5.1 results it is possible to observe that algorithms "D" and "A" algorithms are in general more accurate than "B". Absolute errors are in general well below 10 mHz except for the most severe tests with a square wave. It will be shown in the next subsection that the algorithms perform well in the case of sine waves affected by credible levels of harmonic distortion.

Table 5.1: Test #1-Results with Agilent 33250A as Waveform Generator

| Waveform | Algorithm ID | Mean value [Hz] | Standard deviation | Max AE [Hz] | MAPE [%] |
|---|---|---|---|---|---|
| Sine | B | 50.0010 | 0.00220 | 0.01251 | 0.00369 |
| | D | 50.0011 | 0.00159 | 0.00784 | 0.00309 |
| | A | 50.0011 | 0.00153 | 0.00606 | 0.00305 |
| Triangular | B | 50.0002 | 0.00232 | 0.01185 | 0.00346 |
| | D | 50.0002 | 0.00169 | 0.00838 | 0.00267 |
| | A | 50.0002 | 0.00164 | 0.00878 | 0.00259 |
| Square | B | 50.0026 | 0.03733 | 0.10389 | 0.06081 |
| | D | 50.0022 | 0.03768 | 0.11210 | 0.06132 |
| | A | 50.0022 | 0.03787 | 0.12936 | 0.06098 |

Figure 5.1 depicts the box plots for the sine wave case. For each box, the red central mark represents the mean value whereas the edges denote the 25th and 75th percentiles. The extreme samples that are not considered as outliers are delimited by the black whiskers. The outliers are instead plotted individually with a symbol "+". Algorithms "A" and "D" are clearly characterized by a lower dispersion of measurements and fair lesser number of outliers. A chi-square test was carried out to verify if

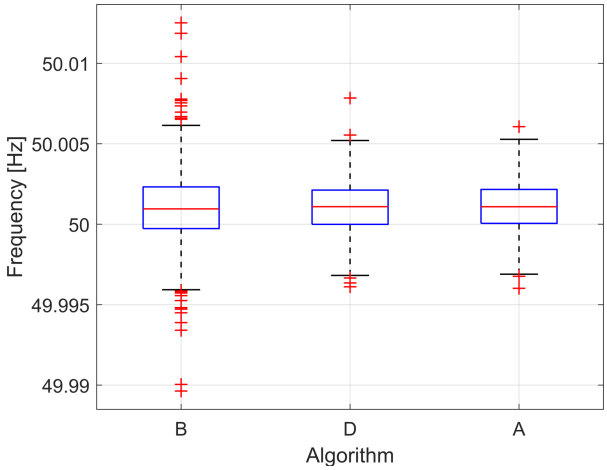


Figure 5.1: Test 1-Box plot of the 50 Hz sine wave test values

data follow a Gaussian distribution. Table 5.2 reports the results of this test applied to the values obtained by the three algorithms in the sinusoidal wave case. By using the hypothesis test method the assumption of Gaussian distribution is rejected for Algorithm "B". This is probably due to the approximations introduced with its formulation as described in Section 5.3.1.

Table 5.2: Test #1-Chi-square test results

| Algorithm | Number of bins | Chi-square | Probability | Rejected (true/false) |
|---|---|---|---|---|
| B | 6 | 18.0391 | $4.3176 \cdot 10^{-4}$ | 1 |
| D | 8 | 3.4183 | 0.6358 | 0 |
| A | 8 | 3.5080 | 0.6222 | 0 |

#### 5.3.3.2 Accuracy Test #2

The aim of this second test was to verify the capability to measure accurately the frequency of sine waveforms in the presence of harmonic distortion, as it may occur in a distribution network. The signal has been generated with a Digilent Analog Discovery 2, a multi-function instrument that allows to generate customized signals with an output accuracy of ±25mV ±0.5%, lower than the one assumed in Test #1. In this test, the following waveforms were considered: a sinusoidal 50 Hz wave without harmonics, two waveforms with THD equal to 5% and 20% respectively, a triangular one. For each waveform, 1000 measurements were performed for each algorithms. As in previous tests, algorithms were run on the same sampled data to allow comparison. Test results, summarized in Table 5.3, confirmed what observed in the first test. Both "D" and "A" algorithms perform better than "B", which is characterized more often by the presence of measurement absolute errors above 10 mHz.

Table 5.3: Test #2-Results with Analog Discovery 2 as waveform generator

| Waveform | Algorithm ID | Mean value [Hz] | Standard deviation | Max AE [Hz] | MAPE [%] |
|---|---|---|---|---|---|
| Sine | B | 50.0003 | 0.00226 | 0.01956 | 0.00329 |
| | D | 50.0003 | 0.00152 | 0.00881 | 0.00242 |
| | A | 50.0003 | 0.00143 | 0.00689 | 0.00233 |
| Sine THD=5% | B | 49.9995 | 0.00213 | 0.02870 | 0.00309 |
| | D | 49.9995 | 0.00150 | 0.00801 | 0.00246 |
| | A | 49.9995 | 0.00143 | 0.00781 | 0.00239 |
| Sine THD=20% | B | 49.9994 | 0.00236 | 0.01637 | 0.00348 |
| | D | 49.9996 | 0.00188 | 0.01744 | 0.00274 |
| | A | 49.9996 | 0.00182 | 0.01747 | 0.00265 |
| Triangular | B | 49.9991 | 0.00220 | 0.01933 | 0.00361 |
| | D | 49.9992 | 0.00159 | 0.00554 | 0.00286 |
| | A | 49.9992 | 0.00155 | 0.00567 | 0.00281 |

It was observed in several numerical tests carried out by applying the proposed algorithm on Matlab simulated waveforms, and here not presented for the sake of

brevity, that the presence of harmonic distortion does not really affect the accuracy. Noticeably in some cases it was possible to obtain results even more accurate than the case with an absence of distortion. These numerical results are confirmed by the experimental ones. The case with a 5% THD is characterized by accuracies very close to the pure sine wave test case. Also the case with a 20% THD is characterized by comparable average results, with the exception of a single case in which all algorithms have made a high absolute error. Although chi-square results are not reported here for the sake of brevity, results show again a non-Gaussian distribution for values measured with the Algorithm "B".

#### 5.3.3.3 Accuracy Test #3

In this third case, the device was tested by measuring the voltage signal output generated by the universal relay testing system SMC Mentor-12. This testing system allows to generate sinusoidal waveforms with a voltage magnitude up to 150 V and high accuracies in both voltage (0.1% of the value ±0.03% of the range) and frequency (1 ppm). The use of this device allows to test the proposed algorithm, in a controlled environment, with voltages which can be typically obtained from real voltage transformers. Although Mentor-12 generates a voltage signal with negligible noise, the measurement chain on this test, is also affected by the errors introduced by the voltage transducer used to adapt the voltage power output to the input channels of the ADC board. The voltage transducer used for tests is characterized by an accuracy of ±2%. Algorithms were tested using sinusoidal voltages at 47.50, 50.00 and 51.50 Hz. Table 5.4 collects the test results obtained with 1000 measurements. Results confirmed the measurement device capability to acquire and process signals in a large interval around the nominal frequency of 50 Hz, with a suitable accuracy. The performances of the three algorithms are comparable in terms of standard deviation. However, Algorithm "B" had worst performances in terms of Max AE and MAPE.

Table 5.4: Test #3-Results with Mentor-12 as voltage generator

| Waveform frequency | Algorithm ID | Mean value [Hz] | Standard deviation | Max AE [Hz] | MAPE [%] |
|---|---|---|---|---|---|
| 47.50 | B | 47.5002 | 0.00358 | 0.01766 | 0.00569 |
| | D | 47.5001 | 0.00350 | 0.01373 | 0.00540 |
| | A | 47.5001 | 0.00347 | 0.01332 | 0.00534 |
| 50.00 | B | 50.0001 | 0.00413 | 0.02422 | 0.00618 |
| | D | 50.0002 | 0.00394 | 0.02174 | 0.00565 |
| | A | 50.0002 | 0.00389 | 0.02138 | 0.00554 |
| 51.50 | B | 51.5000 | 0.00397 | 0.01929 | 0.00581 |
| | D | 51.4999 | 0.00373 | 0.01455 | 0.00532 |
| | A | 51.5000 | 0.00371 | 0.01495 | 0.00528 |

#### 5.3.3.4 Test #4: CPU Timing

Figure 5.2 illustrates total and partial average CPU timings, required for sampling and acquisition, signal conditioning and frequency computation, by each algorithm. To run any of the three algorithms, two entire periods must be sampled. Having conservatively assumed that, in power system operation, frequencies are surely above 45 Hz, the sampling time is set to 46 ms. As shown in Fig. 2, the sampling time is the major bottleneck of the adopted procedure. Algorithm “B” is the fastest one, with an overall time of 80 ms, whereas Algorithm “D” is the slowest, because of the higher computational complexity. Algorithm “A”, with an average computational time very close to Algorithm “B”, provides the best compromise between speed and accuracy. It can be noted that the computation is a minor burden when compared with sampling and pre-processing (sampling, acquisition, conditioning) phases. Computation time in algorithms “A” and “B” is about 10 ms, and this is figure that has to be considered when comparing to other approaches which do not consider sampling and signal conditioning times. This is the timing that characterizes the algorithm solution, whereas different architectures or solvers can be used for signal conditioning and sampling.

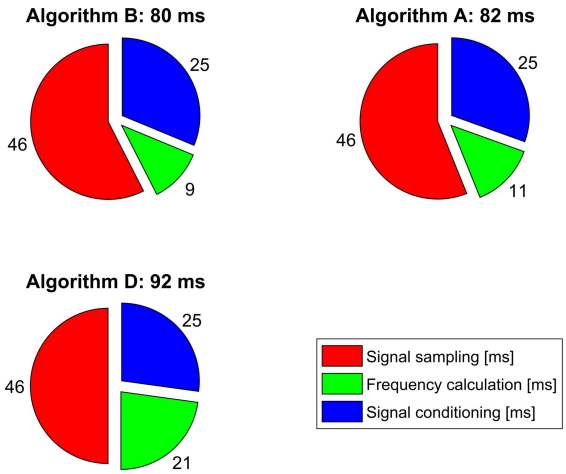


Figure 5.2: Test #1-Average runtime for all algorithms

#### 5.3.3.5 Test #5: RoCoF Assessment

The proposed fast frequency measurement approach was tested using frequency ramps applied to a real system. The frequency was measured at the LabZERO microgrid facility, using the controllable power source Triphase PM15A30F60 in grid-forming mode [177]. The power source was programmed to supply voltage with time-varying frequency profiles, chosen accordingly to the ones suggested by ENTSO-E to assess RoCoF withstand capability of protections [178]. This test was carried out using the over-frequency and under-frequency profiles plotted respectively in Fig. 5.3 and Fig. 5.4. Measurements were obtained considering the Algorithm "A", which guarantees the best compromise between speed and accuracy. The two plots in Fig. 5.3 and Fig. 5.4 show the deviation between the reference frequency profile and the values measured on the microgrid. In both cases, the two plots almost overlap, with a small delay due to the algorithm execution time. Figures 5.5 and 5.6, compare the theoretical RoCoF with the obtained by two subsequent frequency measurements.

Results are very promising, considering that no filters were applied to the RoCoF output and that, according to the IEEE Std. C37.118.1-2011, the expected RFE requirements under frequency ramp tests for synchrophasors is 0.1 Hz/s [179]. Since higher errors can be experienced at RoCoF "transition times", the standard suggests to ignore two subsequent samples after each transition. By neglecting only one sam-

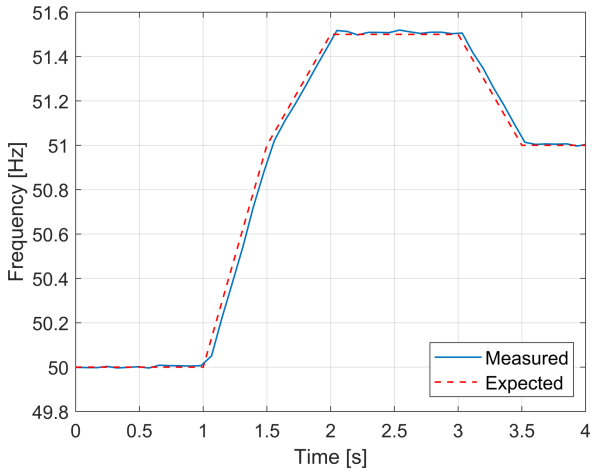


Figure 5.3: Test #5-Frequency measure in the over-frequency case

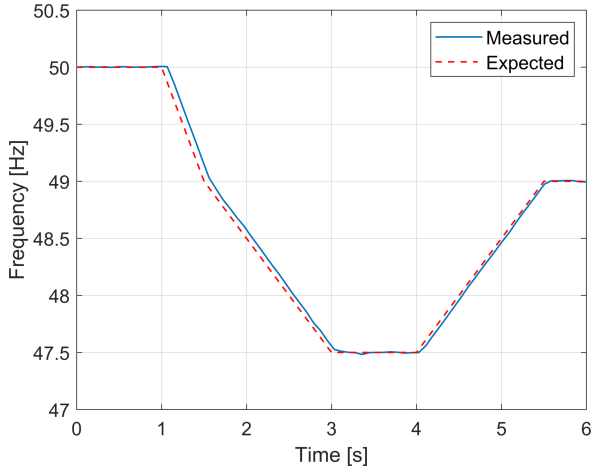


Figure 5.4: Test #4-Frequency measure in the under-frequency case

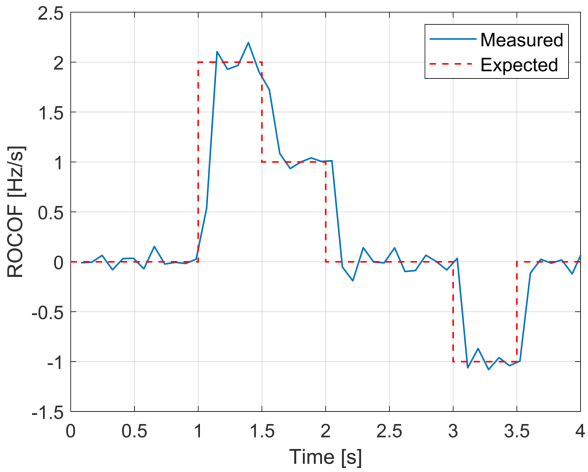


Figure 5.5: Test #5-RoCoF estimation in the over-frequency test

Figure 5.6: Test #4-RoCoF estimation in the under-frequency test

ple after RoCoF transitions the average RFE was assessed in 0.059 Hz/s and 0.049 Hz/s for the over-frequency and the under-frequency test, respectively. In both cases, the maximum RFE was about 0.19 Hz/s. Although the maximum measured RFE appeared higher than the value proposed by the IEEE Std C37.118.1-2011, it should be reminded that the experimental measurements were obtained in a real system affected by noise, whereas standard requirements assume ideal conditions (sinusoidal balanced three-phase voltage waves). The use of a filter allows to reduce the RFE, although it would slow calculations and increase the delay time. The problem of finding the best compromise in terms of noise reduction and delay time will be addressed in future experiments that will test the synthetic inertial response of physical components to the measured RoCoF.

### 5.3.4 Assessment of the proposed algorithms

Test results demonstrated that frequency can be estimated with an accuracy compatible with the European network code on demand connection, and with the more severe ENTSO-E recommendations. A reporting rate smaller than 100 ms was reached for the proposed architecture, with suitable accuracies even in the presence of highly distorted

waveforms. Computation associated with the best algorithm which performs best in terms of accuracy and speed is about 10 ms. A measurement of RoCoF on a real microgrid during a frequency ramp test showed an average error of about 0.05 Hz/s and a maximum RFE of 0.19 Hz/s. This error can be significantly reduced by applying a filter or improving the RoCoF calculation method.

## 5.4 A new controller for SI and FFR

The provision of Synthetic Inertia, or Fast Frequency Response, requires that a power device must be able to detect and respond to frequency variations very rapidly, in a few hundred milliseconds from the beginning of the transient event. As demonstrated in [25], a battery energy storage systems represents one of the best candidates to provide frequency ancillary services thanks to its technical characteristics, such as long discharge time, high ramping rate, and high voltage/frequency control capability of its inverter. As previously specified, the efficacy of a SI control is also severely affected by the quality of frequency and RoCoF measurements. However, authors in [153] even suggested that the assumption of having reliable RoCoF signals at the distribution level may be unrealistic. More advanced frequency measurement systems, such as intelligent electronic devices (IED) or PMUs, might be employed, but they are clearly not suitable for end-user applications due to their high costs [153], [170].

In the literature, several studies demonstrated the possibility of providing fast frequency support at the end-user level by controlling domestic loads, such as refrigerators and boilers [21], [23], or single-phase electric vehicles [180]. In this sense, storage systems are also considered the best source to provide fast frequency control services [165], [181], [25], [182]. Nevertheless, although the idea of using DERs for SI support is generally accepted, few practical implementations can be found in the literature, and the actual controllability of legacy distributed resources was never addressed [161].

Test results previously described proved the capability of the investigated frequency measurement algorithms to be implemented in a low-cost device and comply with end-user applications. Therefore, the possibility to develop a low-cost controller able to autonomously measure frequency and RoCoF, and implement a SI control law

on the management system of remotely controllable DERs was investigated [161], [183]. As a point of strength, the proposed controller has the advantage to be enabled to provide SI response for any distributed component that possesses the ability to receive a remote control signal on a fast communication channel without the need of reprogramming inverter control schemes or management system. Based on this, a real BESS was employed as a controllable DERs to test in a PHIL environment the SI action law provided by the investigated controller.

### 5.4.1 Controller Description

The controller studied in this work is based on a very low-cost architecture (below USD 100), being based on the use of an off-the-shelf single-board computer. In particular, in order to detect and respond more rapidly to frequency variations, a Raspberry Pi 4 Model B (the newest version in its class) was adopted. Clearly, any other similar processing unit could be employed. Differently from its previous version, the Raspberry Pi 4 Model B has the following, more advanced, technical features: 64-bit quad-core processor, 4 GB of RAM, dual-band 2.4/5.0 GHz wireless LAN, Bluetooth 5.0, Gigabit Ethernet, USB 3.0, power over Ethernet capability, and a standard 40-pin GPIO header.

The main purpose of this controller is to estimate RoCoF variations and generate SI control of a BESS, accordingly. SI control is obtained by changing the battery's power output set-points with an additional control signal proportional to RoCoF variations. The SI control can happen even without having to reprogram the BMS, with particular advantages in the case of legacy devices, whose internal control schemes and logic, based on proprietary languages and codes, cannot be modified.

The proposed controller, whose scheme is shown in Figure 5.7, is able to acquire and process grid voltage signals, calculate both frequency and RoCoF, and communicate with other external devices through Ethernet (LAN), Bluetooth, and USB. The GPIO interface of the single-board computer was used to acquire the voltages. The GPIO works with digital signals only, and therefore a voltage transducer and an Analog-to-digital converter are required. The transducer used in this test is a high-

voltage differential probe, with a signal attenuation of 200×, coupled with a DC source used to add a 1.65 V offset in order to adapt the voltage waveform to the ADC-shield input voltage (i.e., 0–3.3 V). A 10-bit ADC, with a cost of about $10, equipped with serial peripheral interface was also mounted on a prototype shield and connected to the GPIO's pins.

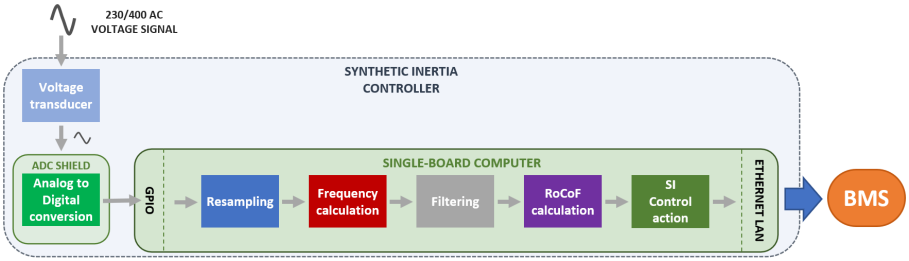


Figure 5.7: Scheme of the investigated SI controller

As a next step, the frequency values are employed to calculate the RoCoF and generate the corresponding SI control law. Nevertheless, as described in Section 5.4.3, due to the presence of noise and distortions on the acquired voltage signal, a filtering process was added between frequency and RoCoF calculation. This filtering stage is also recommended by ENTSO-E in a document discussing frequency and RoCoF measurement requirements [166]. As specified in this report, a wide range of different filter algorithms are available, such as Bessel, Butterworth, Chebyshev, elliptic, etc. However, these filters must be tuned in such a way to minimize the presence of noise without introducing excessive delays. An application case of frequency filtering is presented in [184], in which an appropriate feedback and feedforward filter was applied in order to remove noise as much as possible without affecting the RoCoF behavior. The algorithm is based on a combined version of "comb" filter, which acts by adding a delayed version of the signal to itself and causing constructive and destructive inference that can attenuate the specified frequency signal and its harmonics [185]. In this controller, a less sophisticated filter based on an exponential moving average was employed in order to limit the necessary computational burden. This algorithm is able to reduce lags introduced from the average process by applying more weight to the recent samples than the older ones, and, therefore, results as particularly sensitive

to recent signal changes [186]. According to the measured RoCoF values, the controller generates an SI control law and communicates it to the of the BESS. In these tests, the control law was transferred to the BMS through the LAN and using Modbus TCP/IP protocol.

### 5.4.2 Experimental Tests of SI Control through BESS

In order to assess the performances of the proposed SI controller, PHIL tests were performed by means of a microgrid facility located at LabZERO laboratory of Politecnico di Bari [187]. This facility permits to implement, in a real-time simulating environment, the interaction between the power system and real power devices of the microgrid. Simulation tests performed by the author, not reported here for brevity, demonstrated how this facility is promising, in particular, for testing the provision of AS (e.g. voltage regulation) in real-time co-simulations [143], [188].

The very first step of the performed analysis was to test the behavior of the 5 kVA LiFePO4 BESS currently installed in the LabZERO microgrid when it is controlled to provide Synthetic Inertia during a simulated frequency event. The controlled physical battery interacts with a power system model that reproduces, in real-time, the electromechanical transient following a sudden power imbalance. This first PHIL simulation was used as a benchmark to compare, in the following tests, the SI response of the BESS when it is regulated by the proposed controller. In these additional PHIL tests, the SI control law sent to the BMS is directly generated by the Raspberry controller, which autonomously measures frequency and RoCoF, and controls the battery. These tests were also aimed at demonstrating how, by moving the evaluation of the SI control at field level, it is possible to reduce the delays due to communication and control processes.

The Power Hardware-in-the-Loop test bench is shown in Figure 5.8. The real-time simulator (RTS) OPAL RT5600 (OPAL-RT Technologies, Montreal, QC, Canada) is used to simulate the electromechanical response of a generic power system, whereas the programmable power source Triphase PM15A30F60 (Triphase, Holsbeek, Belgium) is programmed to control the entire microgrid in grid-forming mode. Through

synchronous communication, based on a fiber optics channel, the real-time frequency of the simulated system is sent by the RTS to the programmable source. This frequency value is imposed in real time on the actual microgrid and, therefore, on all its components. In such a way, the frequency excursions following load/generation imbalances, which are controlled through the primary frequency regulation of the simulated system, are applied to the microgrid and to the BESS under study.

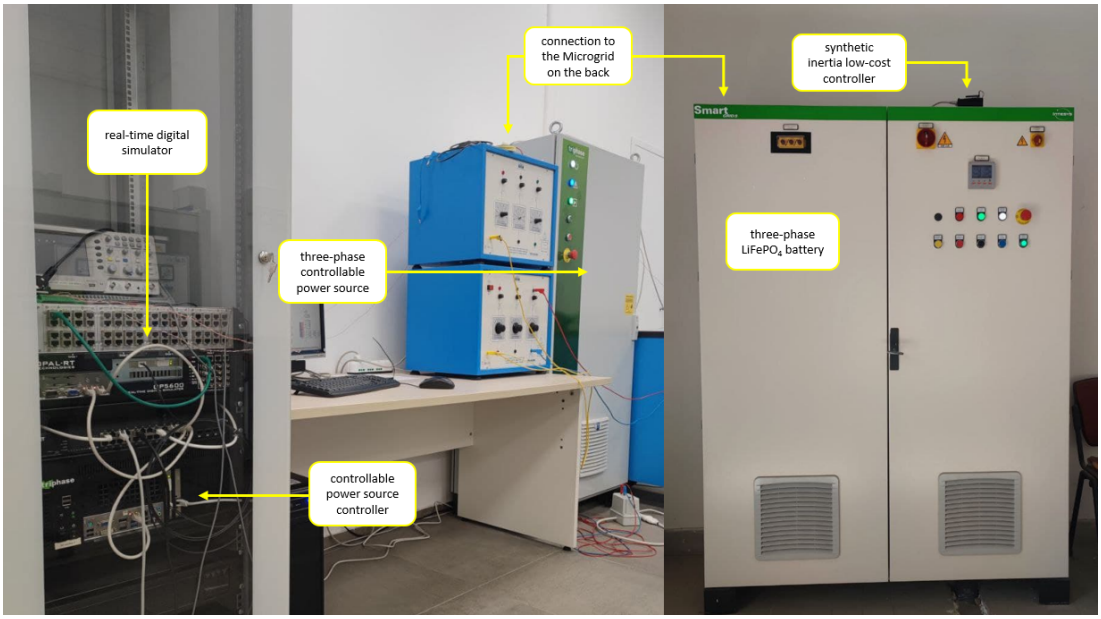


Figure 5.8: Power hardware-in-the-loop test equipment

### 5.4.2.1 System Model and Frequency Response without SI

In Figure 5.9, the block diagram used to build an equivalent model of the power system is shown. The term $\Delta P_L$ is the active power load variation applied to generate a power imbalance, whereas $\Delta P_{SI}$ represents the active power exchanged by BESS to provide SI, and $\Delta P_G$ is the primary frequency regulation following the disturbance. Table 5.5 summarizes the values assigned to the droop $R$ and to the delays $T_G, T_{T1}, T_{T2}, T_{T3}$ of the governor and reheat turbine models. The limits set for the governor model consider the valve opening constraints, whereas limitations imposed on the turbine model take into account the active power limits. A substandard level of system inertia $H$ (3

seconds) was assumed to simulate the arising of reduced total system inertia (TSI) conditions due to the high penetration of inverter-based Renewable Energy Sources. This assumption was made in accordance with [189], where the authors estimated system inertia of the Italian transmission system, highlighting how a TSI even lower than 3 seconds has been experienced during specific real-time conditions.

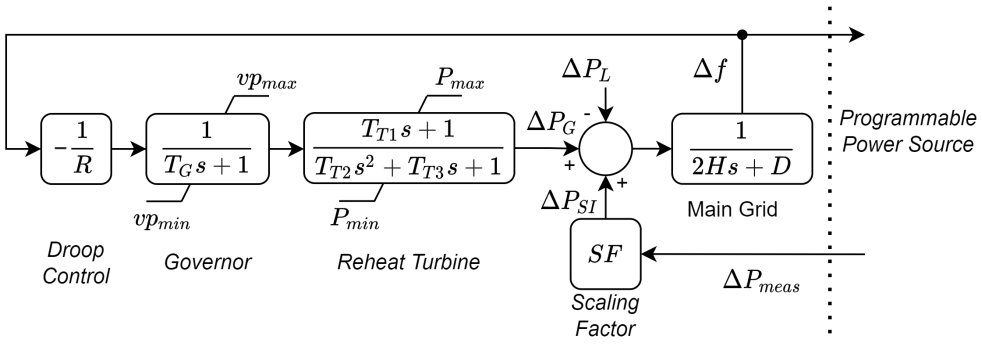


Figure 5.9: Power system model with synthetic inertia contribution

Table 5.5: Power system model coefficients

| $R$ **[p.u.]** | $T_G$ **[s]** | $T_{T1}$ **[s]** | $T_{T2}$ **[s]** | $T_{T3}$ **[s]** | $H$ **[s]** | $D$ | $SF$ **[p.u./kW]** |
|---|---|---|---|---|---|---|---|
| 0.050 | 0.20 | 2.1 | 2.1 | 7.3 | 3.0 | 0.020 | 0.0116 |

Figure 5.10 shows the transient response of the simulated system to a sudden load step change, when only primary frequency regulation is considered (i.e., the term $\Delta P_{SI}$ related to the power contribution of Synthetic Inertia is set to zero). Since the scope of the following tests was to test inertial control, which happens within the first 500–1000 ms of the transient, secondary frequency regulation was not modeled. At the beginning of the simulation ($t < 0$ s), the system was assumed to be in steady-state conditions, with the synchronous generation perfectly balancing the load. At time $t = 0$ s, an instantaneous upward load step change ($\Delta P_{load} = +0.1$ p.u.) was applied. The primary frequency regulation of the synchronous generation regulated the power output of the quantity $\Delta P_{gen}$ so that a new equilibrium point was reached. The primary frequency regulation was modeled according to the transfer functions typical of a thermoelectric

plant, whose parameter values are shown in Figure 5.9.

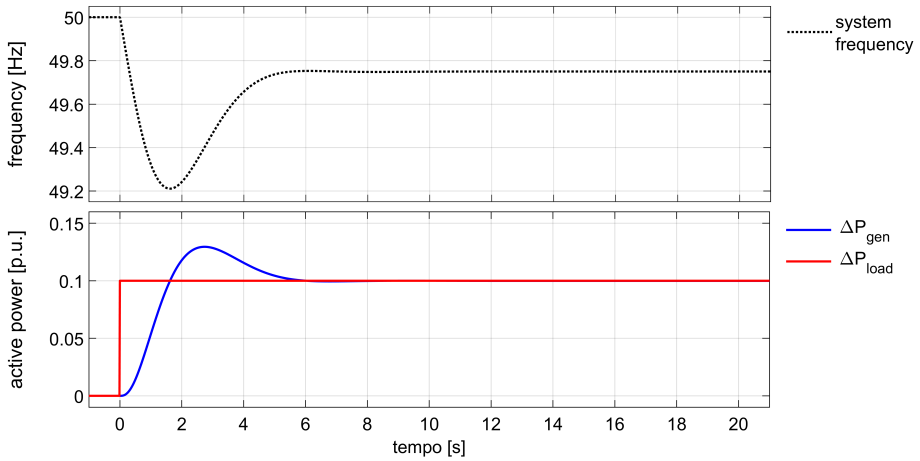


Figure 5.10: Frequency and active power trajectories without SI control

As shown in Figure 5.10, the load step variation gave rise to the frequency transient represented by a dotted black curve. After 1.62 s, the frequency trajectory reached its minimum, or *nadir*, at 49.21 Hz. Then, thanks to primary regulation, system frequency is brought back close to its nominal value, settling to about 49.75 Hz. Without Synthetic Inertia support, frequency control was only provided by the synchronous generators that, by means of the primary frequency regulation, adjusted active power generation according to the simulated response of the turbines' governor. After about 6 seconds from the contingency, the power response $\Delta P_{gen}$, depicted in Figure 5.10 with a continuous blue curve, reached the same value of the applied load variation $\Delta P_{load}$. A power overshoot of about 0.030 p.u. was reached during regulation.

#### 5.4.2.2 PHIL Tests of Synthetic Inertia by Means of BESS

In this subsection, the capability of a BESS to modulate its power output and provide frequency support was investigated. The presence of an additional non-null active power contribution $\Delta P_{SI}$ in the scheme of Figure 5.9 was therefore considered. This additional term takes into account the SI contribution provided by BESS in terms of active power balance. The BESS power output was remotely managed, applying a

current reference set-point $I_{ref}$ to the BMS. This set-point was calculated by a simulated SI controller on the basis of the RoCoF signal, and then sent via Modbus TCP/IP communication. In these tests, the proposed SI controller was only emulated through the RTS. Frequency and RoCoF measurements are ideal signals obtained by the RTS during the transient simulation.

The active power response of the BESS was measured by the controllable power source and fed back to the RTS in order to close the loop of the PHIL simulation. Since the SI active power control should reproduce the response of a larger number of storage units, $\Delta P_{SI}$ was scaled by a factor $SF$ (shown in Figure 5.9). By means of this scaling factor, the real BESS, whose maximum inertial contribution was set to about 3.5 kW, represents in the real-time simulation a BESS with nominal power equal to 4% of the reference power. The Synthetic Inertia control adopted in this test case and simulated through the RTS is represented in Figure 5.11.

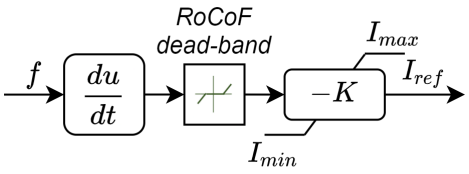


Figure 5.11: Block diagram of the SI controller simulated with the RTDS

With the aim to avoid an excessive control activity of BESS around the frequency equilibrium point and endanger the lifespan of the battery, a 10 mHz/s RoCoF dead-band was assumed. Moreover, the saturation block limited the direct current reference $I_{ref}$ to [−5,+5] A, thus about 3.5 kW in charge/discharge mode.

As previously mentioned, in these tests, an ideal SI controller was just emulated in the RTS. The SI control law was obtained according to the scheme Figure 5.11. The RoCoF signal was calculated during the simulation by deriving the continuous frequency signal. RoCoF was therefore a continuous quantity, known instantaneously at each simulation time step (i.e., 0.125 ms). Due to the absence of delays and measurement errors in the RoCoF signal, as shown in Figure 5.11, no filters were adopted in the control chain.

In tests, increasing values of gain $K$ in the interval 10–25 A/(Hz/s) were used in order to study the dependence of the system frequency response with respect to the amount of active power provided by the inertial control. Figure 5.12 shows the frequency response of the simulated system after the introduction of the SI support with various values of gain $K$.

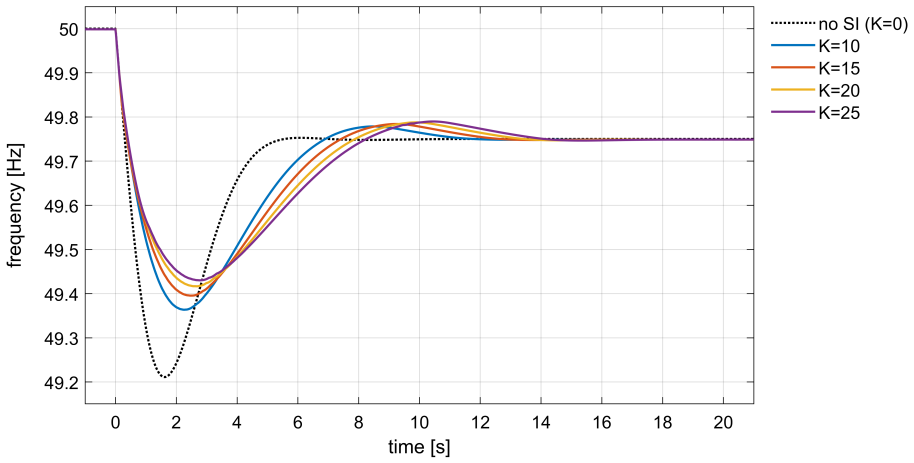


Figure 5.12: Ideal SI controller: frequency response with different gain $K$

The black dashed line represents the system frequency response without any SI support, which was previously calculated and assumed as base case. Differently, all other curves are the frequency trajectories obtained in the presence of BESS Synthetic Inertia control. The observed response is coherent with the typical effects of fast SI control actions [181]. In comparison with the base case (no SI control action), higher frequency *nadir* points were reached, even though the settling time was increased.

In general, it can be observed that an increase of gain $K$ allowed to reduce the frequency derivative in the very first instant and reach a higher *nadir*. However, higher magnitude of inertial control corresponds also to larger second overshoot and longer settling time. From Figure 5.13, it is possible to observe how control gain affects system response. A lower gain reduces the BESS participation in frequency control, letting the synchronous machine more rapidly take care of the power imbalance. The synchronous generator overshoot decreases with SI contribution. In the PHIL tests, this overshoot was reduced from 0.0295 p.u. of the base case to 0.0232 and 0.0230 p.u.

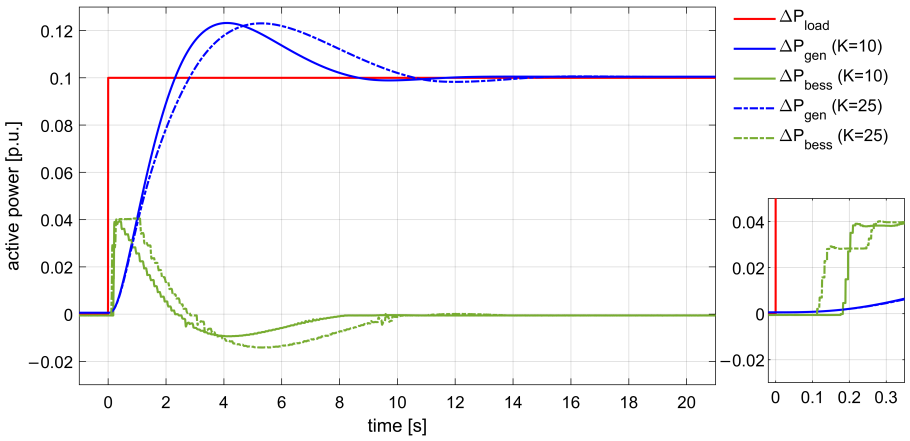


Figure 5.13: Ideal controller: BESS active power response with different gain $K$

for the case with $K = 10$ and $K = 25$, respectively. Having reached the *nadir*, the SI control action changes its sign: for this reason, higher gains cause an increase of the second frequency overshoot and an increase of the time necessary to reach steady state.

Table 5.6 permits to better compare the results obtained using different gains after the same load-step variation. The settling time was calculated considering a 2% tolerance around the steady state value. The fall time is the time necessary for the frequency to drop from 10% to 90% of the settling value. This fall time was used to average the RoCoF value in the initial characteristic of the frequency transient (see Table 5.6). To assess the impact of SI on RoCoF, the average RoCoF value is more suitable than the maximum value, since the latter is always experienced in the very first instant after $t = 0$ s, when no actual regulating response of the BESS is possible (in other words, the maximum instantaneous RoCoF is the same in all simulations). The obtained results demonstrated that fall time and average initial RoCoF improve with SI gain increase. However, it can be noticed how these improvements soon saturate with SI gain increase, whereas settling time continues to increase. This is due to the fact that, in the initial moments when RoCoF reaches its maximum, high gains will cause SI control to hit the maximum active power limits of the battery, and therefore no further frequency response improvement can be obtained.

This is a known problem of SI control, and, in general, two possible solutions can

Table 5.6: Ideal Synthetic Inertia Controller: Characteristics of the Frequency Step Response

| **Gain $K$ [A/(Hz/s)]** | **Frequency Reporting Time [s]** | **Fall Time [s]** | **Average RoCoF [Hz/s]** | **Time *nadir* [s]** | **Frequency *nadir* [Hz]** | **Overshoot [%]** | **Settling Time [s]** |
|---|---|---|---|---|---|---|---|
| 0 | - | 0.242 | 0.824 | 1.616 | 49.211 | 0.050 | 5.063 |
| 10 | inst. | 0.307 | 0.650 | 2.285 | 49.364 | 0.057 | 10.764 |
| 15 | inst. | 0.310 | 0.645 | 2.483 | 49.396 | 0.068 | 11.896 |
| 20 | inst. | 0.312 | 0.640 | 2.672 | 49.417 | 0.076 | 12.800 |
| 25 | inst. | 0.321 | 0.623 | 2.770 | 49.430 | 0.080 | 13.547 |
| 10 | 0.050 | 0.278 | 0.720 | 2.254 | 49.367 | 0.056 | 10.795 |
| 10 | 0.100 | 0.260 | 0.769 | 2.209 | 49.371 | 0.053 | 10.842 |
| 10 | 0.150 | 0.243 | 0.824 | 2.181 | 49.380 | 0.049 | 10.949 |

be adopted. The first solution is to adopt a nonlinear SI control with a gain that is a function of RoCoF. This kind of control allows to exploit all fast frequency regulation resources in the first fall, whereas the SI control action will more rapidly damp out while frequency approaches the *nadir* or the settling value. The disadvantage of this control is that SI response will always be very moderate in frequency events that are not characterized by high-frequency derivatives. Another possible solution is to adapt gain to the specific operating conditions. Gain can be set so that active power control will reach maximum capacity during a credible worst-case event (the one characterized by the highest frequency derivative). In an isolated network, this event might correspond to the sudden loss of the highest load feeder or generating station. Clearly, this kind of approach requires the presence of a control center (a microgrid controller in the case of a small isolated distribution network), plus a communication channel must be established between this control center and the SI controllers installed on the field. Gain $K$ can be easily updated knowing the current battery capability and the expected maximum RoCoF excursion. In both cases, the use of an additional fast frequency control proportional to the frequency deviation (and not to the RoCoF) can help to control transients characterized by small derivatives, but large frequency deviations. Investigations on these control schemes are, however, out of the scope of this test, since the main aim is to test the fast control capability of the proposed controller. Any kind of SI control rule can be easily programmed in the controller.

Figure 5.13 allows to assess the speed of the BESS active power response. The first variation in power exchange was measured by the programmable power source after about 80–100 ms from the load step change. Despite this initial delay, the BESS was able to reach its active power peak within 200 ms. The SI controller was just simulated and therefore there were no delays due to frequency and RoCoF measurements. However, some delays were introduced by the Modbus TCP/IP communication and the use of a master node to control the BMS. In the considered network, these delays are usually in the 50–80 ms range.

Some final PHIL tests were carried out using the simulated ideal controller. These tests, whose results are also synthetically reported in Table 5.6, were aimed to assess the impact of the frequency reporting rate. This is a relevant issue, since the

simulations with a real controller, which will be shown in the next subsection, are characterized by actual measurement delays. So far, frequency and RoCoF measurements were assumed to be continuous variables, known instantaneously at each time step of the simulation. Figure 5.14 shows what happens when the reporting rate of frequency (and RoCoF) assumes values closer to the actual time resolution achievable with hardware instrumentation. These tests were performed using gain $K = 10$.

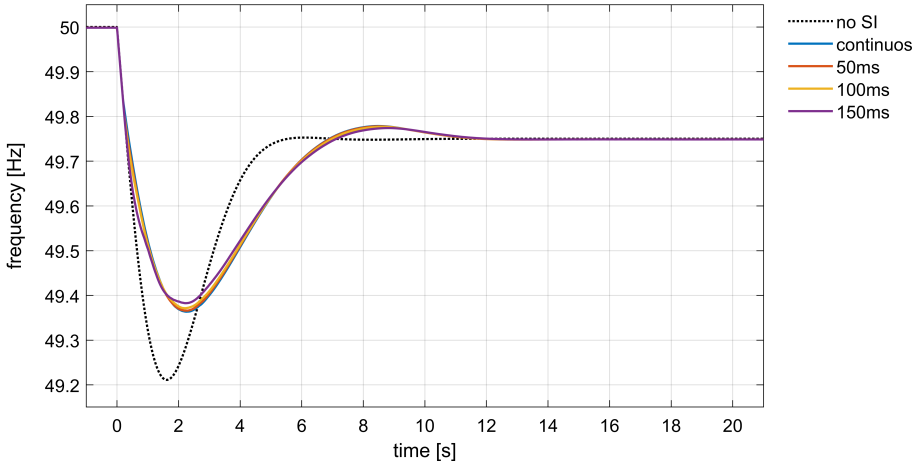


Figure 5.14: Ideal controller: frequency response with different RoCoF reporting time, $K = 10$

If the response of the controlled equipment is slowed by measurement reports, the frequency falls faster. However, up to about 100 ms, the reporting time barely affected the frequency transient. In Figure 5.15, it is possible to notice how with a 150 ms reporting time, the battery was operated close to its maximum capacity for a longer period, even leading to the highest *nadir*. However, this response is more similar to the one obtained by fast frequency regulation schemes that operate with control laws proportional to the frequency deviation; the response is improved in terms of *nadir*, but the initial RoCoF is barely influenced by the BESS control. In this test case, characterized by low inertia and a very fast frequency transient, reporting times equal to or higher than 150 ms cannot produce any improvement in terms of RoCoF reduction. A numerical comparison was peformed between the results of the simulations (Table 5.6) in terms of RoCoF, *nadir*, and settling times. These simulations will also be used as a benchmark for the PHIL tests with the actual controller.

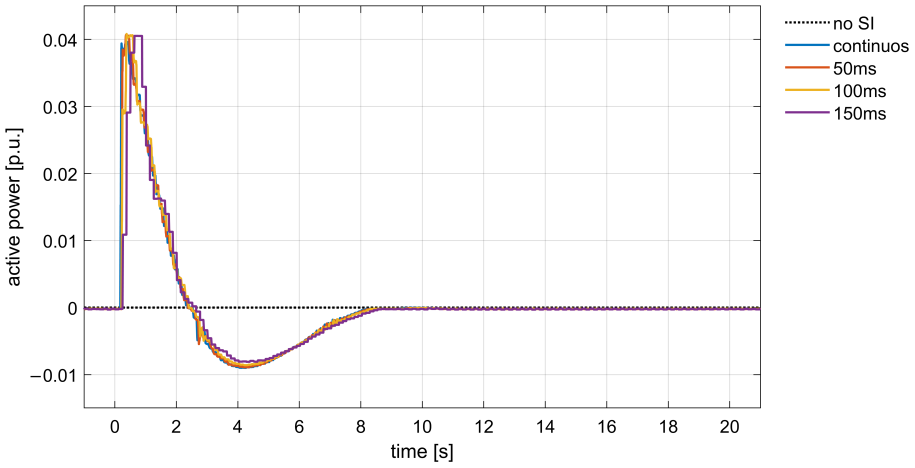


Figure 5.15: Ideal controller: BESS active power response with different RoCoF reporting time, $K = 10$

### 5.4.3 PHIL Tests with the Single-Board SI Controller

Based on previous results, final additional tests were performed with the aim to assess the capability of the proposed SI controller to provide frequency support by means of BESS. Since this controller is able to measure the grid frequency directly from the voltage signal of the BESS busbar, calculate RoCoF, and implement an SI control law on the BMS, in these tests, the RTS was only employed to simulate the power system electromechanical response and provide the frequency reference to the programmable source.

#### 5.4.3.1 Influence of Measurement Errors

Differently from what discussed in the previous subsections, in these tests, the BESS response is affected by both RoCoF sampling period and measurement errors. Due to the methodology used for fast frequency measurement, the reporting time of frequency (and RoCoF) of the controller (Raspberry Pi 4-based) is about 50–60 ms. This time is needed to sample the two entire cycles necessary to evaluate the weighted autocorrelation integral and process the samples to obtain the frequency measurement.

Figure 5.16 shows the frequency response obtained using the proposed SI controller without applying any filter to the RoCoF signal. Even though a very wide

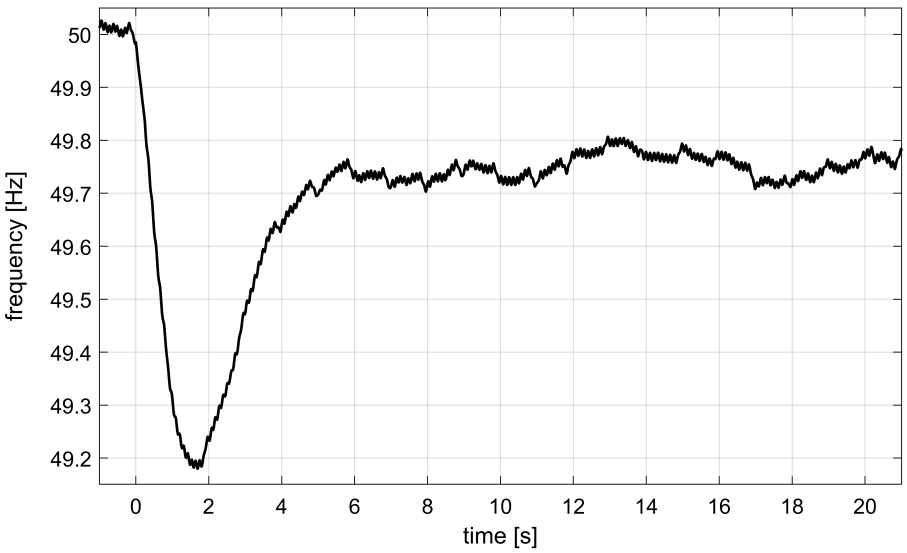


Figure 5.16: Real controller: frequency response without filters on frequency measurements, $K = 10$

RoCoF dead-band ($\pm 0.100$ Hz/s) and a small gain (i.e., $K = 10$) were adopted, the presence of noise on RoCoF introduced excessive errors on BESS control. No improvement was brought to the frequency response in terms of *nadir*. Moreover, measurement errors introduced by the controller resulted in a continuous activation and deactivation of the BESS response, causing unbearable frequency fluctuations around its theoretical steady-state value.

#### 5.4.3.2 Tests with Filtered RoCoF Measurements

Since low-cost applications, such as the one proposed with this single-board controller, cannot make use of high-accuracy transducers and signal processing instrumentation, measurement errors must be filtered. In the following tests, a low-pass filter based on exponential smoothing was applied to frequency measurements. The SI control scheme programmed on the single-board SI controller is shown in Figure 5.17. The filtering action can be modulated by varying the smoothing factor $\alpha$ in the range $[0,1]$. The maximum filtering action is obtained with $\alpha = 0$, whereas the filter is completely deactivated with $\alpha = 1$. Samples $f_{filt}(k)$ and $f(k)$ are, respectively, the $k-th$ sam-

ples of the filtered and not filtered frequency at the time instant $t$. The RoCoF signal $RoCoF_{filt}(k)$ is calculated from the filtered frequency measurements using a discrete derivative function. Smoothing is needed not only to filter measurements but also to reduce the stress on the controlled component and avoid too many sudden power variations that can impact the cells' lifetime.

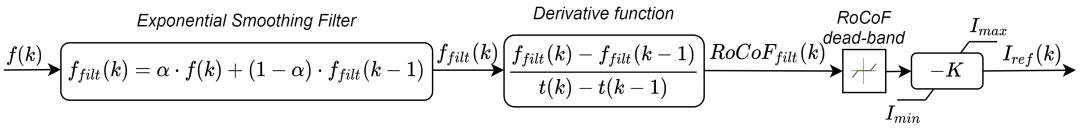


Figure 5.17: Block diagram of the actual SI controller

In Figure 5.18, the frequency response of the simulated power system during a generic frequency event is compared with the filtered and unfiltered frequency values measured by the controller at the microgrid switchboard where the BESS is installed. Figure 5.19 shows the corresponding values of RoCoF. The filtered signals were obtained with a smoothing factor $\alpha$ equal to 0.1. It can be observed that the filtered signals were slightly delayed, but the beneficial effects of the filter during a frequency measurement disturbance, arising around $t = 7.5$ s, are clearly visible. The RoCoF error was drastically reduced, also allowing to keep a small dead-band on RoCoF (i.e., $\pm 0.025$ Hz/s in all simulations with the real controller).

Figure 5.20 shows the system response obtained using the real SI controller, and adopting different values of gain $K$. The characteristics of the frequency response are also reported in Table 5.7.

The smoothing factor was set to 0.1 in all tests. With respect to Figure 5.12, the results obtained with the real controller are slightly worse in terms of initial RoCoF and settling time, but slightly better with regard to *nadir* and second overshoot. It can be observed that higher gains ($K = 20$ and $K = 25$) resulted in bumpier frequency trajectory, due to the amplification of RoCoF errors. Moreover, around the *nadir* point, higher gains created some small oscillations when the RoCoF trajectory entered and exited the dead-band. These small oscillations also introduced some errors in the detection of the *nadir* time and frequency, as in Table 5.7 for the case $K = 25$.

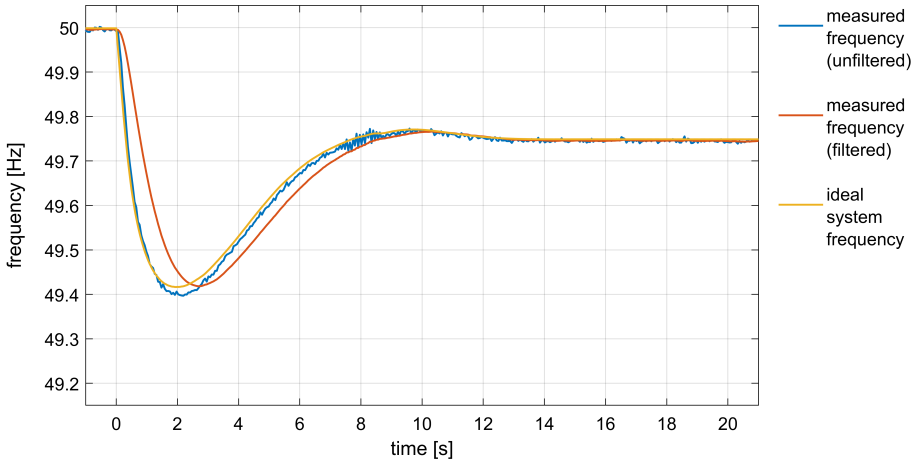


Figure 5.18: Frequency measured by the controller vs. ideal simulated frequency

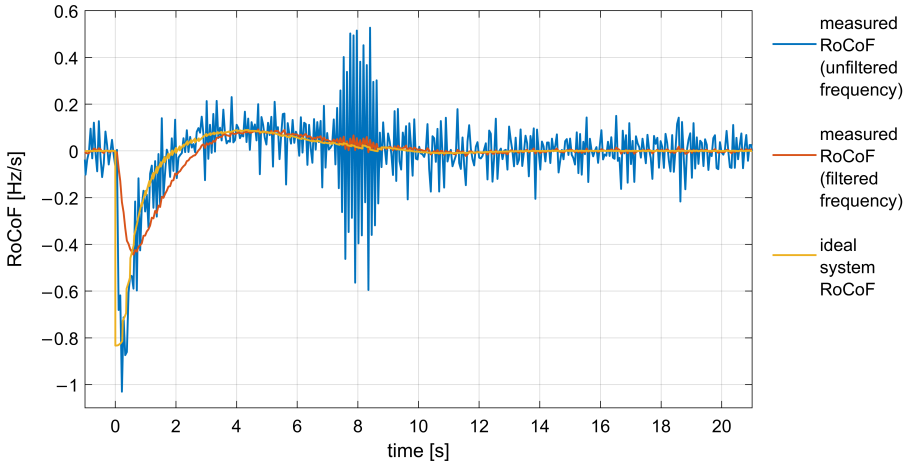


Figure 5.19: RoCoF measured by the controller vs. ideal simulated RoCoF

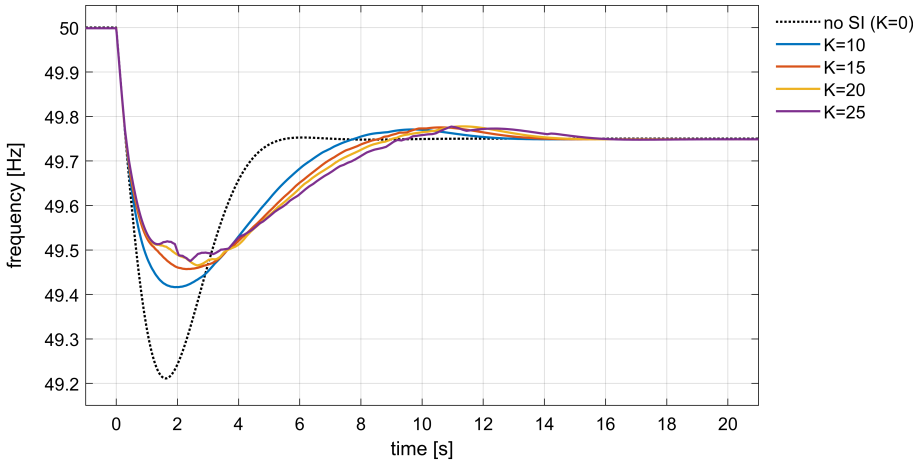


Figure 5.20: Real controller: frequency response with different gain $K$

Figure 5.21 compares the BESS response in the two extreme cases ($K = 10$ and $K = 25$), showing how a lower gain permitted obtaining a smoother response, with limited stress on the controlled component. According to these tests, higher gain levels produced only marginal improvements, which did not compensate the other drawbacks.

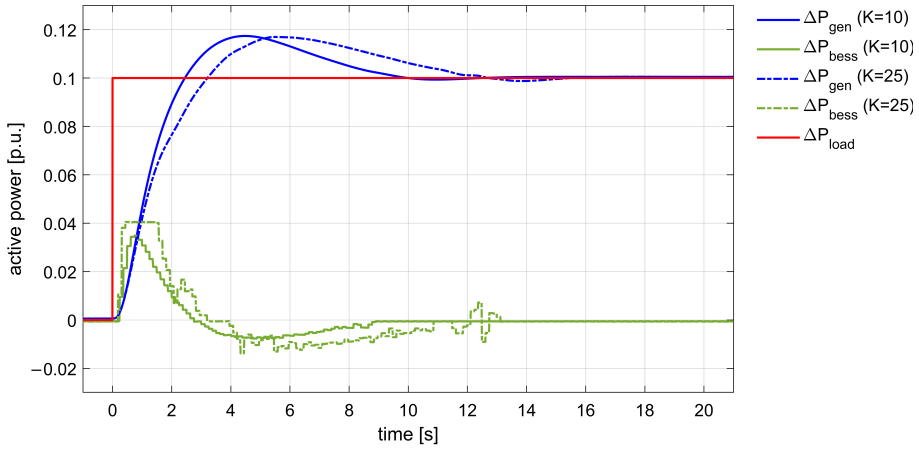


Figure 5.21: Real controller: BESS active power response with different gain $K$

#### 5.4.3.3 Frequency Measurement Reporting Time

Further tests were carried out to investigate the influence of the measurement reporting time with the smoothing factor $\alpha$. As shown in Figure 5.22 and Table 5.8, a higher smoothing factor ($\alpha = 0.25$) allowed reduction of the initial RoCoF, but the frequency response was still characterized by a lower *nadir* and permanent fluctuations due to the effects of RoCoF error. However, since RoCoF estimation is derived from two subsequent frequency measurements, the RoCoF error can be reduced with a slower frequency reporting rate. As observed in [166], since frequency measurement is based on the evaluation of power system voltage, frequency computation can typically be updated every few cycles, 90–120 ms. Since a trade-off between fast enough and accurate frequency measurements is needed, according to ENTSO-E, accurate RoCoF calculations should be based on sliding windows which average results over few consecutive measurements. Robust results can be obtained, for example, in about 0.5 s if a 100 ms time resolution is used. For this reason, some further tests were carried out introducing a small delay in the frequency reporting of the controller, so that more accurate RoCoF estimations can be used by the controller. The effect of increasing the reporting time up to 100 ms is shown in both Figure 5.22 and Table 5.8.

Increasing the reporting time to 100 ms allowed obtaining of more stable frequency responses, but it did not prove useful when a stronger filter was applied ($\alpha = 0.10$). A value of 100 ms reporting time worked well with a higher $\alpha$ ($\alpha = 0.25$), as in the green dotted line in Figure 5.22, obtaining comparable results to the ones obtained with faster reporting rate and $\alpha = 0.10$ (blue line). These results are comparable with the ones obtained with ideal delayed control (see Figure 5.14 and Table 5.6).

This result is significant for several reasons. If a slower reporting rate is employed, the controller has a consistent amount of idle time (in this case more than 40 ms) that can be used either in the implementation of more efficient data processing and filters or in the control of more devices. This means that there is enough time to send more control signals and to deal with different protocols and communication media, extending the range of action of the controller from just one BESS to more coordinated DERs. In a microgrid, where different DERs might provide asymmetric

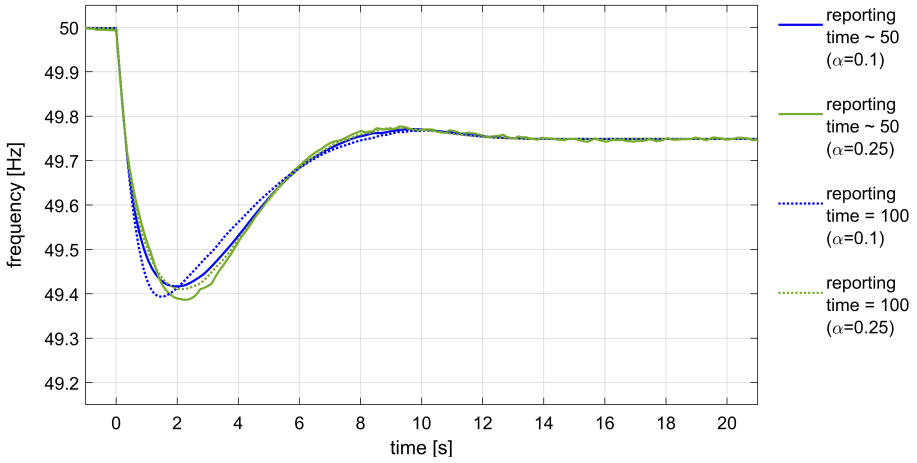


Figure 5.22: Real controller: frequency response with different reporting time and smoothing factor, $K = 10$

frequency control resources (for example, loads vs. renewable sources generation), this is a key improvement since it would allow increasing the extent of the frequency control capacity using just a single controller.

### 5.4.4 Discussion and Future Developments

The results obtained by previous PHIL tests validated the capability of the proposed controller to manage BESS, or other distributed flexible resources, in order to provide frequency support to power systems. The data shown in Tables 5.7 and 5.8 demonstrated that the inertial response can be sensibly improved in terms of frequency *nadir*. A limitation of the proposed approach is that initial RoCoF can only be minimally reduced by SI control. This is due to the unavoidable delays introduced by the measurement, filtering, and communication processes. An effective SI contribution can be reached only after few hundreds of milliseconds (see Figures 5.20 and 5.22). Clearly, the obtained performances cannot be compared with other approaches to virtual inertia, such as, for example, the ones based on virtual synchronous machines, which are able to generate much faster responses. However, one should be reminded that the scope of this test is to prove the feasibility of enabling, through low-cost technologies, Synthetic Inertia control of legacy and distributed devices which cannot be programmed

Table 5.7: Real synthetic inertia controller: characteristics of the frequency step response

| **Gain $K$ [A/(Hz/s)]** | **Frequency Reporting Time [s]** | **Alpha α** | **Fall Time [s]** | **Average RoCoF [Hz/s]** | **Time *nadir* [s]** | **Frequency *nadir* [Hz]** | **Overshoot [%]** | **Settling Time [s]** |
|---|---|---|---|---|---|---|---|---|
| 0 | - | - | 0.242 | 0.824 | 1.616 | 49.211 | 0.050 | 5.063 |
| 10 | ∼0.050 | 0.10 | 0.246 | 0.812 | 1.948 | 49.416 | 0.047 | 11.792 |
| 15 | ∼0.050 | 0.10 | 0.249 | 0.801 | 2.300 | 49.457 | 0.051 | 13.049 |
| 20 | ∼0.050 | 0.10 | 0.249 | 0.801 | 2.641 | 49.465 | 0.055 | 13.825 |
| 25 | ∼0.050 | 0.10 | 0.250 | 0.799 | 2.419 | 49.475 | 0.054 | 15.155 |

Table 5.8: Real synthetic inertia controller: comparison of frequency step response with different reporting time

| **Gain $K$ [A/(Hz/s)]** | **Frequency Reporting Time [s]** | **Alpha α** | **Fall Time [s]** | **Average RoCoF [Hz/s]** | **Time *nadir* [s]** | **Frequency *nadir* [Hz]** | **Overshoot [%]** | **Settling Time [s]** |
|---|---|---|---|---|---|---|---|---|
| 0 | - | - | 0.242 | 0.824 | 1.616 | 49.211 | 0.050 | 5.063 |
| 10 | ∼0.050 | 0.10 | 0.246 | 0.812 | 1.948 | 49.416 | 0.047 | 11.792 |
| 10 | ∼0.050 | 0.25 | 0.251 | 0.797 | 2.285 | 49.386 | 0.054 | 13.526 |
| 10 | 0.100 | 0.10 | 0.244 | 0.817 | 1.496 | 49.393 | 0.047 | 11.785 |
| 10 | 0.100 | 0.25 | 0.246 | 0.812 | 2.100 | 49.410 | 0.047 | 11.663 |

to emulate the behavior of a synchronous generator. These devices could be storage systems, such as in the performed tests, but also other flexible resources which could also have asymmetric active power control capacity (for example, demand response systems, photovoltaics, etc.). Nevertheless, achieved performances are comparable with typical activation times required for wind power or BESS in providing frequency support proportional to the frequency derivative (<0.5 s) [160].

The PHIL tests permitted testing of the response of the proposed control scheme in a realistic scenario, making use of real voltage trajectories affected by noise and including the actual computation and communication delays that can affect the control. Due to the presence of disturbances and uncertainties, such as time delays, and the presence of several blocks that introduce discontinuities (dead-band, saturations, etc.), it was preferred to check the stability of the controller through an extensive set of time-domain simulations and power hardware-in-the-loop tests. These tests were conducted adopting wide ranges of variation of main parameters such as delays, gains, dead-bands, etc. For the sake of brevity, only the results of few tests have been reported in the test. However, the system proved to be stable even in the presence of highly distorted measurements, like also demonstrated in Figures 5.18 and 5.19. The main aim of this work was to check that the performances obtained with an autonomous controller, able to both measure frequency from voltages and produce a control signal, comply with the time requirements needed for inertial support. Future developments will be aimed to investigate further on the design of the measurement filter, with a more analytic stability analysis.

## 5.5 SI and FFR through Public Lighting Systems in small Non-synchronous Power Systems

In addition to the study proposed in Section 5.4, this thesis also investigated the possibility to develop a centralized control aimed at providing fast frequency grid support by means of dispersed resources. In this sense, recent studies demonstrated how dispersed controllable devices (e.g. of public infrastructures) may be harnessed to provide

effective grid services. More in the detail, in this study, the feasibility to provide frequency regulation services like SI and FFR through a centralized control of a public street lighting system was assessed by testing the response of a real LED lamp and of its driver in a PHIL simulation environment [190], [191].

In the literature, a few studies of grid services provision through lighting systems located at the distribution network are provided. In this sense, as specified in [192], [193], dimmable lighting systems represent competitive resources to be employed to provide AS in a Demand Response framework. In particular, Light-Emitting Diode (LED) lamp technologies are very promising from this point of view since they can be rapidly regulated by using remote or local control signals.

Several studies and projects demonstrated how controlling networked LED streetlights is possible in the monitoring and control framework of smart grids [194], to provide demand side management services or optimize energy use through the integration with other urban energy infrastructures such as EV charging stations [195], [196]. Furthermore, dimmable lighting systems can be used for DR as long as illuminance variations are adequately controlled and, then, still acceptable by final users [197]. In [198], the authors demonstrated how SI can be provided by LED lamps without having to add significant BESS or supercapacitors, but simply connecting a DC link capacitor to the lamps. The use of LED lighting system to support BESS [199] and conventional generators [200] during primary frequency regulation has also been investigated. Similarly, a decentralized control strategy for a LED lighting system, aimed to provide primary and secondary frequency regulation is described in [201]. In such control, each lamp independently provides a frequency response contribution by adapting the power consumption to the grid frequency excursions. While, an advanced local control, able to consider entity and duration of frequency deviations, is presented in [202]. Nevertheless, it occurs to consider that these last solutions are based on a decentralized control strategy, with the drawback to require a relevant number of controllers to be installed, one for each lamp, to gather a significant amount of flexibility. This problem might be overtaken by considering clusters of loads to be controlled with a centralized approach. This represents the case of smart city infrastructures, where resources like public lighting lamps could be aggregated with each other by means of

a centralized control to provide grid services. Several projects, such as TeleWatt [195] and EMERA [196], investigated the possibility to exploit existing public lighting infrastructures to provide different services. Both of them were aimed at integrating EV charging stations with public street lighting systems, optimizing their usage in a centralized control architecture.

### 5.5.1 LED Street Lamps as Flexible Control Resources

With LED technologies getting less and less expensive by the day, LED lamps are progressively substituting all others in both new installations and refurbishment projects. Their competitive performances in terms of efficiency, life expectancy, reliability, controllability and Electromagnetic Compatibility (EMC) impacts make them one of the lead technologies in public street lighting systems. According to the standard UNI 11248:2016 [203], if a "Full Adaptive Installation" is employed, the *lighting class* of street lamps can be reduced during low traffic conditions. *Lighting classes*, as defined by the Part 2 of the European standard EN 13201:2015 [204], determine the road lighting conditions to be ensured to guarantee the safety of road users. Illuminance control actions are allowed, as long as they comply with minimum standard requirements.

Various techniques can be used to easily control and dim LED lamps. For example, the *0-10 $V_{DC}$ protocol* is widely adopted for analog dimming. According to this protocol, the lamp scales its light output so that at a control voltage of 10 V its light intensity corresponds to 100% of its rated value, while below 1 V its light intensity is at its minimum value. However, this control technique is not prone to be extended to control several lamps distributed in a large geographical area.

Several protocols, already commercially available, permit to control a larger number of LED drivers. For example, *DALI* controllers allow to manage up to 64 LED lamps, at a maximum distance of about 300 meters. However, time specification of this kind of controllers might not be adequate for applications requiring a very fast device response. The *DMX-512* technology allows instead to control up to 512 networked devices, at a maximum distance of about 300-500 meters, theoretically extendable using repeaters. Since the transmission time for a maximum sized packet with 512 channels

is about 20 ms, this protocol is fast enough to be employed for fast modulation of the light output of LED lamps. Clearly, the use of *DMX-512* implies the installation of a wired communication system among all lamps.

The applicability of wireless controllers has been also proved in [194], where each LED lamp in a networked lighting system has been provided due to a receiver that can collect data packages sent via radio transmission at a frequency of about 900 MHz. GPS applications for the control of lighting systems are also patented. Large geographical areas are therefore theoretically reachable by the same control system, although the easiest solution could be implementing local frequency measure and control at each lighting control box that usually manages few dozens of street lamps. In this sense, an example of low-cost synthetic inertia local controller has been provided in Section 5.4.

However, the implementation of these solutions could be prohibitive in practical applications if the infrastructure is implemented only for frequency support, due to the high investment costs associated with the communication infrastructure, especially if implemented over large geographical areas. However, it could be applied to pre-existing infrastructures (without significant additional costs) and to smart grids in which the remote control of DERs if already implemented (e.g. for energy optimal control) and could be extended to SI and FFR.

The real-time control of LED street lamps here described was proposed to harvest flexible resources for fast frequency regulation. Since the most severe part of a frequency transient is usually extinguished within few seconds from its onset, the time activation of LED lamps control is a crucial aspect in the feasibility of the proposed control. The need of a very fast response introduces for sure some drawbacks in the proposed control scheme, although it also brings some advantages. Given the very short duration of frequency transients, the visual impacts due to this kind of control can be considered comparable to the fluctuations that can be observed during commonly experienced disturbances of power quality such as deep voltage sags or transient voltage interruptions. Due to the very strict requirements in time response, the proposed LED lamp control was tested in a real-time environment through a PHIL test bed. The experimental results were obtained by regulating the power output of an actual LED street lamp according to different frequency-dependant control laws.

### 5.5.2 Characterization of the LED lamp power regulation Response

The first performed tests were aimed at drawing a control characteristic curve of the LED lamp. The lamp was controlled by a LED driver that receives a DC regulating signal in the range $0-10$ V. The higher the voltage, the higher luminous flux is produced by the lamp, and the higher is the electric power absorbed. The control characteristic was obtained through the experimental results collected from the test setup shown in Fig. 5.23. The LED lamp was fed by an AC power source supply, whereas a DC power

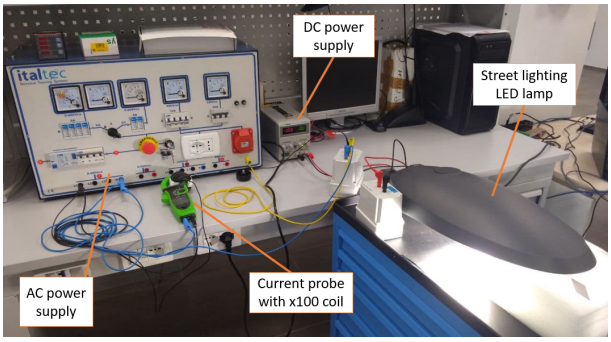


Figure 5.23: Power-Voltage characteristic curve

supply was used to regulate the DC voltage input to the LED driver. The absorbed current was measured using a current probe coupled with a x100 coil to amplify the current signal.

The results obtained by controlling the LED driver with a voltage ranging in the interval $0-10$ V have been collected in Table 5.9. In these tests, the lamp was always fed with the nominal voltage 230 V. These same results are also shown in Fig. 5.24 where the LED lamp power consumption is represented as a function of the DC voltage control input. It can be observed that voltage inputs below 1 V and above 8 V do not produce any significant variation in terms of both absorbed power and luminous flux. Therefore, $1-8$ V is the regulating interval that was used to control the lamp during future tests. In this interval, the characteristic curve appeared to have almost a linear behavior.

According to the results shown in Table 5.9, the lamp under test can be regulated to absorb an electric power ranging from a maximum of 103.6 W to a minimum of

Table 5.9: Test results

| Voltage [V] | Current [A] | Power [W] |
|---|---|---|
| 0.0 | 0.06 | 13.1 |
| 0.5 | 0.06 | 13.1 |
| 1.0 | 0.06 | 13.1 |
| 1.5 | 0.07 | 16.2 |
| 2.0 | 0.10 | 22.7 |
| 2.5 | 0.13 | 29.3 |
| 3.0 | 0.16 | 36.0 |
| 3.5 | 0.19 | 42.4 |
| 4.0 | 0.22 | 49.4 |
| 4.5 | 0.25 | 56.0 |
| 5.0 | 0.28 | 62.8 |
| 5.5 | 0.31 | 69.7 |
| 6.0 | 0.34 | 76.7 |
| 6.5 | 0.37 | 83.6 |
| 7.0 | 0.40 | 90.6 |
| 7.5 | 0.43 | 97.4 |
| 8.0 | 0.46 | 103.6 |
| 8.5 | 0.46 | 103.6 |
| 9.0 | 0.46 | 103.6 |
| 9.5 | 0.46 | 103.6 |
| 10.0 | 0.46 | 103.6 |

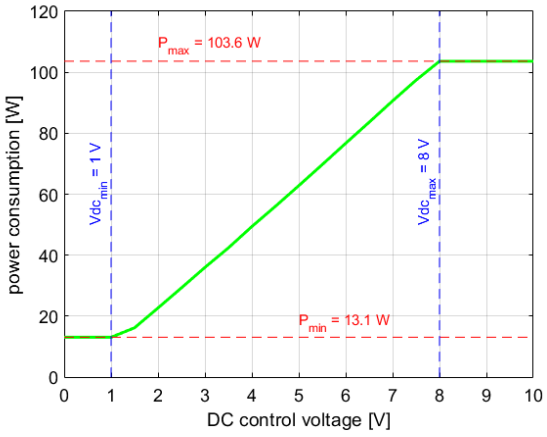


Figure 5.24: Power-Voltage characteristic curve

13.1 W. This means that the lamp can be dimmed in order to reduce its consumption by about 90 %, when operated at full power. Lamps that are operating at half capacity, for example in certain periods of the night when the reduced traffic conditions permit to downgrade the lighting class, could instead theoretically provide instantaneous power control for both upward and downward regulation.

Further tests were also performed to determine the LED lamp time response to a DC control voltage step change and verify if this control is fast enough to be applied for a fast frequency regulation. Fig. 5.25 shows the results obtained by controlling the lamp from one of the extremes of the characteristics curve (Fig. 5.24) to the other, in both upward and downward regulation.

Many other tests, not shown here for the sake of brevity, were conducted by selecting different step change sizes and initial operating points. These results were not conclusive since the observed time delay changed from case to case, with no apparent relation to the inputs, leading to conclude that the delay is due to the inner unknown dynamics of the LED driver. However, in general, it was observed that the delay is in the $400-500$ ms range for upward power regulation, and $500-1400$ ms for downward regulation. Although this delay can be critical for fast frequency regulation applications, since it inevitably reduces the efficacy of the proposed control, in the case of downward power regulation, it will permit to limit the sudden change in illuminance, minimizing visual disturbances to humans and possible hazards to road safety.

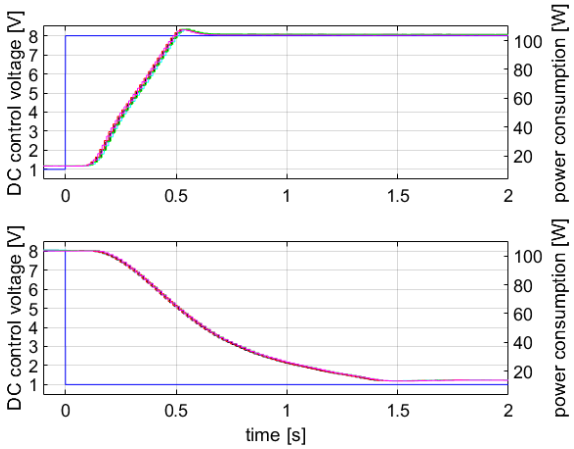


Figure 5.25: Upward and downward device regulations

Following these preliminary results, the effective capability of the actual LED lamp to perform SI and FFR actions was tested in the Power Hardware-in-the-Loop test bed. In particular, PHIL preliminary tests, described in [190], were carried out considering a simplified single-bus electromechanical model of the interconnected power system, neglecting the representation of main grid components, such as power lines or transformers. However, as shown in [205], the presence of grid impedances among regulating resources can affect the overall transient response. Therefore, with the aim to simulate more realistic conditions, further tests were performed [191] considering a more accurate scenario reproducing the behavior of main electrical devices and components in an actual power grid [183]. For the sake of brevity, only simulations performed in this most real scenario have been described in this thesis. However, more details about the first set of tests, performed on the simplified model, are provided in [190].

### 5.5.3 Power Grid Model of a Small Non-interconnected Island

The model employed in the tests hereafter described [191] was detailed enough to describe the influence of high-impedance LV circuits, MV/LV transformers and the actual voltage and power controllers used in a power plant. The adopted representation allowed also to include the presence of multiple LED systems at different buses in the system. This assumption permitted to simulate a more accurate scenario and keep into account the electrical distance with the distributed sources. The assumed grid model represents the MV/LV distribution system of an actual small Italian island, not connected to the main grid. There are multiple rationales under this choice. In the next few years, Italian small islands will continue to be challenged in embracing a significant transformation of their energy generation and network assets [27]. With the mandatory installation of a minimum amount of intermittent renewable sources, small non-synchronous islands, which are inherently characterized by low rotational inertia, will suffer further reductions of inertia and experience harsher frequency events. Therefore, it is essential to develop new ways of ensuring frequency quality, even resorting to demand response approaches. In addition, the adoption of a small-sized test system also allows to ensure suitable details, while respecting the strict computation

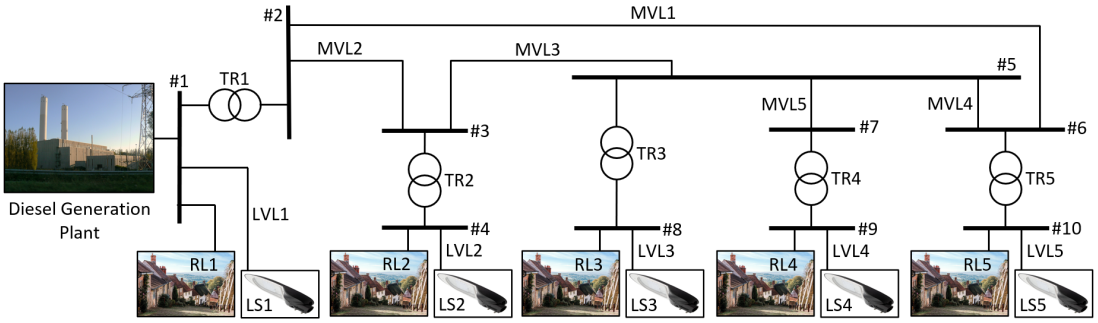


Figure 5.26: modeled small islanded distribution grid

time requirements of real-time simulations and PHIL tests.

The modeled distribution grid is structured as in Fig. 5.26. It mainly consists of five 10 kV MV buses, each one connected through a transformer to a LV bus. Five distribution lines connect the MV nodes, creating a loop that is normally open during operation. Each LV bus supplies electricity to (mostly) residential customers, which have been represented through the equivalent loads RL1-RL5. The installed load capacity $P_n$ at each node is reported in Table 5.10. One of the LV node (bus #1 in Fig. 5.26) supplies the largest number of customers (RL1) and is connected to a generation plant with a 2000 kVA rated power and 50 Hz frequency. The plant is based on a set of diesel generating units and supplies electricity to the local load and to the rest of the island via an elevator transformer (TR1). It should be noted that the detailed model of the generating unit has been represented considering all voltage and mechanical power regulators, a detailed model of the synchronous machine and prime mover dynamics.

Since the proposed control is based on the real-time management of the public LED street lighting system, each LV node was also connected to an additional equivalent circuit, which represents a portion of the street lighting system used to light the entire island. More details are given in the Subsection 5.5.3.1.

The real-time model of the distribution grid is based on a detailed three-phase representation. All system components were modeled using the libraries available in the real-time simulator programming environment. Each component was modeled according to the parameters listed in Table 5.10. These values have been obtained from the data sheets of the components actually installed on the island. Residential loads (RL1-RL5) do not normally participate to frequency control and, therefore, were

modeled using a constant PQ model. This choice permits to simplify the model and reduce the computational efforts required during real-time simulations. A dynamic load model was used instead to represent the power consumption at the street lighting system nodes. Loading levels were set to reproduce conditions of low consumption, usually experienced during the night and far from the tourist season, when the island is more populated. Due to the scarce loading level, the number of active generators is low and the rotational inertia is much reduced. Low inertia conditions can also be due to high Renewable Energy Sources production and the consequent decrease of the number of active synchronous machines.

Table 5.10: Main characteristics of the grid components

| | **TR1** | **TR2** | **TR3** | **TR4** | **TR5** |
|---|---|---|---|---|---|
| $S_n$ [kVA] | 2000 | 400 | 630 | 250 | 630 |
| $V_{1n}$ [kV] | 10.0 | 10.0 | 10.0 | 10.0 | 10.0 |
| $V_{2n}$ [kV] | 0.4 | 0.4 | 0.4 | 0.4 | 0.4 |
| $P_{cc}$% | 0.91 | 1.15 | 1.04 | 1.15 | 1.04 |
| $V_{cc}$% | 6.0 | 4.0 | 4.0 | 4.0 | 4.0 |
| $P_{fe}$% | 0.14 | 0.21 | 0.18 | 0.25 | 0.18 |
| $I_0$% | 0.9 | 1.3 | 1.1 | 1.3 | 1.1 |
| | **RL1** | **RL2** | **RL3** | **RL4** | **RL5** |
| $P_n$ [kW] | 1810 | 590 | 700 | 300 | 650 |
| $V_n$ [kV] | 0.4 | 0.4 | 0.4 | 0.4 | 0.4 |
| | **MVL1** | **MVL2** | **MVL3** | **MVL4** | **MVL5** |
| $Length$ [km] | 0.510 | 0.510 | 0.510 | 0.850 | 0.510 |
| $r_l$ [Ω/km] | 0.387 | 0.387 | 0.387 | 0.253 | 0.387 |
| $x_l$ [Ω/km] | 0.086 | 0.086 | 0.086 | 0.120 | 0.086 |

#### 5.5.3.1 Model of the LED Street Lighting System

The street lighting system has been modeled according to some assumptions. The installed power of the simulated street lighting system was estimated using aggregated data at national level. According to the statistics in [206], in 2017, the electricity consumption of public lighting in Italy was about 6000 GWh. Assuming that the public

lighting lamps are usually switched on less than half a day (about 4000 hours per year) and that they work almost all times at their rated power, it appeared reasonable to consider that the installed power of the lighting systems in Italy in that year was about 1.5 GW. This value is about 3% of the national load peak (55 GW in 2017, as reported in [207] by the Italian TSO). Applying the same percentage to the simulated system, whose peak power demand is about 1.8 MW, it is possible to assume that the installed power of the public street lighting system in the island is about 54 kW.

Having estimated the overall load for street lighting and the total number of lamps, it was assumed to distribute such load on five subsystems, connected at the LV system nodes. The number of lamps for each subsystem is proportional to the installed load capacity at LV level. As represented in Fig. 5.26, each lighting subsystem was modeled using an equivalent three-phase load (LS1-LS5), supplied by an equivalent low-voltage distribution line (LVL1-LVL5). Table 5.11 shows equivalent power and number of installed lamps for each street lighting subsystem (LS1-LS5).

Table 5.11: Power and number of lamps at each LV node

| | **LS1** | **LS2** | **LS3** | **LS4** | **LS5** |
|---|---|---|---|---|---|
| $P_{LS}$ [kW] | 24.20 | 7.76 | 9.32 | 4.04 | 8.69 |
| $N.of\,lamps$ | 234 | 75 | 90 | 39 | 84 |

The equivalent lines LVL1-LVL5 were modeled assuming typical lengths in urban applications and according to the actual data of the urban lighting system in [196]. Cross-section of cables were sized to avoid excessive voltage drops at the terminal of each lighting circuit. The adopted values are summarized in Table 5.12. Please, consider that due to the large number of lamps assigned to LS1, this street lighting system was divided into three parallel sub-circuits, each one supplying one third of the total LS1.

### 5.5.4 Synthetic Inertia and Fast Frequency Response Models

In order to investigate the support that LED street lamps can provide to enhance the grid frequency behavior, two frequency-dependant control laws were proposed,

Table 5.12: Characteristics of the equivalent distribution line of the lighting subsystems

| | **LVL1** | **LVL2** | **LVL3** | **LVL4** | **LVL5** |
|---|---|---|---|---|---|
| *Length* [km] | 0.81 | 0.78 | 0.93 | 0.42 | 0.87 |
| *N.of circuits* | 3 | 1 | 1 | 1 | 1 |
| *Cross-sections* [mm$^2$] | 4x25 | 4x25 | 4x35 | 4x6 | 4x25 |
| $r_l$ [Ω/km] | 0.99 | 0.99 | 0.71 | 4.21 | 0.99 |
| $x_l$ [Ω/km] | 0.093 | 0.093 | 0.089 | 0.114 | 0.093 |

namely *Synthetic Inertia* or *Fast Frequency Response*. These two approaches have never been applied or tested on LED urban lighting systems. An approach somewhat close to what we have proposed was found in [198]. The authors in [198] evaluated the possibility to provide virtual inertia through the energy stored in the capacity of the DC-link that supplies the LED lamp. Due to the limited capability of the DC-link of the lamp driver, this technique can provide a very limited power respect to the SI control proposed in our work that can control up to 90% of the LED lamps rated power (see Subsection 5.5.2). On the other hand, for FFR control, a possible comparison can be done in relation to other primary frequency controls with LED lamps proposed in the literature. The FFR control law here proposed is comparable to the controls in [199] and [202]. In these works, however, the actual response and characteristics of LED lamps and their drivers were not considered. In the described tests, instead, thanks to the PHIL implementation, the behaviour of an actual (commercially available) LED street lamp, with its driver and control system, was thoroughly taken into account. A different control law is proposed in [201] to provide primary frequency support by LED lighting systems. However, this control introduces a fixed delay to reduce the frequency control activation in addition to a dead-band on the frequency deviation. The introduction of this delay does not permit to obtain a prompt response of the devices for very severe contingencies.

A scheme of the SI/FFR controller used for tests is given in Fig. 5.27 where, through a control switch, it is possible to choose the control law to be adopted. The output of the controller is the amount of load to be curtailed. The curtailed load set-point is converted into a DC control voltage set-point using the look-up table obtained

during the characterization tests in Subsection 5.5.2 (see Fig. 5.24). The DC control voltage obtained in this way is applied to the LED driver to regulate the luminous flux, and therefore the power supplied to the lamps. A detail of the SI and FFR functions blocks in Fig. 5.27 is given in the next subsections. Please note that, for the sake of simplicity, in this work, it was assumed to allow SI/FFR control of the street lamps only during underfrequency events, when lamps are working at their maximum power and their power output can only be regulated downward. However, it is possible to imagine that a symmetrical control of loading power could be implemented on the lamps that are working at half capacity during reduced road traffic conditions.

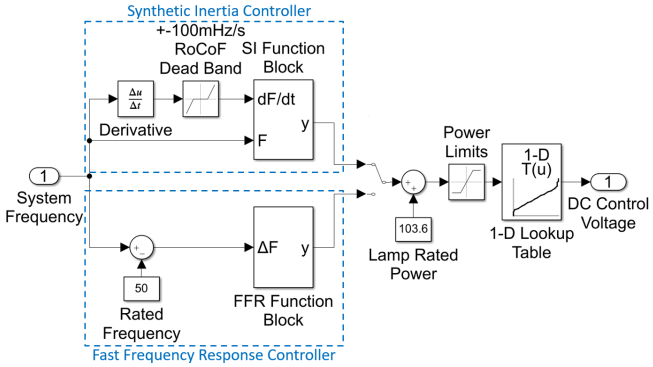


Figure 5.27: Synthetic inertia and fast frequency response control scheme

### 5.5.4.1 Synthetic Inertia control law

As reported in [159], synthetic inertia is obtained by applying a control law proportional to the frequency derivative (RoCoF). Some applications of this control are reported in [161], [162]. However, a control law that follows continuously the RoCoF trajectory can lead to a rise in the frequency response settling time, because of the inertial support given after having reached the *nadir* point. Such drawback can be overcome by adopting the solution proposed in [208] where the SI control is applied only when RoCoF and frequency deviations have the same sign. The SI control adopted in this work and described in [191] is similar to the one proposed in [208], although, in this case, having modeled also secondary frequency regulation, the steady-state value is given by the nominal frequency (50 Hz). As shown in Fig. 5.27, a RoCoF dead

band of $\pm 100$ mHz/s was also introduced in order to avoid unnecessary regulations, due for example to measurement noise. Indeed, RoCoF calculation can be affected by large errors due to noise on frequency measurement. To further reduce the effect of noise, a low-pass filter can be applied to the frequency measurement. According to the step-change responses shown in Fig. 5.25, the dynamic behavior of the controlled LED lamp is characterized by a large delay and is therefore inherently less susceptible to noise, making the use of a filter unnecessary. Assuming $F$ as the frequency sample at the time $t$ and $K_{SI}$ as the applied gain factor, the SI control law implemented in the *SI Function Block* consists of the following *if statement*:

$$\begin{cases} if \quad F \leq 50 \ \ \& \ \ dF/dt < 0.1 \\ \quad y = K_{SI} \cdot dF/dt \\ else \\ \quad y = 0 \end{cases}$$

According to this rule, a non-zero output $y$ of the SI controller is obtained only when the frequency is below its nominal value (50 Hz). The gain factor $K_{SI}$ was sized so that the maximum power variation is obtained when a 0.5 Hz/s RoCoF is reached.

#### 5.5.4.2 Fast Frequency Response control law

As defined in [159], the fast frequency response aims to provide grid support for reduced inertia systems by means of units able to quickly respond to frequency excursions, with an active power response proportional to the frequency deviation. Assuming $\Delta F$ as the measured frequency deviation from the steady-state value, and introducing a 0.1 Hz dead-band to avoid excessive stress to the lamp, the control output $y$ of the *FFR Function Block* in Fig. 5.27 was formulated as follows:

$$\begin{cases} if \quad \Delta F \leq -0.1 \\ \quad y = K_{FFR} \cdot (\Delta F + 0.1) \\ else \\ \quad y = 0 \end{cases}$$

The gain factor $K_{FFR}$ was set in order to obtain the maximum power contribution

with frequency deviations greater than 0.5 Hz.

### 5.5.5 Test Results

This section describes the setup for the Power Hardware-in-the-Loop experimental tests and discusses the results obtained considering the SI and FFR control strategies.

#### 5.5.5.1 Power Hardware-in-the-Loop test bed architecture

The PHIL setup used to investigate the effectiveness of the proposed SI and FFR controls is shown in Fig. 5.28. It consists of a real-time digital simulator (OPAL RT5600), a power amplifier module, managed by an amplifier controller, and a real LED street lamp, whose physical response was applied in PHIL to the simulated power system. As previously described, the real-time simulator, which was interfaced with the amplifier controller by means of an optical fiber channel, simulated both the distribution network described in Section 5.5.3 and the LED lamp controller. The DC-control voltage signal (0–10 V) sent to the LED driver to control the lamp luminous flux was generated by the real-time simulator as an analog output by using the *hardware synchronized mode*.

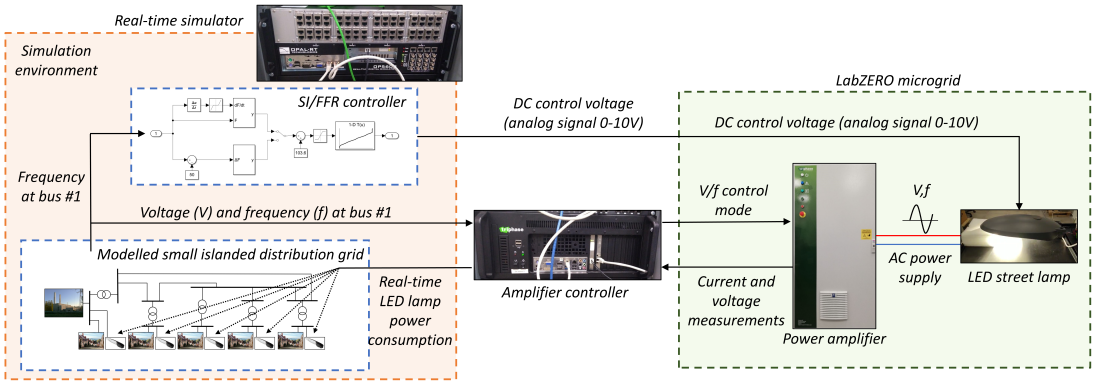


Figure 5.28: Setup of the Power Hardware-in-the-Loop simulation tests

The LED lamp was connected to the LabZERO microgrid [187] at the Politecnico di Bari, which was supplied by the programmable power source operating in voltage source control mode. According to this setup, frequency and voltage signals of the simulated non-synchronous system were communicated to the amplifier controller

and, then, physically applied to the microgrid busbar. The response of the microgrid (and the LED lamp) to the frequency and voltage variations is measured by the programmable power source and transformed into a PQ signal to be fed back to the real-time simulation.

These active and reactive power signals were suitably scaled to reproduce the response of the five street lighting subsystems connected at different LV nodes. Thanks to the characterizations tests, it was proved how LED lamps behavior was not influenced by voltage magnitude in a very large interval. Therefore, the expected response of all simulated lamps can be considered similar to the physical LED lamp as long as the frequency is the same on the entire grid. This condition can be considered true since the system is very small in size and is supplied only by a single power plant.

#### 5.5.5.2 Case 1. SI Control of LED lamps

The proposed SI control was tested applying a sudden load step variation of 180 kW to the simulated grid, in a day characterized by an average power consumption of about 1.25 MW. Given the very low rotational inertia of the diesel power plant (assumed to be 0.3 s with respect to the maximum installed power 2000 kVA), the frequency transient following this disturbance, applied at the generic time $t = 0$ s as in Fig. 5.29, shows a very steep descent with an initial RoCoF higher than 8 Hz/s, and a nadir of about 48.3 Hz, much lower than the 49 Hz minimum suggested by the standard EN-50160 for the quality of frequency in systems with no synchronous connection.

Fig. 5.30 shows how the proposed SI controller can generate a DC control signal adjusting the active power consumption of the LED lamps during the frequency transient.

The effect of this action control is visible in Fig. 5.29 with a non negligible contribution to the nadir, which is now raised to about 48.4 Hz, a reduction of the frequency overshoot and an overall quicker settling time.

As shown in Fig. 5.30, due to the high RoCoF, a maximum power reduction was instantly asked to the LED lamps. Within a few hundred milliseconds, the LED lamps began to reduce their consumption. The SI controlling signal was stopped after having reached the nadir, and the lamps went back to their regular operating point within a

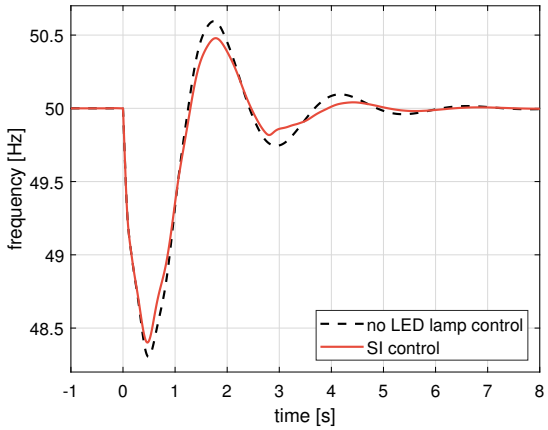


Figure 5.29: Case 1. Frequency response with SI control

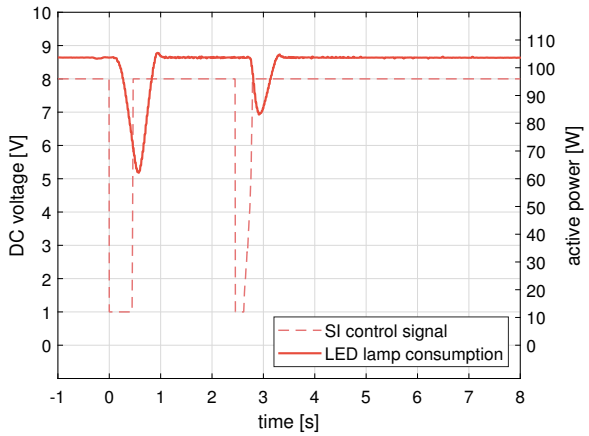


Figure 5.30: Case 1. LED lamp response with SI control

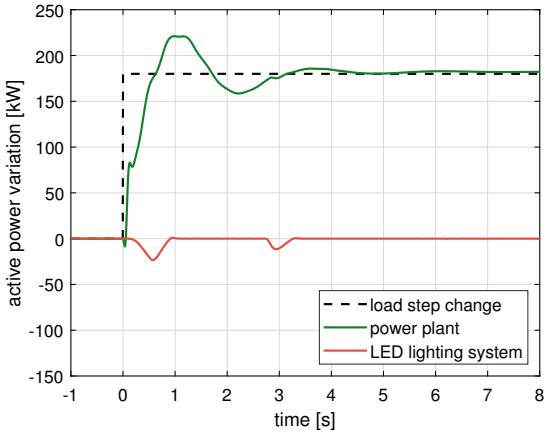


Figure 5.31: Case 1. Active power response with SI control

second from the start of the disturbance. Due to the severity of the transient, a second activation of SI was also requested during a second oscillation.

Fig. 5.31 shows how the power response provided by the diesel generation plant derives from a detailed model of the generating units. Its response is clearly much more significant than the LED lamps, whose consumption is in this case only just about 4% of the overall load. Furthermore, due to the high speed of the system response, the contribution of the lamps to the dynamics can be exploited for a short time only. However, it should be observed that these tests were carried out on particularly stressed conditions. In fact, the model of the non-synchronous system was characterized by an extremely low amount of inertia. The frequency support could have been more significant in systems with more inertia and, then, a delayed nadir time. Nevertheless, from another point of view, the limitation in the active power control of the LED lamps guarantees that the visual impact during the transient is very limited.

#### 5.5.5.3 Case 2. FFR control of LED lamps

This second case is equivalent to the previous one, but this time the presence of a FFR control of the LED lamps was assumed. Fig. 5.32 shows the system frequency response with and without the FFR support. The response was quite similar to the previous case, although a better control of the frequency overshoot and settling time was obtained. Fig. 5.33 shows the LED lamp power response and the control signal applied to its driver.

By comparing the two trends in Fig. 5.30 and Fig. 5.33, it is possible to observe that the FFR control strategy is slightly delayed, but allows a longer activation of the LED lamp active power control. This is due to the fact that, in general, when an imbalance occurs, the RoCoF ($dF/dt$) reaches instantaneously its maximum value, saturating the SI control, and goes rapidly to zero when the nadir is reached. Frequency deviation ($\Delta F$), instead, starts from zero and needs more time to reach the saturation threshold of FFR control (set in this case at $-0.5$ Hz). FFR control is requested until $\Delta F$ is brought back within the dead-band limits (i.e. at 49.9 Hz), with an overall activation of about 1 s. In this case, the LED lamps have enough time to curtail almost all of their consumption, ensuring higher damping and a smaller frequency overshoot. Nadir

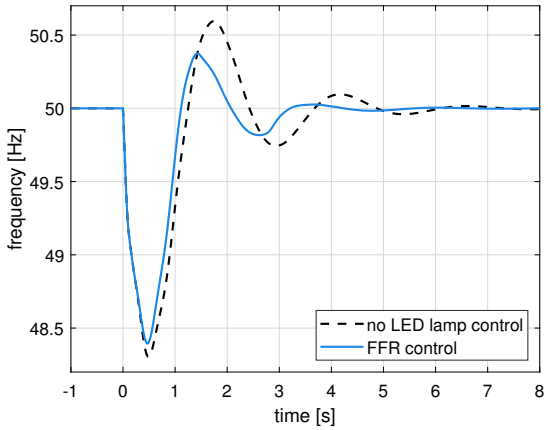


Figure 5.32: Case 2. Frequency response with FFR control

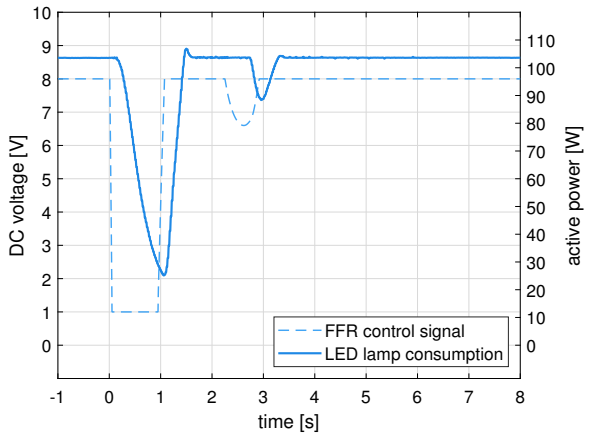


Figure 5.33: Case 2. LED lamp response with FFR control

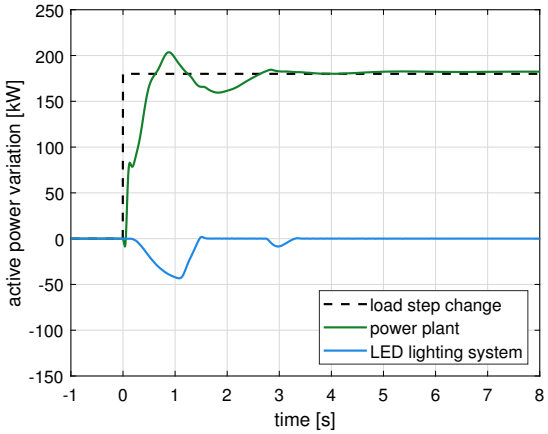


Figure 5.34: Case 2. Active power response with FFR control

point is comparable to the one reached with SI inertia control, although just slightly lower. Fig. 5.34 shows the active power response of both diesel generation plant and LED street lighting systems.

#### 5.5.5.4 Cases 3-5. Further comparison of SI and FFR control

The previous tests assumed a very severe contingency, with values of RoCoF and frequency deviations which rapidly saturated either SI or FFR control. Further tests have been carried out in order to investigate the response of SI and FFR control laws in absence of saturation.

Fig. 5.35 allows to compare the system frequency response obtained with SI and FFR control, applying gradually smaller load step variations. The three cases, namely 3, 4 and 5, are characterized by a 3%, 2% and 1% load variation, respectively. In these cases, the SI controller allowed to improve more visibly the response in terms of nadir with respect to the FFR. With the decreasing of the disturbance severity, RoCoF decreases and the FFR control is activated with larger delays, because of the time necessary for the frequency deviation to reach the dead-band lower limit. In all cases, however, FFR control allows to limit or even avoid the frequency overshoot.

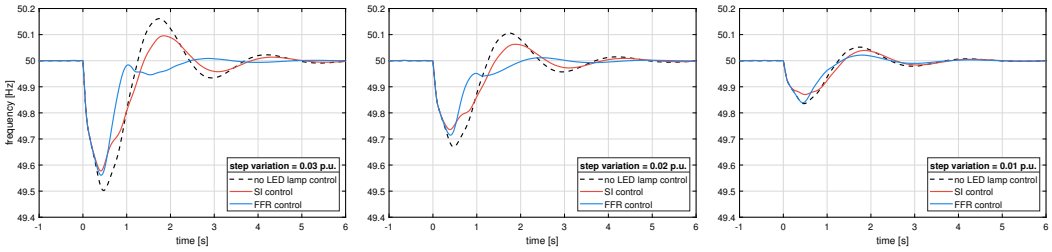


Figure 5.35: Cases 3-5. Frequency response to a 3% (left), 2% (center) and 1% (right) load variation

In addition, having imposed a load variation in the system equal to the installed power of the public street lighting system in the island (3% of the total load), the proposed controls allow to reduce the maximum frequency deviation by 20%. This reduction, using the SI control, increases if the load step change has a magnitude lower than the controlled LED-lamp power volume. Indeed, SI control, being based on RoCoF, is able to provide a contribution even for very modest contingencies. For this reason, SI

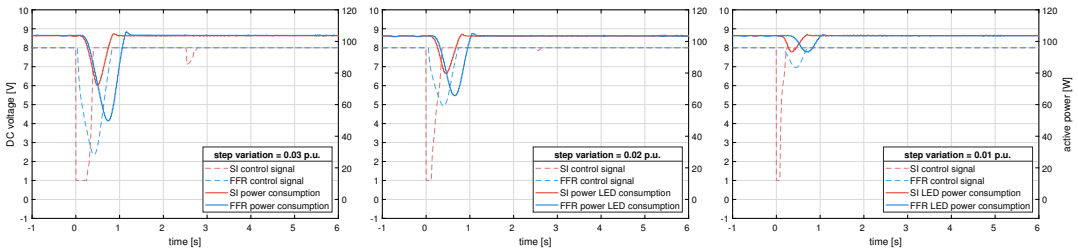


Figure 5.36: Cases 3-5. LED lamp response to a 3% (left), 2% (center) and 1% (right) load variation

controller can be considered preferable as it can provide a better counter-balance for the smaller load variations that most often occur during normal grid operation.

Fig. 5.36 shows the DC control voltage set-points generated by SI and FFR in the three cases, together with the LED lamps active power response. It is possible to observe that, due to the extremely low system inertia conditions and the high values of initial RoCoF, even during small disturbances, SI control is still characterized by a sort of ON/OFF behavior. The FFR control signal, instead, changes more smoothly. However, due to the actual delays in the response of the LED lamp, observed during the characterization tests presented in Section 5.5.2, the active power response follows initially about the same trajectory, with just a little delay in the case of FFR. The main difference of the two controls is again found in the longer activation time of the FFR control. As also previously remarked the delayed response of the lamp allows in any case to minimize the visual impacts which can be considered negligible.

#### 5.5.5.5 Test results discussion

The present investigation addressed the idea of using LED public street lighting systems to obtain an extra grid support in scenarios characterized by very low rotational inertia. The capability of providing a very fast active power regulation, without disconnecting the lamps, was investigated through Power Hardware-in-the-Loop tests. PHIL tests allowed to integrate the simulation of a MV/LV isolated distribution grid with the behaviour of a real LED street lamp controlled to provide SI or FFR control actions.

The simulated grid represents the non-synchronous power system of an actual small Italian island, comprising all main MV/LV components, a detailed diesel gen-

eration power plant and a distributed public street lighting system. This kind of non-synchronous systems is inherently characterized by low total inertia, and will face in the next years the challenge of integrating larger and larger amount of Renewable Energy Sources, with further expected reduction of inertia.

The proposed LED lamp control was tested in a scenario characterized by an extreme reduction of inertia, allowing to prove how a non-negligible contribution to frequency support can be obtained exploiting these controllable resources. Clearly, having limited power with respect to the overall load and being characterized by delays assessed between 400 and 1400 ms, LED lamps cannot substitute other active components, such as batteries or fly-wheels. However, the tests showed how, if suitably controlled, LED lamps can be considered as additional widespread resources to be exploited for supporting the grid and reduce the capacity of other controlling devices.

The PHIL tests showed that FFR control, in case of severe contingencies, allows a more pronounced contribution to enhance the frequency behavior but causes a longer drop in the illumination flux, which has a higher visual impact. On the other hand, SI control has the advantage of reducing impacts on illumination levels, due to a shorter activation time of the dimming control. For this reason, the SI control is preferable with regard to the use of LED street lighting systems to provide AS. In both cases, however, the visual impacts due to the control can be considered negligible and comparable to the same disturbances that can be observed during commonly power quality events, such as deep voltage sags or transient voltage interruptions, which happen hundreds of times in a year (more often than frequency events).

Entity and number of control actions can be reduced by downsizing the gains of the two controllers and increasing the dead bands, respectively. In the implemented controls, the gains were chosen in order to produce an effective control action for most of the test cases presented. No particular problems in terms of stability or interaction with the other controllers were observed, mostly because of the limited power that can be controlled by the lighting systems, even in the case of saturated control laws. However, in practical implementations, the gains can be set according to the typical inertia and droop values adopted in power systems or specified by the national grid codes for the connection of active end-users.

# Conclusions

This thesis investigated a decentralized approach to enable the provision of advanced Ancillary Services by means of DERs. As specified in the first part of this work, the energy transition process is leading power systems toward the dismissal of conventional power plants. In this direction, several initiatives and regulations have been adopted at the European level with the goal to achieve by 2030 a share of Renewable Energy Sources of 40 % and reducing greenhouse gas emissions of at least 55 % with respect to 1990 levels. Although the progressive replacement of fossil-fueled generation with intermittent Renewable Sources is introducing additional uncertainties in power system management, the presence of DERs at DN level represents also an opportunity for power system operators since they can be exploited to provide Ancillary Services. In particular, small dispatchable generators, controllable loads and BESS may be exploited as flexibility resources for improving power system operation and facing power fluctuations introduced by intermittent generation, load changes, line outages, and forecasting errors.

In this perspective, it should be considered that in future scenarios, a significant amount of energy will be produced by Renewable Energy Sources located at the distribution grid level. These aspects demonstrate the relevance for distribution system operators to be enabled in procuring Ancillary Services resources, e.g. to improve the voltage profiles of the nodes of generating units or to eliminate line congestions.

This idea is also shared by Directive 2019/944 on the internal market for electricity, according to each Member State of the European Union must develop a regulatory framework that incentives DSOs to procure the flexible resources necessary to operate their network efficiently and to solve specific operative problems like local conges-

tions. However, in order to use DERs as AS resources, appropriate coordination is required between TSOs and DSOs. Several TSO-DSO coordination schemes have been proposed in the literature with the aim to establish the roles of system operators and their possibility to procure AS to manage their networks.

This thesis proposed a few approaches for enabling the provision of advanced Ancillary Services through Distributed Energy Sources in decentralized architecture, in which each operator is responsible for its own grid. Among the main developed methodologies, an algorithm for mapping the flexibility area at TSO-DSO interconnection point was proposed. Furthermore, two methodologies to aggregate flexibility resources in case of multiple POIs were also derived.

In addition, an algorithm based on Benders Decomposition was also investigated. This method allows a large optimization problem to be decomposed into several subproblems, solvable separately. Therefore, it may be advantageously applied in decentralized TSO-DSO coordination schemes, as it can reduce data to be shared between system operators and distribute the whole computational burden among them [104]. Furthermore, thanks to its mathematical formulation, it is able to perform optimal dispatch in scenarios in which TSOs and DSOs are interfaced in multiple POIs.

The proposed BDA was tested on the Common, Local, and Shared balancing responsibility AS Market models with the aim to dispatch DERs to solve network congestions in a power system including one TN and two DNs. Test results demonstrated the capability of the proposed approach to achieve optimal dispatch solutions while ensuring that TSO and DSO can manage autonomously resources located in their own networks. A study concerning data to be exchanged between TSO and DSO was also carried out for the implemented BDA. This analysis proved that the amount of data to be communicated depends on the number of iterations necessary to achieve the final solution. Whenever a high number of iterations is required (e.g. in larger power systems), data to be exchanged between system operators can be considered as not excessive. This is because a limited number of information is transferred between system operators at each BDA iteration.

Furthermore, the provision of innovative Ancillary Services by means of DERs was also investigated through Power Hardware-in-the-Loop simulations. In particular, SI

and FFRcontributions were provided by means of controllable DERs and LED lamps of public lighting systems. Test results demonstrated the capability of these resources to contribute effectively to the power system stability, also in case of reduced inertia conditions.

In conclusion, the study performed in this thesis demonstrated how an engagement of the DSO at the same level of the TSO, in decentralized approaches, may ensure effective use of DN flexibility resources to provide grid services for the entire power system operation. This was also confirmed by simulation tests carried out according to a PHIL approach, in which DN resources were able to provide innovative Ancillary Services like Fast Frequency Response and Synthetic Inertia, services that will be particularly required in a future scenario characterized by high penetration of Renewable Energy Sources.

# References


[1] The European Commission, "European Green Deal: Commission proposes transformation of EU economy and society to meet climate ambitions," 2021. [Online]. Available: https://ec.europa.eu/commission/presscorner/detail/en/IP_21_3541

[2] ——, "Document 52021PC0557," Brussels, Tech. report, jul 2021. [Online]. Available: https://eur-lex.europa.eu/legal-content/EN/TXT/?uri=CELEX:52021PC0557

[3] S. Impram, S. Varbak Nese, and B. Oral, "Challenges of renewable energy penetration on power system flexibility: A survey," *Energy Strategy Reviews*, vol. 31, p. 100539, 2020.

[4] H. Le Cadre, I. Mezghani, and A. Papavasiliou, "A game-theoretic analysis of transmission-distribution system operator coordination," *European Journal of Operational Research*, vol. 274, no. 1, pp. 317–339, 2019.

[5] S. Bruno, G. Giannoccaro, C. Iurlaro, M. La Scala, L. Notaristefano, and C. Rodio, "Mapping Flexibility Region through Three-phase Distribution Optimal Power Flow at TSO-DSO Point of Interconnection," in *2021 AEIT International Annual Conference*, 2021, pp. 1–6.

[6] J. Villar, R. Bessa, and M. Matos, "Flexibility products and markets: Literature review," *Electric Power Systems Research*, vol. 154, pp. 329–340, 2018.

[7] IEA, "Status of Power System Transformation 2019," IEA, Tech. Report, may 2019. [Online]. Available: https://www.iea.org/reports/status-of-power-system-transformation-2019

[8] C. Zhang, Q. Wang, J. Wang, M. Korpås, and M. E. Khodayar, "Strategy-making for a proactive distribution company in the real-time market with demand response," *Applied Energy*, vol. 181, pp. 540–548, 2016.

[9] S. I. Vagropoulos, P. N. Biskas, and A. G. Bakirtzis, "Market-based TSO-DSO coordination for enhanced flexibility services provision," *Electric Power Systems Research*, vol. 208, p. 107883, 2022.

[10] ARERA, "Relazione 428/2018/I/efr - Stato di utilizzo e di integrazione degli impianti di produzione alimentati dalle fonti rinnovabili," Tech. report, 2018. [Online]. Available: https://www.google.com/url?sa=t&rct=j&q=&esrc=s&source=web&cd=&cad=rja&uact=8&ved=2ahUKEwiLkse8oOj8AhViXfEDHVK4CEcQFnoECB8QAQ&url=https%3A%2F%2Fwww.arera.it%2Fit%2Fdocs%2F18%2F428-18.htm&usg=AOvVaw15XshqVVcX2ZW42OlWvxC4

[11] The European Parliament and the Council of the European Union, "Regulation (EU) 2019/943 on the internal market for electricity," *Official Journal of the European Union*, vol. 62, no. L158, pp. 54–191, 2019.

[12] ——, "Directive (EU) 2019/944 on Common Rules for the Internal Market for Electricity," *Official Journal of the European Union*, no. L158, pp. 125–199, 2019. [Online]. Available: https://eur-lex.europa.eu/eli/dir/2019/944/oj

[13] Terna S.p.A., "Il rapporto con gli operai di settore." [Online]. Available: https://www.terna.it/it/sostenibilita/business-responsabile/rapporto-operatori-settore

[14] H. Gerard, E. Rivero, and J. Vanschoenwinkel, *TSO-DSO Interaction and Acquisition of Ancillary Services from Distribution*. Cham: Springer International Publishing, 2020, pp. 7–23. [Online]. Available: https://doi.org/10.1007/978-3-030-29203-4_2

[15] B. Qin, M. Wang, G. Zhang, and Z. Zhang, "Impact of renewable energy penetration rate on power system frequency stability," *Energy Reports*, vol. 8, pp. 997–1003, 2022. [Online]. Available: https://www.sciencedirect.com/science/article/pii/S2352484722011076

[16] R. Bayindir, S. Demirbas, E. Irmak, U. Cetinkaya, A. Ova, and M. Yesil, "Effects of renewable energy sources on the power system," in *2016 IEEE International Power Electronics and Motion Control Conference (PEMC)*, 2016, pp. 388–393.

[17] H. Khajeh, H. Firoozi, and H. Laaksonen, "Flexibility Potential of a Smart Home to Provide TSO-DSO-level Services," *Electric Power Systems Research*, vol. 205, p. 107767, 2022.

[18] A. G. Givisiez, K. Petrou, and L. F. Ochoa, "A Review on TSO-DSO Coordination Models and Solution Techniques," *Electric Power Systems Research*, vol. 189, p. 106659, 2020.

[19] G. Rancilio, A. Rossi, D. Falabretti, A. Galliani, and M. Merlo, "Ancillary services markets in europe: Evolution and regulatory trade-offs," *Renewable and Sustainable Energy Reviews*, vol. 154, p. 111850, 2022.

[20] E. Papadis and G. Tsatsaronis, "Challenges in the decarbonization of the energy sector," *Energy*, vol. 205, p. 118025, 2020.

[21] D. A. Contreras and K. Rudion, "Improved Assessment of the Flexibility Range of Distribution Grids Using Linear Optimization," in *2018 PSCC*, 2018, pp. 1–7.

[22] C. Madina, P. Kuusela, M. Rossi, and H. Aghaie, "Optimised TSO-DSO Coordination to Integrate Renewables in Flexibility Markets," *International Conference on the European Energy Market, EEM*, vol. 2019-Septe, pp. 1–6, 2019.

[23] V. Trovato, I. M. Sanz, B. Chaudhuri, and G. Strbac, "Advanced Control of Thermostatic Loads for Rapid Frequency Response in Great Britain," *IEEE Transactions on Power Systems*, vol. 32, no. 3, pp. 2106–2117, 2017.

[24] P. A. Lombardi, K. R. Moreddy, A. Naumann, P. Komarnicki, C. Rodio, and S. Bruno, "Data centers as active multi-energy systems for power grid decarbonization: A technical and economic analysis," *Energies*, vol. 12, no. 21, 2019.

[25] J. Le Baut, G. Leclercq, G. Viganò, and M. Z. Degefa, "Deliverable 1.2 - Characterization of flexibility resources and distribution networks," Tech. report, 2017.

[26] G. Migliavacca, M. Rossi, H. Gerard, M. DZvzamarija, S. Horsmanheimo, C. Madina, I. Kockar, G. Leclecq, M. Marroquin, and H. Svendsen, "TSO-DSO coordination and market architectures for an integrated ancillary services acquisition : the view of the SmartNet project," in *CIGRE*, FRA, 2018.

[27] G. Migliavacca, "Introduction," in *TSO-DSO Interactions and Ancillary Services in Electricity Transmission and Distribution Networks: Modeling, Analysis and Case-Studies*, G. Migliavacca, Ed. Cham: Springer International Publishing, 2020, pp. 1–5.

[28] A. Papavasiliou, "Analysis of distribution locational marginal prices," *IEEE Transactions on Smart Grid*, vol. 9, no. 5, pp. 4872–4882, 2018.

[29] M. Rossi, G. Migliavacca, G. Viganò, D. Siface, C. Madina, I. Gomez, I. Kockar, and A. Morch, "TSO-DSO coordination to acquire services from distribution grids: Simulations, cost-benefit analysis and regulatory conclusions from the SmartNet project," *Electric Power Systems Research*, vol. 189, p. 106700, 2020.

[30] H. Gerard, E. I. Rivero Puente, and D. Six, "Coordination between transmission and distribution system operators in the electricity sector: A conceptual framework," *Utilities Policy*, vol. 50, pp. 40–48, 2018.

[31] J. Merino, I. Gomez, E. Turienzo, C. Madina, I. Cobelo, A. Morch, H. Saele, K. Verpoorten, E. R. Puente, S. Haninnen, P. Koponen, C. Evens, N. Helisto, A. Zani, and D. Siface, "Deliverable 1.1 - Ancillary service provision by RES

and DSM connected at distribution level in the future power system," The SmartNet Consortium, Tech. report, dec 2016.

[32] A. Delnooz, J. Vanschoenwinkel, E. Rivero, and C. Madina, "Deliverable 1.3 – Definition of scenarios and products for the demonstration campaigns," Coordinet, Tech. report, jul 2020.

[33] The European Commission, "Regulation (EU) 2017/1485 establishing a guideline on electricity transmission system operation," *Official Journal of the European Union*, no. L 220, pp. 1–120, 2017.

[34] European Commission, "Horizon 2020." [Online]. Available: https://research-and-innovation.ec.europa.eu/funding/funding-opportunities/funding-programmes-and-open-calls/horizon-2020_en

[35] "SmartNet Project." [Online]. Available: https://smartnet-project.eu/

[36] H. Gerard, E. Rivero, and D. Six, "Deliverable 1.3 - Basic schemes for TSO-DSO coordination and ancillary services provision," The SmartNet Consortium, Tech. report, dec 2016.

[37] "The CoordiNet Project." [Online]. Available: https://coordinet-project.eu/

[38] FlexCoop, "Demand response for energy cooperatives." [Online]. Available: https://www.flexcoop.net/

[39] OSMOSE, "Leveraging flexibilities for the European power system." [Online]. Available: https://www.osmose-h2020.eu/

[40] F. Silletti, L. Orrù, M. Di Serafino, L. Bolla, and F. Maso, "H2020 OSMOSE PROJECT: Final results of the experimentation phase of industrial Demand Response (DR)," in *2022 AEIT International Annual Conference (AEIT)*, 2022, pp. 1–6.

[41] G. Pisano, F. Pilo, F. Bignucolo, L. Mantese, R. Langella, M. Pagano, G. Chicco, M. Andrea, F. Spertino, M. La Scala, S. Bruno, C. Rodio,

I. Losa, G. Dondossola, and R. Terruggia, "Deliverable D5.6 - Ex-post market, regulatory and scalability-replicability analysis of the Italian Demo," OSMOSE, techreport, mar 2022. [Online]. Available: https://www.osmose-h2020.eu/wp-content/uploads/2022/04/OSMOSE-D5.6-Final-report-summarizing-main-demo-results_20220427_V1.pdf

[42] InteGRIDy, "Smart grid storage and system integration technologies enabling and increase in renewables." [Online]. Available: https://www.integridy.eu/

[43] EDREAM, "Enabling new Demand Response Advance, Market oriented and secure technologies, Solutions and Business models." [Online]. Available: https://edream-h2020.eu/

[44] ADDRESS, "Towards the smart grids of the future." [Online]. Available: http://www.addressfp7.org/

[45] R. Belhomme, R. Cerero Real De Asua, G. Valtorta, A. Paice, F. Bouffard, R. Rooth, and A. Losi, "ADDRESS - Active Demand for the smart grids of the future," in *CIRED Seminar 2008: SmartGrids for Distribution*, 2008, pp. 1–4.

[46] E. Rivero, Sebastian-Viana, Maria, V. Ulian, and J. Stromsather, "THE evolvDSO PROJECT: KEY SERVICES FOR THE EVOLUTION OF DSOS' ROLES," in *23rd International Conference on Electricity Distribution*, 2015, pp. 1–6.

[47] N. Fonseca, J. Silva, A. Silva, J. Sumaili, L. Seca, R. Bessa, J. Pereira, M. Matos, P. Matos, A. C. Morais, M. Caujolle, and M. Sebastian-Viana, "EvolvDSO grid management tools to support TSO-DSO cooperation," in *CIRED Workshop 2016*, 2016, pp. 1–4.

[48] Energy Department of European Commission, "Clean energy for all Europeans package completed: good for consumers, good for growth and jobs, and good for the planet," 2019.

[49] The European Parliament and the Council of the European Union, "Directive 2009/28/EC of the European Parliament and of the Council," *Official Journal of the European Union*, no. L140, pp. 16–62, 2009. [Online]. Available: https://eur-lex.europa.eu/eli/dir/2009/28/oj

[50] European Commission, "Clean energy for all Europeans package," 2019. [Online]. Available: https://energy.ec.europa.eu/topics/energy-strategy/clean-energy-all-europeans-package_en

[51] ——, "Electricity market design," 2021. [Online]. Available: https://ec.europa.eu/energy/topics/markets-and-consumers/market-legislation/electricity-market-design_en

[52] "ENTSO-E VISION: A Power System for a Carbon Neutral Europe." [Online]. Available: https://www.entsoe.eu/

[53] ENTSO-E, "What are Network Codes?" [Online]. Available: https://www.entsoe.eu/network_codes/

[54] European Commission, "Third energy package," 2021. [Online]. Available: https://ec.europa.eu/energy/topics/markets-and-consumers/market-legislation/third-energy-package_en

[55] The European Commission, "Electricity market design." [Online]. Available: https://energy.ec.europa.eu/topics/markets-and-consumers/market-legislation/electricity-market-design_en

[56] EU DSO Entity, "The EU DSO Entity," 2021. [Online]. Available: https://www.eudsoentity.eu/

[57] Smartgridireland, "Press Release – The official birth of the EU DSO Entity," 2021. [Online]. Available: https://www.smartgridireland.org/press-release-the-official-birth-of-the-eu-dso-entity/

[58] The European DSO Entity, "The EU DSO Entity Missions," 2021. [Online]. Available: https://www.eudsoentity.eu/about/missions/

[59] K. Kris, T. Dimitris, and B. Marco, "D1.1 – Market and regulatory analysis : Analysis of current market and regulatory framework in the involved areas," pp. 1–83, 2020.

[60] The European Parliament and the Council of the European Union, "Regulation (EU) 714/2009 of the European Parliament and of the Council," *Official Journal of the European Union*, no. L211, pp. 15–35, 2009. [Online]. Available: https://eur-lex.europa.eu/legal-content/EN/ALL/?uri=celex%3A32009R0714

[61] T. Schittekatte, V. Reif, and L. Meeus, "The EU Electricity Network Codes," European University Institute, Tech. Rep., 2020.

[62] L. Lid and J. P. C. Ávila, "Deliverable 1.1 - Market and regulatory analysis: Analysis of current market and regulatory framework in the involved areas," The SmartNet Consortium, Tech. report, 2019.

[63] The European Commission, "Regulation (EU) 2016/1388 establishing a Network Code on Demand Connection," *Official Journal of the European Union*, no. L 223, pp. 10–54, 2016.

[64] ——, "Regulation (EU) 2017/2195 establishing a guideline on electricity balancing," *Official Journal of the European Union*, no. L 312, pp. 6–53, 2017.

[65] ENTSO-E, "TERRE," 2021. [Online]. Available: https://www.entsoe.eu/network_codes/eb/terre/

[66] ACER, "Balancing Energy Platforms." [Online]. Available: https://acer.europa.eu/electricity/market-rules/electricity-balancing/implementation/balancing-energy-platforms

[67] ENTSO-E, "Manually Activated Reserves Initiative," 2021. [Online]. Available: https://www.entsoe.eu/network_codes/eb/mari/

[68] ——, "PICASSO," 2021. [Online]. Available: https://www.entsoe.eu/network_codes/eb/picasso/

[69] ——, "Successful launch of the European IN-platform," Tech. Rep., 2021.

[70] ——, "Frequency Containment Reserves (FCR)." [Online]. Available: https://www.entsoe.eu/network_codes/eb/fcr/

[71] Gestore Mercati Energetici, "Spot Electricity Market (MPE) - MGP, MI, MPEG, MSD." [Online]. Available: https://www.mercatoelettrico.org/en/mercati/mercatoelettrico/mpe.aspx

[72] RSE, TERNA, ABB, EGP, ENEL, E2I, COMPENDIA, and EDISON, "Deliverable 5.1- Techno-economic analysis of DSR and RES selected services," OSMOSE Project, Tech. report, oct 2018.

[73] ARERA, "Delibera 300/2017/R/EEL - Prima apertura del mercaprima apertura del mercato per il servizio di dispacciamento (MSD) alla domanda elettrica ed alle unità di produzione anche da fonti rinnovabili non già abilitate nonché ai sistemi di accumulo." Tech. report, may 2017.

[74] ——, "Documento per la consultazione 322/2019/R/eel - Testo Integrato del Dispacciamento Elettrico (TIDE) - orientamenti complessivi -," Tech. report, jul 2019.

[75] ——, "Delibera 628/2018/R/eel - Avvio di procedimento per l'implementazione della regolazione dello scambio dati tra Terna S.p.a., le imprese di distribuzione di energia elettrica e i "significant grid user" ai fini dell'esercizio in sicurezza ..." Tech. report, dec 2018. [Online]. Available: https://www.arera.it/it/docs/18/628-18.htm

[76] ——, "Delibera ARERA 352/2021/R/eel," Tech. report, aug 2021. [Online]. Available: https://www.arera.it/it/docs/21/352-21.htm

[77] ——, "Documento per la consultazione 685/2022/R/eel," Tech. report, dec 2022. [Online]. Available: https://www.arera.it/it/docs/22/685-22.htm

[78] P. De Martini, "Operational Coordination Architecture: New Models and Approaches," *IEEE Power and Energy Magazine*, vol. 17, no. 5, pp. 29–39, 2019.

[79] N. Y. State, "Reforming the Energy Vision." [Online]. Available: https://www3.dps.ny.gov/W/PSCWeb.nsf/All/CC4F2EFA3A23551585257DEA007DCFE2?OpenDocument

[80] M. Zipf and D. Most, "Cooperation of TSO and DSO to provide ancillary services," *International Conference on the European Energy Market, EEM*, vol. 2016-July, 2016.

[81] E. Rivero, D. Six, P. Mallet, M. Sebastian-Viana, J. Stromsather, and M. Baron, "evolvDSO: Assessment of the future roles of the DSOs, future market architectures and regulatory frameworks for network integration of DRES," in *23rd International Conference on Electricity Distribution*, jun 2015, pp. 1–5.

[82] ENTSO-E, "No Title," Tech. Rep., 2022. [Online]. Available: https://www.entsoe.eu/Documents/EDI/Library/HRM/Harmonised_Role_Model_2022-01.pdf75017135029277

[83] "ADDRESSFP7-Towards the smart grids of the future." [Online]. Available: http://www.addressfp7.org/

[84] G. Leclercq, M. Pavesi, T. Gueuning, A. Ashouri, P. Sels, F. Geth, R. D'hulst, and H. Le Cadre, "Deliverable 2.2 - Network and market models," The SmartNet Consortium, Tech. report, feb 2019.

[85] F. Najibi, D. Apostolopoulou, and E. Alonso, "TSO-DSO Coordination Schemes to Facilitate Distributed Resources Integration," *Sustainability*, vol. 13, no. 14, 2021.

[86] D. Badanjak and H. Pandžić, "Distribution-Level Flexibility Markets—A Review of Trends, Research Projects, Key Stakeholders and Open Questions," *Energies*, vol. 14, no. 20, 2021.

[87] W. Zhao, M. Liu, J. Zhu, and L. Li, "Fully decentralised multi-area dynamic economic dispatch for large-scale power systems via cutting plane consensus,"

*IET Generation, Transmission & Distribution*, vol. 10, no. 10, pp. 2486–2495, 2016.

[88] A. Z. Morch, D. Siface, H. Gerard, and I. Kockar, "Market architecture for TSO-DSO interaction in the context of European regulation," in *International Conference on the European Energy Market, EEM*. IEEE, 2019, pp. 1–5.

[89] H. Chen, H. Li, C. Lin, X. Jin, R. Zhang, and X. Li, "An integrated market solution to enable active distribution network to provide reactive power ancillary service using transmission–distribution coordination," *IET Energy Systems Integration*, vol. 4, no. 1, pp. 98–115, 2022.

[90] C. Rodio, G. Giannoccaro, S. Bruno, M. Bronzini, and M. La Scala, "Optimal Dispatch of Distributed Resources in a TSO-DSO Coordination Framework," in *2020 AEIT International Annual Conference*, 2020, pp. 1–6.

[91] N. Natale, F. Pilo, G. Pisano, and G. G. Soma, "Scheduled profile at TSO/DSO interface for reducing balancing costs," in *2019 1st International Conference on Energy Transition in the Mediterranean Area (SyNERGY MED)*, 2019, pp. 1–6.

[92] T. Sousa, T. Soares, P. Pinson, F. Moret, T. Baroche, and E. Sorin, "Peer-to-peer and community-based markets: A comprehensive review," *Renewable and Sustainable Energy Reviews*, vol. 104, pp. 367–378, 2019.

[93] ARERA, "Documento per la consultazione 354/2013/R/eel - Pubblico dibattito per la riforma delle modalità di Approvv. delle risorse per il servizio di Dispacciamento, con riferimento agli impianti di Generazione distribuita e agli impianti dalle fonti rinnovabili," Tech. report, aug 2013. [Online]. Available: https://www.autorita.energia.it/it/docs/dc/13/354-13.jsp

[94] ——, "Documento per la consultazione 354/2013/R/eel - Allegato A," Tech. report, jun 2013. [Online]. Available: https://www.autorita.energia.it/allegati/docs/13/354-13all.pdf

[95] I. Gómez, S. Riaño, C. Madina, M. Rossi, P. Kuusela, P. Koponen, H. Aghaie, G. Migliavacca, E. Rivero, H. Xu, and I. Kockar, "Deliverable 4.3 – Cost-benefit analysis of the selected national cases," The SmartNet Consortium, Tech. report, jun 2019. [Online]. Available: https://smartnet-project.eu/wp-content/uploads/2019/06/D4.3.pdf

[96] K. Purchala, L. Meeus, D. Van Dommelen, and R. Belmans, "Usefulness of DC power flow for active power flow analysis," in *IEEE Power Engineering Society General Meeting, 2005*, 2005, pp. 454–459 Vol. 1.

[97] F. G. Montoya and R. B. Navarro, *Optimization Methods Applied to Power Systems*, volume 1 ed. Bassel: MDPI, jul 2019.

[98] J. Lin, F. Magnago, and J. M. Alemany, "Optimization Methods Applied to Power Systems: Current Practices and Challenges," in *Classical and Recent Aspects of Power System Optimization*, A. F. Zobaa, S. H. E. Abdel Aleem, and A. Y. Abdelaziz, Eds. Elsevier, 2018, pp. 1–18.

[99] G. Tsaousoglou, J. S. Giraldo, and N. G. Paterakis, "Market Mechanisms for Local Electricity Markets: A review of models, solution concepts and algorithmic techniques," *Renewable and Sustainable Energy Reviews*, vol. 156, p. 111890, 2022.

[100] X. Jin, Q. Wu, and H. Jia, "Local flexibility markets: Literature review on concepts, models and clearing methods," *Applied Energy*, vol. 261, p. 114387, 2020.

[101] Z. Li, Q. Guo, H. Sun, and J. Wang, "Coordinated Economic Dispatch of Coupled Transmission and Distribution Systems Using Heterogeneous Decomposition," *IEEE Transactions on Power Systems*, vol. 31, no. 6, pp. 4817–4830, 2016.

[102] ——, "A New LMP-Sensitivity-Based Heterogeneous Decomposition for Transmission and Distribution Coordinated Economic Dispatch," *IEEE Transactions on Smart Grid*, vol. 9, no. 2, pp. 931–941, 2018.

[103] S. Manshadi and M. Khodayar, "A hierarchical electricity market structure for the smart grid paradigm," in *2016 IEEE/PES Transmission and Distribution Conference and Exposition (TD)*, 2016, p. 1.

[104] M. Khorasany, Y. Mishra, and G. Ledwich, "Market framework for local energy trading: a review of potential designs and market clearing approaches," *IET Generation, Transmission & Distribution*, vol. 12, no. 22, pp. 5899–5908, 2018.

[105] P. Bonami, D. Salvagnin, and A. Tramontani, "Implementing Automatic Benders Decomposition in a Modern MIP Solver," in *Integer Programming and Combinatorial Optimization*, D. Bienstock and G. Zambelli, Eds. Cham: Springer International Publishing, 2020, pp. 78–90.

[106] C. Lin, W. Wu, Z. Li, and B. Zhang, "Decentralized economic dispatch for transmission and distribution networks via modified generalized benders decomposition," in *2017 IEEE Power Energy Society General Meeting*, 2017, pp. 1–5.

[107] Z. Li, W. Wu, B. Zhang, and B. Wang, "Decentralized Multi-Area Dynamic Economic Dispatch Using Modified Generalized Benders Decomposition," *IEEE Transactions on Power Systems*, vol. 31, no. 1, pp. 526–538, 2016.

[108] H. Ma and S. M. Shahidehpour, "Transmission-constrained unit commitment based on Benders decomposition," *International Journal of Electrical Power Energy Systems*, vol. 20, no. 4, pp. 287–294, 1998.

[109] X. Lai, L. Xie, Q. Xia, H. Zhong, and C. Kang, "Decentralized Multi-Area Economic Dispatch via Dynamic Multiplier-Based Lagrangian Relaxation," *IEEE Transactions on Power Systems*, vol. 30, no. 6, pp. 3225–3233, 2015.

[110] A. J. Conejo, E. Castillo, R. Mínguez, and R. García-Bertrand, *Decomposition Techniques in Mathematical Programming*, 1st ed., Springer, Ed. Springer Science & Business Media, 2006.

[111] A. M. Geoffrion, "Generalized Benders decomposition," *Journal of Optimization Theory and Applications*, vol. 10, no. 4, pp. 237–260, 1972.

[112] R. Rahmaniani, T. G. Crainic, M. Gendreau, and W. Rei, "The Benders decomposition algorithm: A literature review," *European Journal of Operational Research*, vol. 259, no. 3, pp. 801–817, 2017.

[113] A. Sinha, P. Malo, and K. Deb, "A Review on Bilevel Optimization: From Classical to Evolutionary Approaches and Applications," *IEEE Transactions on Evolutionary Computation*, vol. 22, no. 2, pp. 276–295, 2018.

[114] C. Zhang, Q. Wang, J. Wang, P. Pinson, and J. Østergaard, "Real-Time Trading Strategies of Proactive DISCO With Heterogeneous DG Owners," *IEEE Transactions on Smart Grid*, vol. 9, no. 3, pp. 1688–1697, 2018.

[115] J. Yu, Y. Jiao, X. Wang, J. Cao, and S. Fei, "Bi-level optimal dispatch in the Virtual Power Plant considering uncertain agents number," *Neurocomputing*, vol. 167, pp. 551–557, 2015.

[116] G. K. D. Saharidis and A. Fragkogios, *Open Problems on Benders Decomposition Algorithm*. Cham: Springer International Publishing, 2018, pp. 305–317.

[117] ENTSO-E, "Network Code on Operational Planning and Scheduling," ENTSO-E, Brussels, Tech. Rep., sep 2013.

[118] L. Lopez, A. Gonzalez-Castellanos, D. Pozo, M. Roozbehani, and M. Dahleh, "QuickFlex: a Fast Algorithm for Flexible Region Construction for the TSO-DSO Coordination," p. 6, 2021.

[119] J. Silva, J. Sumaili, R. J. Bessa, L. Seca, M. Matos, and V. Miranda, "The challenges of estimating the impact of distributed energy resources flexibility on the TSO/DSO boundary node operating points," *Computers and Operations Research*, vol. 96, pp. 294–304, 2018.

[120] D. Contreras and K. Rudion, "Computing the feasible operating region of active distribution networks: Comparison and validation of random sampling and optimal power flow based methods," *IET Generation, Transmission  Distribution*, vol. 15, pp. 1600–1612, 2021.

[121] G. Papazoglou and P. Biskas, "Review of Methodologies for the Assessment of Feasible Operating Regions at the TSO-DSO Interface," *Energies*, vol. 15, no. 14, 2022. [Online]. Available: https://www.mdpi.com/1996-1073/15/14/5147

[122] J. Silva, J. Sumaili, B. Silva, L. Carvalho, F. Retorta, M. Staudt, and V. Miranda, "A Data-driven Approach to Estimate the Flexibility Maps in Multiple TSO-DSO Connections," *IEEE Transactions on Power Systems*, pp. 1–12, 2022.

[123] D. Sebastian Stock, L. Löwer, Y. Harms, S. Wende-von Berg, M. Braun, Z. Wang, W. Albers, C. Calpe, M. Staudt, B. Silva, F. Retorta, J. Vieira Silva, and L. Carvalho, "Operational optimisation framework improving DSO/TSO coordination demonstrated in real network operation," in *CIRED 2020 Berlin Workshop (CIRED 2020)*, vol. 2020, 2020, pp. 840–843.

[124] D. S. Stock, S. Talari, and M. Braun, "Establishment of a Coordinated TSO-DSO Reactive Power Management for INTERPLAN Tool," in *2020 International Conference on Smart Energy Systems and Technologies (SEST)*, 2020, pp. 1–6.

[125] M. Heleno, R. Soares, J. Sumaili, R. J. Bessa, L. Seca, and M. A. Matos, "Estimation of the flexibility range in the transmission-distribution boundary," in *2015 IEEE Eindhoven PowerTech*, 2015, pp. 1–6.

[126] M. Mashhour, M. A. Golkar, and S. M. Moghaddas-Tafreshi, "Extending market activities for a distribution company in hourly-ahead energy and reserve markets – Part I: Problem formulation," *Energy Conversion and Management*, vol. 52, no. 1, pp. 477–486, 2011.

[127] C. Rodio, G. Giannoccaro, S. Bruno, and M. La Scala, "Benders Decomposition Methodology for TSO-DSO Cooperation in Ancillary Services Markets," *submitted to IEEE Transactions on Power Systems*.

[128] M. Cheng, J. Wu, S. J. Galsworthy, C. E. Ugalde-Loo, N. Gargov, W. W. Hung, and N. Jenkins, "Power System Frequency Response From the Control of Bitumen Tanks," *IEEE Transactions on Power Systems*, vol. 31, no. 3, pp. 1769–1778, 2016.

[129] S. Bruno, G. Giannoccaro, M. L. Scala, and G. Lopopolo, "First activities and power-hardware-in-the-loop tests at the public research laboratory LabZERO," in *2018 AEIT International Annual Conference*, 2018, pp. 1–6.

[130] S. Bruno, S. Lamonaca, G. Rotondo, U. Stecchi, and M. La Scala, "Unbalanced Three-Phase Optimal Power Flow for Smart Grids," *IEEE Transactions on Industrial Electronics*, vol. 58, no. 10, pp. 4504–4513, 2011.

[131] J. Silva, J. Sumaili, R. J. Bessa, L. Seca, M. A. Matos, V. Miranda, M. Caujolle, B. Goncer, and M. Sebastian-Viana, "Estimating the Active and Reactive Power Flexibility Area at the TSO-DSO Interface," *IEEE Transactions on Power Systems*, vol. 33, no. 5, pp. 4741–4750, 2018.

[132] EPRI, "OpenDSS - Open Distribution System Simulator (v.9)." [Online]. Available: https://www.epri.com/pages/sa/opendss

[133] C. Brezinski, "A Classification of Quasi-Newton Methods," *Numerical Algorithms*, vol. 33, no. 1, pp. 123–135, 2003.

[134] J. Barzilai and J. Borwein, "Two-Point Step Size Gradient Methods," *IMA Journal of Numerical Analysis*, vol. 8, no. 1, pp. 141–148, 1988.

[135] European Committee For Standardization, "EN 50160:2010 - Voltage characteristics of electricity supplied by public electricity networks," pp. 1–34, 2010.

[136] J. F. Benders, "Partitioning procedures for solving mixed-variables programming problems," *Numerische Mathematik*, vol. 4, no. 1, pp. 238–252, 1962.

[137] S. P. Canto, "Application of Benders' decomposition to power plant preventive maintenance scheduling," *European Journal of Operational Research*, vol. 184, no. 2, pp. 759–777, 2008.

[138] Q. Wang, J. D. McCalley, T. Zheng, and E. Litvinov, "Solving corrective risk-based security-constrained optimal power flow with Lagrangian relaxation and Benders decomposition," *International Journal of Electrical Power Energy Systems*, vol. 75, pp. 255–264, 2016.

[139] S. Binato, M. V. F. Pereira, and S. Granville, "A new Benders decomposition approach to solve power transmission network design problems," *IEEE Transactions on Power Systems*, vol. 16, no. 2, pp. 235–240, 2001.

[140] M. Moradi-Sepahvand, T. Amraee, F. Aminifar, and A. Akbari, "Coordinated expansion planning of transmission and distribution systems integrated with smart grid technologies," *International Journal of Electrical Power Energy Systems*, vol. 147, p. 108859, 2023.

[141] Z. Yuan and M. R. Hesamzadeh, "Hierarchical coordination of TSO-DSO economic dispatch considering large-scale integration of distributed energy resources," *Applied Energy*, vol. 195, pp. 600–615, 2017.

[142] C. Rodio, G. Giannoccaro, S. Bruno, and M. La Scala, "Benders Decomposition for TSO-DSO Coordination in Local Ancillary Services Market," in *Accepted with mandatory changes to 2023 IEEE PES General Meeting*.

[143] E. Bompard, S. Bruno, S. Frittoli, G. Giannoccaro, M. La Scala, A. Mazza, E. Pons, and C. Rodio, "Remote PHIL Distributed Co-Simulation Lab for TSO-DSO-Customer Coordination Studies," in *2020 AEIT International Annual Conference*, 2020, pp. 1–6.

[144] M. Jenabi, S. M. T. Fatemi Ghomi, S. A. Torabi, and S. H. Hosseinian, "Acceleration strategies of Benders decomposition for the security constraints power system expansion planning," *Annals of Operations Research*, vol. 235, no. 1, pp. 337–369, 2015.

[145] "Power Systems Test Case Archive." [Online]. Available: https://labs.ece.uw.edu/pstca/

[146] M. E. Baran and F. F. Wu, "Network reconfiguration in distribution systems for loss reduction and load balancing," *IEEE Transactions on Power Delivery*, vol. 4, no. 2, pp. 1401–1407, 1989.

[147] P. Fernández-Porras, M. Panteli, and J. Quirós-Tortós, "Intentional controlled islanding: when to island for power system blackout prevention," *IET Generation, Transmission & Distribution*, vol. 12, no. 14, pp. 3542–3549, 2018.

[148] R. D. Zimmerman, C. E. Murillo-Sánchez, and R. J. Thomas, "MATPOWER: Steady-State Operations, Planning, and Analysis Tools for Power Systems Research and Education," *IEEE Transactions on Power Systems*, vol. 26, no. 1, pp. 12–19, 2011.

[149] H. Wang, C. E. Murillo-Sanchez, R. D. Zimmerman, and R. J. Thomas, "On Computational Issues of Market-Based Optimal Power Flow," *IEEE Transactions on Power Systems*, vol. 22, no. 3, pp. 1185–1193, 2007.

[150] M. Farrokhseresht, N. G. Paterakis, M. Gibescu, Y. Tohidi, and J. G. Slootweg, "A Survey on the Participation of Distributed Energy Resources in Balancing Markets," in *2018 15th International Conference on the European Energy Market (EEM)*, 2018, pp. 1–5.

[151] ENTSO-E, "Need for synthetic inertia (SI) for frequency regulation," ENTSO-E, Brussels, Tech. Rep., mar 2017.

[152] A. Ulbig, T. S. Borsche, and G. Andersson, "Impact of low rotational inertia on power system stability and operation," in *IFAC Proceedings Volumes (IFAC-PapersOnline)*, vol. 19, dec 2014, pp. 7290–7297.

[153] P. Daly, H. W. Qazi, and D. Flynn, "RoCoF-Constrained Scheduling Incorporating Non-Synchronous Residential Demand Response," *IEEE Transactions on Power Systems*, vol. 34, no. 5, pp. 3372–3383, 2019.

[154] Terna S.p.A., "Regolamento per la fornitura del servizio di regolazione primaria della frequenza per il tramite di unità di produzione integrate con sistemi di accumulo." p. 11, 2018.

[155] J. Fang, R. Zhang, Y. Tang, and L. Hongchang, "Inertia Enhancement by Grid-Connected Power Converters with Frequency-Locked-Loops for Frequency Derivative Estimation," in *2018 IEEE Power Energy Society General Meeting (PESGM)*, 2018, pp. 1–5.

[156] T. Kerdphol, F. S. Rahman, M. Watanabe, Y. Mitani, D. Turschner, and H. Beck, "Enhanced Virtual Inertia Control Based on Derivative Technique to Emulate Simultaneous Inertia and Damping Properties for Microgrid Frequency Regulation," *IEEE Access*, vol. 7, pp. 14 422–14 433, 2019.

[157] I. Martínez-Sanz, B. Chaudhuri, A. Junyent-Ferré, V. Trovato, and G. Strbac, "Distributed vs. concentrated rapid frequency response provision in future great britain system," in *2016 IEEE Power and Energy Society General Meeting (PESGM)*, 2016, pp. 1–5.

[158] H. R. Chamorro, A. C. Sanchez, A. Verjordet, F. Jimenez, F. Gonzalez-Longatt, S. Member, and V. K. Sood, "Distributed Synthetic Inertia Control in Power Systems," in *Proceedings of 8th International Conference on Energy and Environment: Energy Saved Today is Asset for Future, CIEM 2017*, 2017, pp. 74–78.

[159] R. Eriksson, N. Modig, and K. Elkington, "Synthetic inertia versus fast frequency response: a definition," *IET Renewable Power Generation*, vol. 12, no. 5, pp. 507–514, 2018.

[160] ENTSO-E, "Future System Inertia 2," techreport. [Online]. Available: https://www.entsoe.eu/Documents/Publications/SOC/Nordic/2018/System-inertia.zip

[161] S. Bruno, G. Giannoccaro, C. Iurlaro, M. La Scala, and C. Rodio, "A Low-cost Controller to Enable Synthetic Inertia Response of Distributed Energy Resources," in *2020 IEEE EEEIC/ICPS Europe*, 2020, pp. 1–6.

[162] M. Rezkalla, A. Zecchino, S. Martinenas, A. M. Prostejovsky, and M. Marinelli, "Comparison between synthetic inertia and fast frequency containment control based on single phase EVs in a microgrid," *Applied Energy*, vol. 210, pp. 764–775, 2018.

[163] L. Meng, J. Zafar, S. K. Khadem, A. Collinson, K. C. Murchie, F. Coffele, and G. M. Burt, "Fast Frequency Response From Energy Storage Systems—A Review of Grid Standards, Projects and Technical Issues," *IEEE Transactions on Smart Grid*, vol. 11, no. 2, pp. 1566–1581, 2020.

[164] D. Ochoa and S. Martinez, "Fast-Frequency Response Provided by DFIG-Wind Turbines and its Impact on the Grid," *IEEE Transactions on Power Systems*, vol. 32, no. 5, pp. 4002–4011, 2017.

[165] S. Bruno, G. De Carne, C. Iurlaro, C. Rodio, and M. Specchio, "A SOC-feedback Control Scheme for Fast Frequency Support with Hybrid Battery/Supercapacitor Storage System," in *2021 6th IEEE Workshop on the Electronic Grid (eGRID)*, 2021, pp. 1–8.

[166] ENTSO-E, "Frequency Measurement Requirements and Usage," techreport January, Final Version 7, 2018.

[167] European Union, "DCC: Commission Regulation (EU) 2016/1388 establishing a network code on Demand Connection," *Official Journal of the European Union*, vol. 2016, no. 14 April 2016, p. 68, 2016.

[168] D. Ibrahim, "Accurate Measurement of the Mains Electricity Frequency," *International Conference on Electrical and Electronics Engineering*, 2011.

[169] M. Kleemann and V. Piskarov, "Rate of change of frequency protection: Towards a viable algorithm for a protective relay," in *CIRED - Open Access Proceedings Journal*, 2017.

[170] P. Tosato, D. Macii, and D. Brunelli, "Implementation of phasor measurement units on low-cost embedded platforms: A feasibility study," in *I2MTC 2017 -*

*2017 IEEE International Instrumentation and Measurement Technology Conference, Proceedings*, 2017.

[171] Z. Huang, T. Zhu, H. Lu, and W. Gao, "Accurate Power Quality Monitoring in Microgrids," in *2016 15th ACM/IEEE International Conference on Information Processing in Sensor Networks, IPSN 2016 - Proceedings*, 2016.

[172] B. Kasztenny, "A new method for fast frequency measurement for protection applications," Edinburgh, 2016, p. 7.

[173] B. Boashash, "Estimating and Interpreting The Instantaneous Frequency of a Signal—Part 1: Fundamentals," *Proceedings of the IEEE*, vol. 80, no. 4, pp. 520–538, 1992.

[174] ——, "Estimating and Interpreting the Instantaneous Frequency of a Signal—Part 2: Algorithms and Applications," *Proceedings of the IEEE*, vol. 80, no. 4, pp. 540–568, 1992.

[175] A. Carcelen-Flores, J. A. Fuentes, A. Molina-Garcia, E. Gomez-Lazaro, and A. Vigueras-Rodriguez, "Comparison of instantaneous frequency estimation algorithms under power system disturbances," in *IEEE Power and Energy Society General Meeting*, 2012.

[176] A. G. Phadke and B. Kasztenny, "Synchronized phasor and frequency measurement under transient conditions," *IEEE Transactions on Power Delivery*, 2009.

[177] G. De Carne, S. Bruno, M. Liserre, and M. La Scala, "Distributed Online Load Sensitivity Identification by Smart Transformer and Industrial Metering," *IEEE Transactions on Industry Applications*, 2019.

[178] ENTSO-E, "Rate of Change of Frequency (RoCoF) withstand capability," ENTSO-E, Brussels, techreport, dec 2018.

[179] I. Power and E. Society, *C37.118.1-2011 - IEEE Standard for Synchrophasor Measurements for Power Systems*, 2011.

[180] M. Rezkalla, A. Zecchino, M. Pertl, and M. Marinelli, "Grid frequency support by single-phase electric vehicles employing an innovative virtual inertia controller," in *2016 UPEC Conference*, 2016, pp. 1–6.

[181] R. Kuga, M. Esguerra, B. Chabot, and A. Avendano Cecena, "EPIC 2.05: Inertia Response Emulation for DG Impact Improvement," Pacific Gas and Electric Company, Tech. Rep., feb 2019. [Online]. Available: https://www.pge.com/pge_global/common/pdfs/about-pge/environment/what-we-are-doing/electric-program-investment-charge/PGE-EPIC-Project-2.05.pdf

[182] J. Fang, Y. Tang, H. Li, and X. Li, "A Battery/Ultracapacitor Hybrid Energy Storage System for Implementing the Power Management of Virtual Synchronous Generators," *IEEE Transactions on Power Electronics*, vol. 33, no. 4, pp. 2820–2824, 2018.

[183] S. Bruno, G. Giannoccaro, C. Iurlaro, M. La Scala, and C. Rodio, "Power Hardware-in-the-Loop Test of a Low-Cost Synthetic Inertia Controller for Battery Energy Storage System," *Energies*, vol. 15, no. 9, 2022.

[184] P. Romano and M. Paolone, "Enhanced interpolated-DFT for synchrophasor estimation in FPGAs: Theory, implementation, and validation of a PMU prototype," *IEEE Transactions on Instrumentation and Measurement*, vol. 63, no. 12, pp. 2824–2836, 2014. [Online]. Available: https://www.scopus.com/inward/record.uri?eid=2-s2.0-84909633088&doi=10.1109%2FTIM.2014.2321463&partnerID=40&md5=042093f6fb7fcf39c037be86f8bd4d59

[185] Z. Zhang, P. Fu, G. Gao, L. Jiang, and L. Wang, "A Rogowski Digital Integrator With Comb Filter Signal Processing System," *IEEE Transactions on Plasma Science*, vol. 46, no. 5, pp. 1338–1343, 2018.

[186] M. E. Haque, M. N. Sakib Khan, and M. R. Islam Sheikh, "Smoothing control of wind farm output fluctuations by proposed Low Pass Filter, and Moving Averages," in *2015 International Conference on Electrical Electronic Engineering (ICEEE)*, 2015, pp. 121–124.

[187] S. Bruno, G. Giannoccaro, M. M. Islam, C. Iurlaro, M. La Scala, M. Menga, and C. Rodio, "Control and Power Hardware-in-the-Loop tests for low-inertia power systems," in *2022 AEIT International Annual Conference*, 2022, pp. 1–6.

[188] E. Bompard, S. Bruno, G. Chicco, G. Giannoccaro, M. La Scala, A. Mazza, E. Pons, and C. Rodio, "Co-simulazione real-time multi-sito e cooperazione tra laboratori," *AEIT*, vol. 106 num. 7, pp. 38–55, 2020.

[189] G. Donnini, E. Carlini, G. Giannuzzi, R. Zaottini, C. Pisani, E. Chiodo, D. Lauria, and F. Mottola, "On the Estimation of Power System Inertia accounting for Renewable Generation Penetration," in *2020 AEIT International Annual Conference (AEIT)*, 2020, pp. 1–6.

[190] S. Bruno, G. Giannoccaro, C. Iurlaro, M. La Scala, C. Rodio, and R. Sbrizzai, "Fast Frequency Regulation Support by LED Street Lighting Control," in *2021 EEEIC/ICPS Europe Conference*, 2021, pp. 1–6.

[191] S. Bruno, G. Giannoccaro, C. Iurlaro, M. La Scala, M. Menga, C. Rodio, and R. Sbrizzai, "Fast Frequency Support Through LED Street Lighting in Small Non-Synchronous Power Systems," *IEEE Transactions on Industry Applications*, pp. 1–11, 2022.

[192] F. Rubinstein, L. Xiaolei, and D. Watson, "Using Dimmable Lighting for Regulation Capacity and Non-Spinning Reserves in the Ancillary Services Market. A Feasibility Study," Lawrence Berkeley Nat. Lab., Berkeley, CA, USA, techrep, 2010.

[193] O. Ma, N. Alkadi, P. Cappers, P. Denholm, J. Dudley, and E. Al., "Demand Response for Ancillary Services," *IEEE Transactions on Smart Grid*, vol. 4, no. 4, pp. 1988–1995, 2013.

[194] M. Shahidehpour, C. Bartucci, N. Patel, T. Hulsebosch, P. Burgess, and N. Buch, "Streetlights Are Getting Smarter: Integrating an Intelligent Communications and Control System to the Current Infrastructure," *IEEE Power and Energy Magazine*, vol. 13, no. 3, pp. 67–80, 2015.

[195] M. Alvarado-Ruiz, F. Abi Abdallah, M. Gagnaire, and Y. Lascaux, "TeleWatt: An innovative electric vehicle charging infrastructure over public lighting systems," 2013, pp. 741–746.

[196] S. Bruno, G. Giannoccaro, M. La Scala, G. Lopopolo, and C. Rodio, "A Microgrid Architecture for Integrating EV Charging System and Public Street Lighting," in *2019 IEEE EEEIC/ICPS Europe*, 2019.

[197] G. R. Newsham, S. Mancini, and R. G. Marchand, "Detection and Acceptance of Demand-Responsive Lighting in Offices with and without Daylight," *LEUKOS*, vol. 4, no. 3, pp. 139–156, 2008.

[198] E. Waffenschmidt, "Virtual inertia grid control with LED lamp driver," in *2016 IESC Conference*, 2016, pp. 1–6.

[199] M. Bagheri-Sanjareh, M. H. Nazari, and G. B. Gharehpetian, "A novel and optimal battery sizing procedure based on MG frequency security criterion using coordinated application of BESS, LED lighting loads, and photovoltaic systems," *IEEE Access*, vol. 8, pp. 95 345–95 359, 2020.

[200] W. Wang, X. Chu, and K. Xiao, "A Distributed Economic AGC Strategy Integrating Dynamic Demand Response," in *2018 IEEE Power & Energy Society General Meeting (PESGM)*. IEEE, 2018, pp. 1–5.

[201] K. Xiao, X. Chu, and Y. Liu, "LED lighting loads actively participating in power system frequency regulation," in *2016 IEEE Power Energy Society ISGT Conference*, 2016, pp. 1–5.

[202] J. Liu, W. Zhang, and Y. Liu, "Primary Frequency Response From the Control of LED Lighting Loads in Commercial Buildings," *IEEE Transactions on Smart Grid*, vol. 8, no. 6, pp. 2880–2889, 2017.

[203] UNI Technical Committee, "UNI 11248:2016 - Road lighting - Selection of lighting classes," pp. 1–38, 2016.

[204] European Committee For Standardization, “EN 13201:2015 - Road lighting - Part 2: Performance requirements,” 2015.

[205] M. G. Ippolito, R. Musca, E. R. Sanseverino, and G. Zizzo, “Frequency Dynamics in Fully Non-Synchronous Electrical Grids: A Case Study of an Existing Island,” *Energies*, vol. 15, no. 6, 2022.

[206] C. Cottarell, C. Valdes, D. Bonata, F. Falchi, and R. Furgoni, “Illuminazione pubblica: spendiamo troppo,” Università del Sacro Cuore - Osservatorio CPI, techreport, may 2018.

[207] Terna S.p.A. e Gruppo Terna, “Dati statistici sull’energia elettrica in Italia,” Terna, Tech. Rep., 2017.

[208] H. R. Chamorro, R. Torkzadeh, M. Eliassi, P. Betancourt-Paulino, M. Rezkalla, F. Gonzalez-Longatt, V. K. Sood, and W. Martinez, “Analysis of the Gradual Synthetic Inertia Control on Low-Inertia Power Systems,” in *2020 IEEE ISIE Conference*, vol. 2020-June, 2020, pp. 816–820.

# Acronyms

**AC** Alternating Current. 71, 72, 74, 99, 180

**ACER** Agency for the Cooperation of Energy Regulators. 25

**AD** analog-to-digital. 138, 146

**ADC** Analog-to-digital converter. 143, 146, 147, 150, 156, 157

**AE** Absolute Error. 147, 150

**aFRR** automatic Frequency Restoration Reserves. ii, 17, 28, 30

**AS** Ancillary Services. vi, 1, 6, 7, 9–16, 20, 22, 23, 26, 27, 30–35, 39, 40, 42–60, 62, 64–67, 70–75, 78–80, 94, 96–102, 105, 106, 110, 115, 119, 120, 122, 124, 132, 134, 158, 177, 197–200

**BDA** Benders decomposition algorithm. 2, 8, 76, 81, 99–101, 103–107, 110, 116, 118–120, 122, 124, 126–128, 132, 133, 199

**BESS** battery energy storage systems. 11, 17, 136, 155, 156, 158, 159, 161–164, 166–170, 172–174, 176, 177, 198

**BMS** battery management system. 156, 158, 162, 166, 168

**BRP** Balance Responsible Party. 27, 38, 68, 69

**BSP** Balancing Service Provider. 27

**CACM GL** Capacity Allocation and Congestion Management Guideline. 26, 28

**CBA** cost-benefit analysis. 64, 66

**CDSO** Closed Distribution System Operator. 26

**CEP** Clean Energy Package. 20, 21

**CM** congestion management. 2, 9, 15, 33, 70–72, 75, 80, 100, 122

**CMP** commercial market parties. 38, 44, 45, 48, 68, 69

**CV** centrlized variant. 42

**DAM** Day-ahead market. 17, 47, 55, 80, 115, 119

**DC** Direct Current. 71, 74, 99, 140, 157, 177, 180, 182, 187, 188, 190, 191, 196

**DCC NC** Demand Connection Code Network Code. 26

**DCO** Consultation Document. 31–33, 62, 64, 65

**DERs** Distributed Energy Resources. i, 1, 2, 6–9, 11–13, 15, 17, 22–24, 31–36, 39, 40, 43, 46–48, 50–54, 56–60, 62, 64, 67, 70, 74, 75, 78–82, 95–100, 106, 120, 127, 130, 134–136, 155, 156, 173, 179, 198–200

**DFT** Discrete Fourier Transform. 138, 139

**DM** Data Manager. 38, 68, 69

**DMS** Distribution Management System. 94

**DN** distribution network. vii, 2, 6–8, 10, 11, 21, 22, 24, 32, 34, 38–58, 60, 62, 64–72, 74–81, 94–102, 106, 107, 110, 115, 116, 118–120, 122, 124, 126–130, 132–134, 137, 198–200

**DR** Demand Response. 6, 18, 24, 26, 27, 137, 177

**DSO** Distribution System Operator. ii, 1, 7–11, 13, 15, 18–27, 32–36, 38–65, 67–72, 74–82, 87, 94–97, 99–102, 104–107, 116, 119, 120, 122, 124, 127, 129, 130, 132, 198–200

**DV** decentrlized variant. 42, 46

**EB GL** Electricity Balancing Guideline. 26–28

**EMC** Electromagnetic Compatibility. 178

**ENTSO-E** European Network of Transmission System Operators. vi, 20, 21, 25, 28–30

**ER NC** Emergency and Restoration Network Code. 26

**EU** European Union. 6, 20, 21, 32, 62, 67

**EV** electrical vehicle. 6, 11, 18, 25, 32, 65, 177, 178

**FA** Flexibility aggregator. 38, 52, 53, 68, 69

**FCA GL** Forward Capacity Allocation Guideline. 26

**FCR** Frequency Containment Reserve. 12, 13, 27, 28, 31, 134, 135

**FFC** Flexibility feasibility checker. 38, 41, 68, 69

**FFR** Fast Frequency Response. ix, 2, 8, 12, 33, 134, 136–138, 155, 177, 179, 183, 187–190, 193–197, 200

**FRD** Flexibility resources dispatcher. 38, 68, 69

**FRR** Frequency Restoration Reserve. 12, 13, 27, 28

**GL** guideline. 25, 26

**GPIO** General Purpose Input/Output. 146, 156, 157

**GPS** Global Positioning System. 179

**HESS** Hybrid Energy Storage System. 17

**HV** high voltage. 83–85, 116

**HVAC** Heating, Ventilation and Air Conditioning. 6, 11, 32, 65

**HVDC NC** High Voltage Direct Current Connections Network Code. 26

**ICA** Ideal Centralized Approach. 107, 110, 115, 116, 118–120, 122, 124, 127

**ICT** Information and Communication Technologies. 51, 53, 54, 60, 67

**IED** intelligent electronic devices. 155

**IF** instantaneous frequency. 139

**IGCC** International Grid Control Cooperation. ii, 28

**IMO** Independent Market Operator. 7, 44–48, 68, 69

**IN** Inbalance Netting. ii, 28

**KKT** Karush–Kuhn–Tucker. 76

**LED** Light-Emitting Diode. v, ix, 2, 8, 134, 177–180, 182–184, 186–197, 200

**LV** low voltage. 82, 84, 85, 87, 183, 184, 186, 191, 196

**MAPE** Mean Absolute Percentage Error. 147, 150

**MARI** Manually Activated Reserves Initiative. ii, 27, 28

**MDR** Measured Data Responsible. 38, 68, 69

**mFRR** manual Frequency Restoration Reserves. ii, 27, 28

**MIPS** Matpower Interior Point Solver. 110

**MO** Market Operator. 38, 42–44, 58, 68, 69, 72

**MP** Master problem. 99, 101, 103, 106, 129, 130

**MSD** Mercato dei Servizi di Dispacciamento. 30, 31

**MV** medium voltage. 82–85, 87, 183, 184, 196

**NC** Network Code. 20, 25, 26

**OPF** optimal power flow. 19, 70–74, 77–80, 82, 86, 96–99, 110, 127

**P2P** peer-to-peer. 19, 59, 61

**PHIL** Power Hardware-in-the-Loop. 2, 134, 156, 158, 162, 163, 166, 167, 174, 176, 177, 179, 183, 184, 187, 190, 196, 197, 199, 200

**PICASSO** Platform for the International Coordination of Automated Frequency Restoration and Stable System Operation. ii, 28

**PMUs** Phasor Measurement Units. 137–139, 155

**POI** point of interconnection. 1, 2, 7, 8, 52, 54–58, 70, 73, 76–81, 83, 87, 92, 94–100, 104, 106, 107, 115, 116, 119, 120, 122, 124, 127, 129, 130, 132, 199

**PS** preliminary step. 106, 116

**PV** photovoltaic. 10, 11, 17, 31, 82, 88

**RA** Reserve Allocator. 38, 68, 69

**RFE** RoCoF error. 137, 138, 152, 154, 155

**RfG NC** Requirements for Generators Network Code. 26

**RoCoF** Rate of Change of Frequency. 8, 134–138, 152, 154–158, 162, 164–170, 173–175, 188, 189, 191, 193, 195, 196

**RR** Replacement Reserve. ii, 12, 27, 30

**RS** Random Sampling. 77, 90, 94

**RTS** real-time simulator. 158, 159, 162, 168

**SAA** smart aggregation approach. iii, viii, 78–80, 95–98, 107, 110, 116, 119, 120, 122, 124, 127–130, 132

**SCADA** Supervisory Control And Data Acquisition. 94

**SGU** significant grid user. 26

**SI** Synthetic Inertia. v, ix, 2, 8, 9, 12, 17, 33, 34, 134, 136–139, 155–164, 166, 168–170, 174, 177, 179, 183, 187–193, 195–197, 199, 200

**SO** System Operator. 1, 10, 13, 26, 32–35, 38, 43, 44, 58, 68, 69

**SO GL** Transmission System Operation Guideline. 26, 28

**SP** Slave problem. 99, 102–104, 122, 129, 132

**SPI** serial peripheral interface. 157

**TERRE** Trans European Replacement Reserves Exchange. ii, 27

**THD** total harmonic distortion. 137

**TN** transmission network. 2, 7, 8, 10, 21, 38, 40–52, 54, 55, 58, 65, 66, 68, 69, 71, 72, 74–76, 78, 80, 81, 94–96, 99–102, 106, 107, 110, 115, 119, 120, 124, 126, 127, 129, 130, 132, 133, 199

**TOPF** three-phase optimal power flow. 7, 74, 82, 85, 87–90, 94

**TSI** total system inertia. 160

**TSO** Transmission System Operator. ii, 1, 7–11, 13, 15, 19–28, 30–36, 39–64, 67–72, 74–83, 87, 94–100, 104–107, 116, 119, 124, 129, 130, 132, 186, 199, 200

**UVA** Unità Virtuali Abilitate. 32

**VPP** Virtual Power Plant. 18, 19

**ZC** zero crossing. 138, 139